**Politecnico di Milano**

School of Civil, Environmental and Land Management Engineering

Master of Science in Environmental and Land Planning Engineering


In collaboration with:
University of Stavanger (UiS)
Department of Mechanical and Structural Engineering and Materials Science

# Mooring systems analysis for floating wind turbines in the Italian seas

Supervisor at UiS: Prof. Ove Tobias Gudmestad
Supervisor: Prof. Giuseppe Passoni

Written by:
Pietro Re
854687

Academic Year 2016/2017

# Acknowledgments

*In this moment, finding the right words in two languages seems a nearly impossible task, but I will do my best. First and foremost, I would like to thank all the people who contributed in the realization of this thesis.*
*All my gratitude, now and forever, goes to the supervisors of this work, Professor Ove Tobias Gudmestad and Professor Giuseppe Passoni, who not only provided fundamental assistance, supervision and precious counsel, but made possible an experience of a lifetime. I also thank Professor Sverre Haver for the fundamental advices in the statistical analysis and Adekunle Orimolade for the help in the use of OrcaFlex.*

*Ora, trattenendo la commozione, mi tornano in mente le parole che scrissi nel 2015 per la mia Laurea e non posso fare altro che rinnovarle: grazie a chiunque è parte della mia vita, c'è una parte di voi non solo in questo lavoro, ma anche in qualsiasi cosa che ho fatto, faccio e farò.*
*Continuiamo così.*

*Grazie*
*Thank you*
*Takk*

# Abstract

In recent years, the interest of exploiting wind power in deep waters has grown, with the realization of floating structures that could accommodate a turbine and produce electricity. One of the many challenges that these projects face, is the position keeping of the system in a defined part of the sea: this is carried out with mooring systems, designed to withstand extreme marine conditions. The first aim of this work is to analyse these systems, to find a general solution for a floating wind farm in the Italian seas. To this end, a numerical model of the floating structure and the environment has been realized using the software OrcaFlex and simulating the 50 and 100 year return period conditions in the Adriatic Sea and in the Strait of Sicily, with different mooring combinations of present day technologies. The model's implementation required environmental and structural parameters: the firsts have been obtained with a statistical analysis of actual recordings of wind speed and wave height and with the official Italian cartography. Structural details have been derived looking at existing floaters, finding the most suitable one for the Italian environment. After sixteen simulations the results are interpreted with a comparison of tension in the lines, vertical forces at the anchors, wires length and mooring footprint, finding out that depth has the greatest impact on these factors. With respect to this, the proposed numerical model can provide a simple indication for the mooring of floating wind turbines in two different areas of the seas surrounding the Italian peninsula: for the Adriatic Sea (shallow waters), suction anchors with chains should be preferred and for the Strait of Sicily (deeper waters), traditional anchors may be considered, with lines composed of chains or a combination of chains with synthetic fibres.

# Riassunto

Negli ultimi anni, è cresciuto l'interesse riguardo allo sfruttamento dell'energia eolica in acque profonde, con la realizzazione di strutture galleggianti in grado di ospitare una turbina e di produrre elettricità. Una delle tante sfide che devono affrontare questi progetti, è il mantenimento della posizione del sistema in una zona definita del mare: questo viene realizzato con sistemi di ancoraggio, progettati per resistere a condizioni ambientali estreme. Il primo obiettivo di questo lavoro è analizzare questi sistemi, per trovare una soluzione preliminare per un parco eolico galleggiante nei mari italiani. A tal fine, un modello numerico della struttura galleggiante e dell'ambiente circostante è stato realizzato, utilizzando il software OrcaFlex e simulando condizioni con tempo di ritorno di 50 e 100 anni nel Mare Adriatico e nello stretto di Sicilia, con diverse combinazioni delle attuali tecnologie riguardo agli ormeggi. L'implementazione del modello ha richiesto parametri ambientali e strutturali: i primi sono stati ottenuti con un'analisi statistica delle registrazioni reali della velocità del vento e dell'altezza delle onde e con la cartografia ufficiale italiana. I dettagli strutturali sono stati ricavati ricercando tra le strutture galleggianti esistenti e trovando la più adatta per l'ambiente italiano. Dopo sedici simulazioni, i risultati sono interpretati con un confronto tra la tensione nelle linee, le forze verticali alle ancore, la lunghezza dei cavi e l'area occupata sul fondale, scoprendo che la profondità ha il maggiore impatto su questi fattori. Rispetto a questo, il modello numerico proposto può fornire una semplice indicazione per l'ormeggio di turbine eoliche galleggianti in due diverse aree dei mari che circondano la penisola italiana: per il Mare Adriatico (acque basse), si dovrebbero preferire ancore a suzione con catene e, per lo stretto di Sicilia (acque più profonde), si possono prendere in considerazione ancoraggi tradizionali, con cavi composti da catene o da una combinazione di catene con fibre sintetiche.

# Estratto

Petrolio, carbone, gas naturali e risorse non rinnovabili in generale oggi coprono la maggior parte del fabbisogno energetico mondiale. Queste fonti sono destinate ad esaurirsi in una scala temporale relativamente breve e nel contempo contribuiscono all'emissione di gas serra e altri inquinanti. Ad oggi, emergono due esigenze in apparenza inconciliabili: combattere l'effetto serra e le emissioni di sostanze dannose per la salute e soddisfare la crescente domanda mondiale di energia. Una possibile risposta è produrre energia elettrica da fonti rinnovabili.
L'energia prodotta tramite aerogeneratori dal vento si colloca in queste ultime: sfrutta una fonte pulita e inesauribile tramite una tecnologia collaudata e sicura. Recentemente, si sta osservando il crescente interesse a sfruttare una produzione non solo basata su turbine terrestri ma anche marittime. Queste ultime sfruttano tecnologie derivate dall'industria petrolifera e, all'inizio, richiamavano strutture offshore tradizionali, con piloni che connettevano la turbina alle fondazioni direttamente costruite sul fondale. La nuova frontiera è sbloccare il potenziale eolico anche in acque profonde, con lo sviluppo di strutture galleggianti capaci di sostenere la turbina e ancorate al fondo del mare.
Una delle sfide che si devono affrontare in questo senso è composta dal progetto di un sistema di ancoraggio che mantenga il sistema galleggiante-turbina in posizione. Questa tesi si colloca in questo ambito, con l'obiettivo di ricercare una soluzione in ambito italiano. La metodologia applicata comprende la realizzazione di un modello numerico tramite software capace di simulare la struttura, le condizioni ambientali e diverse tipologie di ancoraggi, con lo scopo di avere un'indicazione di massima su quale possibilità sviluppare in un progetto ipotetico.
L'implementazione di un modello, seppur con tutte le semplificazioni del caso, richiede la conoscenza di variabili ambientali e tecniche. Per rispondere a questa esigenza si sono dovute svolgere ricerche e analisi volte a chiarire questi parametri.
Per prima cosa si è indagato sui parametri ambientali che governano le simulazioni: condizioni estreme, corrispondenti ai tempi di ritorno di 50 e 100 anni, per quanto riguarda velocità del vento e altezza spettrale delle onde, e profondità del fondale. Questi parametri sono stati ricercati in due località italiane, il mare Adriatico nei pressi di Ancona e lo stretto di Sicilia, nel tratto di mare a sud dell'isola. La scelta di due località è stata presa per simulare due ambienti diversi in termini di fattori ambientali e per la disponibilità di dati. L'analisi per individuare i

parametri richiesti per onde e vento si basa sulla teoria dei valori estremi in statistica e ha richiesto registrazioni di altezza spettrale delle onde e velocità del vento tramite network di monitoraggio gestiti da ISPRA (Istituto Superiore per la Protezione e la Ricerca Ambientale): la Rete Ondametrica Nazionale (RON) per la prima (Rete Ondametrica Nazionale n.d.) e la Rete Mareografica Nazionale (RMN) per la seconda (Rete Mareografica Nazionale (1998-2014) n.d.) (Rete Mareografica Nazionale (2014-2017) n.d.), Figura I. Per quanto riguarda la batimetria, sono stati impiegati i dati cartografici ufficiali italiani, disponibili sul Geoportale Nazionale (Geoportale Nazionale, Bathymetry 2009), Figura I.

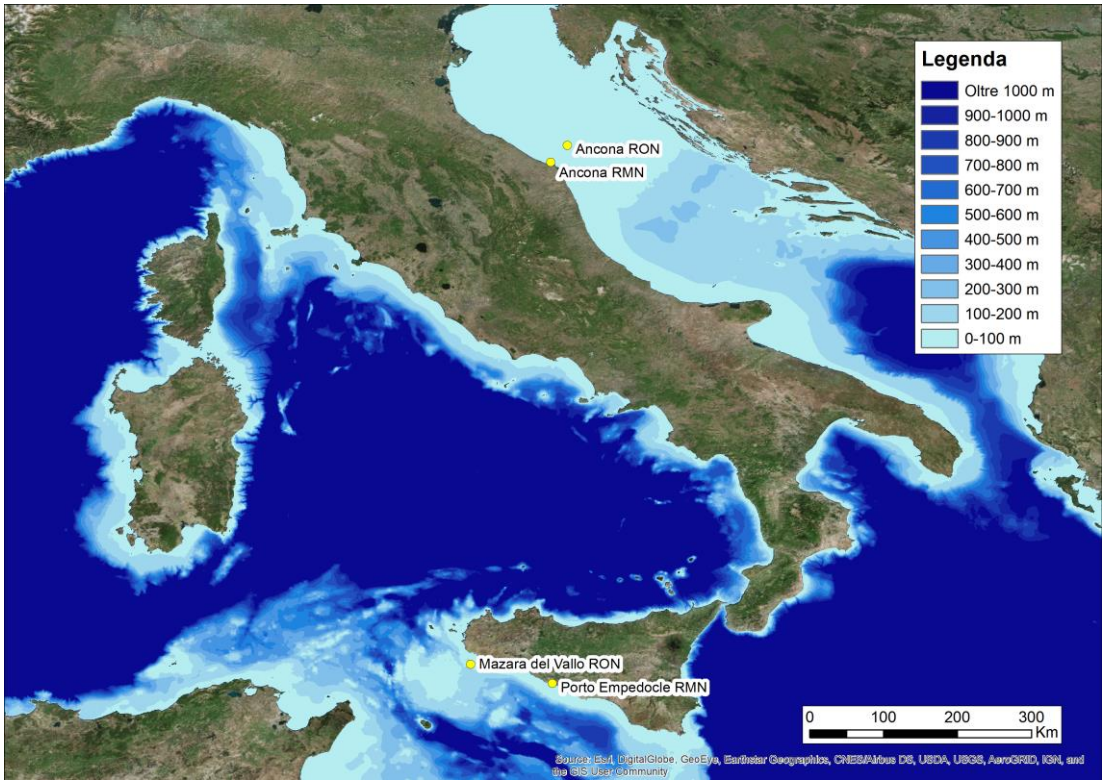


Figura I: batimetria dei mari italiani e posizioni delle stazioni di monitoraggio RMN e RON usate nella tesi.

Una volta raccolti i dati, l'analisi statistica è stata effettuata tramite il software R: usando i dati disponibili della velocità del vento e dell'altezza spettrale delle onde, i massimi mensili sono stati raccolti in un unico dataset e sono stati usati per ottenere, dopo la definizione dei parametri, due distribuzioni, scelte tra quelle più usate nella teoria del valore estremo, Gumbel e Weibull. La stima dei parametri delle distribuzioni è stata effettuata in due modi, sfruttando il pacchetto "fitdistrplus" in R (Delignette-Muller, et al. 2017): stima di massima verosimiglianza e di massima bontà di adattamento. La scelta di quale distribuzione restituisse i migliori valori di 50 e 100 anni di tempo di ritorno è stata basata sul buon adattamento delle distribuzioni teoriche ai dati empirici, osservando i valori della statistica di Kolmogorov-Smirnov e i Q-Q plot restituiti da R.

Dopo i primi risultati si è reso necessario, per una migliore stima dei valori di altezza spettrale d'onda, l'impiego di dataset troncati: sono stati effettuati due tentativi con massimi superiori a 3 e 3.5 metri.

Al fine di definire spettralmente le onde, la cui altezza è stata stimata in precedenza, si è proceduto a determinare il periodo di picco delle stesse: è stato adottato un approccio semplificato, che prevede un'ipotesi di somiglianza. Le onde stimate possiedono un periodo di picco dello stesso ordine di grandezza delle onde più grandi registrate dalla RON, vista la piccola differenza in termini di altezza d'onda spettrale fra di esse.

In tutte le analisi statistiche è emerso uno schema: i migliori risultati sono stati ottenuti con la distribuzione di Gumbel con parametri stimati con la massima bontà di adattamento.

Dopo aver ottenuto i parametri ambientali di riferimento per le simulazioni, si è proceduto con la scelta del tipo di struttura galleggiante e di turbina da modellizzare. L'adozione di turbine eoliche galleggianti diventa conveniente superati i 50 metri di profondità e, ad oggi, tre schemi principali sono stati sviluppati dall'industria (European Wind Energy Association 2013):

1. boa a palo (spar buoy): una boa cilindrica molto larga stabilizza la turbina usando una zavorra. Il centro di gravità è molto al di sotto della superficie del mare, da ciò deriva che le parti inferiori della boa sono pesanti e le parti superiori sono, di solito, vuote;
2. Tension Leg Platform (TLP): una struttura pesante è semi-sommersa e i cavi d'ancoraggio, posti in tensione, la connettono al fondo del mare, contribuendo alla stabilità;
3. piattaforma semi-sommergibile (semi-sub): combina i concetti principali delle soluzioni precedenti, con una struttura semi-sommergibile alla base della turbina per garantire la stabilità.

La scelta della struttura da modellizzare è stata effettuata secondo diversi criteri: grado di sviluppo della tecnologia ad oggi, tecnica costruttiva, adattabilità ai mari italiani e possibilità di realizzazione in Italia o in una nazione vicina appartenente all'Unione Europea. I primi tre fattori sono stati analizzati passando in rassegna i principali progetti che l'industria ad oggi ha sviluppato o è in procinto di sviluppare: Hywind (Statoil n.d.), spar buoy costruita da Statoil, WindFloat (Priciple Power n.d.), piattaforma semi-sommergibile sviluppata da Principle Power, e Pelastar (Glosten 2012), TLP realizzato da Glosten. Le possibilità di realizzazione nazionali o europee sono state affrontate confrontando le dimensioni strutturali dei progetti esistenti con le misure dei bacini di carenaggio dei cantieri navali nei porti italiani, francesi, spagnoli, croati, greci e maltesi.

Il design che si è dimostrato più adatto secondo i parametri fissati è stato la piattaforma semi-sommergibile di WindFloat, Figura II. Questo risulta essere pronto alla commercializzazione dopo anni di test estesi, la struttura semi-sommergibile può essere costruita e assemblata con la turbina in un bacino di carenaggio, il ridotto pescaggio consente l'utilizzo in mari poco profondi come l'Adriatico e, dopo la costruzione, la struttura completa viene trainata da

semplici rimorchiatori in posizione. Tuttavia, le imponenti dimensioni strutturali della base limitano i possibili siti di costruzione, fermo restando che, per il design scelto (Roddier, et al. 2011), la realizzazione resta ipotizzabile in Italia, Francia, Grecia e Malta.

Figura II: rappresentazione di una piattaforma semi-sommergibile del tipo WindFloat (Roddier, et al. 2011).

L'ultimo aspetto da analizzare per il modello numerico è stato l'ancoraggio: in generale un sistema di ancoraggio è richiesto da una piattaforma galleggiante per limitare i suoi movimenti sia in condizioni normali che estreme in mare. Questo consiste essenzialmente in cavi sospesi che connettono la piattaforma ad ancore o altre strutture sul fondo del mare, posizionate a una certa distanza.

I componenti principali da modellare sono quindi linee d'ormeggio e ancore: le prime sono costituite da catene d'acciaio o, più recentemente, fibre sintetiche, le quali compongono una catenaria che agisce tramite tensione per raggiungere l'obiettivo di stabilità. Queste devono trovare un compromesso tra forze agenti sulla struttura e resistenza necessaria a fronteggiare le condizioni del mare. Le ancore sono il componente che fissa l'ancoraggio al fondo del mare, fra i diversi tipi elaborati, per le simulazioni sono state considerate ancore tradizionali, che si basano sul loro peso e l'attrito per mantenere la posizione a scapito di uno stendimento delle linee d'ormeggio più ampio, e ancore a suzione che sono composte da un pilone spinto meccanicamente nel terreno che genera un differenziale di pressione per restare in posizione.

I sistemi modellati sono quattro e sono composti da sistemi generici di ancoraggio, senza progettazione specifica: catene d'acciaio con ancore tradizionali, combinazione di catene d'acciaio e fibre sintetiche con ancore tradizionali, catene d'acciaio con ancore a suzione e fibre sintetiche in tensione con ancore a suzione (taut mooring), Figura III.

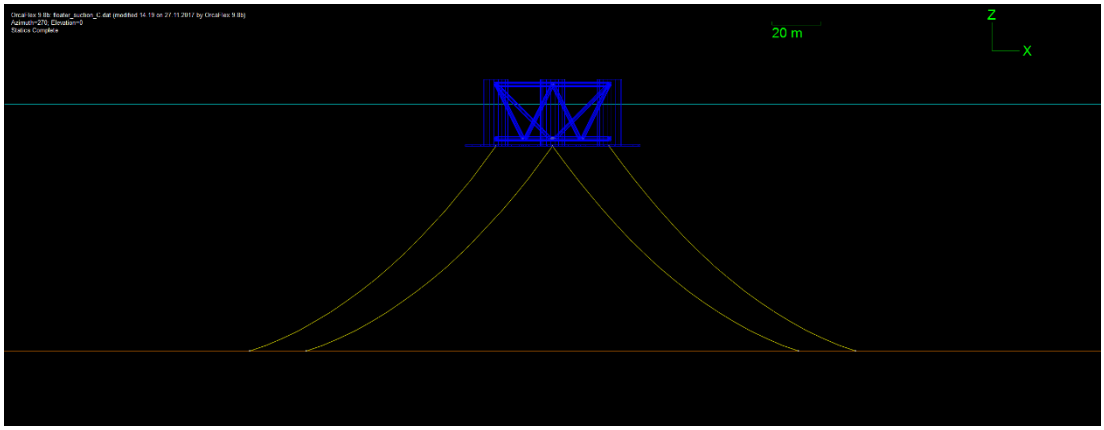


Figura III: esempio di modellazione in OrcaFlex di ancore a suzione con linee d'ormeggio costituite da catene d'acciaio.

Nella simulazione sono stati implementati i parametri ambientali, strutturali e degli ancoraggi che andranno a comporre sedici diversi scenari per le due aree di studio, simulando condizioni di 50 e 100 anni di tempo di ritorno. Le onde, rappresentate tramite lo spettro JONSWAP, e il vento sono state direzionate in modo tale da creare il peggior scenario possibile: perpendicolarmente a un lato della struttura e alla torre (non rappresentata graficamente) con il rotore, Figura IV.

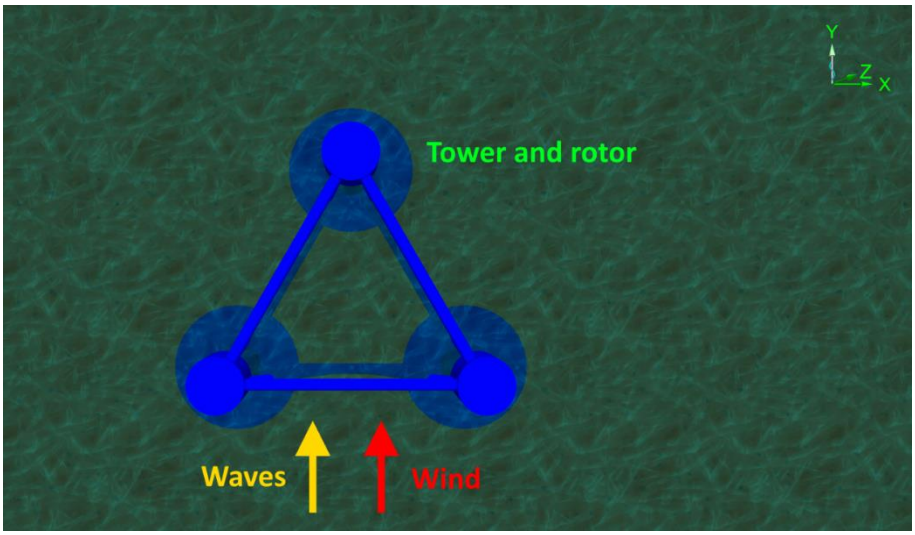


Figura IV: struttura galleggiante e direzione di vento e onde in OrcaFlex.

La simulazione in OrcaFlex è composta da due fasi: la prima è la fase statica, in cui la posizione di equilibrio del sistema è calcolata senza le forze delle onde, la seconda, la cui durata è stata fissata a tre ore, impone il carico derivato dal moto ondoso. Nella prima fase, è stato utile osservare le forze verticali sviluppatesi alle ancore: nulle per quanto riguarda le ancore tradizionali, già importanti per le ancore a suzione. È stato testato con successo un modo per ridurre quest'ultime aumentando lo stendimento orizzontale dell'ancoraggio.

La simulazione dinamica ha richiesto un approccio statistico per l'interpretazione dei risultati: è stato applicato il metodo Peak Over Threshold (POT) usando una distribuzione generalizzata di Pareto per la determinazione dei risultati di tensione nelle linee d'ancoraggio e per le forze verticali alle ancore per due tempeste di 3 e 6 ore. Per quanto riguarda la tensione nei materiali, il punto più stressato, sempre nei pressi della struttura galleggiante, è stato analizzato, concludendo che le forze generate rientravano sempre nei limiti di tolleranza dei materiali.
Per le forze verticali alle ancore, si sono ottenuti anche in questo caso forze nulle per le ancore tradizionali e cicli di carico e scarico per le ancore a suzione.
Dopo un'analisi dei risultati delle simulazioni, si può affermare che la differenza fra simulazioni che rappresentano condizioni di 50 e 100 anni di tempo di ritorno è minima, così come ottenere risultati simulando tempeste di 3 e 6 ore.
Le differenti soluzioni simulate presentano svantaggi e vantaggi, che vengono influenzati soprattutto dalla profondità:

- lunghezza delle linee d'ormeggio: all'aumentare della profondità si rendono necessarie linee più lunghe, le quali aumentano i costi;
- area occupata: all'aumentare della profondità aumenta l'area occupata dagli ancoraggi e quindi lo spazio di un ipotetico impianto costituito da alcune turbine, questo potrebbe causare problemi ambientali per i danni causati al fondale e alle aree di pesca;
- tensione: soprattutto nelle soluzioni con ancore a suzione, all'aumentare della profondità la tensione nelle linee d'ormeggio aumenta, questo nella realtà potrebbe richiedere materiali più resistenti e costosi;
- forze verticali alle ancore: mentre nelle ancore tradizionali a qualsiasi profondità si devono evitare forze verticali che potrebbero provocare un sollevamento, nelle ancore a suzione all'aumentare della profondità queste aumentano, richiedendo un sistema capace di contrastarle, quindi più costoso.

Alla luce degli aspetti analizzati, è stato possibile suggerire una soluzione per l'ancoraggio delle strutture galleggianti nelle due aree di studio: per il mare Adriatico, considerando i 100 metri di profondità modellizzati, ancore a suzione con catene d'acciaio, per lo stretto di Sicilia, visti i 400 metri di profondità, ancore tradizionali con linee d'ancoraggio costituite da catene d'acciaio o una combinazione di catene d'acciaio e fibre sintetiche.
In conclusione, nonostante le semplificazioni adottate, il modello numerico è stato capace di indicare una possibile soluzione per l'ancoraggio di turbine eoliche galleggianti nei mari italiani e di esplorare alcuni aspetti ad esso connessi come la ricerca di parametri di input, la scelta del design più adatto alle esigenze italiane e il confronto tra due diverse località.
Aspetti su cui precisazioni vengono richieste sono: una migliore modellazione ambientale comprendente correnti e materiali del fondo del mare, diversi approcci statistici per ottenere

i valori di progetto di altezza spettrale d'onda e velocità del vento, esplorare la possibilità di risonanza strutturale, elaborare un modello per la precisa modellazione del galleggiamento della struttura e un'analisi economica delle soluzioni scelte.

# Table of contents

# List of figures

# List of tables

# Chapter 1
# Introduction

## 1.1 Background

The principal sources of energy in most part of the world are non-renewable resources like oil, coal, natural gas and nuclear power.
However, these resources present disadvantages and critical issues: burning fossil fuels produces greenhouse gases and other pollutants harmful to the environment and these sources are subjected to limitations and price volatility. Nuclear power is not free from serious problem too: accidental radioactive leaks, nuclear proliferation and safe storage of wastes are only few challenges to be considered.
On the other hand, renewable sources, like wind, have a great potential and great advantages: they are virtually inexhaustible, they produce power without the pollutant emissions and they are freely available in every part of the world. This is greatly in accord to the global goal of reducing greenhouse gas emission, following international agreements, like the Paris one (UNFCCC 2016) or the European Union Renewable Energy directive (European Union 2014). However, renewable sources present some disadvantages for power production like intermittency and predictability.
In recent years, the installations of wind farms are growing not only on the main land but offshore too with a series of advantages:

- the turbine's size is not limited by the existing infrastructure in the manufacturing process when it can be assembled near the shores;
- large sea areas are available, it means that the installations do not cause land consumption or soil degradation;
- the wind generally blows more strongly and steadily over the sea surface, meaning a higher and more constant power production;
- the visual impact and the noise pollution can be eliminated with the turbines' installation at a sufficient distance from the coast line.

However, the previous factors are balanced with some issues:

- the turbines must withstand not only the wind load but they must also resist other environmental challenges like waves and currents, resulting in an increased design complexity and the cost is also affected;
- the turbines have to be marinized and the support structure must be designed, installed and, in the future, decommissioned;
- the offshore wind farms are harder to access than the ones on land, rising the maintenance challenges and costs.

Before 2017, all commercial offshore wind farms are placed within 50 meters of sea depth, connected to the sea bed with structure like monopiles and jackets. These solutions are not economically profitable in deeper waters, where floating structures take the lead: in recent years, the research has been focused in developing the concept of floating wind turbines farms, unlocking the potential of wind in open sea and exploiting the oil and gas industries' experience in terms of mooring and floating structures' design.

The technical realization and profitability of floating structures has been demonstrated by oil and gas industries with long-term floating structures. On the other hand, the development of floating wind turbines designs, capable of conquering a part of the energy market, requires extensive analysis. In the offshore environment, in addiction to wind load, new behaviours must be considered: hydrodynamic loads are the most evident, debris, ice and marine growth build-up must be covered too. The analysis has to account for the coupled motion of the floater and the turbine and for the mooring systems.

2017 has been a turning point: the world's first floating offshore farm began electricity production near the Scottish shores in October. The project is known as "Hywind Scotland", developed and constructed by Statoil in Norway and towed during summer off Aberdeenshire coast (Statoil n.d.), Figure 1.1. It consists of five turbines floating over the deep waters of the North Sea, moored to the sea floor and connected to the Scottish electricity grid through a submarine cable.

Figure 1.1: Hywind Scotland (Statoil n.d.).

The Italian environment nowadays lacks future or potential project of the Hywind-kind even if the potential, that the seas surrounding the Italian peninsula offer, is great. This, coupled with the reduced visual impact (which is and always has been the main opposition for wind turbines' installation in Italy), could lead to the creation of a new and renewable power source, with economical and occupational advantages.

## 1.2 Objectives and procedures

The main goal of the present master thesis work is to analyse and to find a solution for a mooring system connected to a floating wind turbine structure in the Italian seas.
A simplified 3D numerical model of the floater, the mooring and the environment will be developed and subjected to simulations of the combined loads of wind and waves in open sea.
The purpose of the study is to find a preliminary mooring solution for a hypothetical project: a simplified simulation with enough accuracy to provide a clear direction in the design of the structure's position keeping.
This process will be realized by implementing in the simulated environment the present-day technologies for the wind turbine structure, the mooring lines and the anchors. In this way, the results from the simulations will be judged considering several factors: wire length, mooring footprint, tension in the lines, forces at the anchors and their interactions.
The numerical model will be developed using the commercial software OrcaFlex, a fully 3D, nonlinear, time-domain, finite element program, capable of dealing with a wide range of offshore applications, like floating wind turbines and their moorings.
In the process of achieving the main target, several objectives are set:

- underlying the mooring difference between two locations with different sea depth, wind speed and wave height;

- finding the environmental design parameters concerning wind speed and wave height with the application of extreme value statistic theory to dataset of real recordings in the selected areas;
- identifying the most suitable floating wind turbine concept, with respect to characteristics of the Italian seas;
- exploring the possibility for the realization in Italy of the chosen concept from the inception to the construction phase.

The thesis, after the present introduction, is divided in four main chapters, followed by the conclusions, and their general subjects are described below.

In Chapter 2 is presented the process to obtain the environmental design parameters, for the selected locations of the study in the Mediterranean Sea: the Adriatic Sea near Ancona and the part of the Strait of Sicily, near the southern shores of the island. First, descriptions are given of the sources of the data for sea depth, wind speed and wave height. Hereafter, for the last two parameters, the statistical analysis, in which the theory of the extreme values is applied with the help of the statistical software R, is extensively explained: procedure, used distributions and selection of the result. In the end, results and comments are given.

At the beginning of Chapter 3, a general overview of the Italian power production in given along with the potential of the realization of floating farms. After that, a presentation of the existing solutions of floating structures is shown, pointing out the characteristics of the most prominent ones. In the end, the choice of the structure to be modelled is made, considering the compatibility with the Italian seas and the potential construction in an Italian shipyard.

In Chapter 4, the theory behind the numerical model is explained: line types and their characteristics, action of the forces, design and spread. The real mooring hardware to be modelled is presented too: chains, synthetic ropes, anchors and suction anchors.

In Chapter 5, the results and the theory previously presented come together in the actual model and its results. The way in which the software represents the reality, the structure and the mooring parts is explained at the beginning. Follow the static and the dynamic simulations: tension in the wires and forces at the anchors are examined and results are produced. In the end, looking at the previous steps, comparisons and discussions among different locations and simulations are made, with the purpose to find the most suitable mooring solutions.

The final discussion in the conclusions (Chapter 6) leads to considerations with respect to the original objectives, related to the actual results. Suggestions for further works, based on the issues and limitations that were highlighted during the investigations, are also described.

# Chapter 2
# Data collection and statistical analysis

In this chapter will be provided a description of the source of the data used for the mooring modelling, the reason for choosing two different locations, a statistical analysis of the wind and waves condition and a discussion of the results.
The aim of this process is to find the extreme (design) wave and wind condition both for Ancona and southern Sicily, to proceed with the actual numerical modelling. A reliable data source for wind speed and wave height has been searched and found in the Italian agency ISPRA (Istituto Superiore per la Protezione e la Ricerca Ambientale), which runs an extensive monitoring network across the Italian peninsula and the seas around it. To compare different conditions, two different locations (considering water depth, wind speed and sea conditions) have been chosen.
The results are obtained through statistical models which contain the datasets, using a comparison between two different distributions (Gumbel and Weibull) and estimating the wave height and the wind speed for two return periods (50 and 100 years). A way to improve the extreme results for wave height has been taken, cutting the low values of the datasets. Along with the design waves' height, a complete spectral description of the design wave has been provided with the peak periods associated. After that, a comparison of the best results obtained has been made, to underline the differences between two different locations with different conditions. In the end, a discussion regarding other possible approaches to the statistical analysis has been proposed.

## 2.1 Data origin and description

Several data have been searched and used, concerning wind speed, wave height and water depth. For the first two variables, the ISPRA network has been used. It is a public authority, focused on research on environmental themes, and it depends from the Ministry of the Environment and Protection of Land and Sea of Italy (Italian: Ministero dell'Ambiente e della

Tutela del Territorio e del Mare, also known as MATTM) (Istituto Superiore per la Protezione e la Ricerca Ambientale n.d.).
This agency operates several monitoring networks, two of them has been used in this work: the Rete Mareografica Nazionale (National Sea Network, also known as RMN), for the wind speed, and the Rete Ondametrica Nazionale (National Wave Network, also known as RON), for the wave height.
To choose the different locations a measure of the sea depth was needed, this data has been retrieved using ESRI GIS software ArcMap and geographical data available from the National Geoportal. This is a portal, run by the MATTM, in which is available the official Italian cartography for free, following the European normative INSPIRE (Infrastructure for Spatial Information in Europe) (Geoportale Nazionale, INSPIRE n.d.).

### 2.1.1 Rete Mareografica Nazionale

To get uniform measurements, the RMN is well distributed in the Italian territory, using a network of 36 stations, mainly located in several ports (Rete Mareografica Nazionale (2014-2017) n.d.). These stations perform many measurements concerning sea and atmospheric parameters:

- sea level [m];
- water temperature [Celsius];
- air temperature [Celsius];
- humidity [%];
- atmospheric pressure [hPa];
- wind direction [grades north];
- wind speed [m/s].

The stations memorize and manage the data collected and they send them, using cellular network (UMTS), in real-time, to ISRPA headquarters in Rome (Rete Mareografica Nazionale (2014-2017) n.d.).
For this work have been taken into account the wind speed and direction, considering the available data from August 1998 to August 2017. To assemble the dataset two sources have been considered: for data from 1998 to 2014 the older version of the archive (Rete Mareografica Nazionale (1998-2014) n.d.) and for the most recent data the new online portal Linked ISPRA (Rete Mareografica Nazionale (2014-2017) n.d.), from which data can be retrieved using a SPARQL code. For the codes used, refer to Appendix A.
Two stations are available for data collection in the selected areas: Ancona, in the harbour in the Adriatic Sea (LAT: 43° 37’ 29.16” LONG: 13° 30’ 23.46 “ (RMN Ancona n.d.)) and Porto

Empedocle, in the southern shores of Sicily (LAT: 37° 17' 8.72" LONG: 13° 31' 36.64" (RMN Porto Empedocle n.d.)).

Considering Ancona, the dataset available contains measurements starting from June 1999 to August 2017, for the year coverage refer to Figure 2.1. Wind data are measured by the station in a fixed interval, from June 1999 to April 19th, 2011 hourly, from April 20th, 2011 to August 2017 every ten minutes.

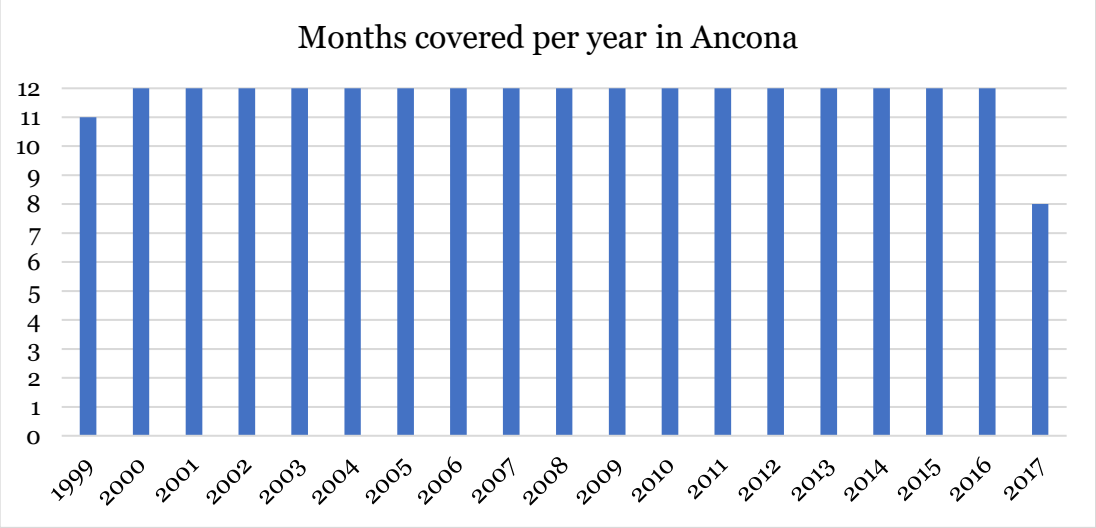


Figure 2.1: histogram of the data covered months in Ancona (RMN).

Considering Porto Empedocle, the data available start from August 1998 to August 2017, for the year coverage refer to Figure 2.2. The frequency used by the measurements follows the same pattern of Ancona.

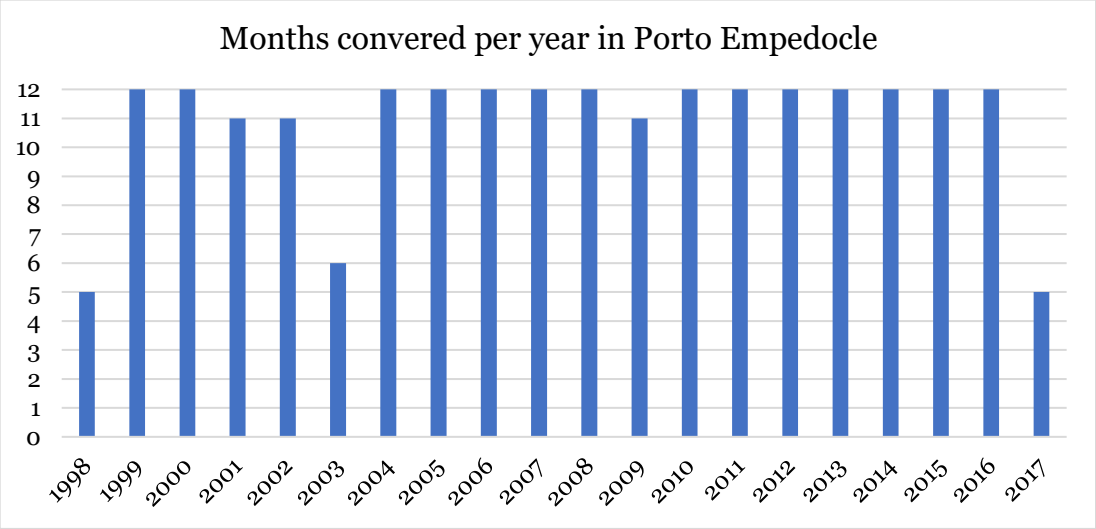


Figure 2.2: histogram of the data covered months in Porto Empedocle (RMN).

The dataset for both location is not uniform, in fact, it presents holes in the measurements that can last for months due to damage to the instruments or renovation of the equipment. Since

none of the available sources tells in detail the cause of the non-uniformity of the datasets and since it does not follow a clear temporal distribution, a decision has been taken to not consider months with a ratio of data measured over data expected less than 75%. For the monthly coverage and the ratio value, refer to Appendix B.

### 2.1.2 Rete Ondametrica Nazionale

The system used to monitor the wave condition in the Italian seas is the RON. It uses fifteen oceanographic buoys in fixed points to gather data that will be collected to describe the sea state. The observations derive from the study of the sea surface, performed in regular intervals according to the World Meteorological Organization guidelines (Rete Ondametrica Nazionale n.d.). The data are sent from the buoys to the mainland in real-time.
The buoy measurements include:

- spectral significant wave height [m];
- mean wave period [s];
- peak wave period [s];
- mean wave direction [grades north].

The RON has been renewed three time since its inception in 1989 and right now (2017) the network is not operational: the available data start from July 1989 to November 2014. For this work is considered the spectral wave height and the measurements are collected from the Linked ISPRA portal (Rete Ondametrica Nazionale n.d.). For the codes used, refer to Appendix A.
Two buoys are available for retrieving data in the location studied: Ancona, in the Adriatic Sea (LAT: 43° 49’ 55.2” LONG: 13° 42’ 36” (RON Ancona n.d.)) and Mazara del Vallo, in the Mediterranean Sea south of Sicily (LAT: 37° 31’ 4.8” LONG: 12° 31’ 58.799” ( (RON Mazara del Vallo n.d.)).
Considering Ancona, the dataset available contains measurements starting from March 1999 to November 2014, for the monthly coverage refer to Figure 2.3. Waves data are measured by the station in a fixed interval, from March 1999 to August 2002 every three hours, from September 2002 to November 2014 every half an hour.

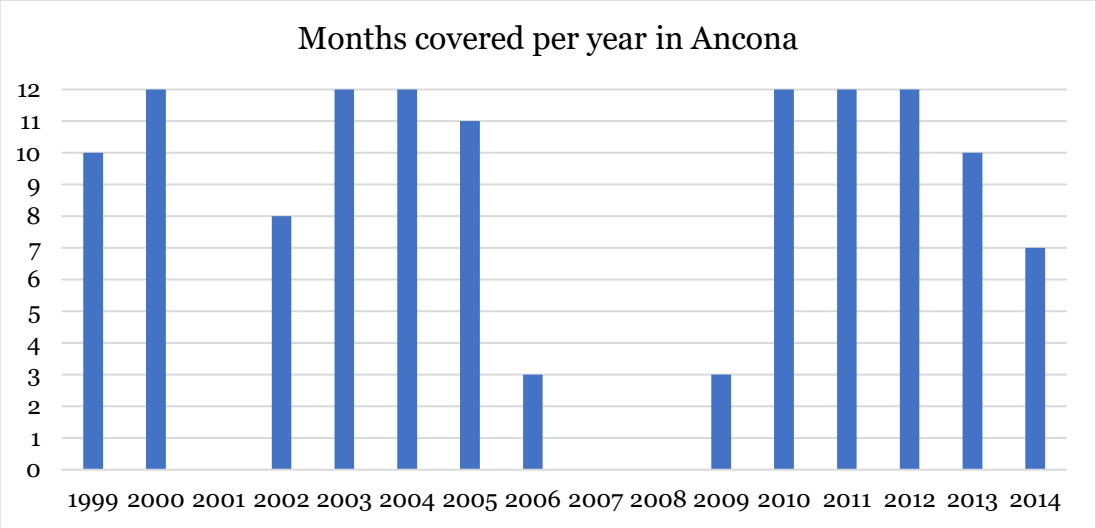


Figure 2.3: histogram of the data covered months in Ancona (RON).

Considering Mazara del Vallo, the data available start from July 1989 to October 2014, for the monthly coverage refer to Figure 2.4. The frequency used by the measurements changes from every three hours to every half an hour in April 2002.

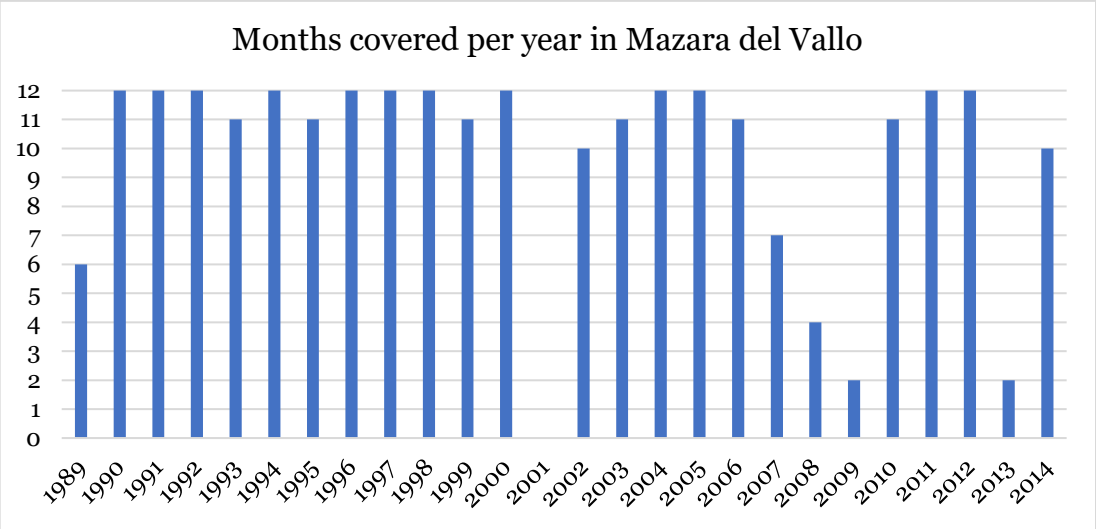


Figure 2.4: histogram of the data covered months in Mazara del vallo (RON).

Like for the RMN the dataset for both location is not uniform, in this case the holes in the data can last for years due to renovation of the network done three times (Rete Ondametrica Nazionale n.d.). The same decision as applied to RMN has been taken for RON too: the months covered with less than 75% of the measurements expected have not been considered, with one exception. Due to the buoys' position in open sea, these instruments often present malfunctions caused by the extreme weather conditions: and since that, in the months with a coverage less than 75% often the maxima are extreme data (waves higher than 3 meters), the assumption that the measurements disruptions were caused by the weather conditions has

been made. In this case, the hypothesis led to consider, in the final datasets, maxima retrieved from months with a coverage less than 75%, taken as significant data measured before the interruption due to extreme conditions, in case these were the highest values for those months. Data without this characteristic have not been considered.

### 2.1.3 Geoportale Nazionale

One of the parameters needed to model the mooring system is the sea depth, obtained through GIS software (ESRI ArcMap), using data from the National Geoportal (Italian: Geoportale Nazionale). The National Geoportal is a geographic database, in which data are freely available following the European normative INSPIRE (Geoportale Nazionale, INSPIRE n.d.). This portal is an infrastructure that allows users to access easily information about the environment and the Italian territory. The cartography is provided with a complete set of metadata concerning the contents of the data itself and this information is uniform through the portal: the data are provided by the Public Administration and the MATTM.
In the current work has been used a dataset concerning the bathymetry of the Italian sea (Geoportale Nazionale, Bathymetry 2009): this dataset allows the user to know the exact sea depth in a certain location, using a very frequent division of the territory in polygons in which the depth is constant. A representation of the cartography involved is given in Figure 2.5.

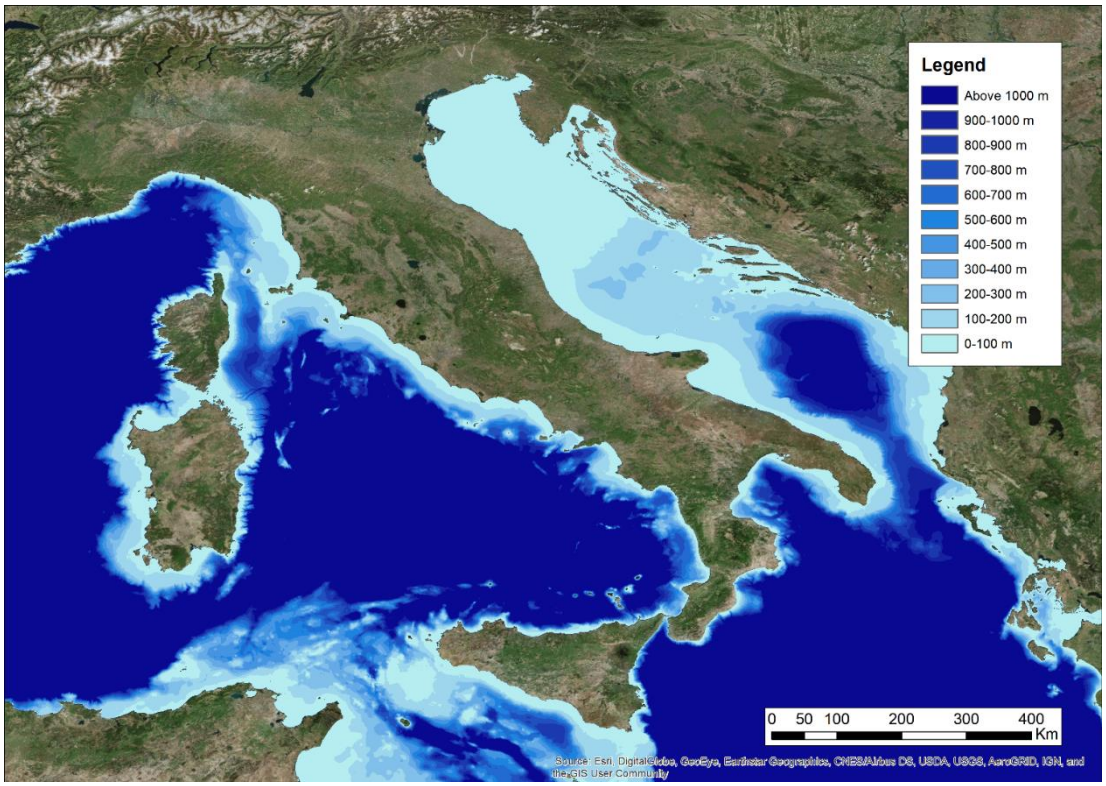


Figure 2.5: Italian seas bathymetry (Geoportale Nazionale, Bathymetry 2009).

## 2.1.4 Selection of locations

The locations for a possible floating wind farm have been chosen following a criterion that would allow to make a comparison between different conditions concerning the sea depth, the wind speed and the wave height. To model and compare those differences, a reliable data source is needed too. Two locations emerged among the others for data availability (presence of both RMN and RON with extensive recorded data) and difference conditions of the sea bed: the part of the Adriatic Sea near Ancona's shores and the portion of the Mediterranean Sea close to the southern shores of Sicily. Considering the first place and referring to Figure 2.5, it can be observed that the seabed is never deeper than 100 meters from the sea surface. This and the different geography surrounding the sea imply different conditions for the considered variables than the southern part of Sicily, in which the bathymetry is higher and the surrounding conditions different. Those decisions have been taken considering a limit for a floating wind turbine mooring set to 1000 meters of depth.
In Figure 2.6 and Figure 2.7 can be observed with a greater level of detail those differences and the locations of the monitoring networks used to develop this work.

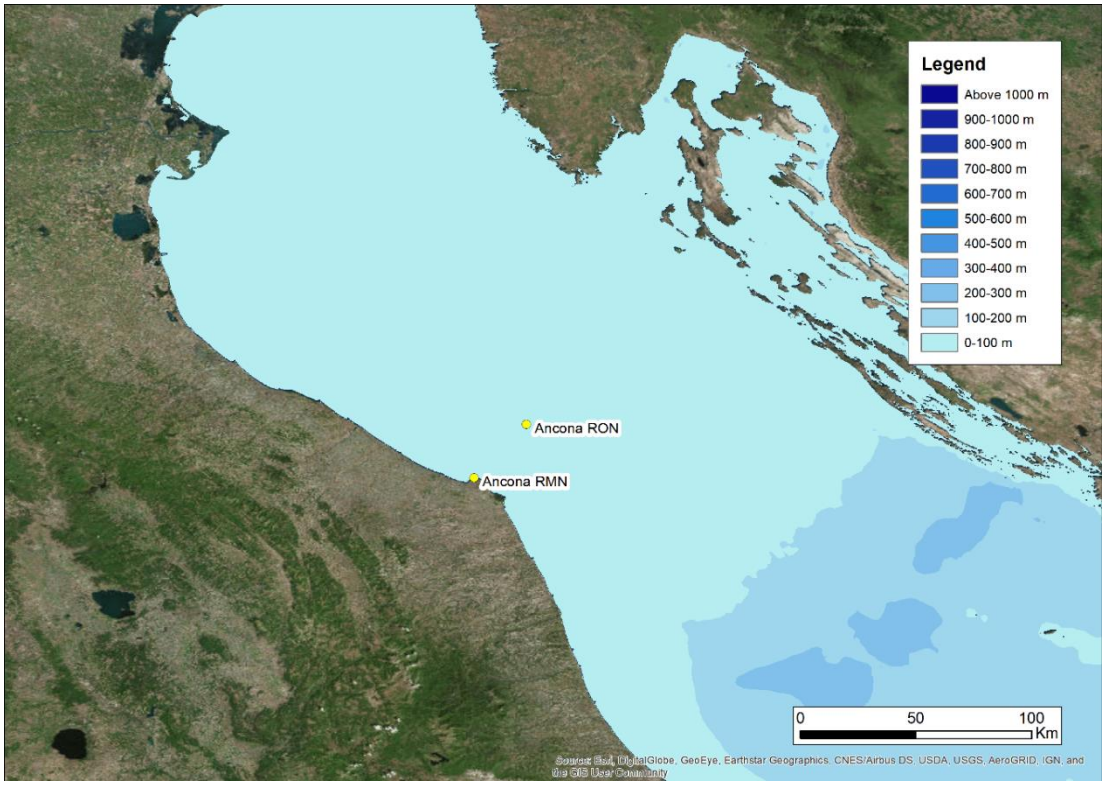


Figure 2.6: bathymetry and positions of the RMN and RON networks for Ancona.

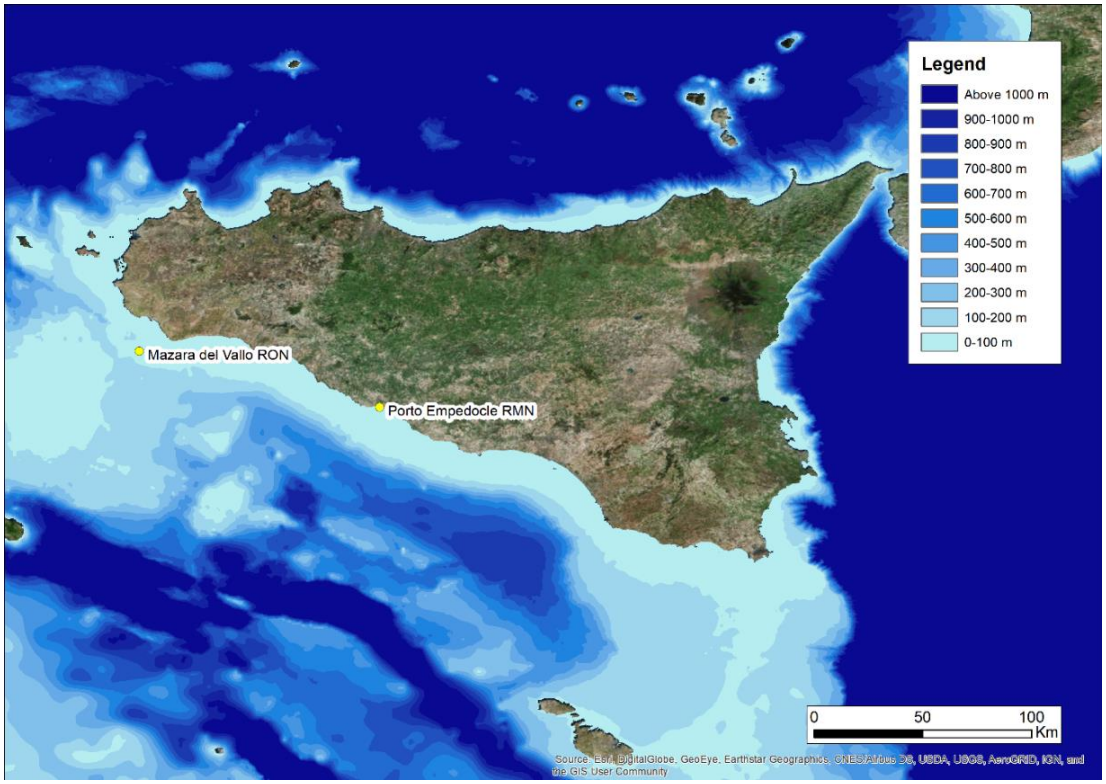


Figure 2.7: bathymetry and positions of the RMN and RON networks for Sicily.

## 2.2 Statistical analysis

Once gathered the data, a statistical analysis has been performed to obtain the extreme values for wind speed and wave height, which will be used for the design of the mooring systems. Using the data available for both variables, the maximum values recorded has been assembled on a monthly base, using the procedure explained in the previous paragraphs. Then, those maxima have been used to obtain, after the parameter's definition, two different distributions, chosen among the most used in the extreme value theory (Johnson, Kotz and Balakrishnan 1994), Gumbel and Weibull distributions for waves and Gumbel for wind, to get the extreme values for two distinct return periods: 50 and 100 years. The choice for the best results has been based upon the goodness of fit (GOF) of the theoretical distributions obtained to the measured data.

Following the results, to obtain better estimations of the extreme values, two different datasets have been considered to get the wave height: two attempts with the maxima above 3 and 3.5 meters.

A simplified approach has been applied to the determination of the waves' peak period: since the estimation of the waves' heights did not provide information about the peak period, a simplified criterion has been used: the peak period chosen for the return period of the design

waves corresponds to a value with the same magnitude as for the ones recorded for the highest waves at the locations of the study. Hereby, are considered only wind waves, not taking into account swell seas. For the present study of anchor design, it is considered that this simplification represents a good approximation to the combined wave height/wave period design criteria.

### 2.2.1 Objective and procedures

Waves and wind speed are phenomena of a stochastic nature and to get extreme values, needed for this work, a statistical method is needed. “Extreme” means very rare in terms of probability or, in other terms, with a high value of return period. The return period (T) of an event is the mean time between the occurrence of two events with the same magnitude and it can be defined considering the probability (p) of exceedance:

$$T = \frac{1}{p} \tag{2.1}$$

Since that extreme values are required, the maximum values recorded every month both for wind speed and wave height have been considered as series of continuous variables and it has been implemented in a new dataset. Every observation (x) in the new datasets, using the software R, has been used to get the Gumbel and Weibull distributions, after the parameters estimations, performed with the same software.

To obtain the required values, given that the cumulative distribution function of a real-valued random variable X is the function given by:

$$F(x) = P(X \leq x) \tag{2.2}$$

Where the right-hand side represents the probability that the random variable X takes on a value less than or equal to x and, recalling the definition of return period ( 2.1 ), the x value with a defined return period ($x_T$) can be derived:

$$\frac{1}{T} = P(X \geq x_T) = 1 - P(X \leq x) = 1 - F(x_T) \tag{2.3}$$

$$F(x_T) = \frac{T-1}{T} \tag{2.4}$$

The R script is based on the previous definition to find the wind speed and the wave height related to the different return periods. It exploits the R package “fitdistrplus” “to help the fit of a parametric distribution to non-censored or censored data” (Delignette-Muller, et al. 2017), along with the distribution parameters estimation, and to give an idea of the goodness of fit of the chosen distribution to the used data.

In the end, the choice of the distribution with the best fit, that will give the best prediction, is made with a comparison between the values obtained by the Kolmogorov-Smirnov statistics (looking at the lower ones) and the observation of the Q-Q plot (quantile-quantile plot), concerning the extreme values.

The R code gives also a graphical comparison between the theoretical and the empirical probability density functions and the theoretical and the empirical cumulative distribution functions with a representation of the P-P plot too. For the codes used, refer to Appendix C, in which the description of the script's steps is introduced with the symbol #.

### 2.2.2 Gumbel distribution

In statistics, the Gumbel distribution (Generalized Extreme Value Distribution Type-I) is used to represent the trend of the maximum (or the minimum) of a number of observation of various distributions (Johnson, Kotz and Balakrishnan 1994).
This distribution might be used to represent the distribution of the maximum level of a variable in many environmental fields like hydrology (river's levels) and geotechnics (extreme earthquakes), in which predictions are useful.
In this work, the Gumbel distribution (concerning the maximum) is used to obtain the values of wind speed and wave height, considering a return period of 50 and 100 years.
It is a two-parameters distribution and the following notation has been used:

- μ: location parameter;
- σ: scale parameter.

Probability density function:

$$f(x) = \frac{1}{\sigma} exp\left(-\frac{x-\mu}{\sigma}\right) exp\left[-exp\left(-\frac{x-\mu}{\sigma}\right)\right], x \in \mathbb{R}, \mu \in \mathbb{R}, \sigma > 0 \quad (2.5)$$

Cumulative distribution function:

$$F(x) = exp\left[-exp\left(-\frac{x-\mu}{\sigma}\right)\right], x \in \mathbb{R}, \mu \in \mathbb{R}, \sigma > 0 \quad (2.6)$$

Quantile function for probability p:

$$Q(p) = \mu - \sigma\, ln[-ln(p)], 0 \leq p < 1, \mu \in \mathbb{R}, \sigma > 0 \quad (2.7)$$

### 2.2.3 Weibull distribution

In probability theory, the Weibull distribution (Generalized Extreme Value Distribution Type-III) is a continuous probability distribution and it is often used in reliability engineering, failure analysis and to represent extreme events.
In this work, the Weibull distribution is used to obtain the values of wave height, considering a return period of 50 and 100 years.
It is a three-parameters distribution and the following notation has been used:

- β: shape parameter;
- μ: location parameter;
- σ: scale parameter.

Frequently (like this case), the location parameter is not used, and the value for this parameter can be set to zero (Johnson, Kotz and Balakrishnan 1994). When this is the case, the probability density function equation reduces to the one of the two-parameter Weibull distribution.

Probability density function:

$$f(x) = \frac{\beta}{\sigma}\left(\frac{x}{\sigma}\right)^{\beta-1} exp\left[-\left(\frac{x}{\sigma}\right)^{\beta}\right], x \geq 0, \beta > 0, \sigma > 0 \quad (2.8)$$

Cumulative distribution function:

$$F(x) = 1 - exp\left[-\left(\frac{x}{\sigma}\right)^{\beta}\right], x \geq 0, \beta > 0, \sigma > 0 \quad (2.9)$$

Quantile function for probability p:

$$Q(p) = \sigma[-ln(1-p)]^{\frac{1}{\beta}}, 0 \leq p < 1, \beta > 0, \sigma > 0 \quad (2.10)$$

## 2.2.4 Estimation of the distribution parameters and goodness of fit choice

To estimate the distributions' parameters two ways have been taken: the maximum likelihood estimation (MLE) and the maximum goodness of fit (MGE). The first one to be performed is the MLE followed by the MGE, based on the Kolmogorov-Smirnov statistics, to see if an improvement in the fit would have been possible.

Maximum likelihood estimation is a method of estimating the parameters of a statistical distribution considering a given dataset, by finding the parameter values that maximize the likelihood of making the observations given the parameters. In general, the likelihood of a dataset is the probability to get the dataset itself, given the distribution model that contains the parameters to estimate: the objective is to get the highest likelihood possible. Putting this into formulas, the first step is to define the joint density function for the observations, considering θ as a vector of the parameters to estimate:

$$f(x_1, x_2, \dots, x_n|\theta) = f(x_1|\theta) \cdot f(x_2|\theta) \cdot \dots \cdot f(x_n|\theta) \quad (2.11)$$

In ( 2.11 ) the observations are considered as fixed values while θ can change freely, this function is called likelihood:

$$\mathcal{L}(\theta;\ x_1, x_2, \dots, x_n) = f(x_1, x_2, \dots, x_n|\theta) = \prod_{i=1}^{n} f(x_i|\theta) \quad (2.12)$$

The software package "fitdistrplus" works with the natural logarithm of the likelihood (Delignette-Muller, et al. 2017), the log-likelihood:

$$ln\,\mathcal{L}(\theta;\ x_1, x_2, \dots, x_n) = \sum_{i=1}^{n} ln\, f(x_i|\theta) \quad (2.13)$$

The MLE method estimates θ, maximizing the likelihood or the log-likelihood function.

The used package gives also a representation of the goodness of fit of the distribution with the estimated parameters, using a value of the Kolmogorov-Smirnov statistic. Considering the possibility of an improvement in the goodness of fit, the package also allows other ways to estimate the parameters like the maximum goodness of fit.

Maximum goodness of fit estimation consists in maximizing a goodness of fit statistics, in this case the Kolmogorov-Smirnov one. The Kolmogorov–Smirnov (KS) statistic quantifies a distance between the empirical distribution function of the datasets and the theoretical cumulative distribution function.

The KS statistics D can be written, considering $F_n(x)$ as the empirical distribution function as:

$$D = \sup_x |F_n(x) - F(x)| \qquad (2.14)$$

The MGE makes the term ( 2.14 ) to tend to zero. In this case too, a value of the resulting KS statistics is given by the software.

This value, looking at the lowest, along with the Q-Q plots, has been used to make a comparison between the different estimation methods and the different distributions. To choose the best fit to the wind and wave data: this pair can provide an assessment of the goodness of fit both numerical, concerning a distance, like in the KS statistic, and graphical, like in the Q-Q plot. For the explanation of the need of using both the GOF ways and the Q-Q plot details refer to 2.2.5.

### 2.2.5 Possible variations for better estimation of the waves extreme values

The decision of which distribution can represent better the datasets and give the best estimations concerning the extreme values, has been further considered, given the Q-Q plots provided by R. This led to regard a truncated dataset concerning the waves as a possible solution to improve the estimations, considering the weakness of the KS statistic into the tails of the distributions (Johnson, Kotz and Balakrishnan 1994).

Q-Q (quantile-quantile) plot is a probability plot, which is a graphical method for comparing two probability distributions by plotting their quantiles against each other (Johnson, Kotz and Balakrishnan 1994). Q-Q plots are commonly used to compare a dataset to a theoretical model. This can provide an assessment of the goodness of fit that is graphical, rather than reducing to a numerical summary, like when it is used a KS statistic (Johnson, Kotz and Balakrishnan 1994). In general, the basic idea is to compute the theoretically expected value for each data point based on the distribution in question. If the data indeed follow the assumed distribution, then the points on the Q-Q plot will fall approximately on a straight line.

The Q-Q plots with the complete datasets presented a deviation of the empirical quantiles from the theoretical ones concerning the highest values of the distributions, or, in other terms, the

ones required to model the extreme wave height values. To reduce this deviation two attempts have been made, considering two truncated datasets for every location with less data, concerning the lower values: the first one presents wave height data above 3 meters only and the second one performs a further data refinement considering data above 3.5 meters only.
The final decision of which distribution and which distribution's parameters are the best to fit the datasets has been made considering both the values of the KS statistics and the Q-Q plots, aiming to the best estimation possible.

### 2.2.6 Waves' peak period

The waves' datasets provide much information, including the peak period associated with the recordings (refer to 2.1.2). Since the estimated wave heights do not correspond to a measured wave with information about the period and frequency, an assumption of similarity has been made: the waves corresponding to the design heights have a peak period with the same magnitude as the ones recorded by the stations for the biggest waves. The assumption is supported by the fact that the difference between the biggest wave heights recorded and the estimated is a matter of centimetres and thus the design waves likely would follow a similar trend in terms of peak period.

## 2.3 Results

### 2.3.1 Wind

For the wind, the results show a clear pattern: the best values are obtained using the maximum goodness of fit in the estimation of the Gumbel distribution parameters; this led to choose the wind speed for a return period of 50 and 100 years obtained with MGE. The decision has been supported with both the value of Kolmogorov-Smirnov statistics and the Q-Q plot comparison.

#### *Ancona*

A total of 222 monthly maxima has been used in the analysis for Ancona: the distribution can be seen in Figure 2.8 with the help of a histogram. It denotes a large concentration of wind speed values in the range 10-15 m/s.

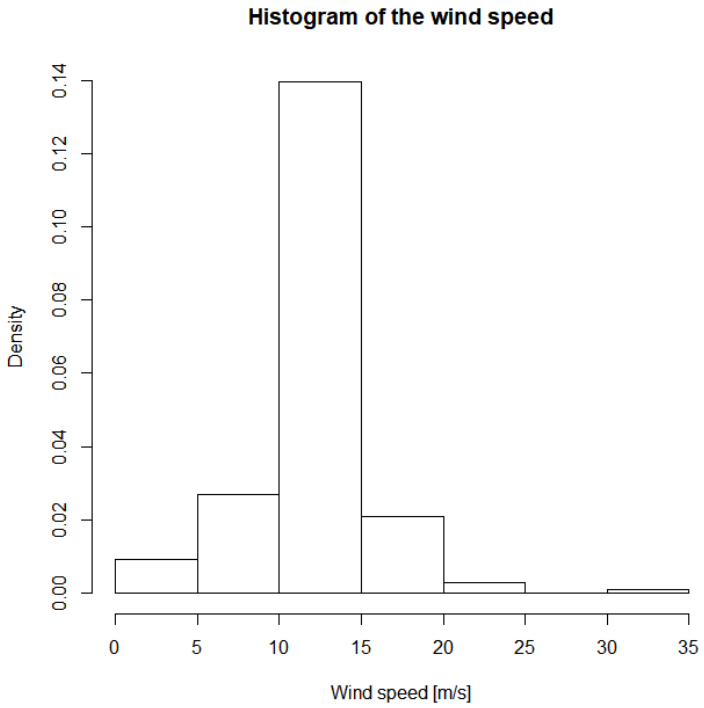


Figure 2.8: histogram of the maxima of the wind speed recorded in Ancona.

The analysis has been performed through an implementation of a Gumbel distribution in which the parameters has been estimated with MLE and MGE. The parameters, the associated KS statistics and the variables estimation have been collected in Table 2.1.

| | **MLE** | **MGE** |
|---|---|---|
| **μ** | 10.492468 | 11.1990706 |
| **σ** | 3.4121975 | 2.487064 |
| **KS statistic** | 0.1683476 | 0.08050747 |
| **Wind speed (T=50 years)** | 23.84481 m/s | 20.90345 m/s |
| **Wind speed (T=100 years)** | 26.23407 m/s | 22.63994 m/s |

Table 2.1: results for wind speed in Ancona.

The value of the KS statistics is better with MGE method, in fact this outcome led to prefer the results obtained with this computation.

A further comparison of the parameters has been done through the observation of the Q-Q plots obtained with the different methods. These graphs, along with a representation of the PDFs and CDFs (empirical and theoretical) and the P-P plots, are collected in Figure 2.9 and Figure 2.10.

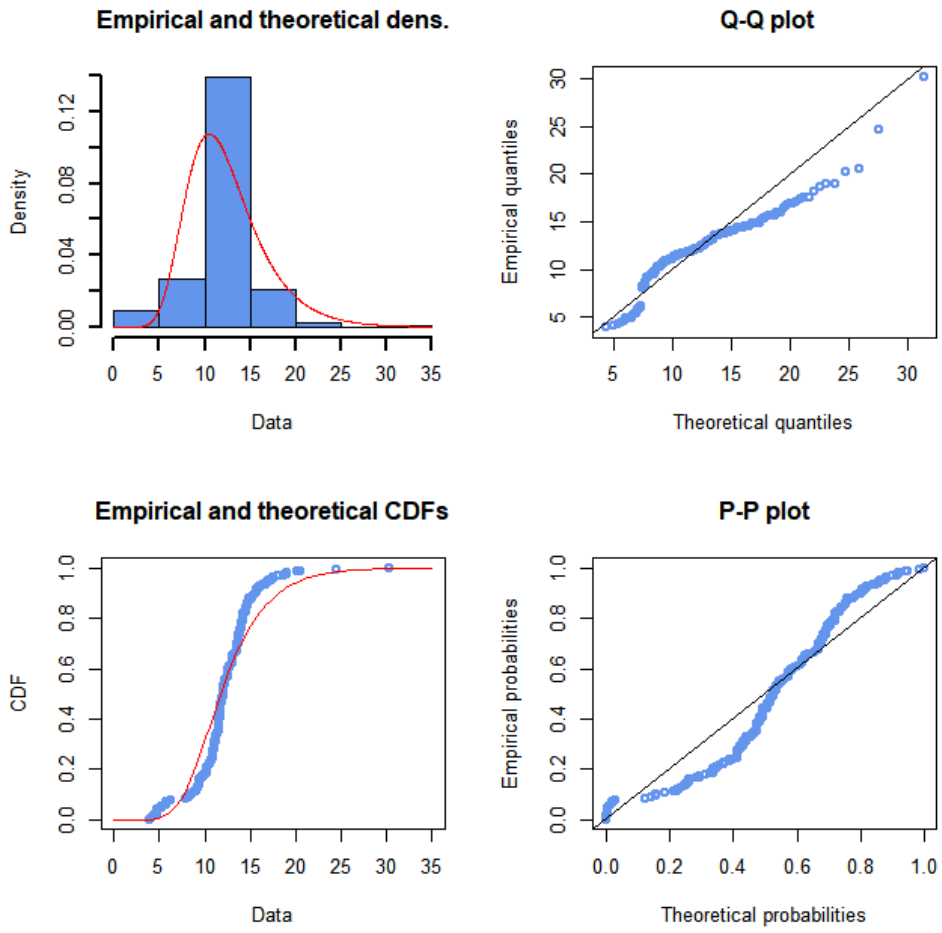


Figure 2.9: PDF, CDF, Q-Q plot and P-P plot for wind speed in Ancona (MLE), observations in light blue.

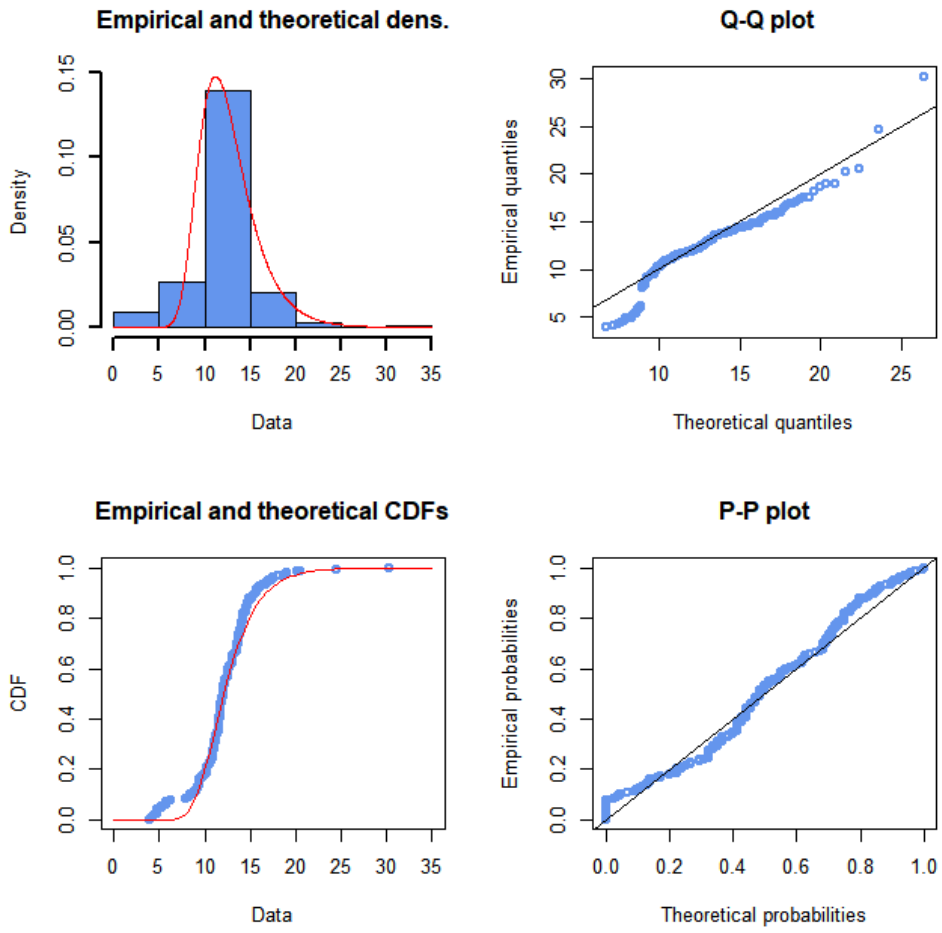


Figure 2.10: PDF, CDF, Q-Q plot and P-P plot for wind speed in Ancona (MGE), observations in light blue.

The Q-Q plots comparison confirms the first choice: in the MLE method the deviation between empirical and theoretical quantiles, in the part of the graph concerning the results, is bigger than in the MGE method. The values chosen are the ones obtained through the Gumbel distribution with parameters estimated with maximum goodness of fit.

## *Porto Empedocle*

A total of 207 monthly maxima has been used in the analysis for Ancona: the distribution can be seen in Figure 2.11 with the help of a histogram. It denotes a large concentration of wind speed values in the range 10-25 m/s, with the presence of extreme values above 40 m/s (144 km/h), which have been largely recorded during spring 2001.

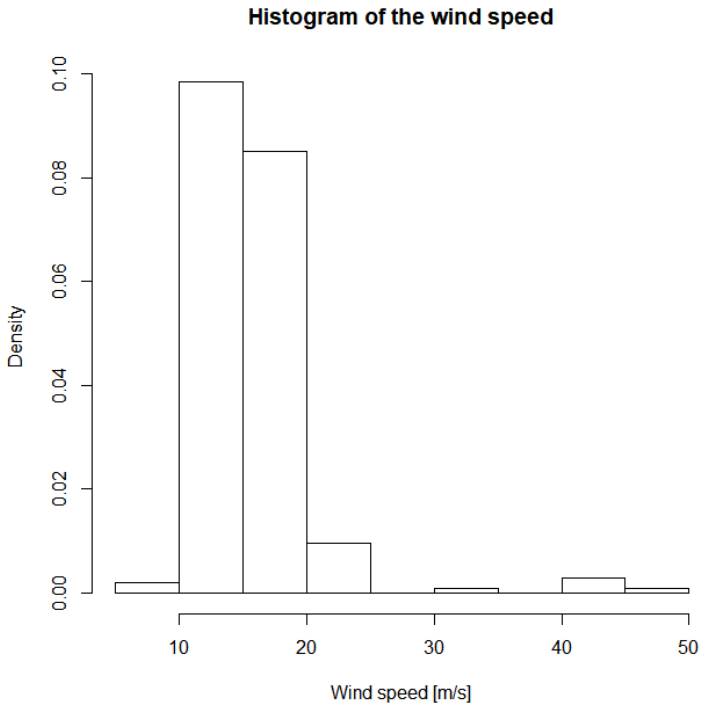


Figure 2.11: histogram of the maxima of the wind speed recorded in Porto Empedocle.

The analysis has been performed with the same procedure of Ancona. The parameters, the associated KS statistics and the variables estimation have been collected in Table 2.2.

| | **MLE** | **MGE** |
|---|---|---|
| **μ** | 14.406073 | 14.485472 |
| **σ** | 2.502472 | 2.031465 |
| **KS statistic** | 0.0829856 | 0.04413119 |
| **Wind speed (T=50 years)** | 24.17056 m/s | 22.41213 m/s |
| **Wind speed (T=100 years)** | 25.91782 m/s | 23.83052 m/s |

Table 2.2: results for wind speed in Porto Empedocle.

The value of the KS statistics is better with MGE method, in fact this outcome led to prefer the results obtained with this computation. The same graphical comparison performed with Ancona results has been made and the associated graphs can be seen in Figure 2.12 and Figure 2.13.

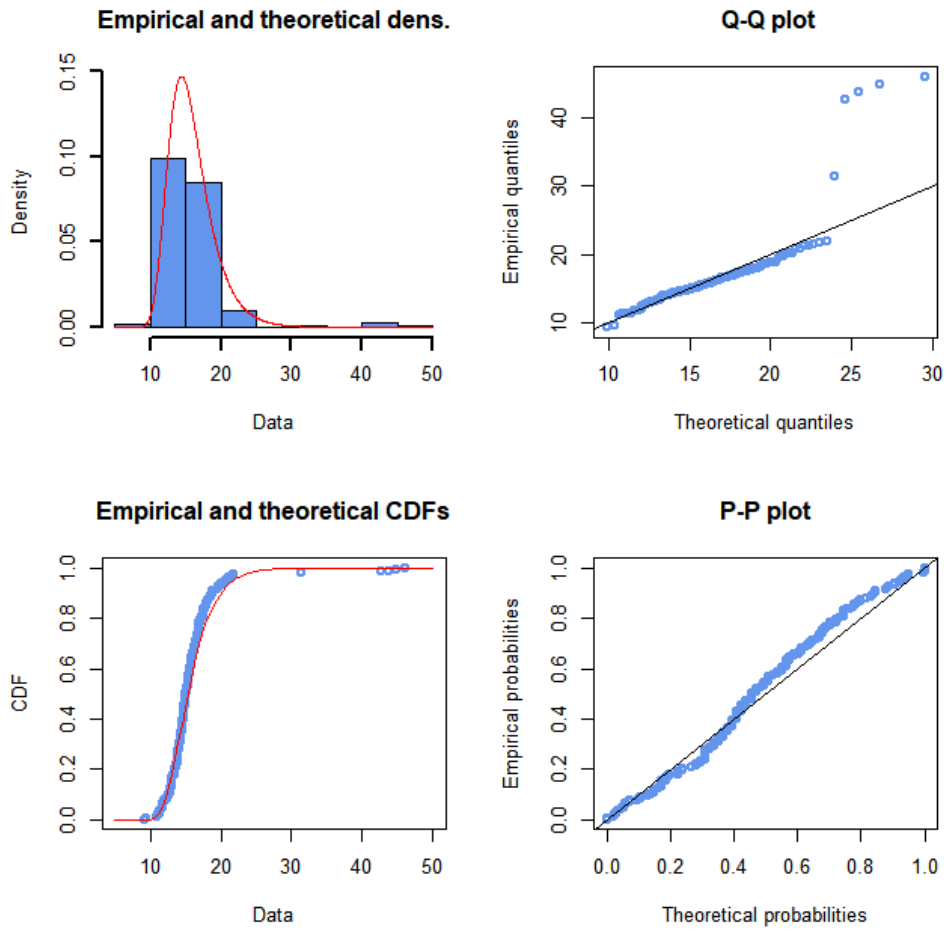


Figure 2.12: PDF, CDF, Q-Q plot and P-P plot for wind speed in Porto Empedocle (MLE), observations in light blue.

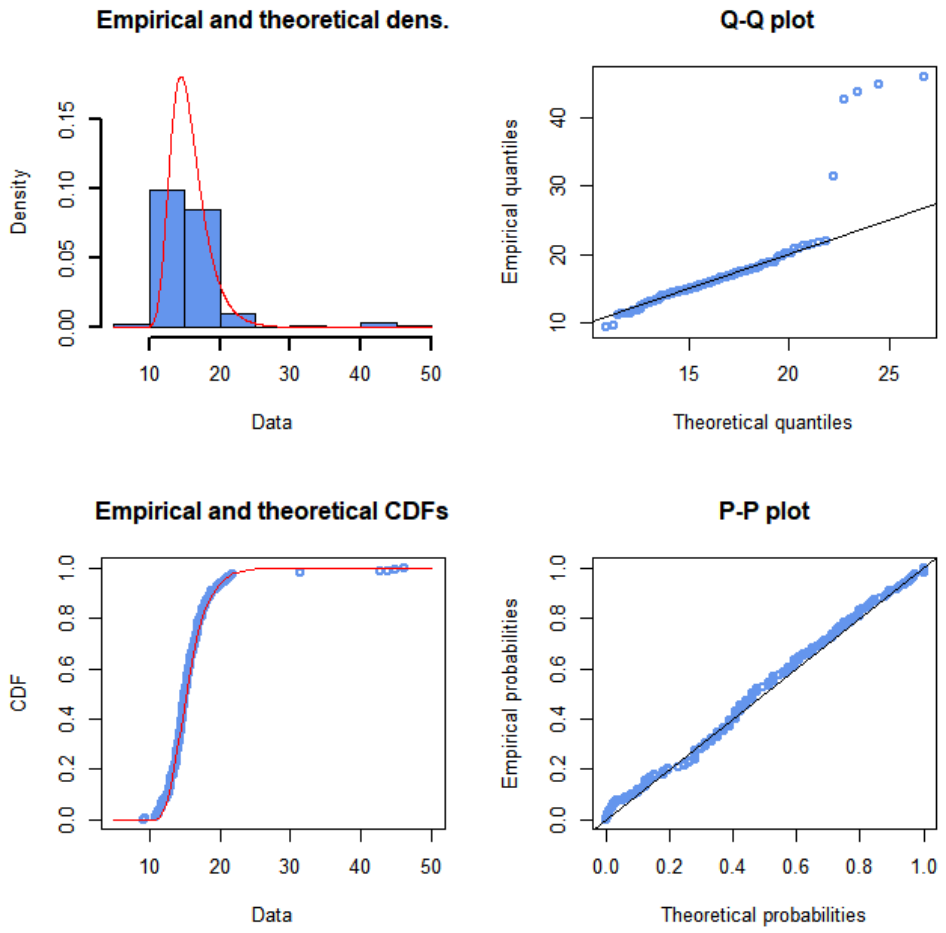


Figure 2.13: PDF, CDF, Q-Q plot and P-P plot for wind speed in Porto Empedocle (MGE), observations in light blue.

The Q-Q plots comparison confirms the first choice: in the MLE method, the deviation between empirical and theoretical quantiles, in the part of the graph concerning the results, is bigger than in the MGE method, in which the observations are almost superimposed to the theoretical quantiles line. It must be denoted that is present a huge variation in the data where wind speed is more than 40 m/s. These events have a probability of occurrence extremely low (lower than the ones associated to the return period implemented) as it can be observed in the comparison between empirical and theoretical CDFs. The values chosen are the one obtained through the Gumbel distribution with parameters estimated with maximum goodness of fit.

## 2.3.2 Waves with complete dataset

The wave height analysis provided good results in term of statistics fit: low values of the Kolmogorov-Smirnov statistic have been obtained both in Ancona and Mazara del Vallo with a Weibull distribution with parameters estimated with MGE. However, the observation of the

Q-Q plots caused the decision of the need of a further data refinement because of the distance between the empirical and theoretical quantiles in both locations. This led to not consider wave height values in the location under 3 and 3.5 meters in two attempts to get better estimations.

## *Ancona*

A total of 105 monthly maxima has been used in the analysis for Ancona: the distribution can be seen in Figure 2.14 with the help of a histogram. It denotes a large concentration of wave height values in the range 2.5-3.5 m, with a consistent presence of waves higher than 5 meters.

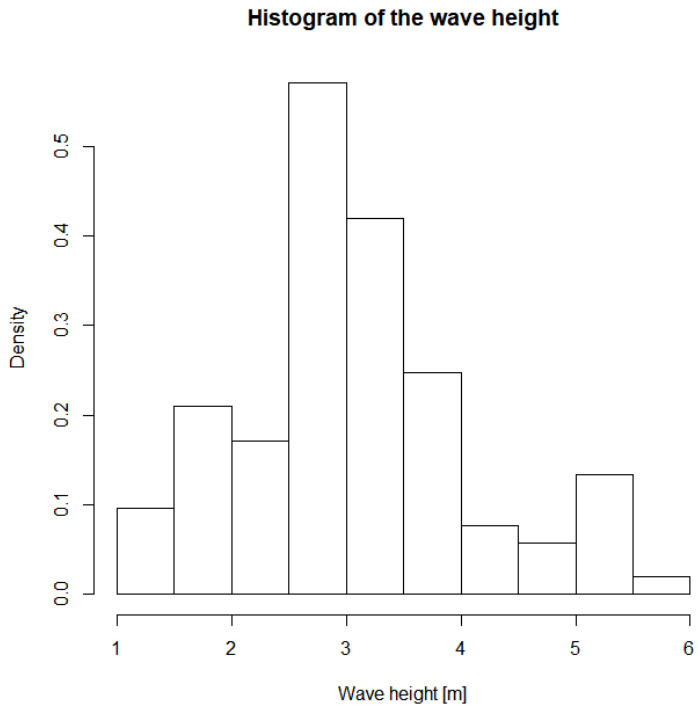


Figure 2.14: histogram of the maxima of the wave height recorded in Ancona.

| | Gumbel distribution | | Weibull distribution | |
|---|---|---|---|---|
| | **MLE** | **MGE** | **MLE** | **MGE** |
| **β** | - | - | 3.288662 | 3.805482 |
| **μ** | 2.5877345 | 2.684678 | 0 | 0 |
| **σ** | 0.8842025 | 0.821553 | 3.413948 | 3.316665 |
| **KS statistic** | 0.1212030 | 0.0779636 | 0.1099881 | 0.07545757 |
| **Wave height (T=50 years)** | 6.037839 m | 5.890327 m | 5.16882 m | 4.746486 m |
| **Wave height (T=100 years)** | 6.655198 m | 6.463944 m | 5.43167 m | 4.954371 m |

Table 2.3: results for wave height in Ancona.

The analysis has been performed through an implementation of both a Gumbel and a Weibull distribution in which the parameters has been estimated with MLE and MGE. The parameters, the associated KS statistics and the variables estimation have been collected in Table 2.3.
The best value of the KS statistics is obtained with the Weibull distribution with parameters estimated through MGE: this outcome led to prefer the results obtained with this computation.
A further comparison of the parameters is needed for the huge difference between the results and to confirm the previous statement and it has been done through the observation of the Q-Q plots obtained with the different methods. These graphs, along with a representation of the PDFs and CDFs (empirical and theoretical) and the P-P plots, are collected in Figure 2.15, Figure 2.16, Figure 2.17 and Figure 2.18.

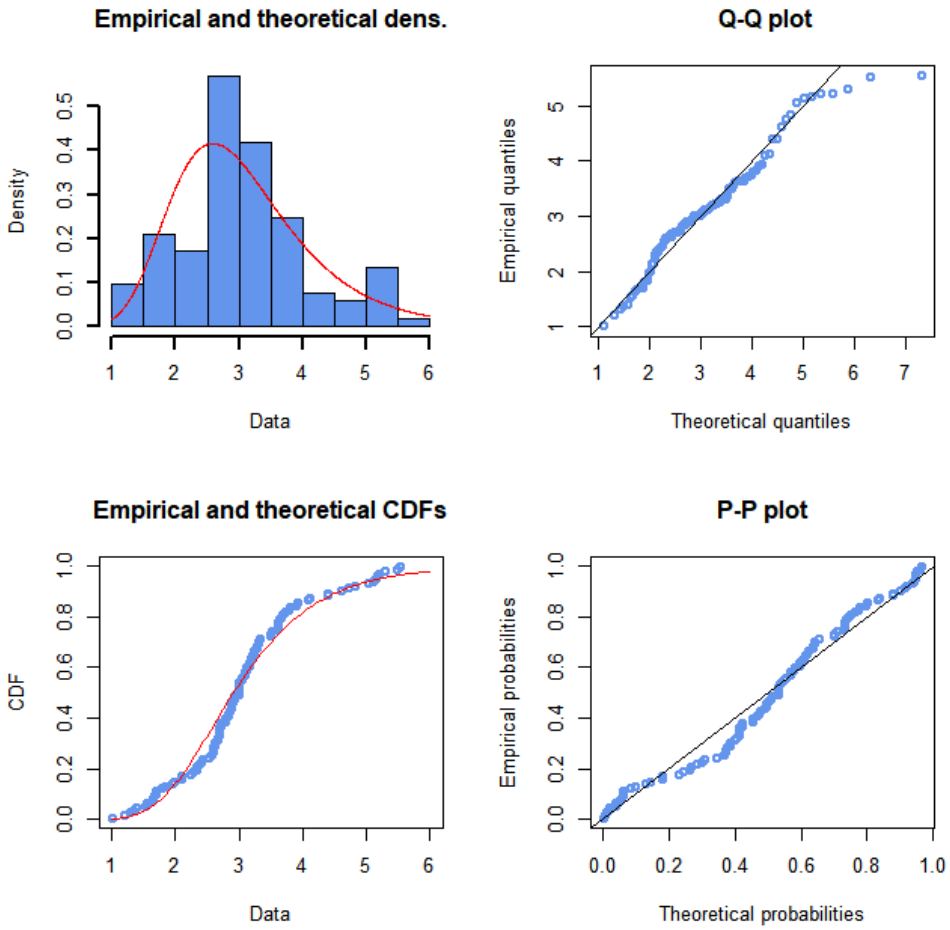


Figure 2.15: PDF, CDF, Q-Q plot and P-P plot for wind speed in Ancona (Gumbel MLE), observations in light blue.

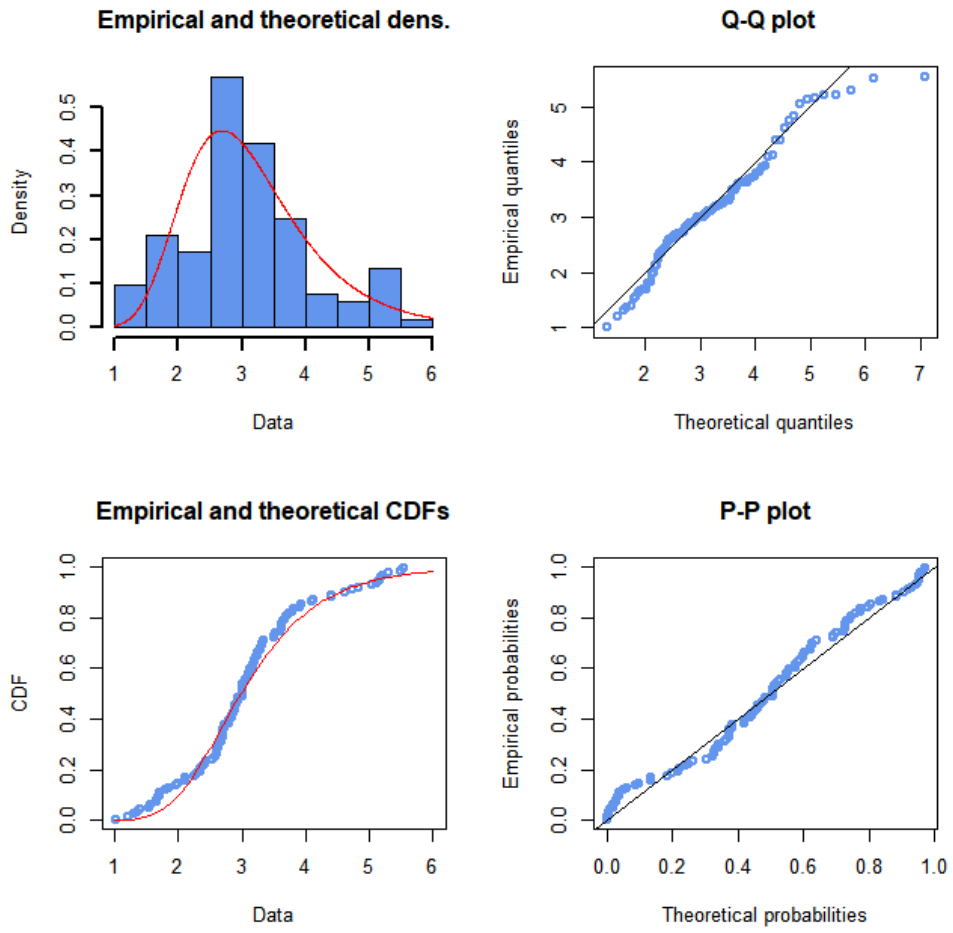


Figure 2.16: PDF, CDF, Q-Q plot and P-P plot for wind speed in Ancona (Gumbel MGE), observations in light blue.

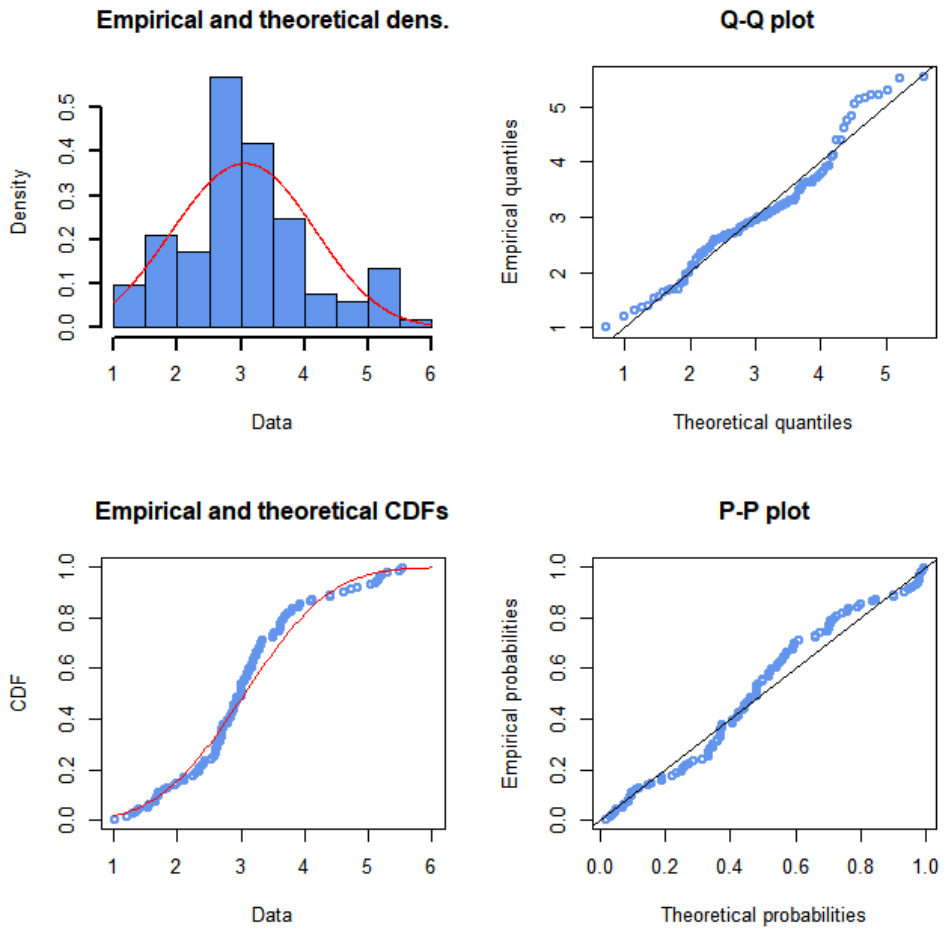


Figure 2.17: PDF, CDF, Q-Q plot and P-P plot for wind speed in Ancona (Weibull MLE), observations in light blue.

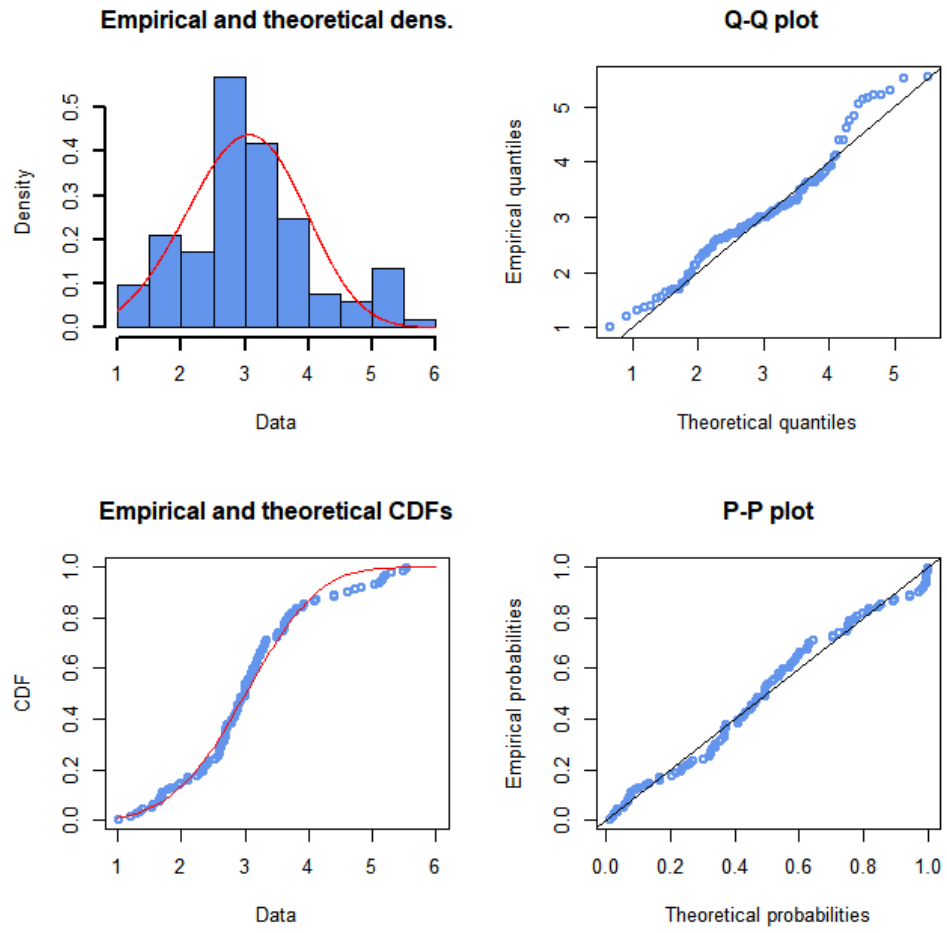


Figure 2.18: PDF, CDF, Q-Q plot and P-P plot for wind speed in Ancona (Weibull MGE), observations in light blue.

The Q-Q plots analysis confirms the need of a further data refinement: in the area related to the values obtained the deviation between theoretical and empirical quantiles is significative and therefore the estimations are not considered accurate even with the good levels of fit given by the KS statistics. This caused the decision to try to improve the results with a lower truncation of the dataset, considering wave heights above 3 and 3.5 meters.

## *Mazara del Vallo*

A total of 219 monthly maxima has been used in the analysis for Mazara del Vallo: the distribution can be seen in Figure 2.19 with the help of a histogram. It denotes a large concentration of wave height values in the range 2-4 m, with a presence of waves higher than 6 meters.

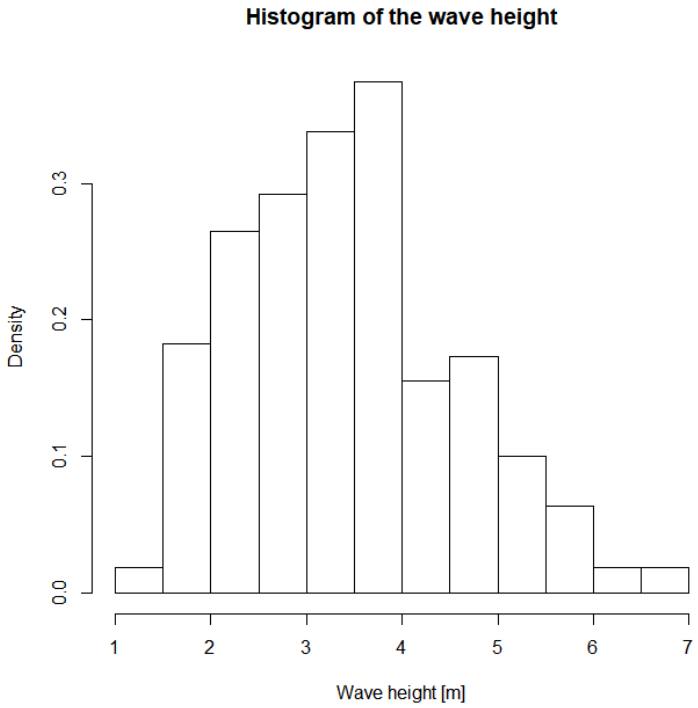


Figure 2.19: histogram of the maxima of the wave height recorded in Mazara del Vallo.

The analysis has been performed with the same procedure of Ancona. The parameters, the associated KS statistics and the variables estimation have been collected in Table 2.4.

| | **Gumbel distribution** | | **Weibull distribution** | |
|---|---|---|---|---|
| | **MLE** | **MGE** | **MLE** | **MGE** |
| **β** | - | - | 3.315391 | 3.536775 |
| **μ** | 2.9106139 | 2.928833 | 0 | 0 |
| **σ** | 0.9462657 | 1.021264 | 3.836545 | 3.773902 |
| **KS statistic** | 0.05693139 | 0.04840359 | 0.06381818 | 0.04617256 |
| **Wave height (T=50 years)** | 6.602884 m | 6.913741 m | 5.789252 m | 5.54994 m |
| **Wave height (T=100 years)** | 7.263577 m | 7.626799 m | 6.08122 m | 5.811912 m |

Table 2.4: results for wave height in Mazara del Vallo.

The best value of the KS statistics is obtained with the Weibull distribution with parameters estimated through MGE: this outcome led to prefer the results obtained with this computation. A similar consideration to Ancona about the observation of the Q-Q plots can be made. These graphs, along with a representation of the PDFs and CDFs (empirical and theoretical) and the P-P plots, are collected in Figure 2.20, Figure 2.21, Figure 2.22 and Figure 2.23.

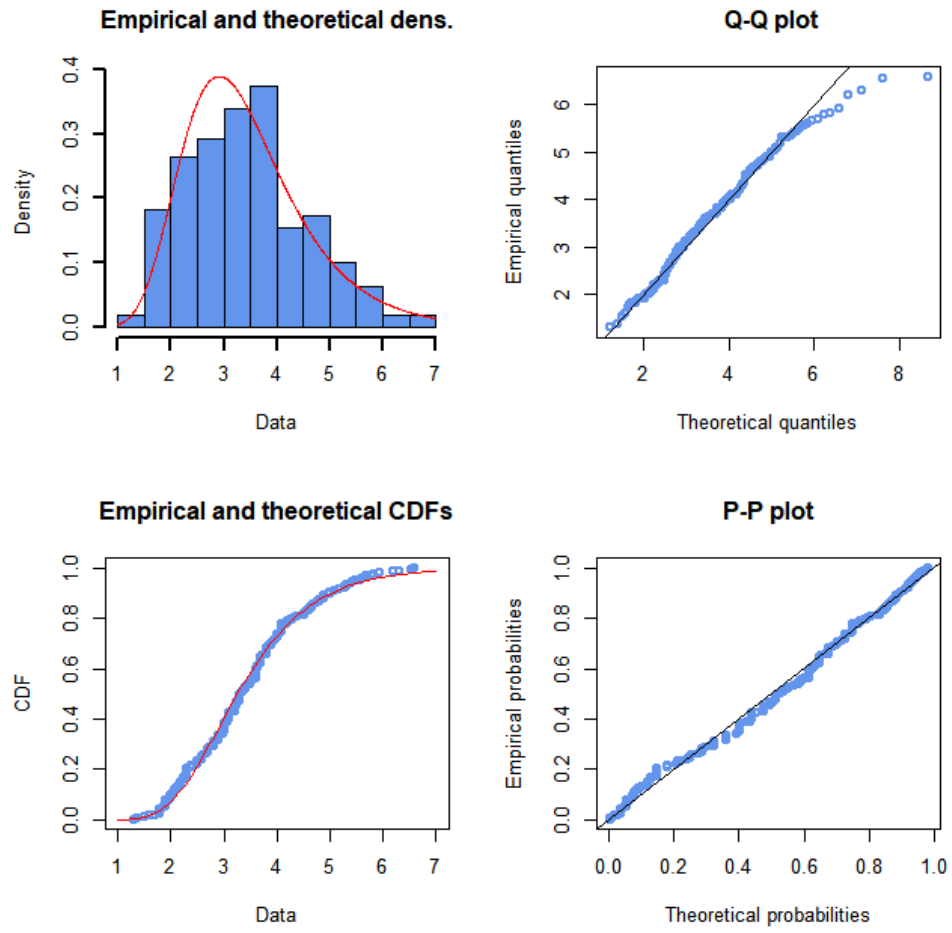


Figure 2.20: PDF, CDF, Q-Q plot and P-P plot for wind speed in Mazara del Vallo (Gumbel MLE), observations in light blue.

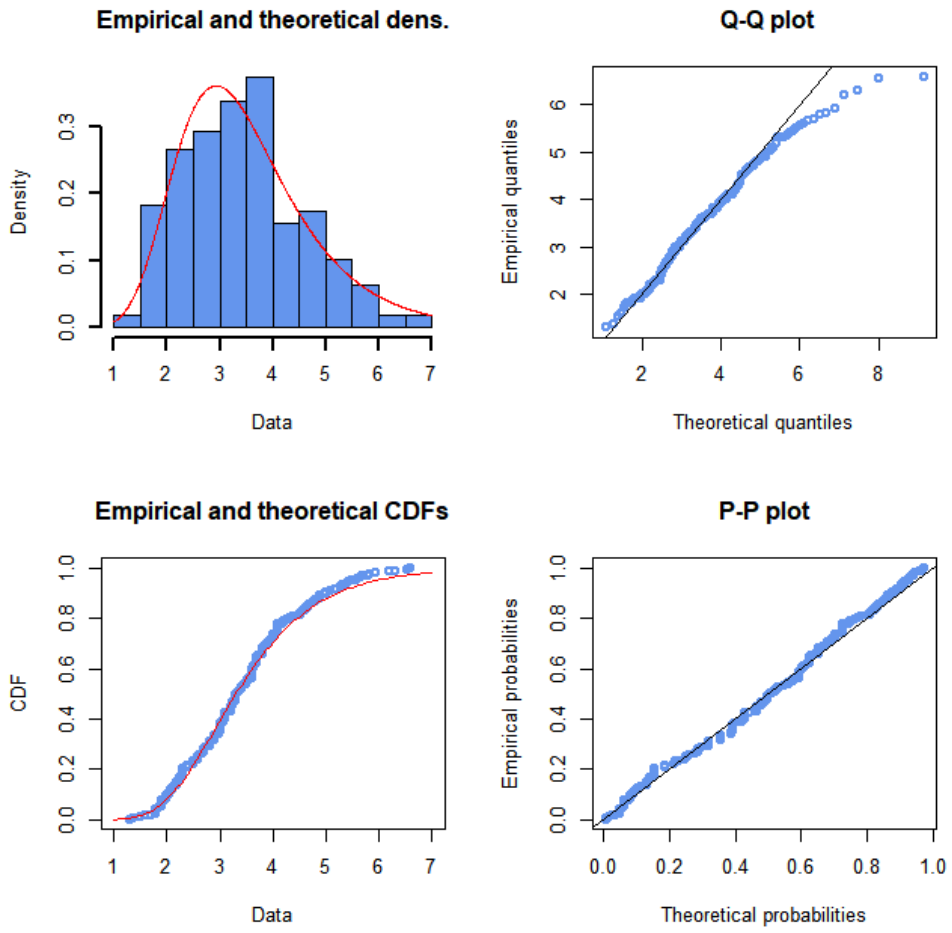


Figure 2.21: PDF, CDF, Q-Q plot and P-P plot for wind speed in Mazara del Vallo (Gumbel MGE), observations in light blue.

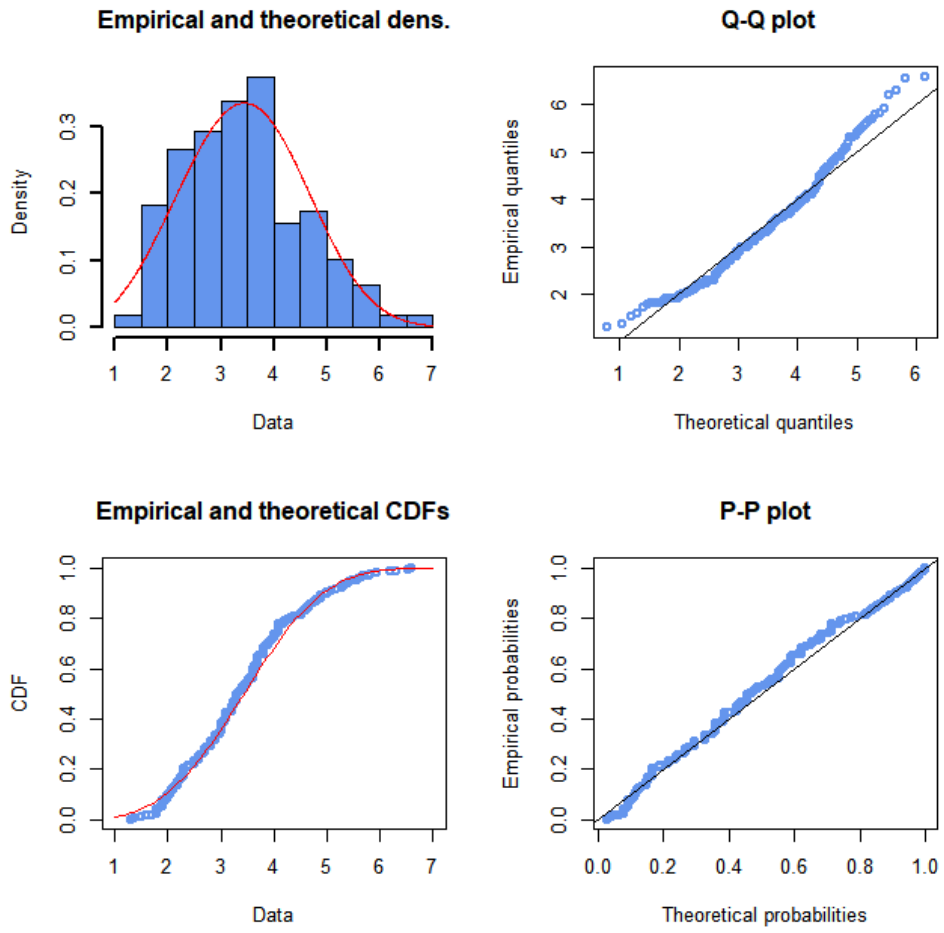


Figure 2.22: PDF, CDF, Q-Q plot and P-P plot for wind speed in Mazara del Vallo (Weibull MLE), observations in light blue.

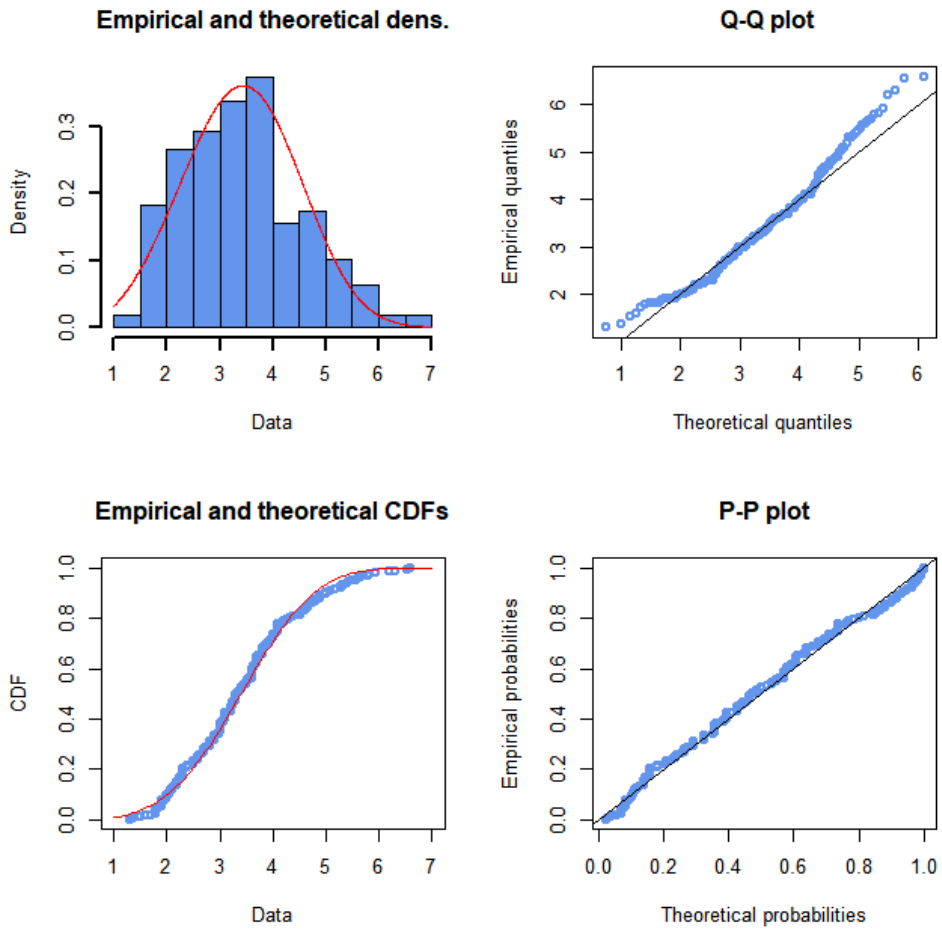


Figure 2.23: PDF, CDF, Q-Q plot and P-P plot for wind speed in Mazara del Vallo (Weibull MGE), observations in light blue.

The Q-Q plots lead to the same decision made with the Ancona Dataset even with better values of the KS statistic. The refinement of the observation has been performed in the same way: only waves higher than 3 and 3.5 meters have been considered.

### 2.3.3 Waves with truncated dataset

The truncation of the dataset has been effective: a better graphical fit, considering the Q-Q plots, has been obtained, with a tolerable increase of the Kolmogorov-Smirnov statistics. The best estimations are given in both locations by a Gumbel distribution with parameters estimated with a maximum goodness of fit estimation, considering a dataset with wave height values above 3 meters.

## *Ancona*

A great reduction in the available data has been made considering waves height above 3 and 3.5 meters: from 124 observations, 50 maxima has been used in the first case and 28 in the second. The distributions can be seen in Figure 2.24 and Figure 2.25.

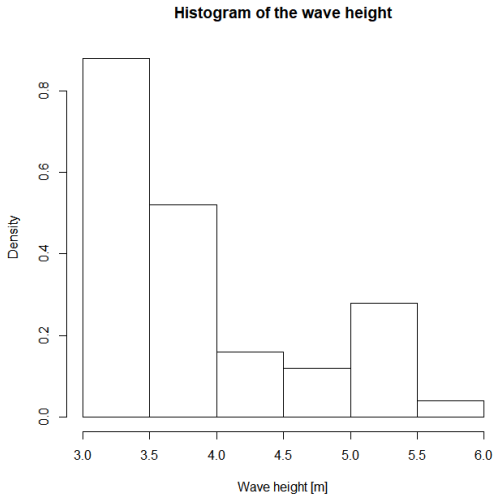


Figure 2.24: histogram of the maxima of the wave height (>3 m) recorded in Ancona.

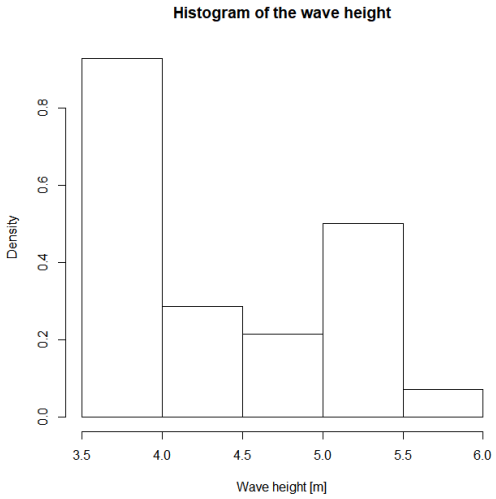


Figure 2.25: histogram of the maxima of the wave height (>3.5 m) recorded in Ancona.

The analysis has been performed with the same procedure described in the chapters with a complete dataset. The parameters, the associated KS statistics and the variables estimation have been collected in Table 2.5 and Table 2.6.

| | **Gumbel distribution** | | **Weibull distribution** | |
|---|---|---|---|---|
| | **MLE** | **MGE** | **MLE** | **MGE** |
| **β** | - | - | 5.096906 | 6.390132 |
| **μ** | 3.5037231 | 3.4555748 | 0 | 0 |
| **σ** | 0.5304505 | 0.5552263 | 4.167385 | 4.007164 |
| **KS statistic** | 0.1432639 | 0.1074065 | 0.1908960 | 0.1484142 |
| **Wave height (T=50 years)** | 5.573508 m | 5.622034 m | 5.446171 m | 4.960698 m |
| **Wave height (T=100 years)** | 5.943875 m | 6.009699 m | 5.623293 m | 5.088963 m |

Table 2.5: results for wave height (dataset >3 m) in Ancona.

The best value of the KS statistics is obtained with the Gumbel distribution with parameters estimated through MGE in the dataset that considers wave heights above 3 meters.

A further comparison of the results is needed for the general higher values of the KS statistics than the case with the complete dataset. It has been done through the observation of the Q-Q plots obtained with the different methods and different datasets. These graphs, along with a representation of the PDFs and CDFs (empirical and theoretical) and the P-P plots, are

collected in Figure 2.26, Figure 2.27, Figure 2.28, Figure 2.29, Figure 2.30, Figure 2.31, Figure 2.32 and Figure 2.33.

| | Gumbel distribution | | Weibull distribution | |
|---|---|---|---|---|
| | **MLE** | **MGE** | **MLE** | **MGE** |
| **β** | - | - | 6.902176 | 7.023911 |
| **μ** | 4.0182392 | 3.9794504 | 0 | 0 |
| **σ** | 0.5310922 | 0.6051899 | 4.640101 | 4.547281 |
| **KS statistic** | 0.1652376 | 0.1265550 | 0.1879755 | 0.1582316 |
| **Wave height (T=50 years)** | 6.090528 m | 6.340864 m | 5.653999 m | 5.52195 m |
| **Wave height (T=100 years)** | 6.461343 m | 6.763414 m | 5.789216 m | 5.651693 m |

Table 2.6: results for wave height (dataset >3.5 m) in Ancona.

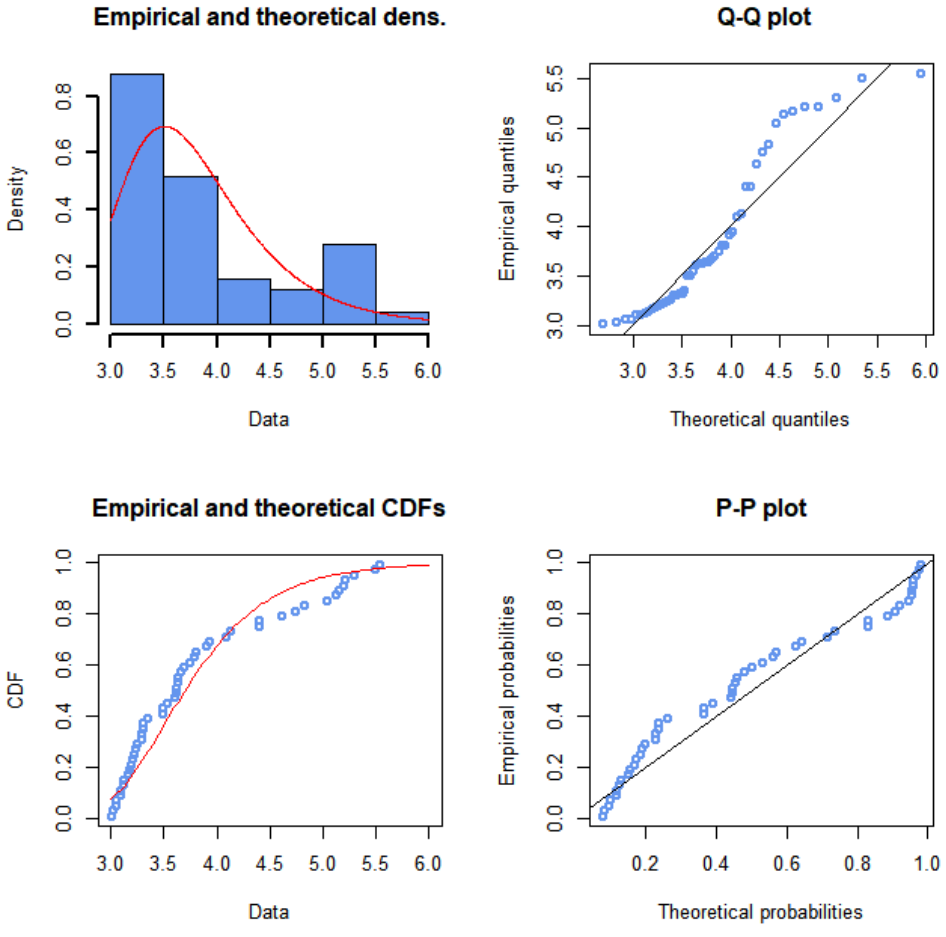


Figure 2.26: PDF, CDF, Q-Q plot and P-P plot for wind speed in Ancona (Gumbel MLE, dataset >3 m), observations in light blue.

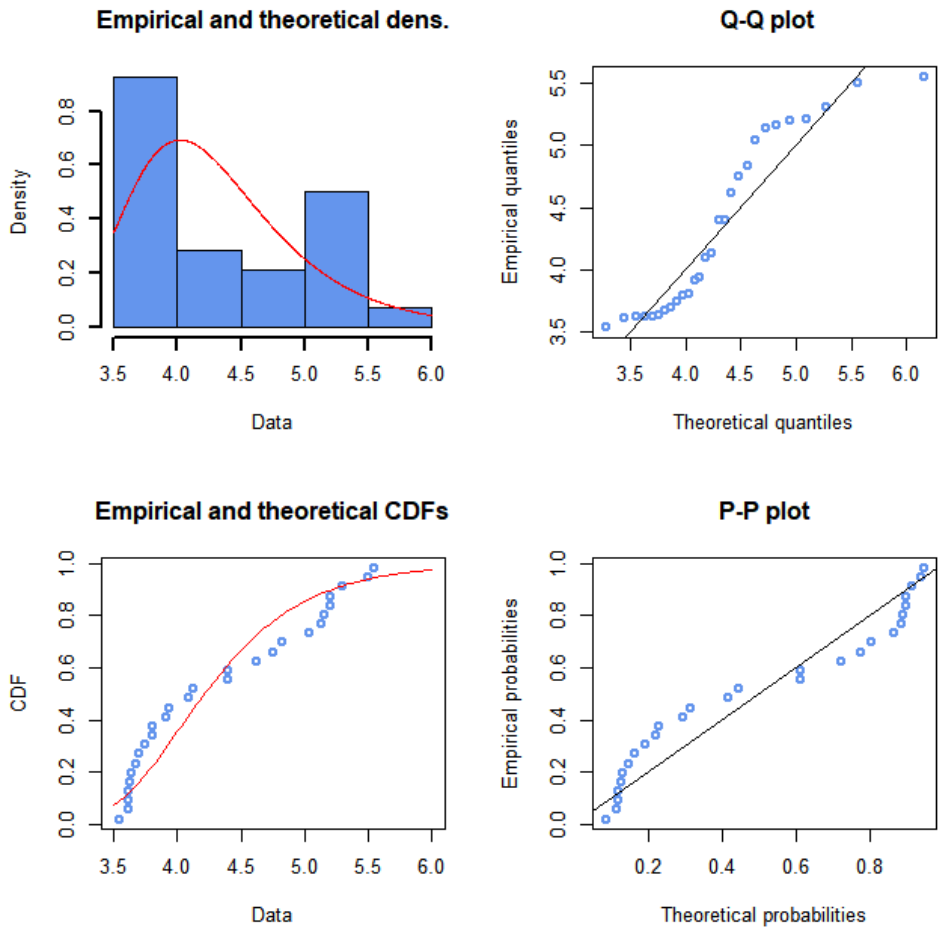


Figure 2.27: PDF, CDF, Q-Q plot and P-P plot for wind speed in Ancona (Gumbel MLE, dataset >3.5 m), observations in light blue.

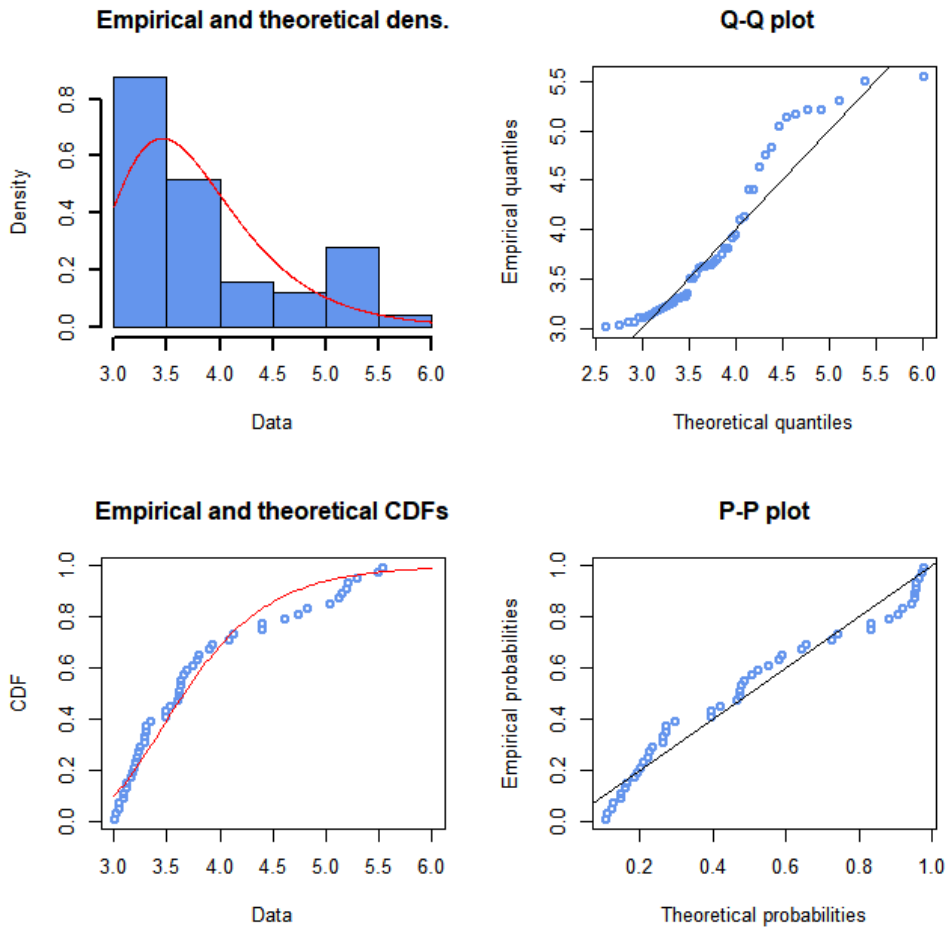


Figure 2.28: PDF, CDF, Q-Q plot and P-P plot for wind speed in Ancona (Gumbel MGE, dataset >3 m), observations in light blue.

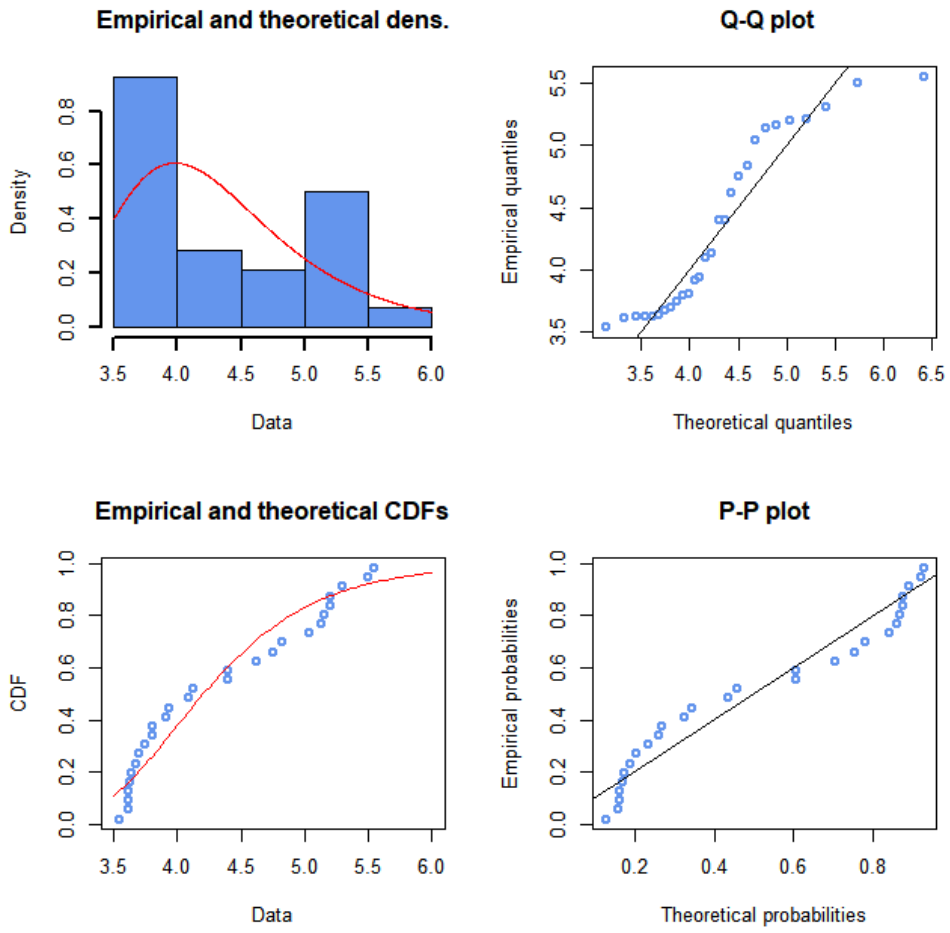


Figure 2.29: PDF, CDF, Q-Q plot and P-P plot for wind speed in Ancona (Gumbel MGE, dataset >3.5 m), observations in light blue.

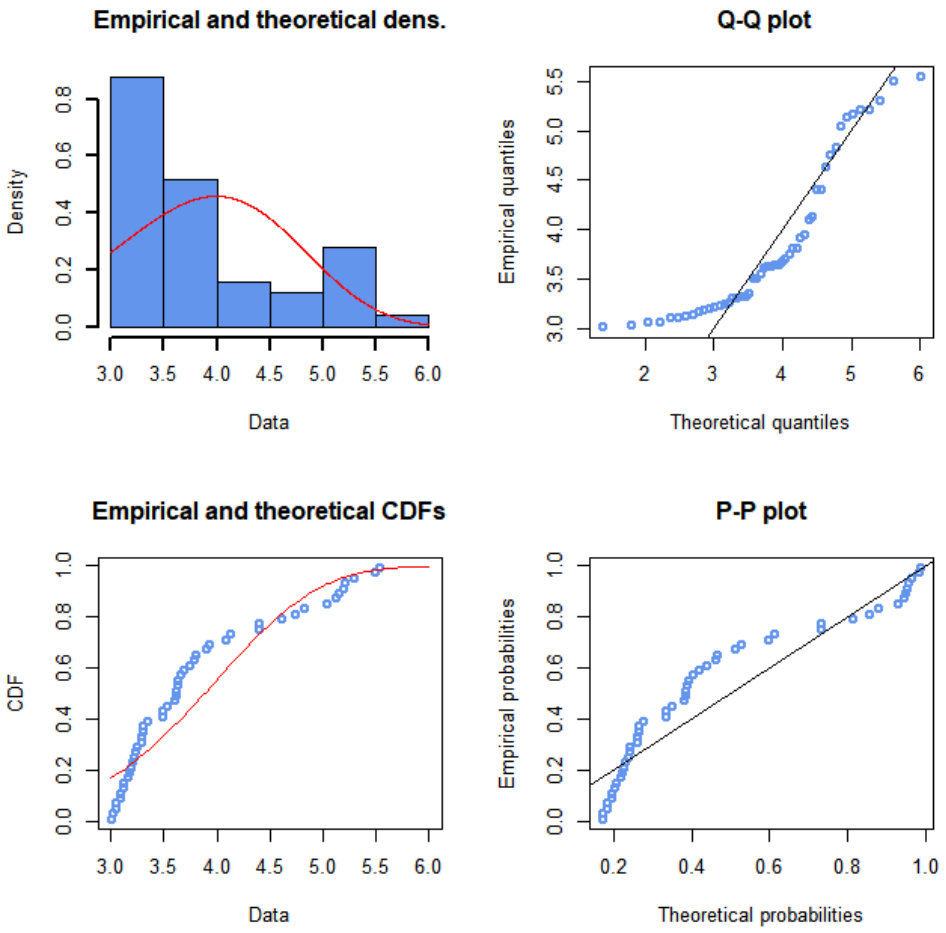


Figure 2.30: PDF, CDF, Q-Q plot and P-P plot for wind speed in Ancona (Weibull MLE, dataset >3 m), observations in light blue.

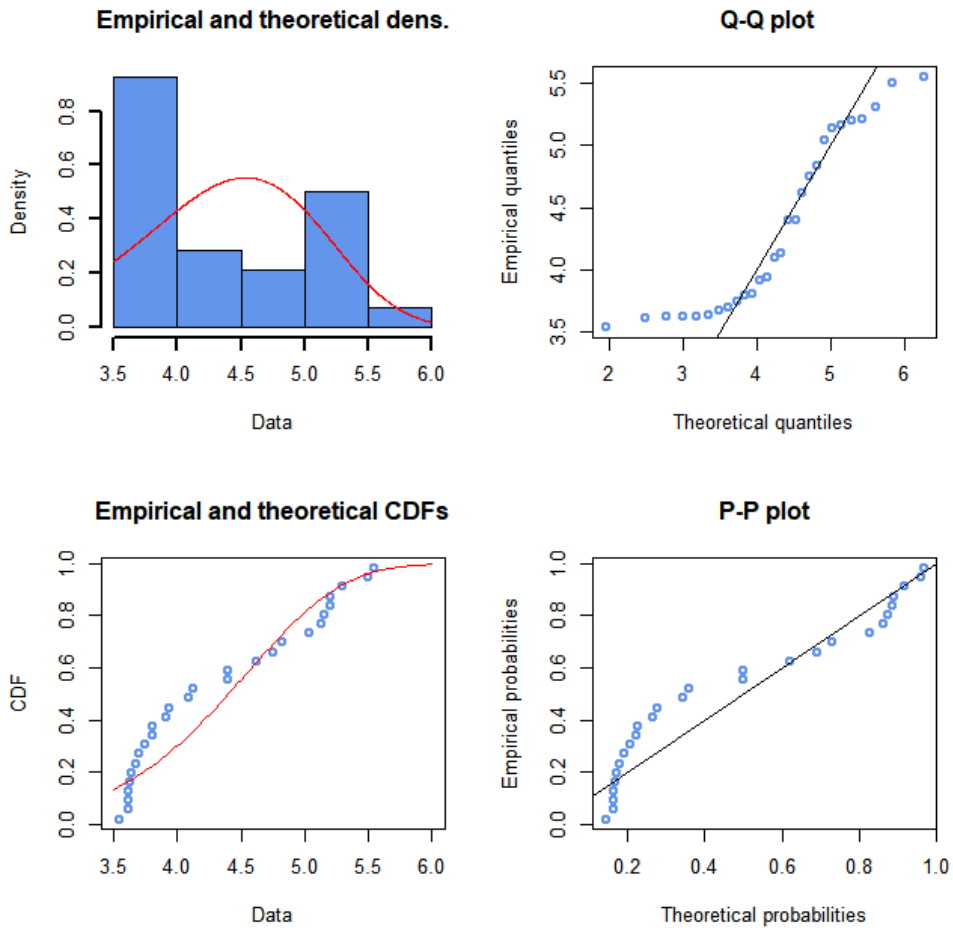


Figure 2.31: PDF, CDF, Q-Q plot and P-P plot for wind speed in Ancona (Weibull MLE, dataset >3.5 m), observations in light blue.

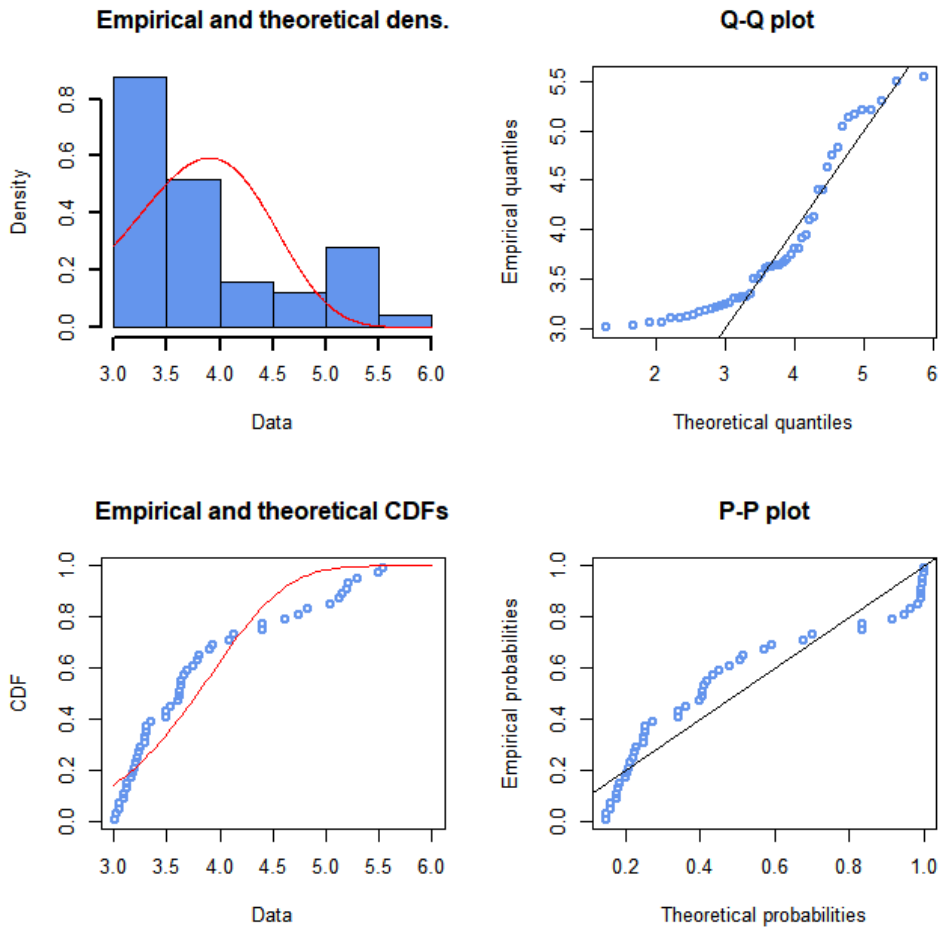


Figure 2.32: PDF, CDF, Q-Q plot and P-P plot for wind speed in Ancona (Weibull MGE, dataset >3 m), observations in light blue.

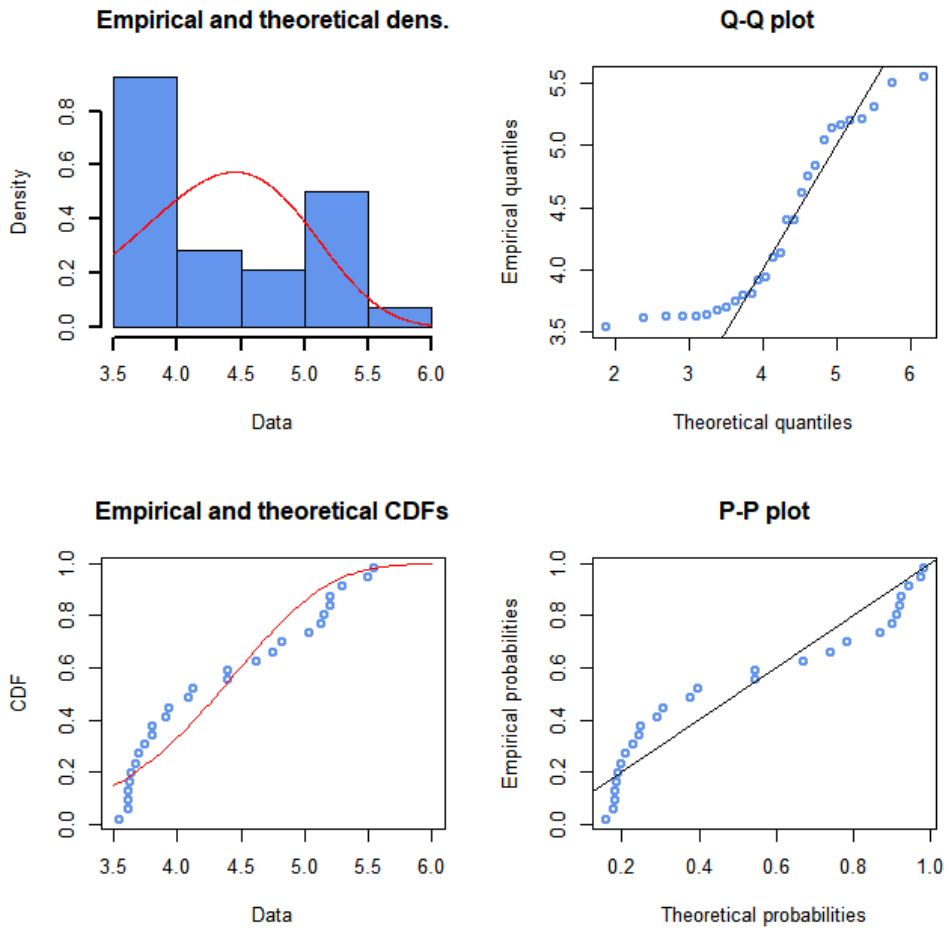


Figure 2.33: PDF, CDF, Q-Q plot and P-P plot for wind speed in Ancona (Weibull MGE, dataset >3.5 m), observations in light blue.

The Q-Q plots analysis confirms the indication given by the KS statistics: the best compromise to obtain a good prediction is to consider a Gumbel distribution, parameters estimated with MGE, with a dataset that contains values of wave height above 3 meters. The lower distance between the empirical and theoretical quantiles, in the results area, justifies the increase of the KS statistic compared to the value obtained with a complete dataset.

## *Mazara del Vallo*

The available data in Mazara del Vallo are more than in Ancona even with the truncations performed to the dataset: considering waves higher than 3 meters, 136 observations remained and 99 observations are at disposal in the 3.5 meters higher dataset. The distributions can be seen in Figure 2.34 and Figure 2.35.

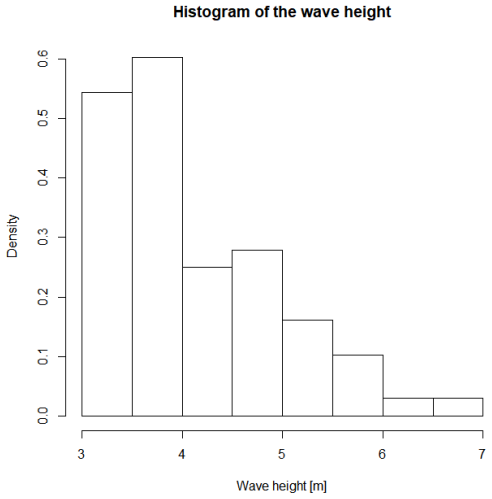


Figure 2.34: histogram of the maxima of the wave height (>3 m) recorded in Mazara del Vallo.

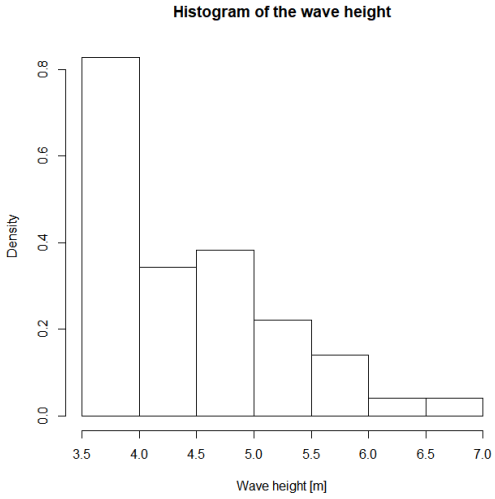


Figure 2.35: histogram of the maxima of the wave height (>3.5 m) recorded in Mazara del Vallo.

The analysis has been performed with the same procedure described in the previous chapter. The parameters, the associated KS statistics and the variables estimation have been collected in Table 2.7 and Table 2.8.

| | **Gumbel distribution** | | **Weibull distribution** | |
|---|---|---|---|---|
| | **MLE** | **MGE** | **MLE** | **MGE** |
| **β** | - | - | 4.858632 | 6.215009 |
| **μ** | 3.7273280 | 3.693101 | 0 | 0 |
| **σ** | 0.6170447 | 0.645047 | 4.459583 | 4.282276 |
| **KS statistic** | 0.08223152 | 0.06200983 | 0.1541464 | 0.1091355 |
| **Wave height (T=50 years)** | 6.134998 m | 6.210035 m | 5.905026 m | 5.333257 m |
| **Wave height (T=100 years)** | 6.565826 m | 6.660414 m | 6.106649 m | 5.475092 m |

Table 2.7: results for wave height (dataset >3 m) in Mazara del Vallo.

| | **Gumbel distribution** | | **Weibull distribution** | |
|---|---|---|---|---|
| | **MLE** | **MGE** | **MLE** | **MGE** |
| **β** | - | - | 4.858632 | 6.215009 |
| **μ** | 3.7273280 | 3.693101 | 0 | 0 |
| **σ** | 0.6170447 | 0.645047 | 4.459583 | 4.282276 |
| **KS statistic** | 0.08223152 | 0.06200983 | 0.1541464 | 0.1091355 |
| **Wave height (T=50 years)** | 6.134998 m | 6.210035 m | 5.905026 m | 5.333257 m |
| **Wave height (T=100 years)** | 6.565826 m | 6.660414 m | 6.106649 m | 5.475092 m |

Table 2.8: results for wave height (dataset >3.5 m) in Mazara del Vallo.

The best value of the KS statistics is obtained with the Gumbel distribution with parameters estimated through MGE in the dataset that considers wave heights above 3 meters.
A further comparison of the results has been performed: it has been done in the same way described in the previous chapter. The Q-Q graphs, along with a representation of the PDFs and CDFs (empirical and theoretical) and the P-P plots, are collected in Figure 2.36, Figure 2.37, Figure 2.38, Figure 2.39, Figure 2.40, Figure 2.41, Figure 2.42 and Figure 2.43.

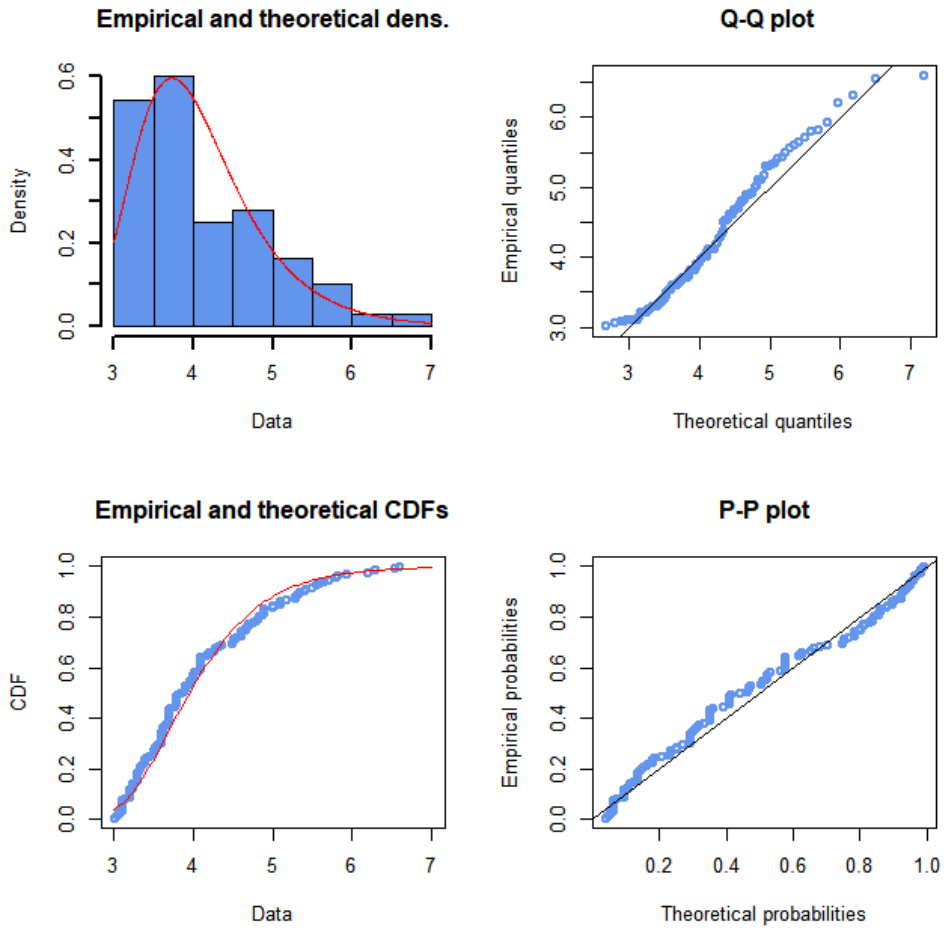


Figure 2.36: PDF, CDF, Q-Q plot and P-P plot for wind speed in Mazara del Vallo (Gumbel MLE, dataset >3 m), observations in light blue.

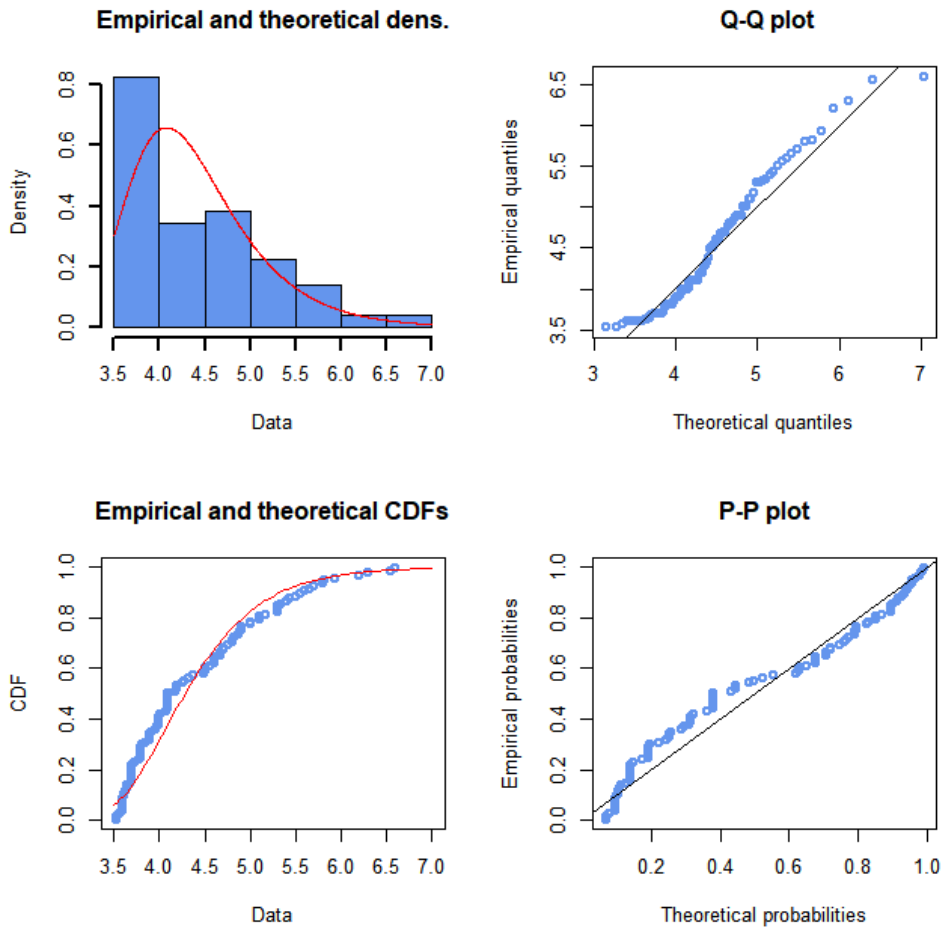


Figure 2.37: PDF, CDF, Q-Q plot and P-P plot for wind speed in Mazara del Vallo (Gumbel MLE, dataset >3.5 m), observations in light blue.

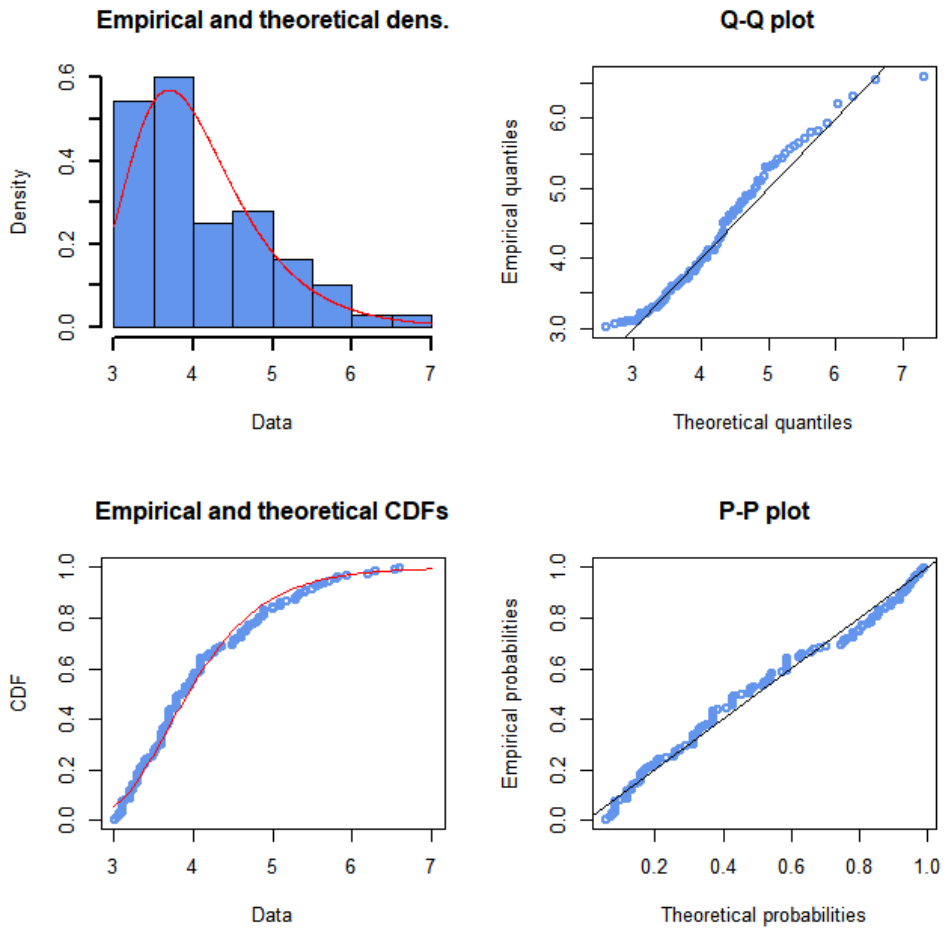


Figure 2.38: PDF, CDF, Q-Q plot and P-P plot for wind speed in Mazara del Vallo (Gumbel MGE, dataset >3 m), observations in light blue.

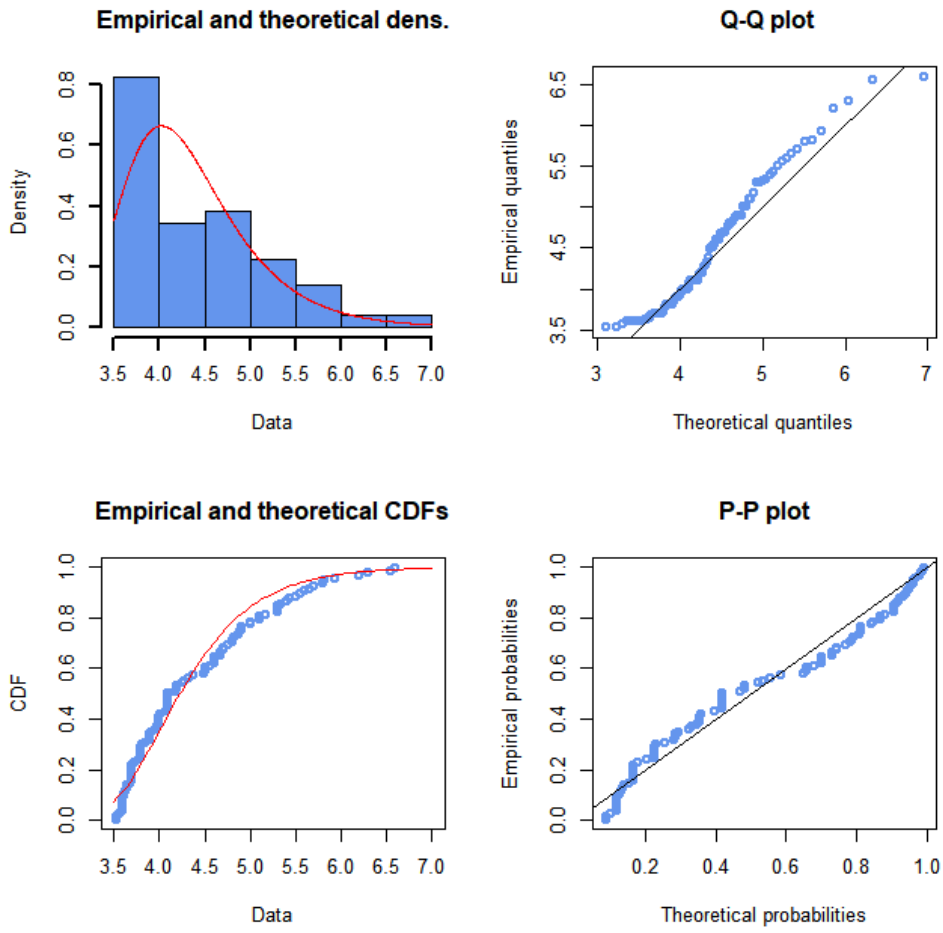


Figure 2.39: PDF, CDF, Q-Q plot and P-P plot for wind speed in Mazara del Vallo (Gumbel MGE, dataset >3.5 m), observations in light blue.

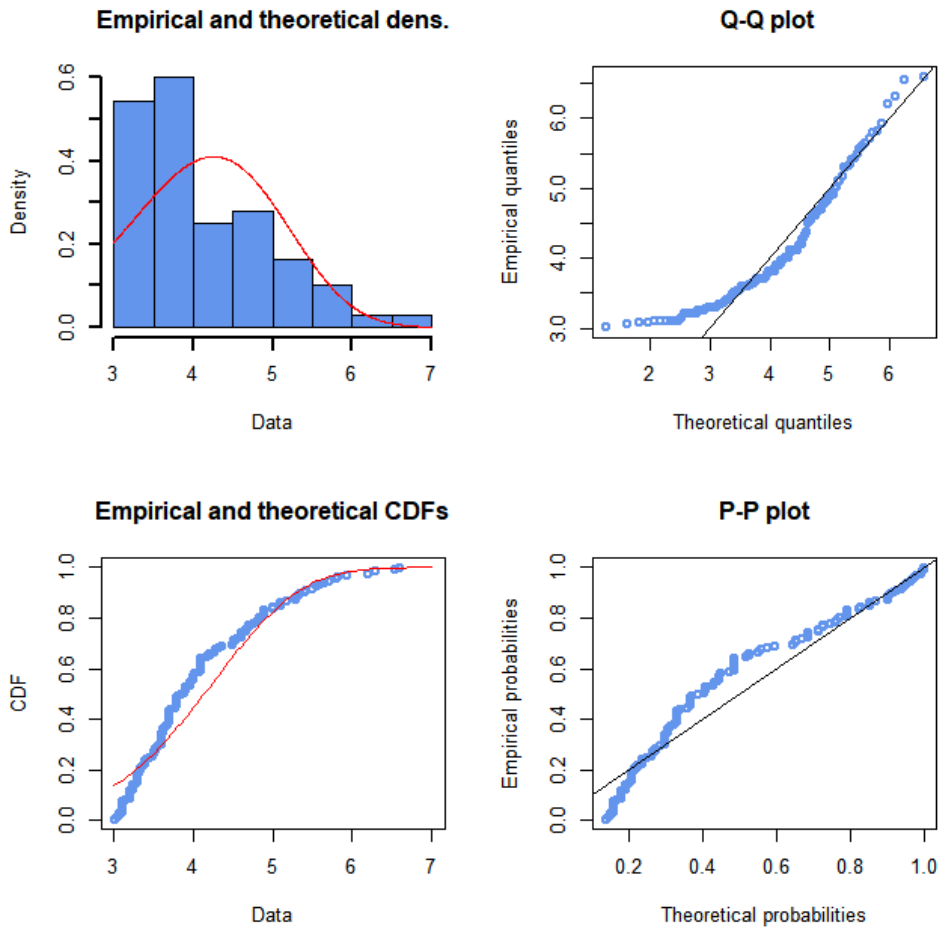


Figure 2.40: PDF, CDF, Q-Q plot and P-P plot for wind speed in Mazara del Vallo (Weibull MLE, dataset >3 m), observations in light blue.

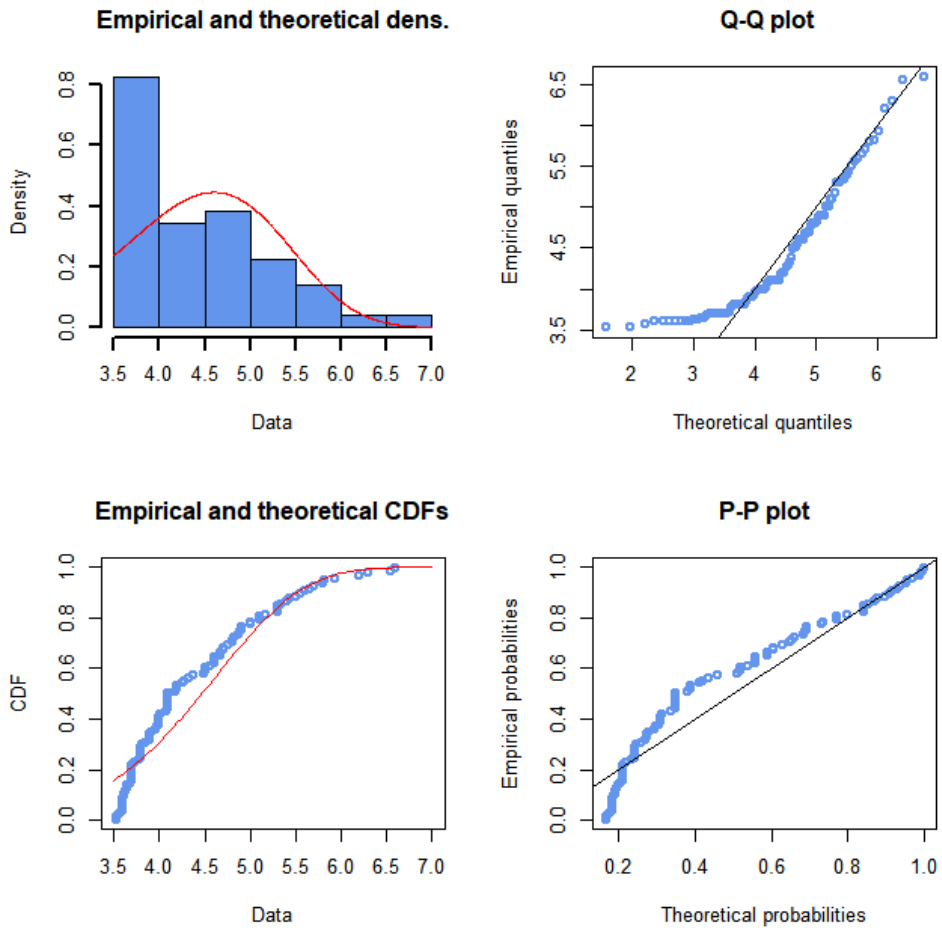


Figure 2.41: PDF, CDF, Q-Q plot and P-P plot for wind speed in Mazara del Vallo (Weibull MLE, dataset >3.5 m), observations in light blue.

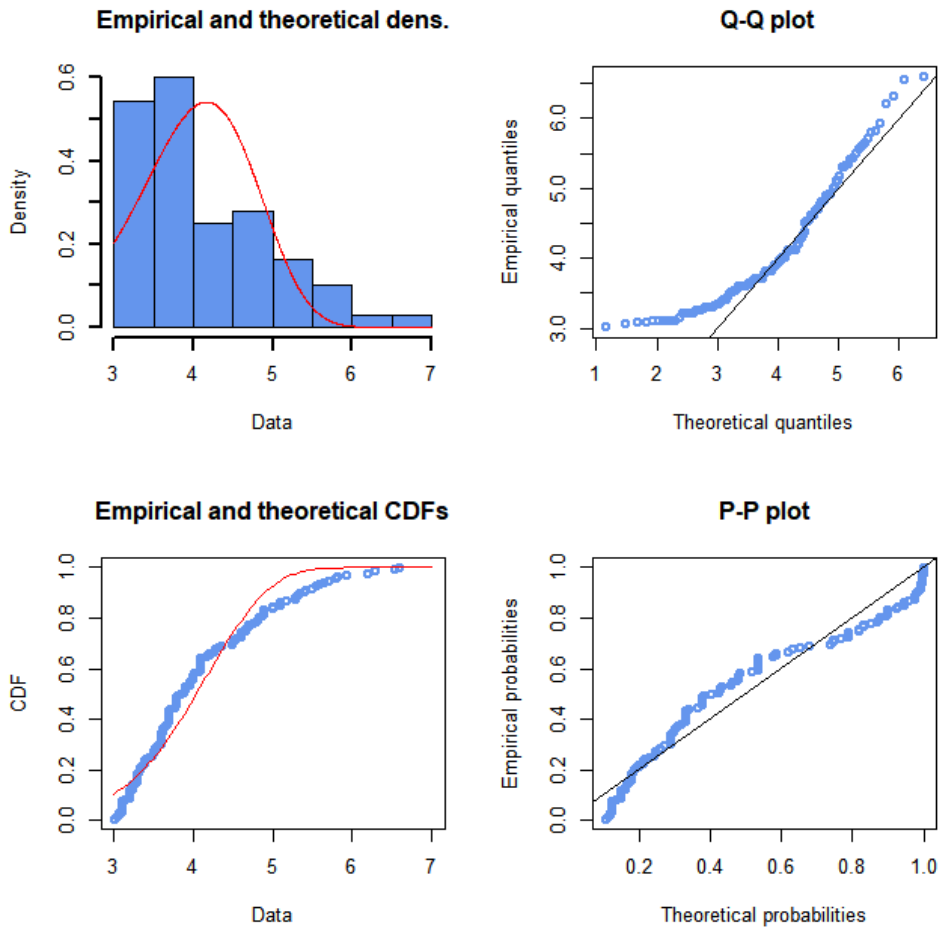


Figure 2.42: PDF, CDF, Q-Q plot and P-P plot for wind speed in Mazara del Vallo (Weibull MGE, dataset >3 m), observations in light blue.

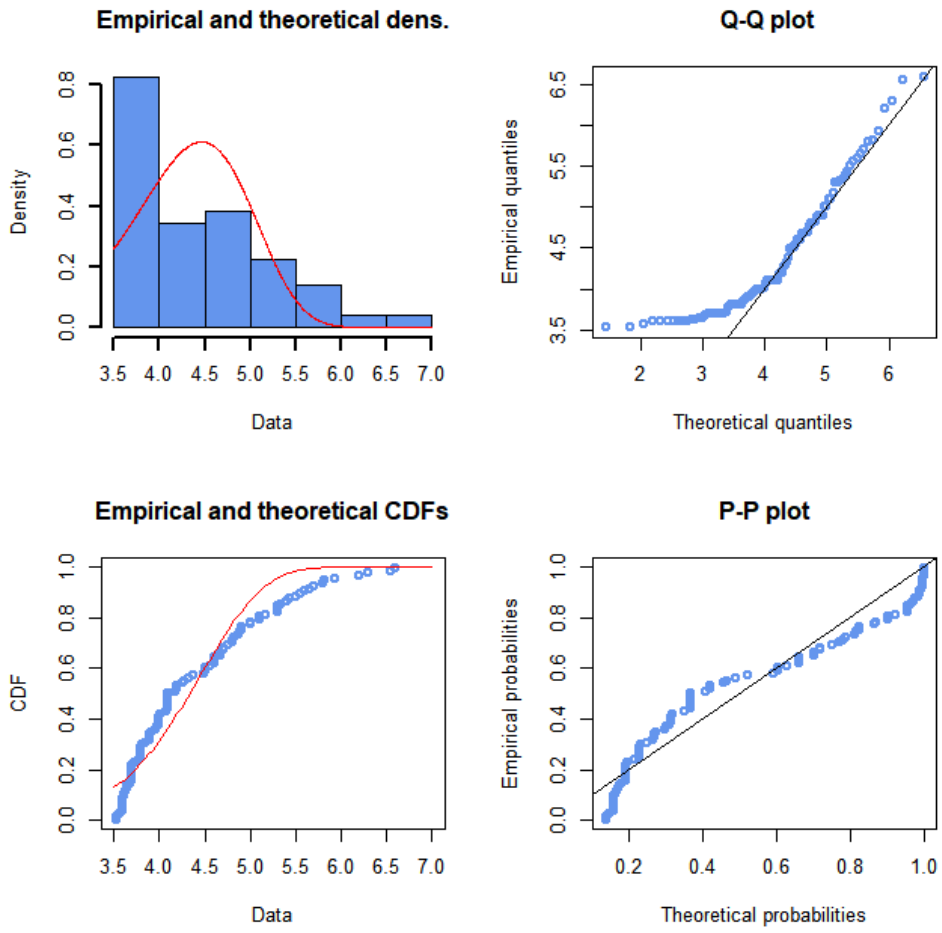


Figure 2.43: PDF, CDF, Q-Q plot and P-P plot for wind speed in Mazara del Vallo (Weibull MGE, dataset >3.5 m), observations in light blue.

The indication given by the Q-Q plots strengthen the KS statistic value: the best predictions are given by a Gumbel distribution (MGE) with a dataset that contains wave heights data above 3 meters. In this case too, like in Ancona, there is an increase in the KS statistic, compensated by a better distance between empirical and theoretical quantiles.

## *Peak period*

For Ancona, to obtain the peak period associated with the design waves, only recorded waves above 5 meters have been considered. The corresponding data show that, in this location, the highest waves mostly have a peak period around 9.5 seconds.

For Mazara del Vallo, the considered waves are above 6 meters of height: the corresponding waves' peak period has a value of around 11 seconds.

## 2.4 Discussion of the results

In all the analysis emerged a clear pattern: the best results are obtained through a Gumbel distribution with parameters estimated with maximum goodness of fit procedure. This has been confirmed by identifying the lowest values of the Kolmogorov-Smirnov statistics and the Q-Q plot observations, that together provide an indication of the fit of the measured data to the statistical distribution, like described in 2.2.4:

- for the wind in Ancona: Table 2.1 and Figure 2.10;
- for the wind in Porto Empedocle: Table 2.2 and Figure 2.13;
- for the waves in Ancona: Table 2.5 and Figure 2.28;
- for waves in Mazara del Vallo: Table 2.7 and Figure 2.38.

This led to the decision of the design wind speed and wave height to be used in the mooring analysis. These values, along with the waves' peak periods, are summarized in Table 2.9.

| Return Period | Design wind speed | | Design wave height | | Design peak period | |
|---|---|---|---|---|---|---|
| | Ancona | Porto Empedocle | Ancona | Mazara del Vallo | Ancona | Mazara del Vallo |
| **50 years** | 20.90 m/s | 22.41 m/s | 5.62 m | 6.21 m | 9.5 s | 11 s |
| **100 years** | 22.64 m/s | 23.83 m/s | 6.01 m | 6.66 m | | |

Table 2.9: design wind speed, wave height and peak period for 50 and 100 years return period.

The design wind speed is higher in southern Sicily than in Ancona: this must be considered when computing the mooring system. On one side, higher cost for the anchor system are prevented to withstand the stronger force impressed by the wind, on the other, a wind that blows faster allows a higher energy production and less time to compensate the building costs. The same tendency emerges from a comparison between the design wave height values: in the southern Sicily waves are around 60 cm higher than in the central Adriatic. This, in addition to a deeper seabed (refer to Figure 2.5), can rise the building cost and make the site less desirable even with a higher energy production from wind.

Peak periods are parameters to consider in the waves' spectral definition for the numerical analysis of the moorings and, in general, for the structural calculations: the foundation structure must not have a natural frequency close to wave peak frequency. This could lead to resonances and a potential structural failure that could endanger the whole project.

## 2.5 Other approaches in statistical analysis

To have at disposal more data, the extreme value problem could be faced using all the data recorded by the stations to increase the population. Since that the recording is not continuous

but performed at specific intervals of time: this could present troubles regarding the monthly coverage (like said in 2.1.1 and 2.1.2 is not uniform) and the use of the extreme value theory. In this work, the extreme value theory has been followed: the first step is to extract from the whole observations a series of the maxima (Johnson, Kotz and Balakrishnan 1994), that in this case has proven to be numerous both for wind and for waves. The maxima have been extracted following a coverage and significance criteria, that would allow us to regard those data extracted like real maxima.

Another approach could be performed regarding the goodness of fit choice: a chi-squared test (like the Pearson's one (Johnson, Kotz and Balakrishnan 1994)) instead of a Kolmogorov-Smirnov statistic could be used. The chi-squared test is used to determine whether there is a significant difference between the expected frequencies and the observed frequencies in one or more categories. The reasons that KS statistic has been preferred in our analysis are the selection of categories themselves: the value of the chi-square test statistic is dependent on how the data is binned. There is no optimal choice for the categories' width, since the optimal bin width depends on the distribution (Johnson, Kotz and Balakrishnan 1994).

To get reasonable values, in this work, the bins often require to be combined at the tails of the distributions: this aspect is not present in KS statistic and it depends on the operator intervention. This aspect led us to prefer a search of the lowest distance (indicated by the lowest value of the KS statistic) in the empirical and theoretical CDFs that is being used to obtain the design values.

# Chapter 3
# Wind turbine design

In this chapter, will be presented the path that has led to the wind turbine design chosen to be implemented the mooring analysis. First, an overview of the present and, potential, future Italian energy production from wind is given, along with the possibilities that the country should offer concerning power production from off-shore wind turbines. In this process, the indications by the European and the Italian normative have been considered.
Second, a presentation of the available technologies in the design of floating wind turbine is performed: different projects are being developed around the world with different designs above the sea surface and under. These various design approaches lead to different dimensions of the structure to be assembled at the sites involved: a focus is provided to the construction modalities that lead to specific shape. For this reason, a presentation is given of the main Italian and Mediterranean dry docks, to explore the possibility of an all-around Italian project, starting from the locations to arrive to the construction and operation, and to improve the competition between shipyards.
In the end, is given a comparison between the floating wind turbine technologies and the pros and cons of their realization and operation in the Italian seas, a choice of the most suitable design for the current study has been made.

## 3.1 Italian framework

During the year 2016, the Italian energy production was 289768 GWh, 37.91% (109847 GWh) of which came from renewable sources (Terna n.d.). Wind energy occupied the fourth place among the renewable sources, accounting for a 16% among them, as can be seen in Figure 3.1.

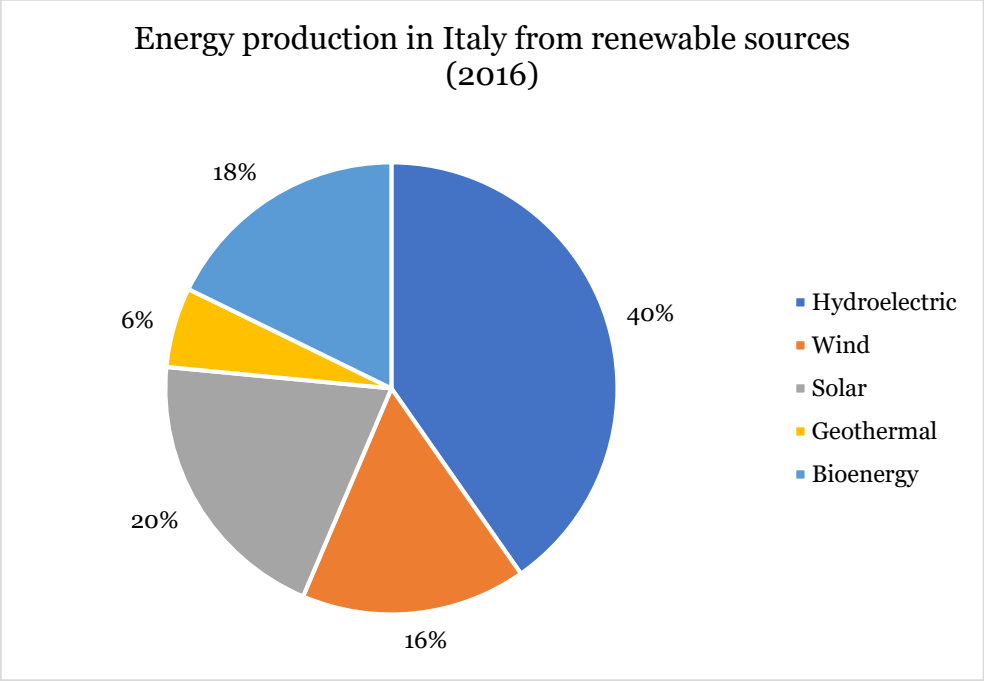


Figure 3.1: energy production in Italy from renewable sources (2016) (Terna n.d.).

Considering the national energy demand, Italy satisfies it with 33.2% of renewable sources (Terna n.d.). This percentage has been calculated computing the imported amount of energy from abroad.

The 2020 target imposed by the European Union with the Renewable Energy Directive, that imposes to Italy to reach a 17% of energy needs by renewable sources (European Union 2014), seems to be reachable, concerning at least electricity. However, in a global viewpoint, Italy must fulfil the Paris agreement: "the Paris Agreement's central aim is to strengthen the global response to the threat of climate change by keeping a global temperature rise this century well below 2 degrees Celsius above pre-industrial levels and to pursue efforts to limit the temperature increase even further to 1.5 degrees Celsius." (UNFCCC 2016). This goal should be reached with National Determined Contributions (NDC), different for each country, considering the greenhouse gases emissions (UNFCCC 2016). Currently Italy occupies the 16$^{th}$ place in the world for $CO_2$ emissions with 389674.86 Ktons emitted in 2013 (European Commission 2014).

Among the power sources, wind produces very little impact on $CO_2$ emissions and it produces many other advantages. During 2016 Italy produced 16 TWh of energy from wind, capable to satisfy 16 million people, avoiding the use of 21 million barrels of oil (11 million tons of $CO_2$) (Associazione Nazionale Energia dal Vento 2017). Wind energy could improve economy too: if 17150 MW of wind power plants were installed in Italy, it would help to increase occupations by 67200 jobs, mostly in the south (Associazione Nazionale Energia dal Vento 2017). Every

year wind power generates 3.5 billion euros of investments and it occupies 26000 people (Associazione Nazionale Energia dal Vento 2017).

The National Energetic Strategy 2017-2020 (Strategia Energetica Nazionale) pushes in the renewable energy direction: it "furtherly promotes the diffusion of renewable technologies with low emissions [...]. Italy, concerning its positions, has at its disposal a huge potential to exploit to reach the EU targets" (Ministero dello Sviluppo Economico 2017).

Offshore wind turbines could be a part of the strategy: the European Wind Energy Association (EWEA), in a 2013 report, states that "that by 2020, 40 GW offshore wind capacity could be operational in European waters, producing 148 TWh, provided that the right framework conditions are in place. This is enough to power the equivalent of 39 million households. By 2020 offshore wind will represent 30% of the new installation annual wind market." (European Wind Energy Association 2013). The same reports state that the Mediterranean Sea could exploit the 8% of that potential, 3.2 GW (European Wind Energy Association 2013). A part of the potential, 950 MW, could be in Italy, providing 1200 jobs (Associazione Nazionale Energia dal Vento 2017).

While the future seems promising, the reality presents a different scenario: traditionally Italy has been a territory with a scarce will to build wind power plants with the main opposition regarding landscape impact (La Stampa 2014). The offshore power plants, while with a lower impact, are currently following this path: during the past years 15 projects have been presented and none has been completed (Legambiente 2015). For all the projects presented, authorizations problems arose, even with a positive environmental impact assessment: administrative appeals, vetoes from Ministry of Cultural Heritage and various commissions, problems with Regions and local Authorities (Legambiente 2015). Only one project is currently under realization in Taranto: a traditional off-shore plant capable of 30 MW in front of the port (Corriere di Taranto 2017).

Italy, even with a great potential in off-shore wind energy production and the need to fulfil international agreements, struggles to invest in new, clean and reliable energy sources: the only ongoing project passed through a maze made of bureaucracy and it seems that every new proposal could have the same fate.

New projects concerning the floating wind turbine could avoid partially these contrasts, since they are built away from coastline, off sight, in areas already interested by off-shore structures like oil platforms (Legambiente 2015). These structures have also a limited impact on the environment, not only avoiding environmental problems but creating a biodiversity zones in the mooring area too (Lindeboom, et al. 2011). Despite the many advantages and the Italian potential, currently no floating wind turbine projects are being developed in the country.

# 3.2 Floating wind turbine's concepts

The passage between a traditional off-shore structure, with piles and foundations directly into the sea bed, to a floating wind turbine is based on the water depth. Different characteristics and solutions had been found and applied dividing the water level in three main zones: shallow (less than 20 meters deep), transitional (between 20 and 50 meters) and deep (greater than 50 meters) (Roddier, et al. 2011) as shown in Figure 3.2.

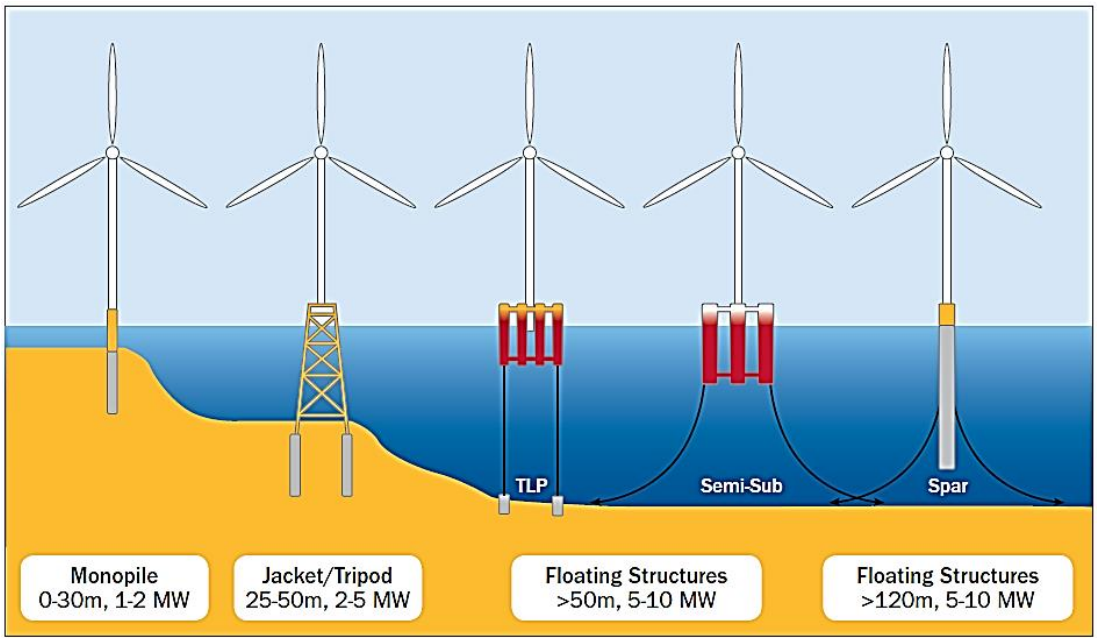


Figure 3.2: off-shore wind turbine designs (Roddier, et al. 2011).

Considering off-shore wind farm, currently, three main technologies, inspired by off-shore oil platforms, are applied for foundations and mooring, recalling the EWEA definitions (European Wind Energy Association 2013):

1. spar buoy: a very large cylindrical buoy stabilises the wind turbine using ballast. The centre of gravity is much lower in the water than the centre of buoyancy. Whereas the lower parts of the structure are heavy, the upper parts are usually empty elements near the surface, raising the centre of buoyancy;
2. Tension Leg Platform (TLP): a very buoyant structure is semi submerged. Tensioned mooring lines are attached to it and anchored on the seabed to add buoyancy and stability;
3. semi-submersible: combining the main principles of the two previous designs, a semi submerged structure is added to reach the necessary stability.

In all categories, the challenge is the stability (Roddier, et al. 2011): wind turbines have a large mass in the nacelle and in the rotor, structures 80-100 meters above the sea surface. Several

industries are developing projects that face that challenge in different approaches, which consider both logistical and economical approaches.

Taking a spar buoy, it's possible to use current technologies concerning wind turbine, but the depth necessary to the stability cannot be less than 120 meters (Roddier, et al. 2011) and the installation must be performed in a sheltered area: these factors can preclude a large portion of locations considering depth and weather. The semi-submersible design can be more flexible: it uses too the current technologies in wind turbines, but the structure can be assembled in a dry dock and towed to destination for its high stability in different conditions. The required depth is also less significant than the one needed for a spar. Considering a TLP, it's possible to use the same technologies in the matter of the turbine like the previous one, but the project can be difficult to assess (Roddier, et al. 2011): a similar natural frequency can be present between the wind turbine and the tendons of a TLP, this system requires expensive stability devices when it's not moored and a sea bed preparation, that can increase significantly the cost, if needed. Furthermore, when the project is developed in an area with less than 100 meters depth, tide must be considered: finding a location free of significant tides could be limiting and challenging.

A selection of the preliminary ongoing projects can be seen in Table 3.1, with details about the country origin, the construction year and the technology used. Further details, like power installed, manufactures and dimensions, are given in the following paragraphs for the most prominent project for each floating concept, ready or almost ready to be used in commercial operations (Hywind, WindFloat and PelaStar).

| Name | Origin | Year | Technology |
|---|---|---|---|
| Hywind | Norway | 2009 | Spar buoy |
| WindFloat | Portugal | 2011 | Semi-submersible |
| Blue H TLP | Netherlands | 2015 | TLP |
| WINFLO | France | 2013 | Semi-submersible |
| PelaStar | United States | 2011 | TLP |
| Sway | Norway | 2007 | Spar |
| VertiWind | France | 2011 | Semi-submersible |

Table 3.1: ongoing floating wind turbine projects (European Wind Energy Association 2013) and (Roddier, et al. 2011).

### 3.2.1 Hywind

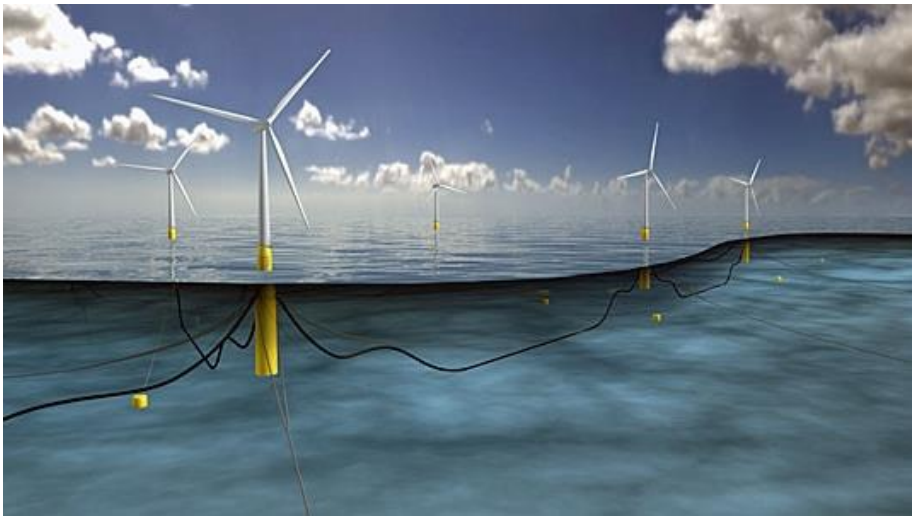

Figure 3.3: Hywind representation (Statoil n.d.).

| | Hywind (prototype, 2009) | Hywind Scotland (commercial, 2017) |
|---|---|---|
| **Location** | Karmøy, NO | Buchan Deep, UK |
| **Turbine capacity** | 2.3 MW | 6 MW |
| **Mass** | 5300 ton | 11200 ton |
| **Draught** | 100 m | 78 m |
| **Hub height** | 65 m | 98 m |
| **Water depth** | 220 m | 105 m |
| **Substructure diameter** | 8.3 m | 14.4 m |
| **Rotor diameter** | 85 m | 154 m |
| **Type of floater** | Spar buoy | Spar Buoy |

Table 3.2: Hywind design parameters (Statoil n.d.).

Hywind is a project made by Statoil in Norway, started in 2009, and it is "a floating wind turbine design based on a single floating cylindrical spar buoy moored by cables or chains to the sea bed. Its substructure is ballasted so that the entire construction floats upright." (Statoil n.d.). The spar buoy floater objective is to minimize the area subjected to wave load and it also reduces the construction costs. The mooring system is composed of three cables that connect the hull to the sea bed. These cables prevent excessive rotation around the vertical axes and they are designed with redundancy: they have enough strength to keep the structure in position even with a cable failure. The substructures and the turbines are separately assembled onshore, then the substructure is put in vertical position and towed to the assembly site where a crane finally fixes the turbine. The combination of substructure and turbine is then towed to the final location. After 8 years of testing, the Hywind project demonstrated its value and

Statoil invested 2 billion Norwegian kroner to build the first floating wind farm in Scotland: it consists of 5 turbines with an installed capacity of 30 MW, capable to power around 22000 homes, and the export cable to the mainland is 30 km (Statoil n.d.).

### 3.2.2 WindFloat

Figure 3.4: WindFloat representation (Roddier, et al. 2011).

| | **Windfloat (prototype, 2011)** | **Winfloat** (Roddier, et al. 2011) | **Windfloat Pacific (project, 2017)** |
|---|---|---|---|
| **Location** | Aguçadoura, PT | - | Coos Bay, US |
| **Turbine capacity** | 2 MW | 5 MW | 6 MW |
| **Mass** | 2800 ton | 4640 ton | 6000 ton |
| **Draught** | 13.7 m | 17 m | 18 m |
| **Tower height** | 56 m | 86 m | 88 m |
| **Operational water depth** | 40 m | 40 m | 40 m |
| **Column height** | 23.2 m | 27 m | 27.5 m |
| **Column diameter** | 8.2 m | 10 m | 10.5 m |
| **Column centre to centre** | 38 m | 46 m | 50 m |
| **Water entrapment plate edge** | 12 m | 15 m | 13.2 m |
| **Minimum width** | 53.7 m | 65.8 m | 66.2 m |
| **Maximum width** | 62 m | 76 m | 76.4 m |
| **Rotor diameter** | 80 m | 126 m | 154 m |
| **Type of floater** | Semi-sub | Semi-sub | Semi-sub |

Table 3.3: WindFloat design parameters (Bureau of Ocean Energy Management 2014) and (Priciple Power n.d.).

The WindFloat design is composed by a semi-submersible floater with plates at the base of each column. The subsea metal plates allow to improve dynamic stability, while maintaining shallow draft, by lowering wave and turbine induced motion utilizing a tri-column triangular structure with the wind turbine positioned on one of the three columns (Roddier, et al. 2011). The triangular structure leads to different dimensions regarding the width, when the plate edges and the triangular orientation are considered, for further details about the structure refer to Figure 3.5 and Figure 3.6.

Figure 3.5: WindFloat hull and turbine (Roddier, et al. 2011).

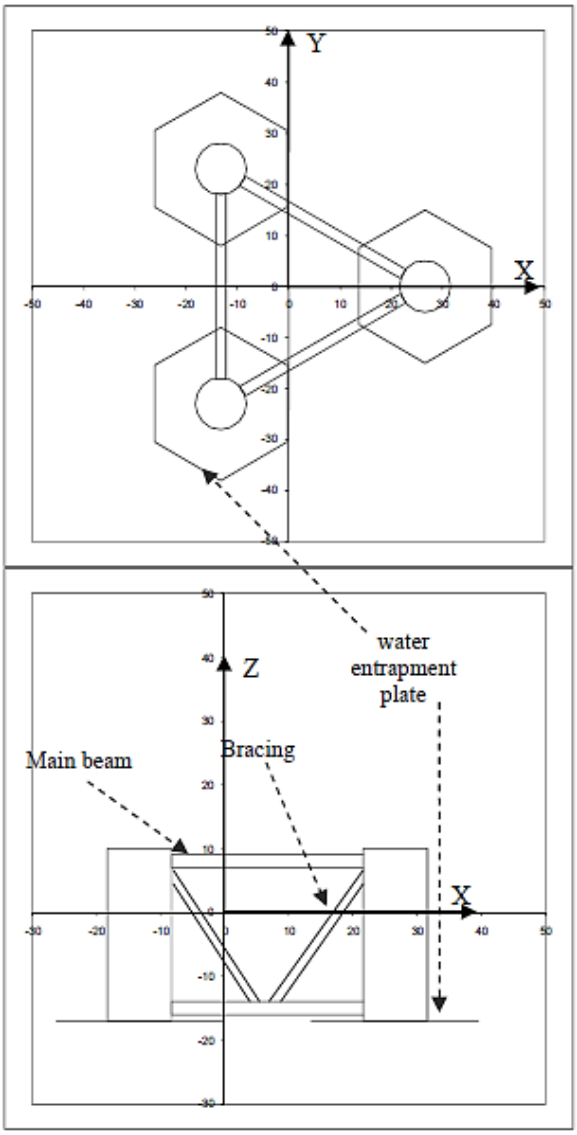


Figure 3.6: [top] top view of Windfloat and [bottom] elevation with the waterline at Z = 0 m (Roddier, et al. 2011).

The mooring system employs conventional components such as chain and polyester lines to minimise cost and complexity, allowing flexibility in the site choosing. Using pre-laid drag embedded anchors, site preparation and impact is reduced. The WindFloat design allows the structure to be built on-shore and then towed to destination, allowing to not consider weather in the construction process like with a spar buoy (Priciple Power n.d.). A prototype was installed in 2011 by Principle Power off the Portuguese coast and it was tested during the following five years: this procedure proved that the technology is valid and ready to be developed in commercial projects (Priciple Power n.d.). After the prototype decommissioning in 2016, several projects are being developed all around the world: Windfloat Pacific in the United Stated, Windfloat Atlantic in Portugal, Les Eoliennes Flottantes du Golfe du Lion in France and Windfloat Japan (Priciple Power n.d.). The projects are following the same pattern:

a 24 MW wind farm composed by four 6 MW turbine, with expected commissioning by the end of 2017 or beginning 2018 (Priciple Power n.d.).

### 3.2.3 Pelastar

Figure 3.7: PelaStar representation (Glosten 2012).

| | **PelaStar** (Glosten 2012) |
|---|---|
| **Location** | - |
| **Turbine capacity** | 6 MW |
| **Mass** | 1400 ton |
| **Draught** | 22 m |
| **Hub height** | 100 m |
| **Water depth** | 50-200 m |
| **Substructure diameter** | 25 m |
| **Rotor diameter** | 150 m |
| **Type of floater** | TLP |

Figure 3.8: PelaStar design parameters (Glosten 2012).

PelaStar is a Tension Leg Platform foundation system developed by Glosten that can be coupled with existing offshore wind turbines. This TLP concept has a large buoyancy held to the sea bed by tension cables: these solutions allow to reduce the total weight and to increase the overall turbine stability, reducing the overturning moment. No TLP prototype has been yet deployed, but PelaStar is certainly the most advanced study in this field. A study has been commissioned by the Energy Technologies Institute (UK), coupling the foundation with a General Electric Heliade 150 6 MW turbine with the purpose to develop a full-scale demonstrator, facing a commercial debut in the mid-20s (Glosten 2012). The demonstrator realization in the United Kingdom has been scraped, due to delays in planning and authorization, and currently Glosten is in search for a test site to realize the 6 MW prototype during 2018 (Glosten 2012). The construction can be done on-shore and then the structure can be towed into position or transported using special ships. Compared to a spar or a semi-submerged technology and facing the limitations previously quoted, TLP is not ready yet for a commercial use.

## 3.3 Construction aspect

Different approaches mean different construction techniques: spar buoys are constructed horizontally at a yard or in a dock and the turbine and the submersible structure are separately built in the ports (Roddier, et al. 2011). However, for the final assembly this solution requires heavy crane vessels and a spot in the sea with favourable weather and sea condition during the whole time of the upending procedure (Roddier, et al. 2011). In addition, spar buoys, once assembled, need a consistent sea depth for the towing in their final position, considered their large draft (Roddier, et al. 2011).

Figure 3.9: Hywind final assembly in a fjord near Stord, Norway, summer 2017 (Statoil n.d.).

Semi-submersible structures take huge advantages in the construction process: they can be built and assembled completely in dry docks, using conventional structures already present in the ports like heavy-lifting cranes: in this way, the tubular base and the turbines could be assembled and coupled. Then, the shipyard's dock can be flooded and the structures, considering their low draft, can be towed to their destination with simple tug boats. On the other hand, semi-submersible structures require big dry docks to be assembled, a condition that it's not often satisfied, refer to 3.3.1 for the requirements.

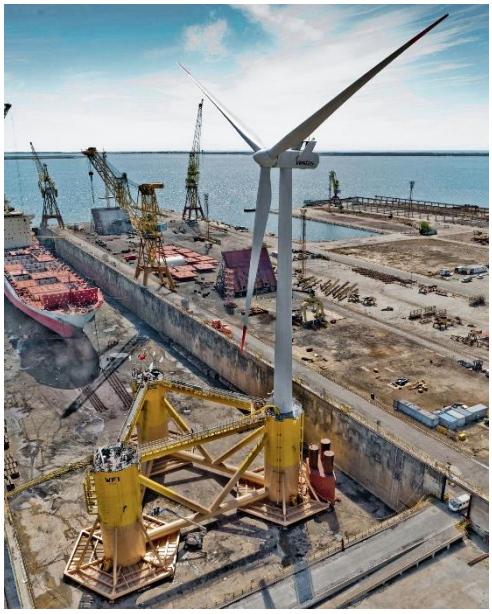

Figure 3.10: WindFloat assembly in a dry dock, Portugal (Priciple Power n.d.).

TLP structures are assembled in a port, like the semi-submersible one, requiring in the meantime less space in the dry dock: the steel-made base is thereafter coupled with a traditional wind turbine in the shipyard. After the construction, the structure can be towed to destination or be transported using special barges. The installation, however, requires specific vessels to keep in a steady position the structure and to connect it to the tendons and it must be performed with good weather and sea conditions (Roddier, et al. 2011). The required draft in case of towing is higher than for a semi-submersible structure (Roddier, et al. 2011).

The construction parameters of the analysed solutions are summarized in Table 3.4.

| | **Assembly** | **Vessel** | **Draft** |
|---|---|---|---|
| **Spar buoy** | Off-shore | Special floating cranes<br>Tug boats | High |
| **Semi-submersible** | In a dock | Tug boats | Low |
| **TLP** | In a dock | Tug boats/barges<br>Specific installation vessels | Medium |

Table 3.4: floating wind turbine construction summary.

Dry docks have a great part in the construction of the previous structures, especially for semi-submersibles and TLPs: the possibility of the realization of a possible floating wind turbine project in Italy has been explored first collecting and comparing the dimension of the Italian dry docks. To improve the number of suitable construction sites and to create competition between shipyards, similar information has been searched and collected in the Mediterranean area.

### 3.3.1 Dry docks in Italy

Dry docks in Italy are well distributed all around the peninsula in the main commercial ports. There is the presence of both graving and floating basins. In general, the structures are owned by the State that gives in concession the use of them to a variety of companies for ship buildings and maintenance.

Spar buoys and TLP structure do not require extreme dimensions for construction in the dry docks: the first technology is assembled off-shore, coupling the turbine with the underwater pile, and the second requires a width wider than 25 meters, considering the PelaStar design (Glosten 2012). Different considerations are made regarding at a semi-submersible structure: the width required for the structure stability in way bigger than the other technologies, at least 54 meters, considering the WindFloat prototype (Priciple Power n.d.).

To find a suitable location for construction, information about the dry docks wider than 25 meters have been collected and they are shown, with other characteristics like cranes and lifting capacity (for floating basins), in Table 3.5, ordered by decreasing width. The port locations, in relation to the study zones, are shown in Figure 3.11.

| Location | Name | Length | Width | Depth | Annex structures | Source |
|---|---|---|---|---|---|---|
| Palermo | Graving dock 4 | 370 m | 68 m | 11.35 m | Crane (x2): 120 ton<br>Crane (x2): 20 ton | (Fincantieri 2010) |
| Livorno | Accosto 77 | 350 m | 56 m | 9.7 m | Crane (x3): 20 ton<br>Crane (x1): 90 ton | (Porto di livorno n.d.) |
| Trieste | Graving dock 4 | 295 m | 56 m | 11 m | Crane (x2): 60 ton<br>Crane (x2): 10 ton | (Fincantieri 2010) |
| Palermo | Floating dock 3 | 286 m | 46.2 m | 4 m | Lifting: 52000 ton<br>Crane (x3): 15 ton | (Fincantieri 2010) |

| | | | | | | |
|---|---|---|---|---|---|---|
| Livorno | Bacino Azimuth | 180 m | 42 m | 2.4 m | | (Porto di livorno n.d.) |
| Genova | Dry dock 4 | 267 m | 40 m | 11.5 m | Crane (x1): 10 ton<br>Crane (x1): 40 ton | (Ente bacini di Genova n.d.) |
| Napoli | Dry dock 3 | 335 m | 40 m | 10.6 m | | (Cantieri del Mediterraneo n.d.) |
| Genova | Dry dock 5 | 249 m | 38 m | 8.7 m | Crane (x1): 10 ton<br>Crane (x1): 30 ton | (Ente bacini di Genova n.d.) |
| La Spezia | Dock 1 (floating) | 246.4 m | 38 m | 9.5 m | Lifting: 40000 ton<br>Crane (x2): 12 ton | (Fincantieri 2010) |
| Napoli | Dry dock 5 | 227 m | 35 m | 7 m | | (Cantieri del Mediterraneo n.d.) |
| Palermo | Floating dock 2 | 193 m | 30.18 m | 3.1 m | Lifting: 19000<br>Crane (x2): 8 ton | (Fincantieri 2010) |
| Genova | Dry dock 3 | 200 m | 30 m | 9.1 m | Crane (x1): 10 ton<br>Crane (x1): 20 ton | (Ente bacini di Genova n.d.) |
| Trieste | Graving dock 4 | 206 m | 28.6 m | 6 m | Crane (x2): 10 ton<br>Crane (x2): 60 ton | (Fincantieri 2010) |
| Ravenna | | 180 m | 27 m | 5 m | Crane (x1): 12 ton<br>Crane (x2): 25 ton<br>Crane (x1): 40 ton<br>Crane (x1): 60 ton<br>Crane (x1): 75 ton | (Naviravenna n.d.) |

Table 3.5: Italian dry docks (width > 25 m) parameters, by decreasing width.

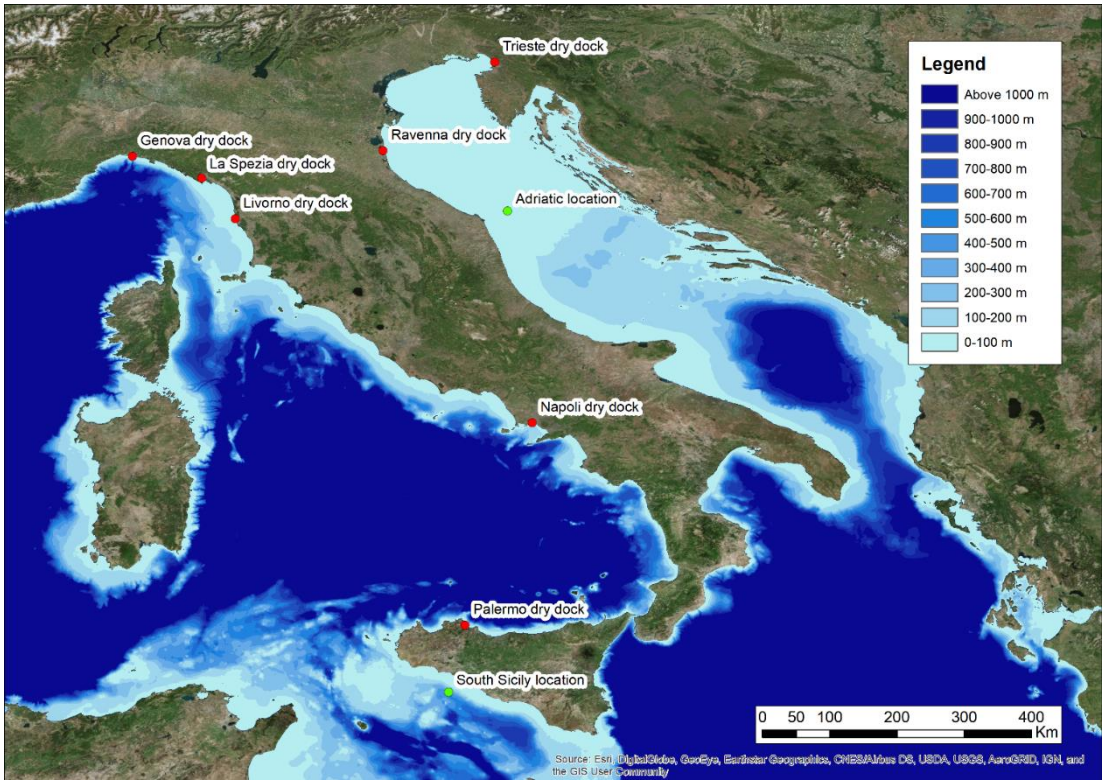


Figure 3.11: dry docks location in relation with study areas.

## 3.3.2 Dry docks in the Mediterranean area

Like for Italy, in the Mediterranean area the main dry docks are positioned in the principal commercial ports of the Sea. The criterion was the same used in 3.3.1 to find suitable places for the construction, along with suitable industrial and technological knowledge. The structures' details are collected in Table 3.6, ordered by decreasing width. The port locations, in relation to the study zones, are shown in Figure 3.12.

| Location | Country | Name | Length | Width | Depth | Annex structures | Source |
|---|---|---|---|---|---|---|---|
| Marseille | France | Forme 10 | 465 m | 85 m | 9.2 m | Crane (x1): 50 ton<br>Crane (x1): 150 ton<br>Crane (x1): 40 ton | (Marseille port n.d.) |
| Skaramagas | Greece | Dock 1 | 421 m | 75 m | 5.5 m | | (Hellenic Shipyards n.d.) |
| Valletta | Malta | Graving dock 6 | 362 m | 62 m | 9.3 m | Crane (x1): 30 ton<br>Crane (x2): 40 ton | (Palumbo n.d.) |

| | | | | | | | |
|---|---|---|---|---|---|---|---|
| | | | | | | Crane (x1): 150 ton | |
| Skaramagas | Greece | Dock 2 | 335 m | 53.6 m | 7.9 m | | (Hellenic Shipyards n.d.) |
| Marseille | France | Forme 8 | 320 m | 53 m | 11.7 m | Crane (x1): 50 ton<br>Crane (x1): 150 ton<br>Crane (x1): 40 ton | (Marseille port n.d.) |
| Rijeka | Croatia | Dock 11 | 261.7 m | 53 m | 9.5 m | Crane (x2): 18 ton<br>Crane (x1): 25 ton | (Viktor Lenac Shipyards n.d.) |
| Toulon | France | Grand bassins Vauban | 422 m | 40.7 m | | | (Structurae n.d.) |
| Toulon | France | Grand bassins Vauban | 422 m | 40.7 m | | | (Structurae n.d.) |
| Valletta | Malta | Graving dock 4 | 262 m | 40 m | 8.53 m | Crane (x2): 5 ton<br>Crane (x1): 10 ton<br>Crane (x1): 50 ton | (Palumbo n.d.) |
| Marseille | France | Forme 9 | 250 m | 37 m | 7.7 m | Crane (x1): 50 ton<br>Crane (x1): 150 ton<br>Crane (x1): 40 ton | (Marseille port n.d.) |
| Skaramagas | Greece | Floating dock 1 | 252 m | 37 m | 8.5 m | Lifting: 33000 ton | (Hellenic Shipyards n.d.) |
| Valletta | Malta | Graving dock 7 | 98 m | 35 m | 3.03 m | Crane (x1): 20 ton | (Palumbo n.d.) |
| Barcelona | Spain | Dry dock | 215 m | 35 m | 6.5 m | | (Port de Barcelona n.d.) |
| Skaramagas | Greece | Floating dock 2 | 232 m | 34 m | 6 m | Lifting: 20000 ton | (Hellenic Shipyards n.d.) |
| Rijeka | Croatia | Dock 5 | 201.5 m | 33.8 m | 6 m | Crane (x2): 15 ton | (Viktor Lenac Shipyards n.d.) |

| | | | | | | | |
|---|---|---|---|---|---|---|---|
| Skaramagas | Greece | Floating dock 3 | 196 m | 32 m | 6.5 m | Lifting: 9000 ton | (Hellenic Shipyards n.d.) |
| Valletta | Malta | Graving dock 5 | 216 m | 27.4 m | 8.53 m | Crane (x2): 5 ton<br>Crane (x1): 10 ton<br>Crane (x1): 50 ton | (Palumbo n.d.) |
| Valletta | Malta | Graving dock 2 | 164.1 m | 25 m | 8.83 m | Crane (x3): 5 ton | (Palumbo n.d.) |

Table 3.6: Mediterranean dry docks (width > 25 m) parameters, by decreasing width.


Figure 3.12: Mediterranean dry docks location in relation with study areas.

# 3.4 Floater choice

In the floater choice, four main factors have been considered: the structural dimensions, the building structure, the sea depth and phase of development of the technology.

TLP structures are still in a testing phase, with prototypes yet to be built to demonstrate the project validity, furthermore there are computational difficulties regarding tides, tendons natural frequency and sea bed preparation. For these factors, the installation process could be very difficult and this technology has been rejected in this work.

The two remaining technologies (spar buoy and semi-submersible structure) are already in the commercial phase, with a Hywind plant built in 2017 and several WindFloat farms in the commissioning phase. The technologies have been proven reliable and ready with a series of testing in the past years, the differences are in the structural dimensions and in the

construction procedures: spar buoys have a simple design that allows serial production and smaller dimensions, but they are constrained to deep waters due to the large draft (that can also limit the repair possibility in ports) and they require large vessels and heavy cranes to be assembled off-shore in a location with favourable weather. To build Hywind Scotland, Statoil assembled the turbines in a sheltered area in a fjord near Stord in Norway, using Saipem 7000 floating crane (world second largest vessel of its kind, Figure 3.9) and then the finished turbines were towed to their destination (Statoil n.d.).

Semi-submersible structures take advantages in the location flexibility and in the assembling procedures: the low draft makes them able to operate in shallow waters and for this reason they are eligible for in port construction and repairs, with simple tug vessels to tow them. However, they are complex structure to assembly and they can have large dimensions that would limit the port availability to construction and maintenance.

Considering the construction factors, the Italian ports, the sea depths and the will to explore the possibility of an Italian project from the inception to the realization, a decision to choose a semi-submersible structure has been made.

The presence of shallow waters and the assembly process led to exclude the possibility of a spar buoy: this technology would exclude almost the entire Adriatic Sea for its shallow depth and, not considering the need of large crane vessels and good weather, the draft would exclude the towing in the Mediterranean Sea between Tunisia and Sicily and in the sea part between Tuscany and Corse for the same reason. The only limiting factor for a semi-submersible structure in the Italian environment is the dry dock, with its dimensions: considering the Italian ports (Table 3.5) and the smallest WindFloat dimension (Table 3.3), only three ports are eligible for the construction, Palermo, Livorno and Trieste. The ports choice reduces to Palermo only if highest turbine powers are needed. However, the advantage of this choice is multiple: the towing process to location would not be limited by draft or sea depth or specific vessels need and the on-shore construction and maintenance process is simpler than the one required for spar buoy. For example, considering the Palermo dry dock and the ideal 5 MW WindFloat (Roddier, et al. 2011), at the same time four semi-submersible structure can be built in the same shipyard, with conventional cranes and techniques.

For the realization of a semi-submersible structure, a selection of EU shipyards is available, and an Italian construction is possible: the larger availability of dry docks means increasing the competition between companies. This aspect could lead to lower prices in the whole construction process. Considering the smallest WindFloat measurement requirements, three shipyards are available in Marseille, Skaramagas and Valletta. This addition to the number of construction sites increases the number of available construction sites to six: if the highest-powered turbines are going to be built, the choice reduces to Palermo, Marseille and Skaramagas. The eligible Italian and EU ports for construction and the towing distance to the location of the study are shown in Figure 3.13 and Figure 3.14.

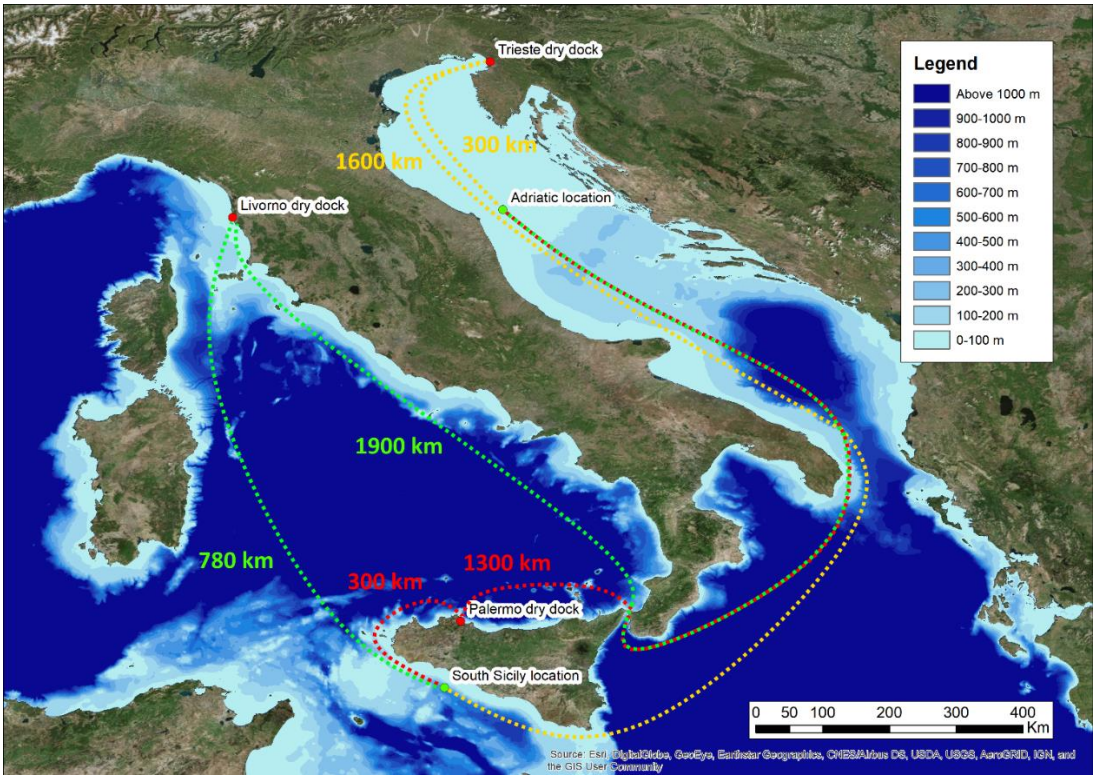


Figure 3.13: Italian ports for a WindFloat design construction and towing distances to the study locations.

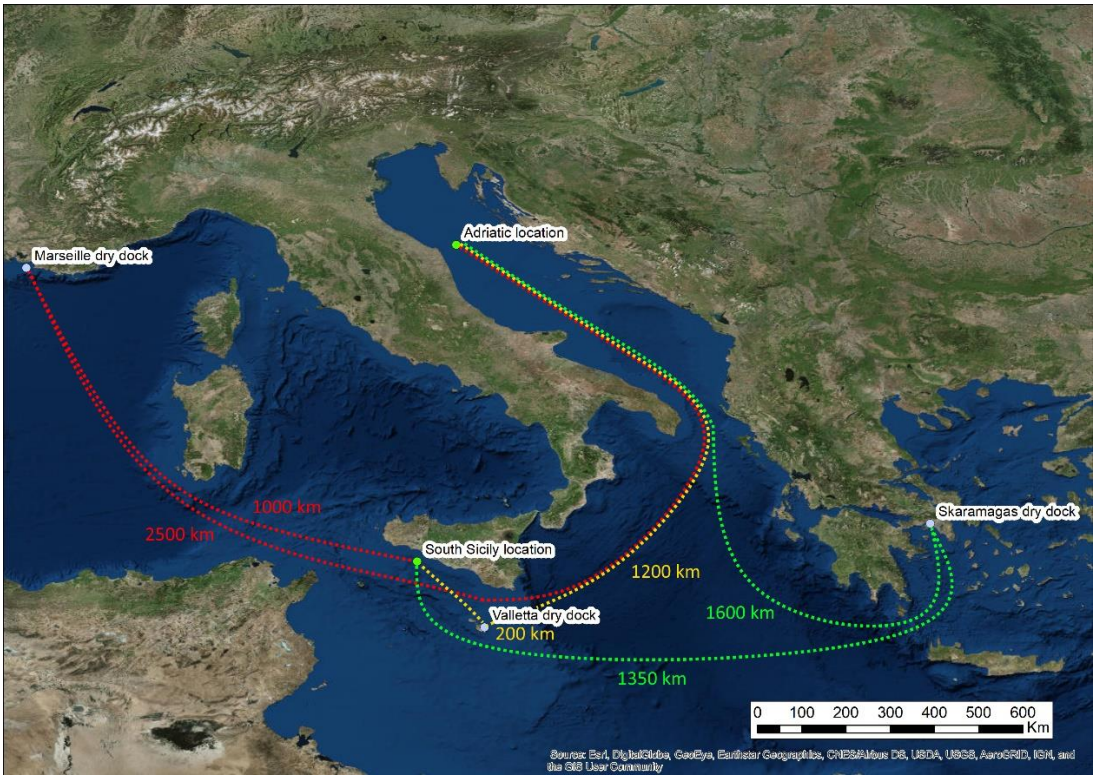


Figure 3.14: eligible EU ports for a WindFloat design construction and towing distances to the study locations.

# Chapter 4
# Mooring

In this chapter, a general description of the moorings systems will be given: starting from the characteristics required in terms of duration and sea conditions, describing in detail the current mooring types and the forces which they are subjected to. Then, the design procedures are explained, underlying the differences between the static, the quasi-static and the dynamic approach. In the end, a description of the mooring components is given: both the wires and the hardware that connects them to the sea bed are covered, explaining the pro and cons of each solution and the field of use.

A general mooring system is required for a floating offshore platform to fix its position at a predetermined location and to limit its movements under the typical (i.e. normal service load) and extreme sea conditions (i.e. ultimate state condition). It "consists of freely hanging lines connecting the surface platform to anchors, or piles, on the seabed, positioned at some distance from the platform" (Chakrabarti 2015).

Over the years, steel chains, steel wires and synthetic ropes have been used to connect floating objects to the sea bed: the lines compose a catenary shape, that acts on its tension (increasing or decreasing it as the catenary lifts off or lays on the sea bed) to stabilize the platform subjected to sea forces. The catenary mooring system has been deployed with success in shallow waters. With the need to exploit resources in deep waters, the suspended weight of the lines is becoming a limiting factor (Gudmestad 2015): steel chains are currently less used in deep water applications, now being replaced by synthetic fibre ropes, that are reducing the wire length, the overall tension and the total costs (Chakrabarti 2015). However, this solution, compared to the traditional steel chains, is rather recent and it lacks extensive test data (Chakrabarti 2015).

Mooring systems must find a balance between the need to avoid excessive forces acting on the platform and the requirement to stiffness necessary to withstand the sea conditions and to avoid damage to the structure. This compromise is rather easily achievable for medium depths, but it becomes harder to find as the water depth increases (Chakrabarti 2015).

Recently, dynamic thrusters have been used to improve the moorings systems, especially in oil production platforms, but this is not the case of a floating wind turbine, that must be easy to build and easy to manage as well as being cost effective.

# 4.1 Characteristics

Numerous industrial standards and requirements are to be fulfilled when mooring systems are considered. Among them can be listed (Chakrabarti 2015):

- offset limitations;
- lifetime before replacement;
- installability;
- positioning ability.

The focus on which requirement is needed more than other ones depends on the floater: the design return period can vary from 50 to 100 years, the resistance in a storm can be higher or lower, the design lifetime of the components can be higher than 10 years or lower and a fatigue analysis can be required or not (Chakrabarti 2015).
Other variables can be related to the environmental conditions: arctic conditions can be challenging and soft sea beds can cause that a line is stuck that creates additional forces (Gudmestad 2015).

# 4.2 Line types

Two main line types are currently deployed in the sea: a traditional and tested catenary line and a rather new taut synthetic line. In this paragraph is presented how they works, describing the forces that the systems are dealing with, and their advantages or disadvantages.

## 4.2.1 Catenary lines

In Figure 4.1 is represented a catenary line that connects the sea bed (point B) to a submerged point on a vessel (point A). Some dimensional clarification for Figure 4.1: part of the line is laying on the sea bed and, usually, the horizontal dimension, a, is 5-20 times higher than the vertical dimension, b (Chakrabarti 2015).

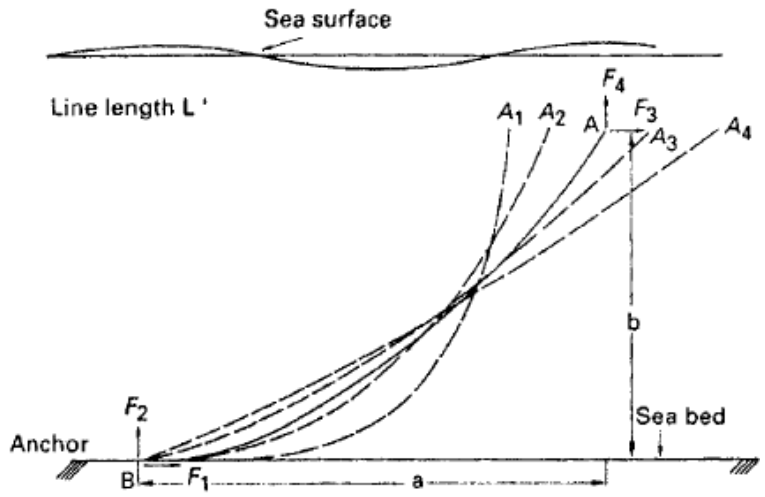


Figure 4.1: catenary mooring line (Chakrabarti 2015).

When the floater is moving horizontally, the point A shifts from $A_1$ to $A_4$, the part of the catenary that is on the sea bed reduces its length arriving to none at $A_4$. Since the tension is proportional to the part of the chain suspended, the progressive increasing of the catenary part suspended increases the overall tension (Chakrabarti 2015).

The line's behaviour can be described by the catenary equations, obtaining the tension and shape: these equations are developed using a mooring line represented in Figure 4.2. Some assumptions have been made: horizontal sea bed and ignored bending stiffness. The forces acting on a single element of the catenary are represented in Figure 4.3.

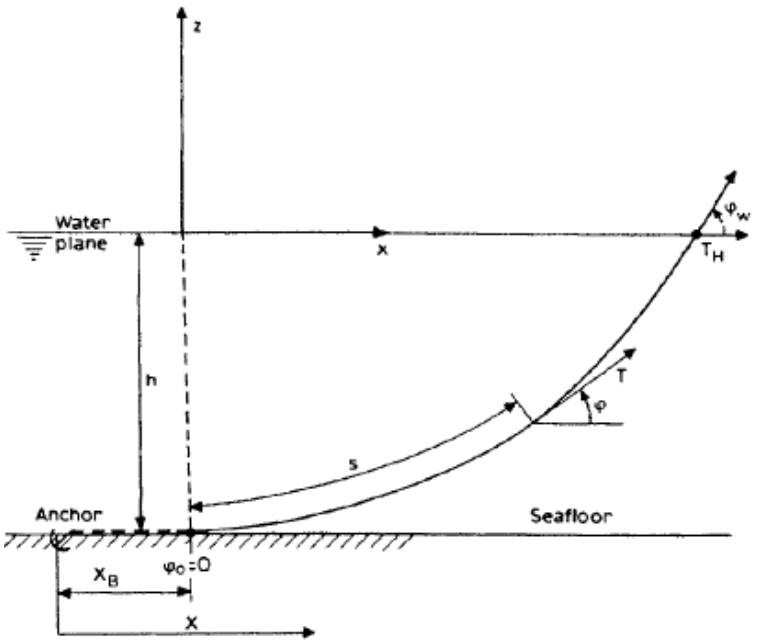


Figure 4.2: catenary mooring line considered in the equations (Chakrabarti 2015).

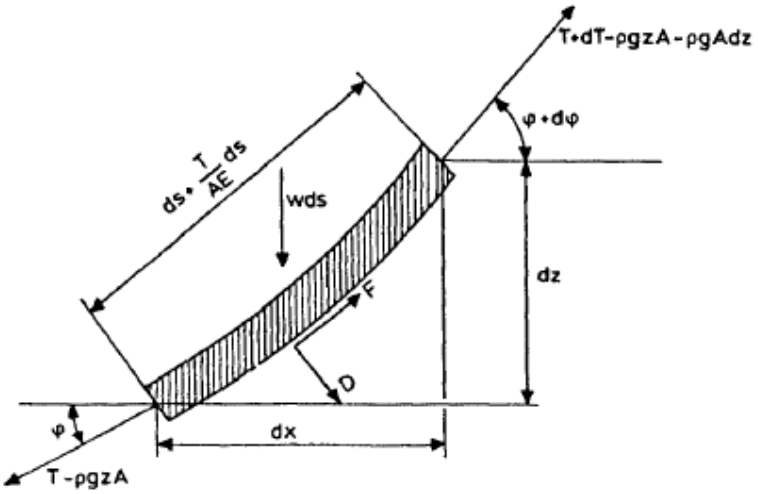


Figure 4.3: forces acting on a single element of the catenary (w: line weight per unit length; T: line tension; A: area of the cross-section; E: elastic modulus) (Chakrabarti 2015).

Referring to Figure 4.3 and considering that the mean hydrodynamic forces on the element are given by D and F per unit length, we get:

$$dT - \rho g A dz = \left[w \sin\phi - F\left(\frac{T}{EA}\right)\right] ds \quad (4.1)$$

$$T d\phi - \rho g A z d\phi = \left[w \cos\phi + D\left(1 + \frac{T}{EA}\right)\right] ds \quad (4.2)$$

Ignoring the forces F and D can lead to the equations' simplification and we obtain the suspended line length s and the vertical dimension h:

$$s = \left(\frac{T_H}{w}\right) \sinh\left(\frac{wx}{T_H}\right) \quad (4.3)$$

$$h = \left(\frac{T_H}{w}\right)\left[\cosh\left(\frac{wx}{T_H}\right) - 1\right] \quad (4.4)$$

Obtaining the tension in the line at the top, written in function of the depth d:

$$T = \frac{w(s^2 + d^2)}{2d} \quad (4.5)$$

## 4.2.2 Synthetic lines

As said in the previous paragraphs, in deep water conditions the mooring system are relying more and more on synthetic fibre lines. This decision is taken due to the many advantages that this type of mooring has over traditional catenary systems: the lines are considerably lighter, more flexible and they can absorb dynamic motions through extension without causing excessive tension (Chakrabarti 2015). Another significant advantage can be seen in Figure 4.4: a reduction of the line length and of the space occupied on the seabed.

The disadvantages in the synthetic lines come from the material mechanical properties: they are more complex and less observed in action than a catenary line. This factor could lead to

overconservative designs that frustrate a part of the advantages, in the name of safety (Chakrabarti 2015).

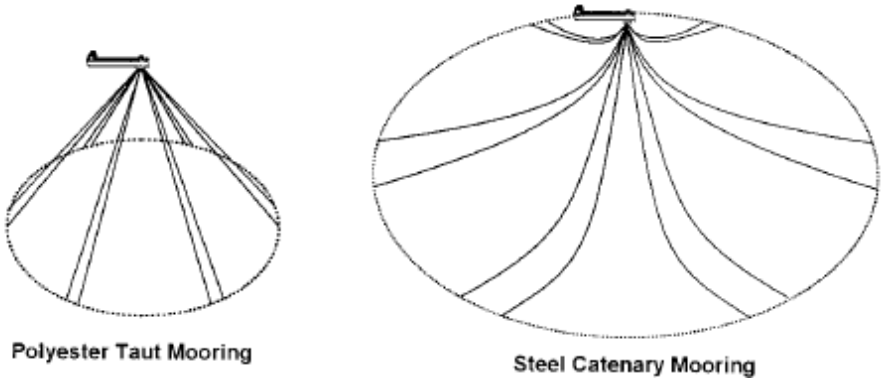


Figure 4.4: comparison between polyester and catenary mooring (Chakrabarti 2015).

Numerical models should be implemented when dealing with synthetic ropes and they must consider several parameters like the ones listed (Chakrabarti 2015):

- stiffness: the elongation of the fibre ropes allows them to extend 1.2 to 20 times as much as steel, the stiffness is not constant but varies with the loading conditions and the age of the material;
- hysteresis and heat build-up: a cycle of loading induces energy in the wire that is dissipated through heat that comes is addition to the one produced by friction; this could be a problem with large diameters that do not allow an efficient heat dissipation;
- fatigue: in certain points (especially the terminations) the rope present compression instead of tension; this factor could lead to damage to the fibres, endangering the whole mooring system;
- other issues: with equal diameters, the strength of a synthetic fibre rope is about half of a steel rope; the creep behaviour must be considered; and the fibre could be cut by sharp objects and fish bites.

# 4.3 Forces

Several forces act on a moored object (Chakrabarti 2015): for a constant weather condition, in the design process, the current forces are considered temporally constant with variation with depth in direction and profile. Wind loads also are considered constant, while wave forces produce motions of the structure in all six degrees of freedom: surge, sway, heave, roll, pitch and yaw. This scheme of forces can be seen in Figure 4.5.

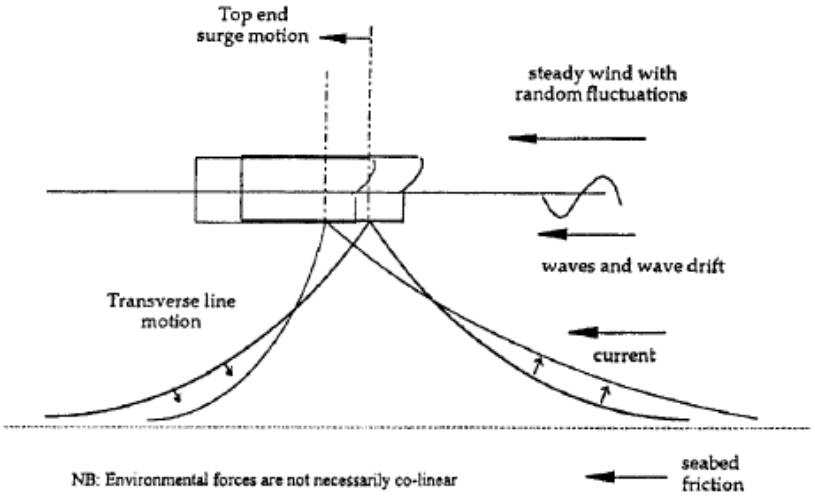


Figure 4.5: forces acting on a moored object with catenary lines (Chakrabarti 2015).

Drifting of the object in the horizontal plane could cause high loads on the mooring lines: the forces are increased if the object is not heading against the wave direction. This occurs because "the frequency of the drift forces results in translations that usually correspond to the natural frequency of the vessel restrained by the mooring system. Consequently, it is essential to quantify the level of damping in the system, as this quantity controls the resonant motion amplitude." (Chakrabarti 2015).

Many damping forces acts on the floating object and the moorings (Chakrabarti 2015), that increases with large waves and strong winds and currents:

- wind damping: caused by the frictional drag between air and the object, the effects are small;
- viscous flow damping: caused by currents and the slow object motion;
- hydrodynamic drag damping: a relatively small horizontal translation of the object can result in transverse motion over the centre section of the line that can be several times larger than the object translation itself;
- line internal damping: friction between components could lead to an increase of the total damping;
- sea bed interaction: soil friction leads to reduced tension fluctuations in the ground portion of line effectively increasing the line stiffness.

Furthermore:

- vortex-induced vibration: vortex formations could increase the in-line drag forces, it's considered negligible for chains.

# 4.4 Design

In this section, the available design approaches for a catenary mooring system are presented, underlining the differences and the outcomes. Static, quasi-static and dynamic designs are different ways to obtain a result that must be confronted with standards of safety and strength, in relation to the environment. The last sub-paragraph presents the mooring spread or the positioning of the mooring lines around a floating object.

## 4.4.1 Static design

This approach often is the first step on the project of a mooring system (Chakrabarti 2015): the forces acting on a single line are determined ignoring the interactions with fluids.
This outcome is obtained through the equations described in 4.2.1 to get the forces acting on the object from each line, known the coordinates on the vessel and on the seabed and the lengths and elasticity. The forces are then summed to obtain the resultant horizontal and vertical restoring forces on the object: the most excited line is then found displacing the object through prescribed horizontal drifting caused by environmental action.
Some simplifications applied: it's often assumed that it is necessary that the part of the line on the sea bed has no vertical forces at the anchor, otherwise the overall length must be incremented. After having checked this, the load of the most stressed line is compared with a prescribed breaking strength, if it's too high some changes must be made: change the material, the positioning and repeating the calculation. After finding the complete system, a new computation must be made in case of failure of the most stressed line.
The disadvantages of this method are evident (Chakrabarti 2015): it is over-conservative and large safety factors are required to face the hypothesis made; also, significant dynamic parameters are ignored.

## 4.4.2 Quasi-static design

This procedure is more difficult to perform than the static one and it presents two different approaches (Chakrabarti 2015):

1. time domain simulation: it performs the simulation considering the forces acting on the object at their frequency, but considers the wind and current forces as steady, using the mooring stiffness curve without considering line dynamics;
2. frequency response method: the mooring stiffness curve is treated as linear and low-frequency dynamic responses to both wave drift and wind gust effects are calculated as if for a linear single degree of freedom system.

The main difference between the static and quasi-static method is that the equations of motion are integrated in a time domain (Chakrabarti 2015).

### 4.4.3 Dynamic design

The dynamic analysis is the most complete and used tool in the design of mooring systems and it provide the most reliable outcomes (Chakrabarti 2015).
It begins with a static configuration with non-linear time domain solutions: the lines are decomposed into a large number of elements and, in general, the object's motion is computed separately from the line dynamics. This is an over-simplification in deep water, in which the mutual interaction in very important in the result (Chakrabarti 2015).
Compared to static and quasi-static methods, the dynamic analysis considers the interaction between line, object and fluids (Chakrabarti 2015).
This analysis is, on the other hand, computationally intensive and it presents some difficulties (Chakrabarti 2015):

- time steps must be small so that wave-induced line oscillations are included;
- runs must be long to allow for the object drift oscillation period, which in deep water may be of the order of 5 min;
- for a typical floating object mooring system design, the weather is multi-directional and a number of test cases must be considered.

### 4.4.4 Mooring spread

Mooring spread could be symmetrical or asymmetrical: even if the first choice is the simplest in terms of design, it could not be the best in terms of performance. Some considerations must be made (Chakrabarti 2015):

- directionality of the weather: if the weather actions come from a dominant direction, it could be useful to use an asymmetrical mooring system to balance those forces;
- directionality of the currents: the same consideration of the directionality of the weather can be made for currents, an asymmetrical mooring system can balance the forces applied by strong currents
- subsea spatial layout: equipment positioned on the sea bed could restrict the available positions for the moorings;
- other space restriction: it could be useful to couple moorings lines to gain further space.

Figure 4.6 shows a representation of several mooring patterns, symmetrical and asymmetrical.

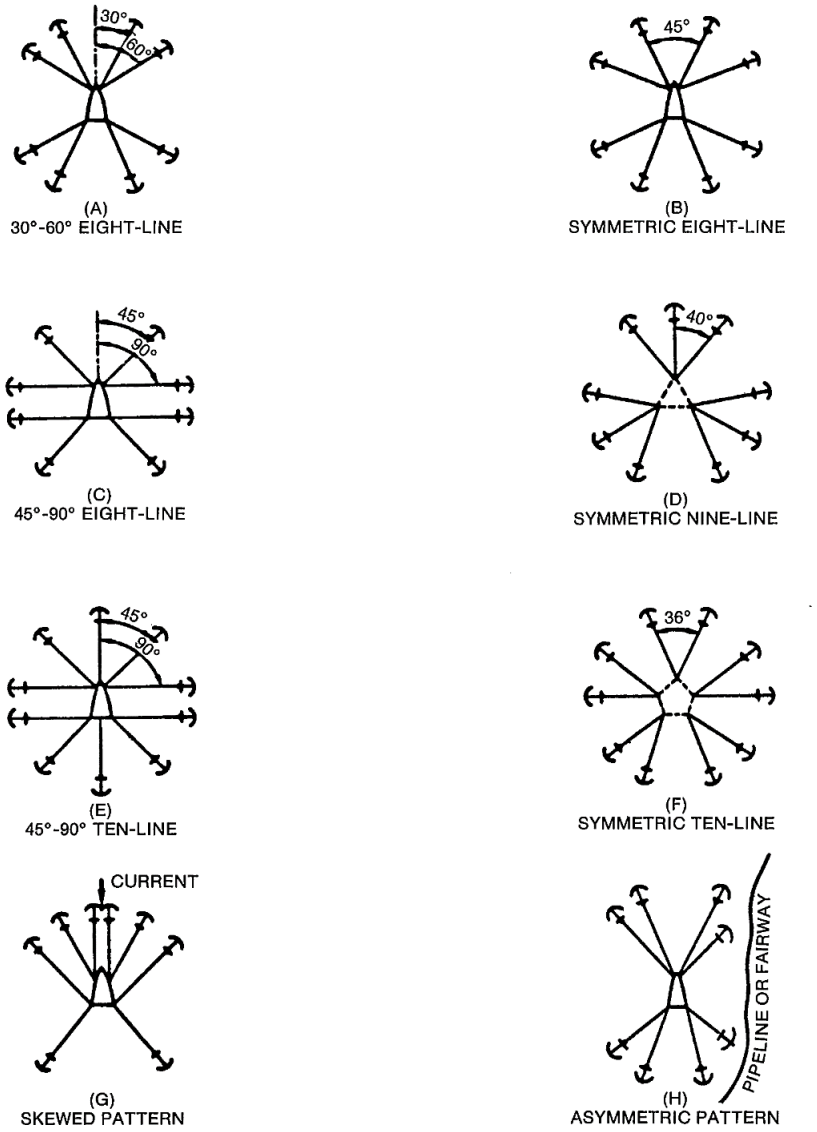


Figure 4.6: mooring patterns (American Petroleum Institute 1987).

# 4.5 Components

In general, several parts compose a mooring system and they can be listed as (Chakrabarti 2015): chain, wire, ropes, anchors, turrets, winches, power supplies and riggings. In the following paragraphs, the main components of a mooring system for a floating wind turbine are described in detail: this hardware and its combinations are going to be numerically modelled in Orcaflex for the analysis.

## 4.5.1 Chain

Chains could provide the necessary strength in a mooring system as described previously. Two main construction approaches are currently used (Chakrabarti 2015) and they can be seen in Figure 4.7: stud-link chain, in shallow waters, and stud-less chain, used recently in deep waters.

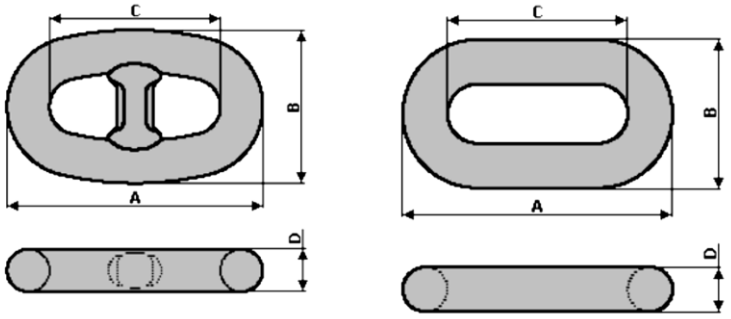


(a) Stud-Link (b) Studless Chain

Figure 4.7: (a) stud-link and (b) studless chain (Chakrabarti 2015).

The first approach is widely used and it is strong, reliable and easy to handle (Chakrabarti 2015): the studs provide stability to the chain and they ease the positioning.

The second approach removes the studs (Chakrabarti 2015): this action provides weight reduction and it increases the chain fatigue life, while the handling is harder.

Chains can be produced in several grades, which are characterized by a different strength (American Petroleum Institute 1987): grade 4 (R4) is the highest grade available, but different specifications can be made in different operational scenarios.

## 4.5.2 Synthetic lines

The main alternative to the use of the chains is to employ synthetic lines, which can be made with different materials: nylon, polyester, polypropylene, Kevlar and polyethylene.

The outer part of the ropes is designed in order to minimize the disadvantages quoted in 4.2.2: an external jacket protects the inner core against corrosion, frictions and fish bites while dissipating the heat and maintaining the flexibility and lightness.

The realization of a synthetic line consists of individual wires wound in a helical pattern to form a “strand”. The pitch of the helix determines the flexibility and axial stiffness of the strand. The composition of a wire is shown in Figure 4.8 while the main industrial constructions can be seen in Figure 4.9.

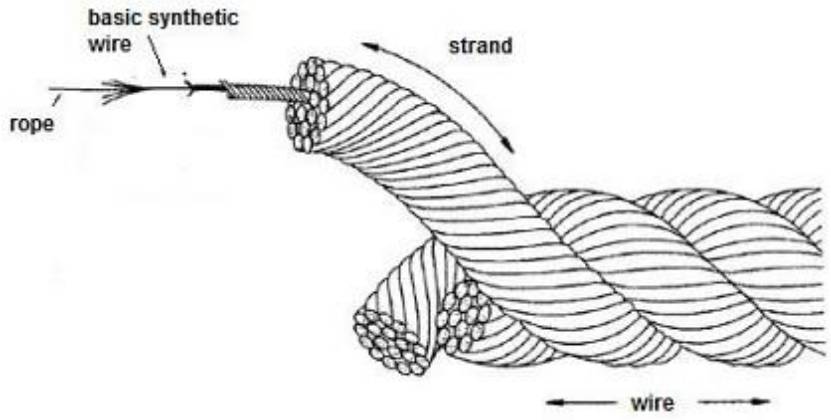


Figure 4.8: synthetic wire composition (American Bureau of Shipping 1999).

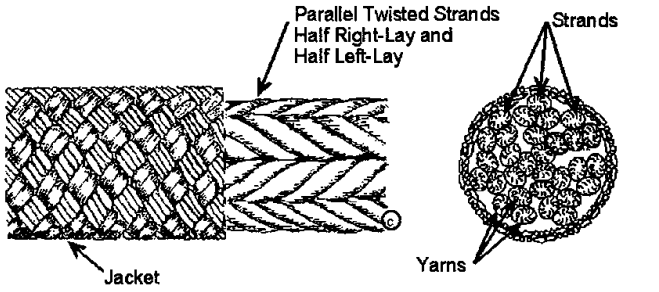


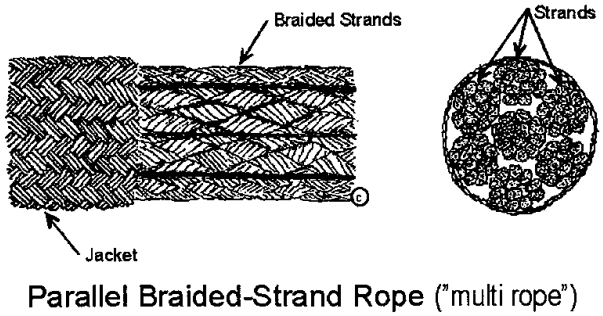


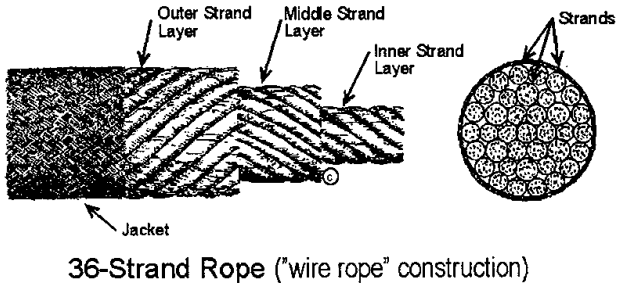


Figure 4.9: typical synthetic rope constructions (American Bureau of Shipping 1999).

## 4.5.3 Wire rope

Wire ropes are very similar to synthetic lines and they are constructed in the same way, except for the materials (Chakrabarti 2015): three main typologies can be used, spiral strand, six strand and multi-strand ropes and they can be seen in Figure 4.10.

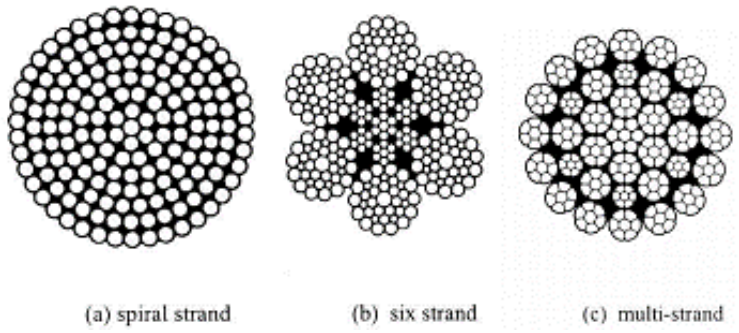


Figure 4.10: wire ropes construction, (a) spiral strand, (b) six strand, (c) multi-strand (Chakrabarti 2015).

Multi-strand wire ropes may contain either a fibre or a metallic core. The core is important for support of the outer wires, especially on a drum, and in some applications to absorb shock loading. Fibre core (FC) ropes are not generally used for heavy duty marine applications. Metallic core ropes may be one of the two types: independent wire rope core (IWRC) or wire-strand core (WSC). IWRC is the most common core filling for heavy marine applications.

## 4.5.4 Anchors

Two main types of anchors are available (Chakrabarti 2015): the first relies on self-weight to keep the final part of the mooring still, the second is based on suction forces.
The traditional anchors' holding capacity is generated by one or more dead weights providing friction between the sea bed and the anchor itself: the holding power depends strongly on the weight and on the materials of the sea bed. An example can be seen in Figure 4.11.

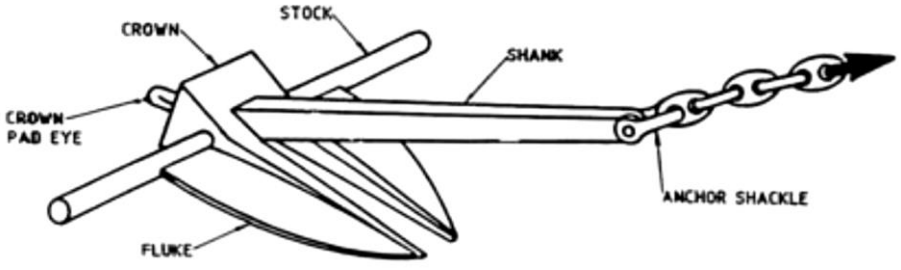


Figure 4.11: drag anchor (Chakrabarti 2015).

In the suction anchors, horizontal and vertical holding capacity is generated by pushing a pile mechanically or from the pressure difference into the ground (Chakrabarti 2015). This

technique provides friction along the length of the pile in contact with the material composing the sea bed. A representation and the installation process can be seen in Figure 4.12.

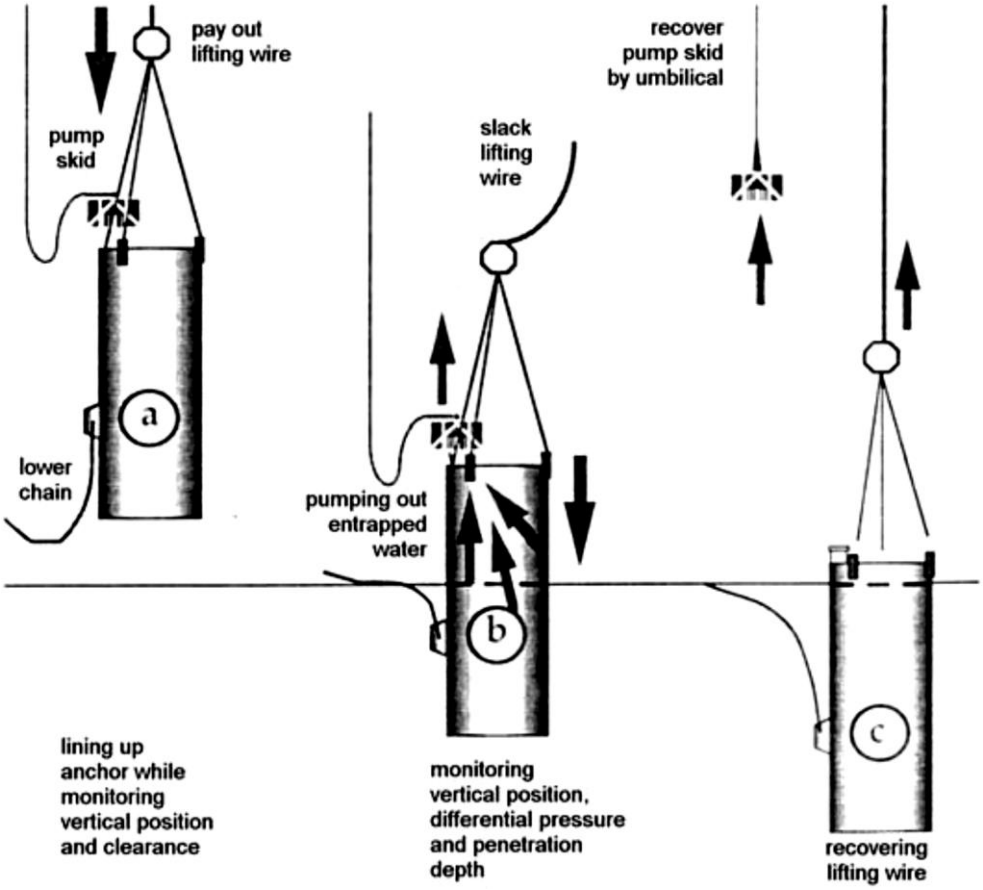


Figure 4.12: suction anchor installation sequence (Chakrabarti 2015).

# Chapter 5
# Mooring modelling

In this chapter, will be presented the mooring modelling in the two areas of the study, offshore south Sicily and in the Adriatic Sea, performed with the commercial software OrcaFlex, developed by Orcina (Orcina n.d.).

The mathematical model of the real-world system is built using the various modelling capabilities provided by OrcaFlex (Orcina n.d.) and the equations that rule it are explained in the first paragraph of this chapter. The model consists of the marine environment to which the system is subjected, the wind turbine floater, the mooring lines, the anchors placed in the environment and their connection. The objects in the model represent the structures being analysed and the environment determines the wind load and wave excitation to which the objects are subjected.

After that, the simulation conditions are given: it is explained how the environment of the two areas of the study has been recreated in terms of water depth, waves representation with JONSWAP spectrum, wind characteristics and time of the simulation, distinguishing the different return periods of 50 and 100 years.

Then, a description of the implemented floater is given, which includes the realization of the chosen WindFloat design with all its characteristics like columns, connections and water entrapment plates. Alongside, is explained how the floater reacts to external excitation like waves and wind: its response to waves is provided through the Response Amplitude Operator (RAO) and the wind response is implemented in the software using the areas subjected to the wind forces and specifying the application point on the structure.

The mooring characteristics are then explained: traditional anchors and suction anchors have been represented into the model. Different solutions concerning the mooring lines have been explored: chains, chains with synthetic fibres and synthetic fibres only. The first two cases led to a catenary design for the wires and in the last one the possibility of a taut mooring has been tested. Dimensions and the material's parameters are given considering the environmental differences between locations.

In the end, the results of the simulations are presented: static and dynamic. The first provides the equilibrium position of the system and the starting point for the dynamic simulation, in which are applied the wave loads. In the static results, the vertical component of the forces at the anchor is analysed to obtain a starting parameter for a possible design for the anchor itself. Concerning the suction anchor, is explored a way to reduce this force, increasing the horizontal mooring spread, and a comparison of the same forces is made between synthetic ropes for the taut mooring design and traditional chains.
In the dynamic simulations, both the wires and at the anchors, are analysed for the two values of the return period. In every simulation, the most stressed point in every wire is identified and it is then subjected to an extreme statistical analysis to find a reference value concerning the tension for two storms with durations of 3 and 6 hours, respectively. Focus has also been put on the forces at the anchors: if the difference in the values is significant between static and dynamic simulations (like for suction anchors), the same statistical computation is applied to find a design value for vertical forces for every anchor subjected to storms with the same duration as the ones used for the tension analysis.
Finally, a discussion of the results is given, comparing mooring length, footprint, tension and vertical forces at the anchors, along with a proposal of a mooring solutions for the locations of the study.

# 5.1 Mathematical model

In the present work, numerical modelling uses mathematical models to describe the physical conditions of the marine scenarios using numbers and equations. In this way, objects and their interactions are represented, over a period of time, under predetermined environmental conditions.
OrcaFlex uses several frames of reference, each of which consists of a reference origin and a set of axes directions, to represent different coordinate systems (Orcina n.d.). Firstly, there is one global frame of reference, G. The reference origin is the global origin and GX, GY and GZ are the global axes directions. For the local coordinate systems for each type of object, typically the origin is at a selected fixed point on the object and the axes are in particular fixed directions, such as the surge, sway and heave directions for a vessel. A representation of the references frames is given in Figure 5.1.

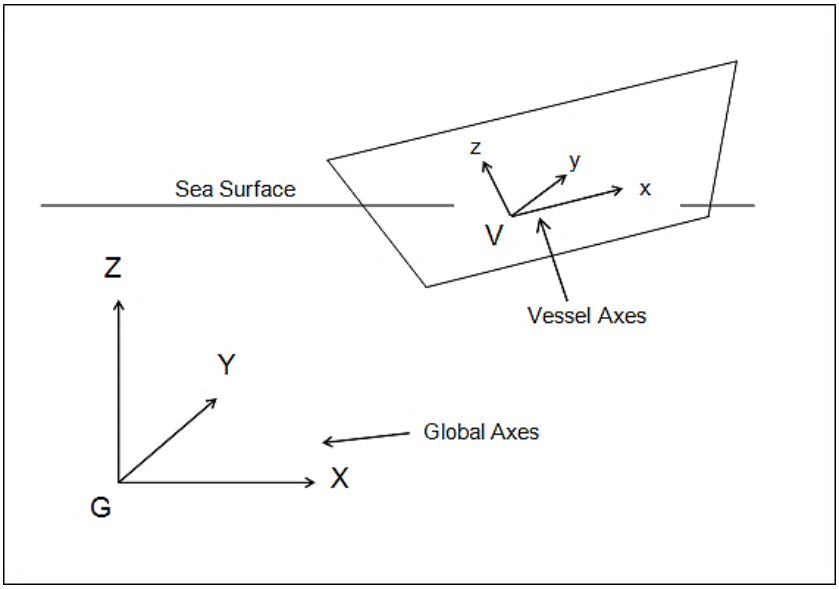


Figure 5.1: OrcaFlex coordinate systems (Orcina n.d.).

The modelled system is composed by the environment, the floater coupled with the wind turbine and the moorings. The environment defines the conditions to which the objects in the model are subjected: it consists of the sea, waves, seabed and wind (Orcina n.d.). For further details about the modelled variables refer to Figure 5.2 and 5.2.

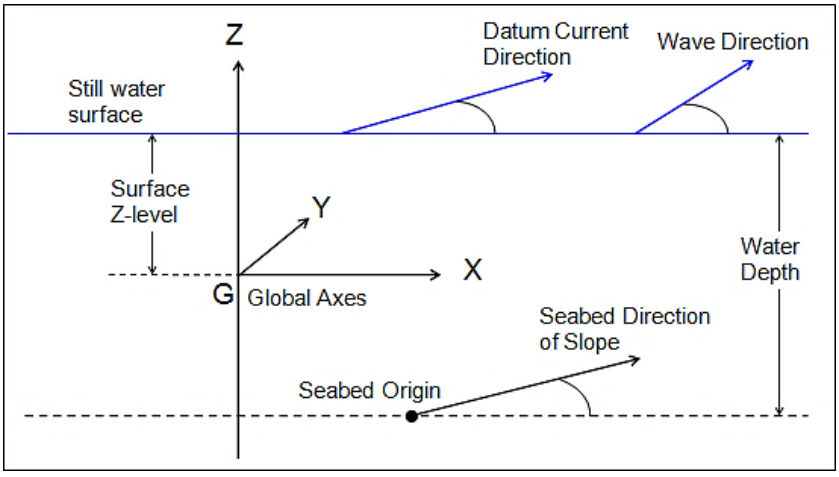


Figure 5.2: environment modelling in OrcaFlex (Orcina n.d.).

To represent the floater system, a vessel has been used in OrcaFlex: OrcaFlex vessels are primarily intended to model rigid bodies that are large enough for wave diffraction to be significant, such as floating platforms. In this situation, the vessel motion is based on RAOs. More details are given in 5.3.

The moorings are modelled through lines (Orcina n.d.): lines are flexible linear elements used to model cables, hoses, chains or other similar items. Lines are represented in OrcaFlex by a lumped mass model. That is, the line is modelled as a series of lumps (Orcina n.d.) of mass joined together by massless springs. The lumps of mass are called nodes and the springs

joining them are called segments. Each segment represents a short piece of the line, whose properties (mass, buoyancy, drag etc.) have been lumped, for modelling purposes, at the nodes at its ends, Figure 5.3.

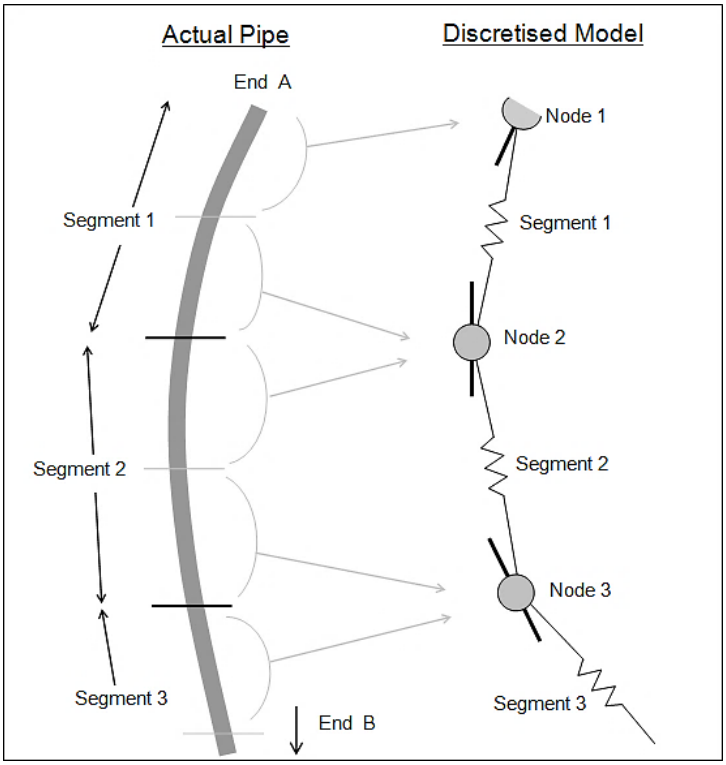


Figure 5.3: OrcaFlex line model (Orcina n.d.).

Referring to Figure 5.3, for the present model purposes, End A is connected to the vessel and End B is in contact with the sea floor, further details are given in 5.4. OrcaFlex calculates hydrodynamic loads on lines, 3D buoys and 6D buoys using an extended form of Morison's equation (Orcina n.d.): there are two force components, one related to water particle acceleration, the inertia force, and one related to water particle velocity, the drag force. The extended form of Morison's equation used in OrcaFlex is (Orcina n.d.):

$$f = \left(\Delta a_f + C_a \Delta a_r\right) + \frac{1}{2}\rho C_d A v_r |v_r| \qquad (5.1)$$

Where:

- f is the fluid force;
- Δ is the mass of fluid displaced by the body;
- $a_f$ is the fluid acceleration relative to earth;
- $C_a$ is the added mass coefficient for the body;
- $a_r$ is the fluid acceleration relative to the body;
- ρ is the density of water;
- $v_r$ is the fluid velocity relative to the body;
- $C_d$ is the drag coefficient for the body;

- A is the drag area.

The term within round brackets in ( 5.1 ) is the inertia force, the other term is the drag force. The inertia force consists of two parts, one proportional to fluid acceleration relative to earth (the Froude-Krylov component), and one proportional to fluid acceleration relative to the body (the added mass component) (Orcina n.d.). The Froude-Krylov force is the integral over the surface of the body of the pressure in the incident wave, undisturbed by the presence of the body. The added mass component is due to the motion of the body.

The first step of the analysis is the static simulation, in which two objectives are set (Orcina n.d.):

1. to determine the equilibrium configuration of the system under weight, buoyancy, hydrodynamic drag, etc;
2. to provide a starting configuration for dynamic simulation.

Static equilibrium is determined in a series of iterative stages (Orcina n.d.):

1. at the start of the calculation, the initial values of all degrees of freedom are defined by the data;
2. in the line statics, the equilibrium configuration for each line is then calculated;
3. in the whole system statics, the out-of-balance load acting on each free body is then calculated and a new position for the body is estimated.

The second step of the analysis is the dynamic simulation in a time domain, which is fully nonlinear. Mass, damping, stiffness, loading etc. are evaluated at each time step in which the domain is divided, solving the following equation of motion (Orcina n.d.):

$$M(p,a) + C(p,v) + K(p) = F(p,v,t) \qquad (5.2)$$

Where:

- M(p, a) is the system inertia load;
- C(p, v) is the system damping load;
- K(p) is the system stiffness load;
- F(p, v, t) is the external load;
- p, v, a are position, velocity and acceleration respectively;
- t is the time variable.

An implicit time domain integration scheme has been applied (Orcina n.d.): it re-computes the system geometry at every time step and so the simulation takes full account of all geometric nonlinearities, including the spatial variation of both wave loads and contact loads.

At the beginning of the ODEs integration, the initial positions and orientations of all objects in the model, including all nodes in all lines, are known from the static analysis. The forces and moments acting on each free body and node are then calculated. Forces and moments considered include (Orcina n.d.): weight, buoyancy, hydrodynamic and aerodynamic drag, hydrodynamic added mass effects (calculated using ( 5.1 )), tension and shear, bending and

torque, seabed reaction and friction, contact forces with other objects, forces applied by links and winches. The equation of motion (Newton's law) is then formed for each free body and each line node (Orcina n.d.):

$$M(p)a = F(p, v, t) - C(p, v) - K(p) \quad (5.3)$$

This is not the system-wide equation of motion, but a local equation of motion for each free body and each line node: solving each of these equations of motion merely requires the inversion of a 3×3 or 6×6 mass matrix (Orcina n.d.). The system equation of motion is solved at the end of the time step: because p, v and a are unknown at the end of the time step an iterative solution method is required. The position, velocity and acceleration at time step t are $p_t$, $v_t$ and $a_t$ respectively, then for a time step dt, the values at the end of the time step, at time t+dt, are given by:

$$v_{t+dt} = v_t + dta_t \quad (5.4)$$

$$p_{t+dt} = p_t + dtv_{t+dt} \quad (5.5)$$

At the end of each time step, after the iterations, the positions and orientations of all nodes and free bodies are again known and the process is repeated. For details about the static and dynamic simulations implemented in the present work refer to 5.2, 5.5 and 5.6.

# 5.2 Simulation conditions

The simulation conditions comprehend both environmental characteristics and time of the dynamic simulation. For all locations and return periods, the time of the dynamic simulation has been set to 3 hours with constant environmental loads (i.e. we select one value for the wave spectrum and consider the situation during one storm). The integration of the equations of motion of the floater is set with an implicit time domain integration: the system equation of motion is solved at the end of the time step and since position, velocity and acceleration are unknown at the end of the time step an iterative solution method is used (Orcina n.d.). Parameters concerning the time step duration and iteration limitations are set to default.

Concerning the environmental modelling, parameters concerning sea bed, waves and wind are set. The sea bed is considered flat and elastic: The elastic model treats the seabed as a simple elastic in both the seabed normal direction and the seabed shear directions. This gives a seabed normal resistance that is proportional to the penetration, and a seabed lateral resistance that is proportional to the lateral displacement of the contact point from its undisturbed position (Orcina n.d.). The water depths used at the locations of the study are summarised in Table 5.1.

| Location | Depth |
|---|---|
| Adriatic Sea | 100 m |
| South Sicily | 400 m |

Table 5.1: models' water depths for study locations.

Concerning wind and waves, the parameters obtained in Chapter 2 have been used to model these environmental effects, creating simulations with 50 and 100 years return period. To represent waves, a JONSWAP spectrum has been used, specifying spectral wave height, peak period and peak enhancement factor: for more details about the theory and the used parameters refer to 5.2.1 and Appendix D.
Alongside the wind and wave intensity, the directions of both variables have been specified in order to create a worst-case scenario: wind and wave are directed towards the structure, refer to Figure 5.4, perpendicularly to the rotor blades and a side of the triangular floater, to obtain the maximum loads effects on the whole floater.

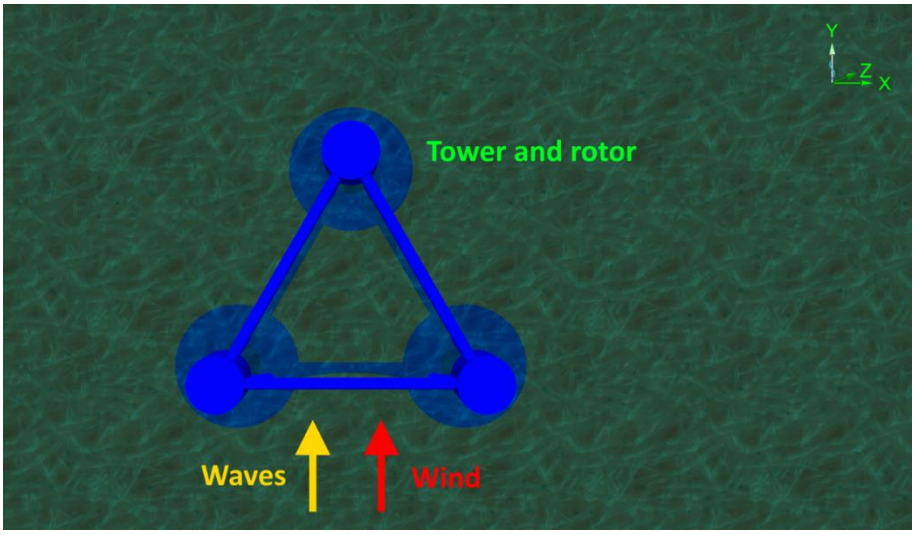


Figure 5.4: wind and waves directions with respect to the floater.

## 5.2.1 JONSWAP spectrum

A wave spectrum is used to define the characteristics of the waves generated by a given wind condition. A wave spectrum consists in a plot of the wave energy density at each component period or frequency versus the range of component periods or frequencies.
In general, the spectrum of the sea surface does not follow any specific mathematical form. However, under certain wind conditions the spectrum does have a specific shape. A series of empirical expressions have been found which can be fit to the spectrum of the sea surface elevation. These are called parametric spectrum models, and are useful for routine engineering applications. In describing these spectra, one or more parameters are needed.
The JONSWAP (Joint North Sea Wave Project) spectrum was developed from wave and wind measurements with sufficient wind duration and provides a fetch limited spectrum. The spectrum gives a relation between wave frequency, wind speed and fetch. The data used to develop the JONSWAP spectrum were collected for relatively light wind conditions, but data collected at higher wind velocities compared reasonably well with this spectral formulation.

Since that no information are available about the fetches in areas considered and the significant wave height and the peak period are known, a decision to use a "partially specified" spectrum has been taken: once specified the known parameters and the calculated peak enhancement factor OrcaFlex calculates the other parameters (Orcina n.d.).
The JONSWAP spectrum may be expressed as (Holthuijsen 2010):

$$S(f) = \frac{\alpha g^2}{(2\pi)^4 f^5} exp\left[-\frac{5}{4}\left(\frac{f}{f_P}\right)^{-4}\right] \gamma^{exp\left[-\frac{(f-f_P)^2}{2\sigma^2 f_P^2}\right]} \quad (5.6)$$

With (Holthuijsen 2010):

- $\sigma = \sigma_1 = 0.07$ if $f \leq f_P$
- $\sigma = \sigma_2 = 0.09$ if $f > f_P$

$$\gamma = 4.42\left(\frac{f_p U_{10}}{g}\right)^{\frac{3}{7}} \quad (5.7)$$

Where $\alpha$ is the modified Philips constant, $\sigma$ is the spectral width parameter, $\gamma$ is the peak enhancement factor, $f_P$ is the frequency at the spectral peak, $U_{10}$ is the wind speed at 10 meters above the sea surface.
The spectra and their associated parameters are shown in Appendix D.

## 5.3 Floater model

The WindFloat floater has been modelled in OrcaFlex through the use of a vessel, a rigid body subjected to a motion due to wind and waves: the dimensions concerning each element are the same as the one shown in Table 3.3. Motion derived from waves is governed by the Response Amplitude Operator, which is an engineering statistic, or set of such statistics, that are used to determine the likely behaviour of a ship or a floating platform when operating at sea (Orcina n.d.). More details about the used RAO are given in 5.3.1.
The wind loads are proportional to the area exposed to the wind flow and the wind speed, which is considered constant in this study, refer to 5.3.2 for more details.
The vessel has been modelled like an equilateral triangle which has, on the top, the effective representation of the WindFloat structure: a series of elastic shapes, which in Orcaflex are simple 3-dimensional geometric objects, used to model physical obstacles. Elastic solids are intended only for modelling the overall limitation on movement that a physical barrier presents (Orcina n.d.). Those solids are anchored to the vessel and they move according to the vessel's motion.
Two-dimensional and three-dimensional representations of the floater are given in Figure 5.5, Figure 5.6 and Figure 5.7.

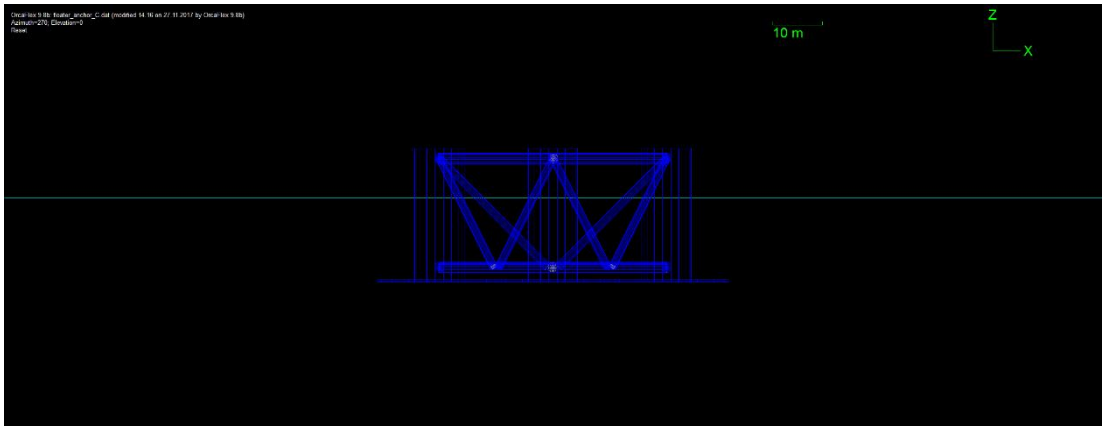


Figure 5.5: 2D floater representation.

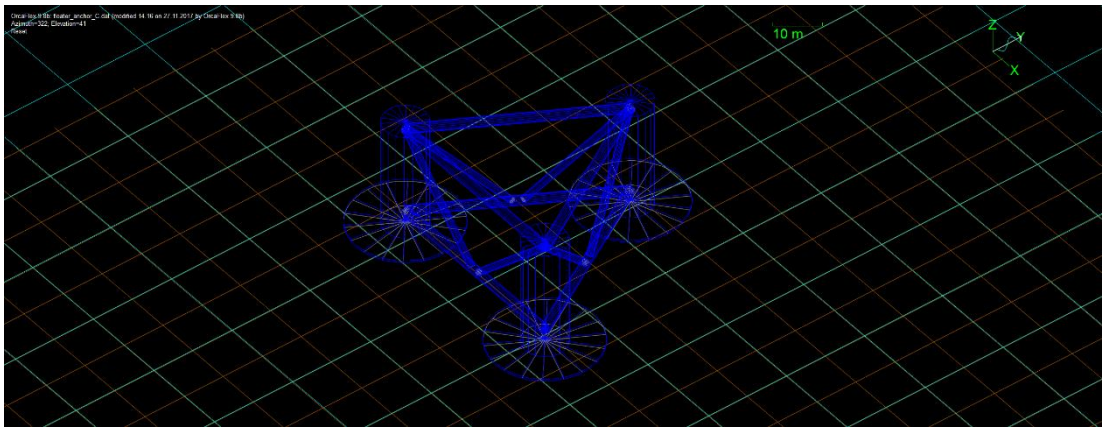


Figure 5.6: 3D floater representation.

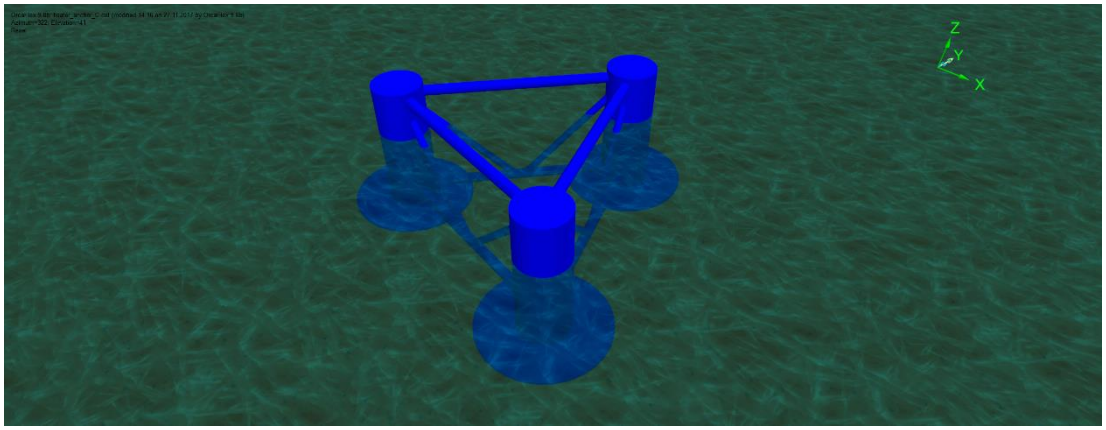


Figure 5.7: enhanced 3D floater representation.

### 5.3.1 Response Amplitude Operator

RAOs are effectively transfer functions used to determine the effect that a sea state will have upon the motion of a ship through the water.

Each RAO consists of a pair of numbers that define the vessel response, for one particular degree of freedom, to one particular wave direction and period. The two numbers are an amplitude, which relates the amplitude of the vessel motion to the amplitude of the wave, and a phase, which defines the timing of the vessel motion relative to the wave (Orcina n.d.).
The vessel has 6 degrees of freedom: 3 translations (surge, sway, heave) and 3 rotations (roll, pitch, yaw), so the RAO data consists of 6 amplitude and phase pairs for each wave period and direction. The RAO amplitude and phase vary for different types of vessel, and for a given vessel type they vary with draught, wave direction, forward speed and wave period (or frequency).

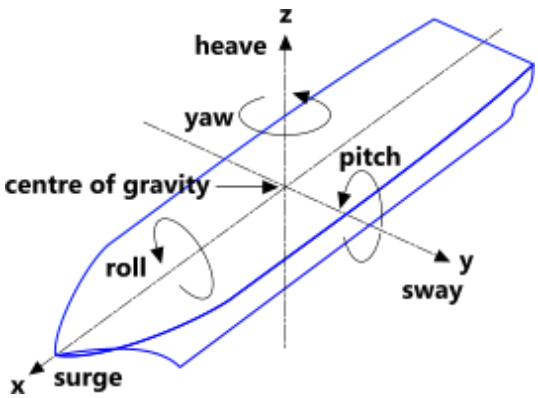


Figure 5.8: generic vessel motion.

Since that the RAO's generation is a long and elaborated process and counting that the present study is focused on the mooring, an existing RAO has been used. This set of equation has been taken from an example available on the Orcina website, regarding a structure like WindFloat's one: a generic semi-submersible platform used in the oil industry (Orcina n.d.), with RAO specified for 0°, 45° and 90° directions. The structural similarities along the wind response modelling are taken to give reliable answers regarding the mooring systems and their loads. Details about period, amplitude and phase, along with their graphical representation, are given in Appendix E. It should be noted that for a real design, the specific RAOs must be developed and possibly tested in a wave tank.

## 5.3.2 Wind Load

Wind drag loads on a vessel are loads due to the relative velocity of the fluid past the vessel. Since that the structure is correlated with energy production from wind, the loads are expected to be significant. Wind loads are proportional to the areas subjected to the flow: in OrcaFlex are specified the surge area, the sway area and the yaw area moment. The surge area comprehends the whole area covered by the rotor's blades and the yaw area moment is calculated according to The Oil Companies International Marine Forum (OCIMF) directive (Orcina n.d.):

$$Yaw\ area\ moment = LA_{sway} \quad (5.8)$$

Giving the results:

| Parameter | Value |
|---|---|
| $A_{surge}$ | 12561 m² |
| $A_{sway}$ | 394 m² |
| Y | 15681 m³ |
| L | 40 m |

Table 5.2: wind load parameters.

Where $A_{surge}$ is the surge area, $A_{sway}$ is the sway area, Y is the yaw area moment and L is the length between perpendicular of the floater.

Even if, in the tower, the rotor and the nacelle are not graphically represented, the wind loads are applicated at the position of the nacelle, to influence realistically the floater response in such situations.

## 5.4 Mooring types

The mooring has been represented in OrcaFlex using lines, which connect the floater to the sea bed: 4 wires of equal length and specifications link the floating structure to the sea bed. Different solutions with different characteristics have been applied: traditional anchors, with mooring lines composed by chains and a combination of chains and synthetic fibres, and suction anchors, with mooring lines composed by chains and synthetic fibres.

In the mooring type with a combination of suction anchor and synthetic fibres rope a taut mooring system has been simulated, in the other cases a traditional catenary system has been applied.

The same type of chain and synthetic rope have been used in all cases. The chosen characteristics are in accord with the regulations needed for offshore operations (DNV GL n.d.) (DNV GL 2016) and they are summarised in Table 5.3 and Table 5.4.

| Parameter | Value |
|---|---|
| Mooring type | Chain |
| Bar diameter | 0.05 m |
| Link type | Stud-link |
| Grade | R4 |
| Weight in air | 0.537 kN/m |
| Displacement | 0.071 kN/m |
| Weight in water | 0.466 kN/m |
| Breaking load | 2740 kN |

Table 5.3: mooring chain parameters (DNV GL n.d.).

| Parameter | Value |
|---|---|
| Mooring type | Synthetic rope |
| Diameter | 0.08 m |
| Type | 8-strand polyester |
| Standard | ISO 10556 |
| Weight in air | 0.050 kN/m |
| Displacement | 0.037 kN/m |
| Weight in water | 0.013 kN/m |
| Breaking load | 1091 kN |

Table 5.4: synthetic mooring rope parameters (DNV GL 2016).

### 5.4.1 Anchor

The traditional anchor mooring system has been modelled using the option “anchored” in OrcaFlex for the end of line touching the seabed: this will simulate the friction and the behaviour of an anchor in the simulations.

The mooring lines follow a catenary shape and two simulations, for each return period, have been performed with two different wires composition: the first using a chain (Figure 5.9) and the second using chains, in proximity of the anchor and the floater, and synthetic ropes in the middle (Figure 5.10).

From now on these conventions are applied for the simulations:

| Simulation number | Location | Mooring system | Wind and waves return period |
|---|---|---|---|
| 1 | Adriatic Sea | Anchor with chains | 50 years |
| 2 | Adriatic Sea | Anchor with chains | 100 years |
| 3 | South Sicily | Anchor with chains | 50 years |
| 4 | South Sicily | Anchor with chains | 100 years |
| 5 | Adriatic Sea | Anchor with chains and synthetic ropes | 50 years |
| 6 | Adriatic Sea | Anchor with chains and synthetic ropes | 100 years |
| 7 | South Sicily | Anchor with chains and synthetic ropes | 50 years |
| 8 | South Sicily | Anchor with chains and synthetic ropes | 100 years |

Table 5.5: simulation name convention for traditional anchor systems.

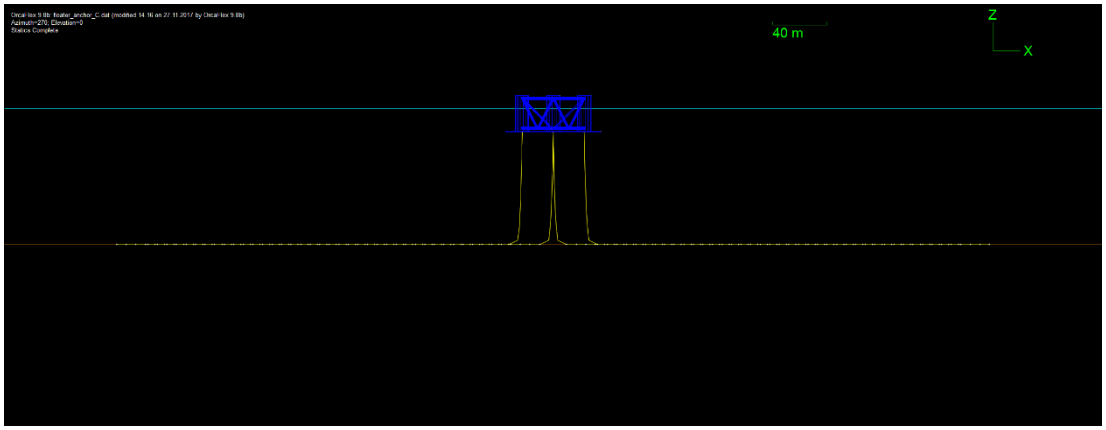


Figure 5.9: anchor mooring system with chains (yellow).

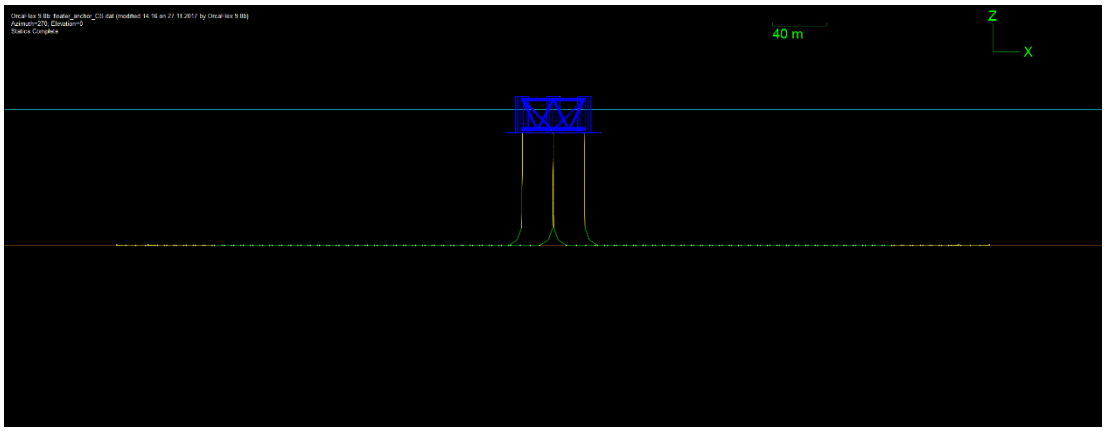


Figure 5.10: anchor mooring system with chains (yellow) and synthetic ropes (green).

The distance between the anchor and the fairlead on the floater, over the horizontal axes, has been set, using a practical rule for traditional anchors systems (Chakrabarti 2015), proportional to three time the water depth, as can be seen in Figure 5.11.

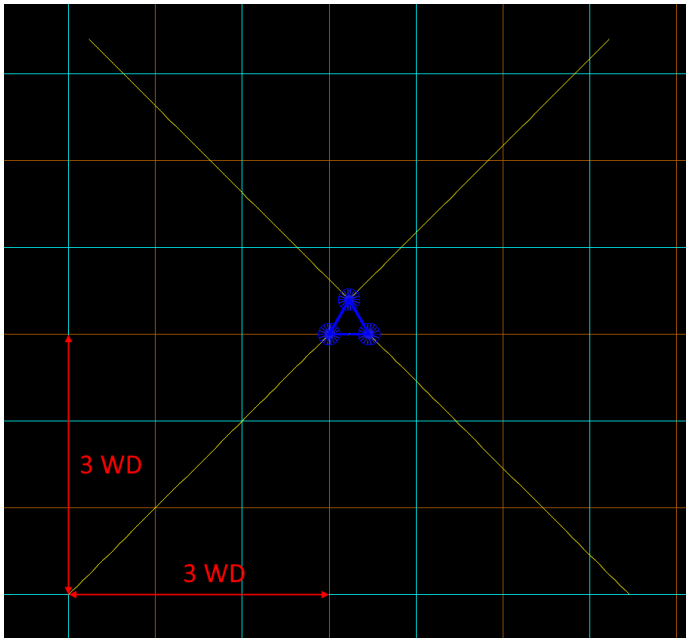


Figure 5.11: distance over the horizontal axes between the anchor and the fairlead on the floater (WD: water depth).

The wire length for the different simulations and locations is summarized in Table 5.6 and Table 5.7.

| **Adriatic Sea** | |
|---|---|
| Chain length | 500 m |
| **South Sicily** | |
| Chain length | 2000 m |

Table 5.6: mooring wires length for chain-only simulation (anchor).

| **Adriatic Sea** | |
|---|---|
| Top chain length | 70 m |
| Synthetic rope length | 360 m |
| Bottom chain length | 70 m |
| **South Sicily** | |
| Top chain length | 200 m |
| Synthetic rope length | 1600 m |
| Bottom chain length | 200 m |

Table 5.7: mooring wires length for chain and synthetic fibres simulation (anchor).

## 5.4.2 Suction anchor

Since that a suction anchor is a system that uses suction forces rather than friction, limiting the horizontal motion with a sea bed penetration, it has been modelled in OrcaFlex using the option “fixed” in OrcaFlex for the end of line touching the sea bed. This choice fixes the

extremity of the mooring line to a prescribed point, in which is possible to analyse the horizontal and vertical forces in order to obtain the first design parameters for the anchor.
Two simulations, for each return period, have been planned with two different wires composition: in the first (Figure 5.12), the mooring line is made by a chain and its shape follows the catenary rule, in the second one (Figure 5.13), synthetic ropes only are used with a taut design. In the first case, the touchdown point of the chain correspond to the suction anchor.
From now on these conventions are applied for the simulations:

| Simulation number | Location | Mooring system | Wind and waves return period |
|---|---|---|---|
| 9 | Adriatic Sea | Suction anchor with chains | 50 years |
| 10 | Adriatic Sea | Suction anchor with chains | 100 years |
| 11 | South Sicily | Suction anchor with chains | 50 years |
| 12 | South Sicily | Suction anchor with chains | 100 years |
| 13 | Adriatic Sea | Suction anchor with synthetic ropes | 50 years |
| 14 | Adriatic Sea | Suction anchor with synthetic ropes | 100 years |
| 15 | South Sicily | Suction anchor with synthetic ropes | 50 years |
| 16 | South Sicily | Suction anchor with synthetic ropes | 100 years |

Table 5.8: simulation name convention for suction anchor systems.

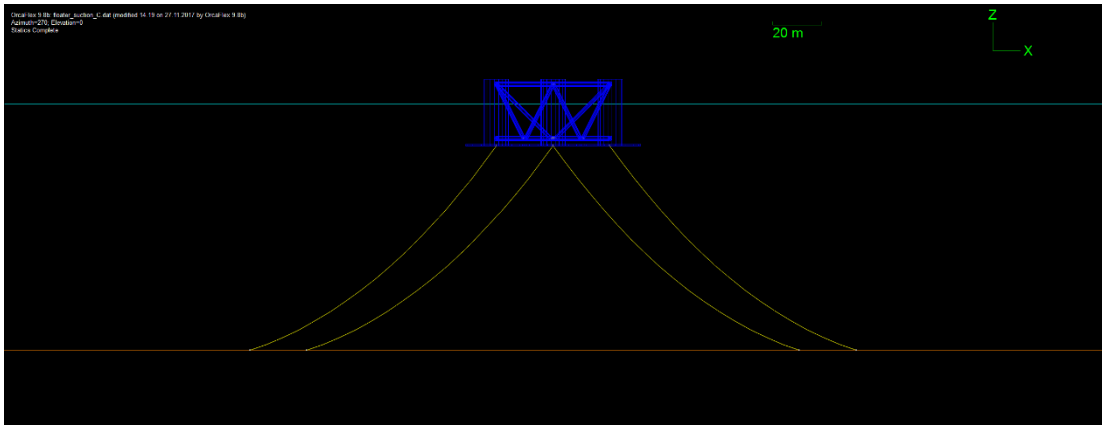


Figure 5.12: suction anchor mooring system with chains (yellow).

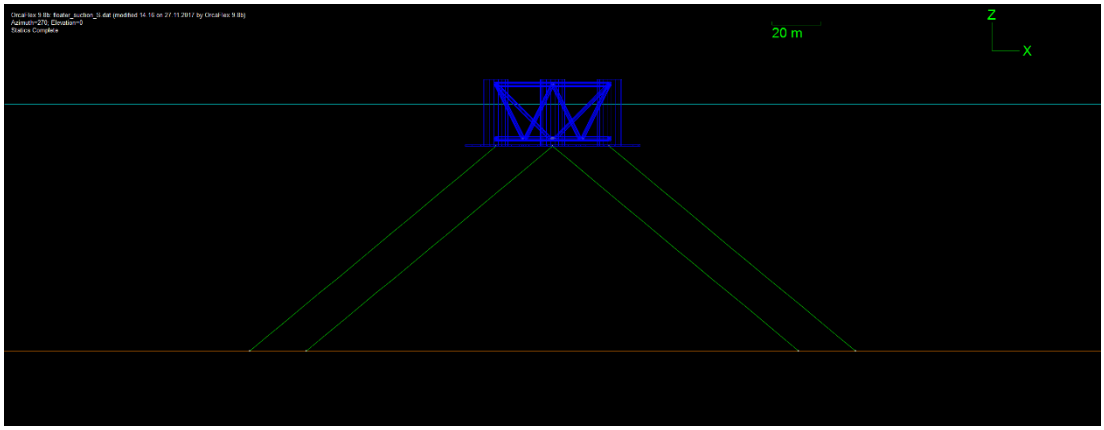


Figure 5.13: suction anchor mooring system with synthetic ropes (green).

The distance between the anchor and the fairlead on the floater, over the horizontal axes, has been set, using a practical rule for suction anchors systems (Chakrabarti 2015), proportional to the water depth, as can be seen in Figure 5.14.

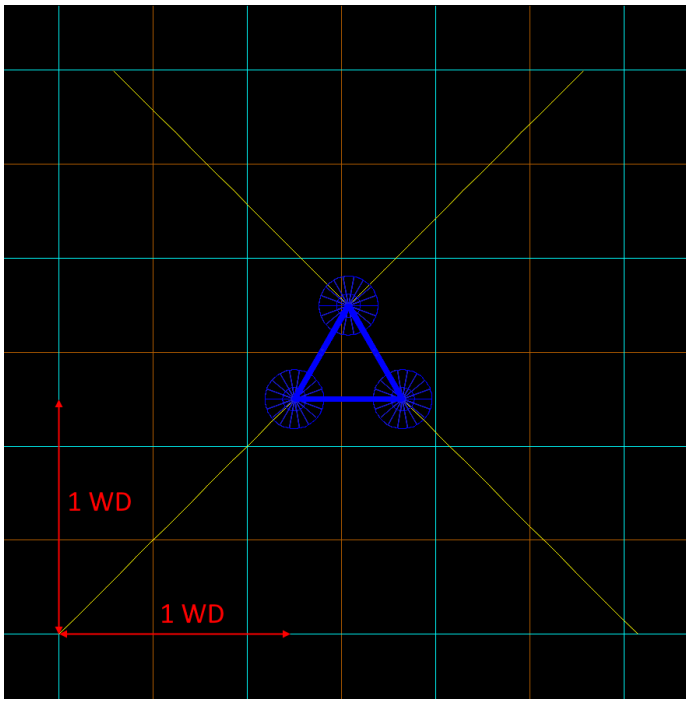


Figure 5.14: distance over the horizontal axes between the suction anchor and the fairlead on the floater (WD: water depth).

The wire length for the different simulations and locations is summarized in Table 5.9 and Table 5.10.

| **Adriatic Sea** | |
|---|---|
| Chain length | 166 m |
| **South Sicily** | |
| Chain length | 690 m |

Table 5.9: mooring wires length for chain simulation (suction anchor).

| **Adriatic Sea** | |
|---|---|
| Synthetic rope length | 145 m |
| **South Sicily** | |
| Synthetic rope length | 600 m |

Table 5.10: mooring wires length for synthetic rope simulation (suction anchor).

## 5.5 Static simulation

The first step of the simulations is the static analysis, in which OrcaFlex calculates the static equilibrium position of the model: wind loads are included, but not wave loads. Since the difference concerning wind speed between the values found for 50 years and 100 years of return period is very little in both locations, the analysis of the result will be focused on 100 years return period scenarios.

During this phase of simulations, attention has been put into the values of the forces at the anchors, especially the vertical ones, for every situation. In the traditional anchor system, vertical tension forces are not present in both cases, there are horizontal traction forces sustainable by the materials chosen.

Vertical traction forces are present and significant in both cases when suction anchors are modelled: a possible solution for a reduction of these forces has been explored for the simulations with chains as mooring lines. An increase of the horizontal spreading of the lines proved that a reduction is possible at the cost of an augmented footprint of the mooring system.

The case with the highest values of forces at the anchors is the taut mooring simulation: a comparison between forces at the anchor and mooring wires' length has been made in both cases with suction anchors, showing that using shorter mooring lines is possible (taut system) with a suction anchor capable of withstanding larger vertical forces.

In all the results is followed the OrcaFlex convention for forces sign in the interaction between objects: a positive value corresponds to a compression and a negative value to a traction.

Abbreviation convention for all tables:

- End A: terminal part of the mooring line in contact with the fairlead on the floater;
- End B: terminal part of the mooring line in contact with the anchor;
- GX: horizontal global axis X of the reference system in OrcaFlex (see Figure 5.7 for a visual representation);
- GY: horizontal global axis Y of the reference system in OrcaFlex (see Figure 5.7 for a visual representation);
- GZ: horizontal global axis Z of the reference system in OrcaFlex (see Figure 5.7 for a visual representation).

## 5.5.1 Anchor

In both the simulation performed in the Adriatic Sea and in South Sicily, values of the tension in the mooring wires respected the allowable loads for the material in every section. Concerning the forces at the anchor, in both simulation are present horizontal forces of traction and vertical forces of compression: the compression is probably due to the weight of the material composing the end of the wire, since that it lies on the sea bed for the larger part not producing angles with the sea bed itself. A decreasing of the magnitude of the force applied to the floater in the passage from chain-only wire to the hybrid composition chain and synthetic rope, for the increased elasticity in the wire composition due to the use of synthetic fibres.

Details about the forces are shown in Table 5.11, Table 5.12, Table 5.13 and Table 5.14. Only the 100 years return period scenarios are considered. For list of simulation scenarios, see Table 5.5.

| **Simulation 2** | | | | |
|---|---|---|---|---|
| **End A components** | | | | |
| **Load** | **Magnitude** | **GX** | **GY** | **GZ** |
| Force [kN] | 56.1351 | -0.6026 | -0.6026 | -56.1286 |
| **End B components** | | | | |
| **Load** | **Magnitude** | **GX** | **GY** | **GZ** |
| Force [kN] | 2.485 | -0.6026 | -0.6026 | 2.3343 |

Table 5.11: simulation 2 static results.

| **Simulation 4** | | | | |
|---|---|---|---|---|
| **End A components** | | | | |
| **Load** | **Magnitude** | **GX** | **GY** | **GZ** |
| Force [kN] | 211.7494 | -12.092 | -12.092 | -211.0577 |
| **End B components** | | | | |
| **Load** | **Magnitude** | **GX** | **GY** | **GZ** |
| Force [kN] | 17.265 | -12.092 | -12.092 | 2.376 |

Table 5.12: simulation 4 static results.

| **Simulation 6** | | | | |
|---|---|---|---|---|
| **End A components** | | | | |
| **Load** | **Magnitude** | **GX** | **GY** | **GZ** |
| Force [kN] | 49.0751 | -0.0573 | -0.0573 | -49.075 |
| **End B components** | | | | |
| **Load** | **Magnitude** | **GX** | **GY** | **GZ** |
| Force [kN] | 2.3337 | -0.0573 | -0.0573 | 2.3323 |

Table 5.13: simulation 6 static results.

| Simulation 8 | | | | |
|---|---|---|---|---|
| **End A components** | | | | |
| **Load** | **Magnitude** | **GX** | **GY** | **GZ** |
| Force [kN] | 112.5143 | -0.573 | -0.573 | -112.5113 |
| **End B components** | | | | |
| **Load** | **Magnitude** | **GX** | **GY** | **GZ** |
| Force [kN] | 2.4708 | -0.573 | -0.573 | 2.3342 |

Table 5.14: simulation 8 static results.

## 5.5.2 Suction anchor

For the suction anchors models, vertical forces at the anchors are substantially increased than in 5.5.1, since that the angle between line and sea bed is more than zero at the anchor and, in the taut system, tension in the line plays a fundamental role for the floater stability.
Details about the forces are shown in Table 5.15, Table 5.16, Table 5.17 and Table 5.18. Only the 100 years return period scenarios are considered. For list of simulation scenarios, see Table 5.8.

| Simulation 10 | | | | |
|---|---|---|---|---|
| **End A components** | | | | |
| **Load** | **Magnitude** | **GX** | **GY** | **GZ** |
| Force [kN] | 155.5961 | -72.6366 | -72.6366 | -116.8673 |
| **End B components** | | | | |
| **Load** | **Magnitude** | **GX** | **GY** | **GZ** |
| Force [kN] | 107.4547 | -72.6366 | -72.6366 | -31.5334 |

Table 5.15: simulation 10 static results.

| Simulation 12 | | | | |
|---|---|---|---|---|
| **End A components** | | | | |
| **Load** | **Magnitude** | **GX** | **GY** | **GZ** |
| Force [kN] | 616.0105 | -287.8885 | -287.8885 | -462.2871 |
| **End B components** | | | | |
| **Load** | **Magnitude** | **GX** | **GY** | **GZ** |
| Force [kN] | 428.1114 | -287.8885 | -287.8885 | -132.3624 |

Table 5.16: simulation 12 static results.

| Simulation 14 | | | | |
|---|---|---|---|---|
| **End A components** | | | | |
| **Load** | **Magnitude** | **GX** | **GY** | **GZ** |
| Force [kN] | 914.7821 | -556.8228 | -556.8228 | -465.5353 |
| **End B components** | | | | |
| **Load** | **Magnitude** | **GX** | **GY** | **GZ** |
| Force [kN] | 913.2249 | -556.8228 | -556.8228 | -462.4677 |

Table 5.17: simulation 14 static results.

| Simulation 16 | | | | |
|---|---|---|---|---|
| **End A components** | | | | |
| **Load** | **Magnitude** | **GX** | **GY** | **GZ** |
| Force [kN] | 970.2048 | -566.0435 | -566.0435 | -548.1667 |
| **End B components** | | | | |
| **Load** | **Magnitude** | **GX** | **GY** | **GZ** |
| Force [kN] | 965.2572 | -566.0435 | -566.0435 | -539.3616 |

Table 5.18: simulation 16 static results.

Concerning the case with a chain-only wire an attempt to reduce these forces has been done increasing progressively the horizontal spread of the mooring lines from one time the water depth to three times. The same line characteristic has been kept: the touchdown point has always been maintained at the suction anchor. Results show a clear pattern: increasing the mooring spread and decreasing the angle between sea bed and wire at the proximity of the suction anchor, the vertical forces decrease. In this process, the chain becomes more and more close to a traditional anchor system. The decrease of vertical forces permits the use of a less performant (and so less expensive) suction anchor, at the cost of using more material and forming a larger footprint on the sea bed. This process is confirmed in both location and can be seen, along with the angle between wire and sea bed, in Figure 5.15 and Figure 5.16.

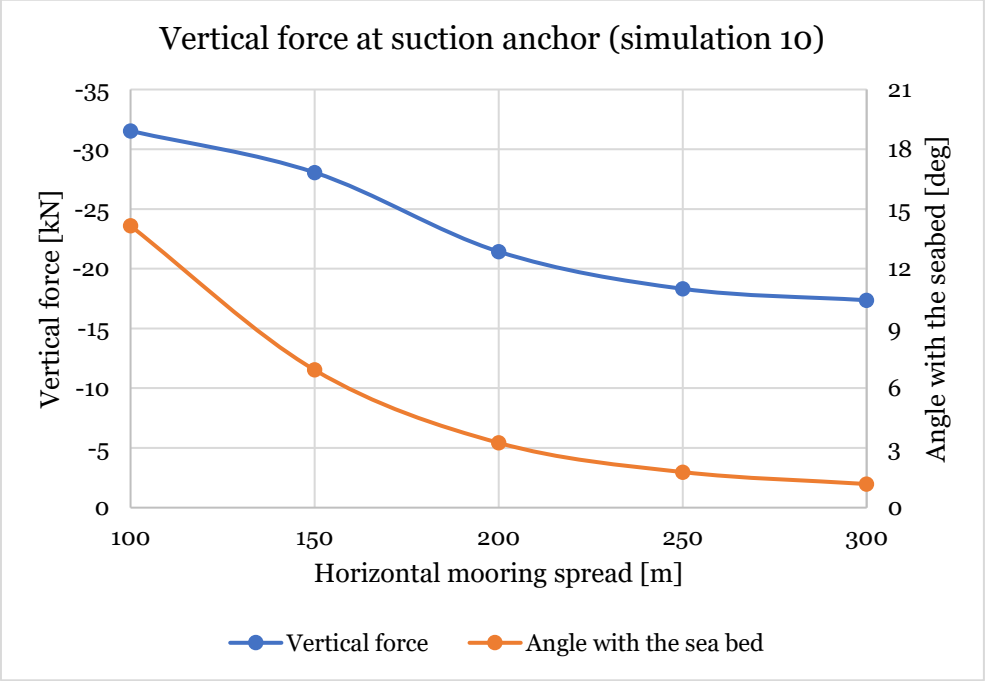


Figure 5.15: vertical force at suction anchor (simulation 10, Adriatic Sea, suction anchor mooring system with chains, 100 years return period).

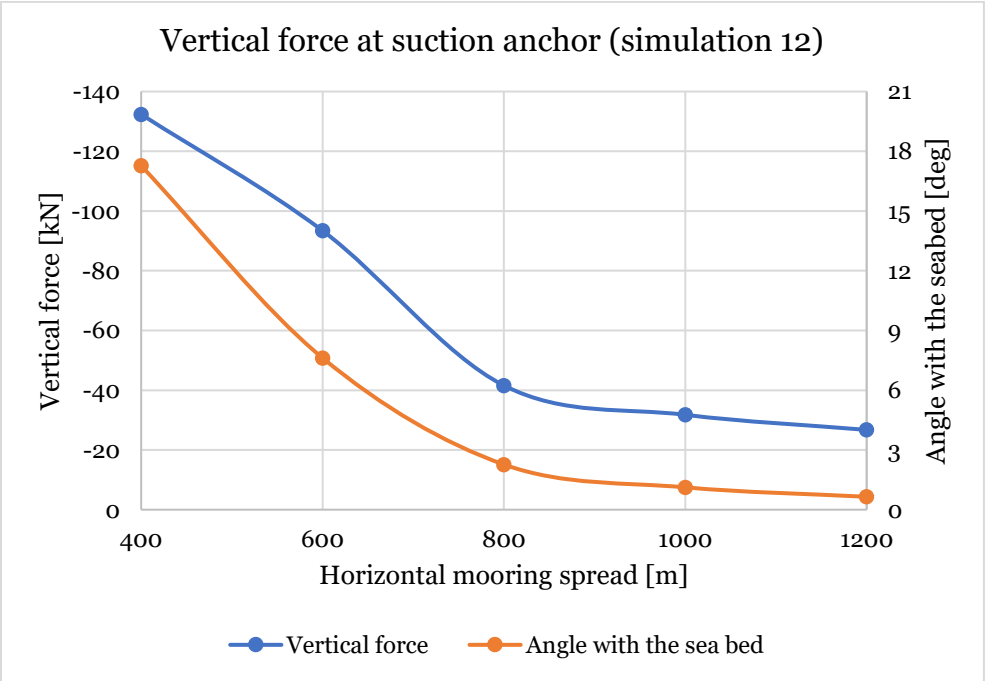


Figure 5.16: vertical force at suction anchor (simulation 12, South Sicily, suction anchor mooring system with chains, 100 years return period).

The taut system, compared to the coupling suction anchor and chain shows, a massive increment concerning the vertical forces with a little reduction into the wire length: this factor leads to the requirement of a much more capable suction anchor with a possible reduction in

the material use for the mooring lines. A comparison between these solutions is shown in Table 5.19.

| **Simulation 10 vs 14** | |
|---|---|
| Vertical force increase | 430.93 kN |
| Wire length reduction | 21 m |
| **Simulation 12 vs 16** | |
| Vertical force increase | 407.00 kN |
| Wire length reduction | 90 m |

Table 5.19: comparison in suction anchors solutions between chain and synthetic fibres composing mooring lines.

# 5.6 Dynamic simulation

In the dynamic analysis, OrcaFlex carries out a time simulation of the response of the system to waves and wind, based on user-defined inputs. The dynamic simulation uses the static analysis as its initial configuration and time then evolves forward from there. The results of the dynamic analysis can be used to determine the design criteria for the range of mooring systems and anchor's technology.

The analysis of the result has been focused on the tension in the wires and on the forces at the anchors: simulation has been performed for both return periods and for every wire and anchor, then the design data obtained have been compared.

These results have been obtained through the analysis of the time history of the simulation that produces cycles of loading and unloading on the wires and the anchor: the peak values have been implemented in a statistic concerning the extremes, using the OrcaFlex option "extreme values statistics" (Orcina n.d.). In this procedure, a Generalized Pareto distribution gave results and their consequent confidence limits, both for tensions and anchors forces, simulating two storms, lasting for 3 and 6 hours.

The resulting values for tension present common patterns both for the Adriatic Sea and South Sicily: the most stressed part in the wire is in proximity of the floater, the limit loads are never exceeded. The difference between a simulation with 50 years return period and one with 100 is negligible and the variation of the storm duration affects the results poorly.

The values concerning the loads at the anchors presents differences between traditional and suction anchors: in the first case, they are nearly not affected by the simulation and the values are very close to the static analysis ones, in the second case they present peaks of loading and unloading. There is also a difference in simulated suction anchors with chains and taut: the vertical load from the dynamic analysis is the first case differs from the static values more than second case. Like for the tension values, the difference between results, obtained with a 3 hours

lasting storm and a 6 hours one and with environmental loads with 50 and 100 years return period, is negligible.

Considering the OrcaFlex reference system, since that the floater is symmetric in the X direction and the loads are applied only in the Y direction (Figure 5.4), following the conventions shown in Figure 5.17, line 1 presents the same results if line 2 and line 3 presents the same results of line 4. For this reason, are presented only the result obtained with line 1 and line 3. This is valid also for the anchors. For the abbrevation convention in the tables in the following paragraphs, see 5.5.

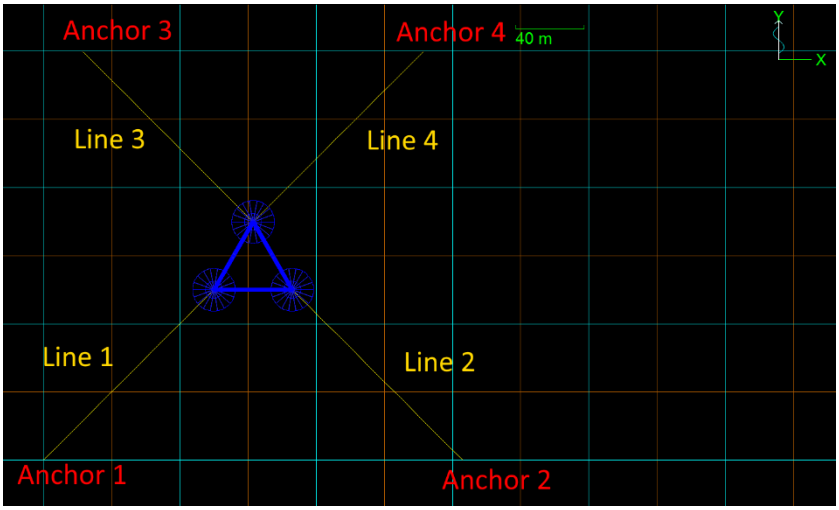


Figure 5.17: mooring lines (yellow) and anchors (red) names convention.

## 5.6.1 Extreme value statistics

The goal to the dynamic analysis to predict the extreme responses of the system composed by the floater and the moorings in terms of tension and forces at the anchors, to determine the design parameters for those objects. OrcaFlex can estimate extreme values for any given time domain result variable by analysing the simulated time history of the variable using extreme value statistical methods (Orcina n.d.).

The simulations data are analysed using the peak over a threshold method (POT), using a Generalized Pareto distribution (GPD) (Orcina n.d.).

The GPD is a family of continuous probability distributions that is often used to model the tails of another distribution (Gudmestad 2015). The GPD is specified by three parameters, which OrcaFlex estimate with the maximum likelihood method (Orcina n.d.):

- β: shape parameter;
- μ: location parameter;
- σ: scale parameter.

And the probability density function is given by (Gudmestad 2015):

$$f(x) = \frac{1}{\sigma}\left(1 + \beta\left(\frac{x-\mu}{\sigma}\right)\right)^{-\frac{1}{\beta+1}}, x \in \mathbb{R}, \beta \in \mathbb{R}, \mu \in \mathbb{R}, \sigma > 0 \quad (5.9)$$

The cumulative distribution function is given by (Gudmestad 2015):

$$F(x) = 1 - \left(1 + \beta\left(\frac{x-\mu}{\sigma}\right)\right)^{-\frac{1}{\beta}}, x \in \mathbb{R}, \beta \neq 0, \mu \in \mathbb{R}, \sigma > 0 \quad (5.10)$$

And (Gudmestad 2015):

$$F(x) = 1 - \exp\left(\frac{x-\mu}{\sigma}\right), x \in \mathbb{R}, \beta = 0, \mu \in \mathbb{R}, \sigma > 0 \quad (5.11)$$

Historically, the Weibull distribution has often been used for marine systems, but the Generalised Pareto is preferred by the extreme value statistics community because of its sound mathematical foundations (Orcina n.d.).

The POT takes the peaks over a certain threshold for a simulation into account (Figure 5.18): mathematical theory states that as the size of the dataset and the threshold for fitting increase, the peaks over the threshold converge in distribution to a Generalised Pareto distribution (Gudmestad 2015).

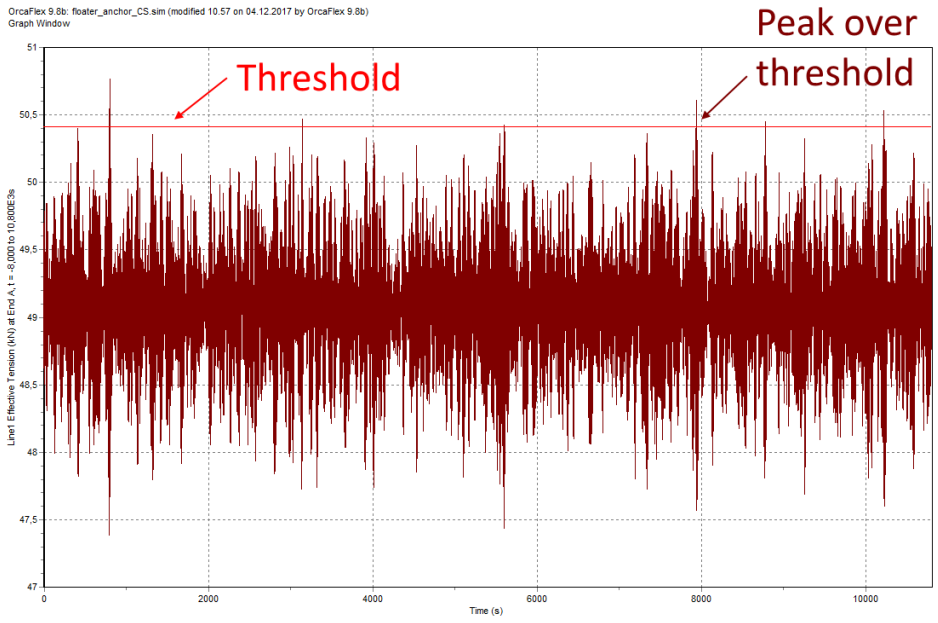


Figure 5.18: simulated time series shows threshold and peak over threshold.

An important assumption underpinning the maximum likelihood method is that the data are independent. In a 3-hour simulation, it is not the case: OrcaFlex gets closer to the independence sub-sampling the data, performing a declustering and ensuring that the points we choose are sufficiently far apart as to be approximately independent (Orcina n.d.).

In all the statistical analysis performed, the default declustering procedure (mean up-crossing (Orcina n.d.)) has been set in OrcaFlex, with the threshold suggested by the software. For the

analysis of the vertical loads at the suction anchors, since that the analysis gave negative values, the peaks implemented in the statistics are under the threshold, in order to identify the highest vertical forces (for the signs convention refer to 5.5).
Two storm durations have been set, 3 and 6 hours: storm duration is the return period for which the return parameter (tension or vertical load) is reported. The length of the simulation, relative to this duration, determines the accuracy of the estimation for the return parameter (Orcina n.d.).
The maximum likelihood fitting procedure used for the GPD allows the estimation of a confidence interval (CI) for the return parameter, for a specified confidence level, set to 95%: the reported return parameter is defined to be the parameter whose expected number of exceedances in the specified storm duration is one (Orcina n.d.). These are the values referred to in the tables in the following paragraphs as our design values.

## 5.6.2 Wires tension

The analysis for the tension in the wires has been performed finding the most stressed part of them in the whole simulation. This procedure is possible using the OrcaFlex function “range graph”, which shows the minimum, mean and maximum values that the tension took during the simulation (Orcina n.d.).
In all the simulation, this part is always located in proximity of the floater: this part of the mooring line sustains the environmental loads and the submerged weigh of the suspended part of the wire.
The difference between simulations with the same mooring characteristics but different return period conditions is negligible (i.e. lower than 20 kN in every case), as well as for the different storm duration (i.e. less than 10 kN in most of the cases). A comparison, between simulation with the same modelled characteristics but different return period environmental conditions, has been made after the data exposition in the following paragraphs.
In Appendix F are reported for every simulation:

- range graphs for line 1 and line 3;
- time history graphs with thresholds for the statistical analysis performed for line 1 and line 3;
- fitted GPD parameters for line 1 and line 3.

### *Anchor*

For the traditional anchors simulation, the tension follows a common scheme: a rapid decrease from the highest value in proximity of the floater until a constant value after the touchdown point. In the simulations 5/6/7/8 the synthetic wires present a component of compression in

near the touchdown point, probably due to the elasticity of the material which is subjected to loading and unloading cycles. Similar values both for tension and CI are given from the statistical analysis for storms of 3 and 6 hours. Note that the values of CI are defined in 5.6.1 above.

The results of the statistical analysis are presented in Table 5.20, Table 5.21, Table 5.22, Table 5.23, Table 5.24, Table 5.25, Table 5.26 and Table 5.27. For list of simulation scenarios, see Table 5.5.

| | | **Simulation 1** | | |
|---|---|---|---|---|
| | | Lower CI [kN] | Tension [kN] | Upper CI [kN] |
| **Line 1** | 3 h storm | 57.8263 | 57.9715 | 58.5858 |
| | 6 h storm | 57.8888 | 58.0423 | 59.4600 |
| **Line 3** | 3 h storm | 60.6445 | 61.306 | 65.9583 |
| | 6 h storm | 60.9261 | 61.7711 | 71.7233 |

Table 5.20: simulation 1 dynamic analysis results for tension.

| | | **Simulation 2** | | |
|---|---|---|---|---|
| | | Lower CI [kN] | Tension [kN] | Upper CI [kN] |
| **Line 1** | 3 h storm | 57.9857 | 58.0289 | 58.1329 |
| | 6 h storm | 58.0098 | 58.0453 | 58.1918 |
| **Line 3** | 3 h storm | 61.2138 | 61.4857 | 62.1016 |
| | 6 h storm | 61.3642 | 61.6281 | 62.4362 |

Table 5.21: simulation 2 dynamic analysis results for tension.

| | | **Simulation 3** | | |
|---|---|---|---|---|
| | | Lower CI [kN] | Tension [kN] | Upper CI [kN] |
| **Line 1** | 3 h storm | 226.5300 | 230.9402 | 252.9705 |
| | 6 h storm | 228.0937 | 234.9000 | 279.5950 |
| **Line 3** | 3 h storm | 236.2290 | 239.0648 | 250.8267 |
| | 6 h storm | 237.5129 | 240.8051 | 259.5306 |

Table 5.22: simulation 3 dynamic analysis results for tension.

| | | **Simulation 4** | | |
|---|---|---|---|---|
| | | Lower CI [kN] | Tension [kN] | Upper CI [kN] |
| **Line 1** | 3 h storm | 227.6176 | 229.2149 | 234.7186 |
| | 6 h storm | 227.4826 | 230.0666 | 239.0978 |
| **Line 3** | 3 h storm | 237.4656 | 239.7343 | 244.9749 |
| | 6 h storm | 238.6840 | 241.1706 | 248.3094 |

Table 5.23: simulation 4 dynamic analysis results for tension.

| | | Simulation 5 | | |
|---|---|---|---|---|
| | | Lower CI [kN] | Tension [kN] | Upper CI [kN] |
| **Line 1** | 3 h storm | 50.5496 | 50.6701 | 51.2244 |
| | 6 h storm | 50.6001 | 50.7238 | 52.1967 |
| **Line 3** | 3 h storm | 53.2386 | 53.9155 | 59.2559 |
| | 6 h storm | 53.5102 | 54.4184 | 66.2998 |

Table 5.24: simulation 5 dynamic analysis results for tension.

| | | Simulation 6 | | |
|---|---|---|---|---|
| | | Lower CI [kN] | Tension [kN] | Upper CI [kN] |
| **Line 1** | 3 h storm | 50.6574 | 50.6574 | 50.9336 |
| | 6 h storm | 50.6834 | 50.7782 | 51.0191 |
| **Line 3** | 3 h storm | 53.7814 | 54.0370 | 54.6726 |
| | 6 h storm | 53.9257 | 54.1824 | 55.0074 |

Table 5.25: simulation 6 dynamic analysis results for tension.

| | | Simulation 7 | | |
|---|---|---|---|---|
| | | Lower CI [kN] | Tension [kN] | Upper CI [kN] |
| **Line 1** | 3 h storm | 119.5879 | 120.0995 | 121.9094 |
| | 6 h storm | 119.8559 | 120.2666 | 123.5335 |
| **Line 3** | 3 h storm | 125.8506 | 129.0953 | 156.1920 |
| | 6 h storm | 126.9039 | 131.9151 | 197.2419 |

Table 5.26: simulation 7 dynamic analysis results for tension.

| | | Simulation 8 | | |
|---|---|---|---|---|
| | | Lower CI [kN] | Tension [kN] | Upper CI [kN] |
| **Line 1** | 3 h storm | 119.5247 | 119.9996 | 121.5961 |
| | 6 h storm | 119.7483 | 120.2644 | 122.9735 |
| **Line 3** | 3 h storm | 126.3183 | 127.9930 | 135.5978 |
| | 6 h storm | 127.0513 | 129.1861 | 142.6389 |

Table 5.27: simulation 8 dynamic analysis results for tension.

The difference in the tension values between simulation with the same mooring characteristics but different return period is negligible considering a certain grade of uncertainty. This small difference is shown in Table 5.28, Table 5.29, Table 5.30 and Table 5.31.

| | | Simulation 2 vs 1 |
|---|---|---|
| | | Difference in tension [kN] |
| **Line 1** | 3 h storm | 0.0574 |
| | 6 h storm | 0.0030 |
| **Line 3** | 3 h storm | 0.1797 |
| | 6 h storm | -0.1430 |

Table 5.28: difference in the tension values between simulation 2 and 1.

| | | Simulation 4 vs 3 |
|---|---|---|
| | | Difference in tension [kN] |
| **Line 1** | 3 h storm | -1.7253 |
| | 6 h storm | -4.8334 |
| **Line 3** | 3 h storm | 0.6695 |
| | 6 h storm | 0.3655 |

Table 5.29: difference in the tension values between simulation 4 and 2.

| | | Simulation 6 vs 5 |
|---|---|---|
| | | Difference in tension [kN] |
| **Line 1** | 3 h storm | -0.0127 |
| | 6 h storm | 0.0544 |
| **Line 3** | 3 h storm | 0.1215 |
| | 6 h storm | -0.2360 |

Table 5.30: difference in the tension values between simulation 6 and 5.

| | | Simulation 8 vs 7 |
|---|---|---|
| | | Difference in tension [kN] |
| **Line 1** | 3 h storm | -0.0999 |
| | 6 h storm | -0.0022 |
| **Line 3** | 3 h storm | -1.1023 |
| | 6 h storm | -2.7290 |

Table 5.31: difference in the tension values between simulation 8 and 7.

## *Suction anchor*

For the suction anchors simulations, the maximum tension recorded in the wires follows a different path with respect to traditional anchors: the most stressed point is near the floater in this case too, but the decreasing of tension along the wire is almost linear. This decrease is more significant in the simulations in which the mooring lines are represented with chains, while in the taut mooring system the tension is nearly constant. While different storm durations for the statistical analysis do not affect the result significantly, for simulation 11 and 12, the discrepancy is more than 10 kN.

Confidence intervals and the tension value for line 1 and 3 are reported in Table 5.32, Table 5.33, Table 5.34, Table 5.35, Table 5.36, Table 5.37, Table 5.38 and Table 5.39. For list of simulation scenarios, see Table 5.8.

| | | Simulation 9 | | |
|---|---|---|---|---|
| | | Lower CI [kN] | Tension [kN] | Upper CI [kN] |
| **Line 1** | 3 h storm | 195.8603 | 198.6366 | 205.9508 |
| | 6 h storm | 197.1484 | 200.2663 | 209.6685 |
| **Line 3** | 3 h storm | 193.6938 | 202.1199 | 228.8819 |
| | 6 h storm | 197.0520 | 208.5098 | 250.9081 |

Table 5.32: simulation 9 dynamic analysis results for tension.

| | | Simulation 10 | | |
|---|---|---|---|---|
| | | Lower CI [kN] | Tension [kN] | Upper CI [kN] |
| **Line 1** | 3 h storm | 202.1888 | 213.9080 | 234.6363 |
| | 6 h storm | 206.1896 | 216.9051 | 235.1147 |
| **Line 3** | 3 h storm | 196.5679 | 202.9657 | 222.6793 |
| | 6 h storm | 198.8413 | 207.0938 | 236.0463 |

Table 5.33: simulation 10 dynamic analysis results for tension.

| | | Simulation 11 | | |
|---|---|---|---|---|
| | | Lower CI [kN] | Tension [kN] | Upper CI [kN] |
| **Line 1** | 3 h storm | 804.9377 | 830.7138 | 948.8001 |
| | 6 h storm | 815.8615 | 847.9487 | 1054.9280 |
| **Line 3** | 3 h storm | 772.0310 | 793.2182 | 925.6318 |
| | 6 h storm | 780.4233 | 808.3258 | 1069.6997 |

Table 5.34: simulation 11 dynamic analysis results for tension.

| | | Simulation 12 | | |
|---|---|---|---|---|
| | | Lower CI [kN] | Tension [kN] | Upper CI [kN] |
| **Line 1** | 3 h storm | 820.0695 | 840.1612 | 930.4509 |
| | 6 h storm | 828.6044 | 852.7245 | 1000.5857 |
| **Line 3** | 3 h storm | 776.1794 | 792.1074 | 868.0766 |
| | 6 h storm | 783.2289 | 802.9811 | 939.6502 |

Table 5.35: simulation 12 dynamic analysis results for tension.

| | | Simulation 13 | | |
|---|---|---|---|---|
| | | Lower CI [kN] | Tension [kN] | Upper CI [kN] |
| **Line 1** | 3 h storm | 951.6614 | 953.0595 | 956.8501 |
| | 6 h storm | 952.3543 | 953.8713 | 958.6900 |
| **Line 3** | 3 h storm | 949.3661 | 951.6178 | 958.5418 |
| | 6 h storm | 950.4872 | 952.9988 | 963.0834 |

Table 5.36: simulation 13 dynamic analysis results for tension.

| | | Simulation 14 | | |
|---|---|---|---|---|
| | | Lower CI [kN] | Tension [kN] | Upper CI [kN] |
| **Line 1** | 3 h storm | 957.7721 | 961.2738 | 984.6681 |
| | 6 h storm | 959.3167 | 963.5503 | 1018.0987 |
| **Line 3** | 3 h storm | 951.8960 | 953.7490 | 958.9283 |
| | 6 h storm | 952.8370 | 954.3942 | 963.1950 |

Table 5.37: simulation 14 dynamic analysis results for tension.

| | | Simulation 15 | | |
|---|---|---|---|---|
| | | Lower CI [kN] | Tension [kN] | Upper CI [kN] |
| **Line 1** | 3 h storm | 983.2169 | 984.1853 | 987.7350 |
| | 6 h storm | 983.6098 | 984.8282 | 990.3431 |
| **Line 3** | 3 h storm | 980.8847 | 981.4666 | 987.4475 |
| | 6 h storm | 981.1534 | 981.8007 | 999.1678 |

Table 5.38: simulation 15 dynamic analysis results for tension.

| | | Simulation 16 | | |
|---|---|---|---|---|
| | | Lower CI [kN] | Tension [kN] | Upper CI [kN] |
| **Line 1** | 3 h storm | 984.8140 | 985.8408 | 989.5719 |
| | 6 h storm | 985.3052 | 986.4433 | 992.6756 |
| **Line 3** | 3 h storm | 982.0787 | 982.5171 | 983.7012 |
| | 6 h storm | 982.3157 | 982.7094 | 984.4186 |

Table 5.39: simulation 16 dynamic analysis results for tension.

The difference in the tension values between simulation with the same mooring characteristics but different return period is more pronounced for line 1 for the simulation with chain modelled (9, 10, 11, 12), but always inferior than 20 kN. For the other lines and simulations, pattern and considerations are similar to the one made in the previous paragraph. The difference is shown in Table 5.40, Table 5.41, Table 5.42 and Table 5.43.

| | | Simulation 10 vs 9 |
|---|---|---|
| | | Difference in tension [kN] |
| **Line 1** | 3 h storm | 15.2714 |
| | 6 h storm | 16.6388 |
| **Line 3** | 3 h storm | 0.8458 |
| | 6 h storm | -1.4160 |

Table 5.40: difference in the tension values between simulation 10 and 9.

| | | Simulation 12 vs 11 |
|---|---|---|
| | | Difference in tension [kN] |
| **Line 1** | 3 h storm | 9.4474 |
| | 6 h storm | 4.7758 |
| **Line 3** | 3 h storm | -1.1108 |
| | 6 h storm | -5.3447 |

Table 5.41: difference in the tension values between simulation 12 and 11.

| | | Simulation 14 vs 13 |
|---|---|---|
| | | Difference in tension [kN] |
| **Line 1** | 3 h storm | 8.2143 |
| | 6 h storm | 9.679 |
| **Line 3** | 3 h storm | 2.1312 |
| | 6 h storm | 1.3954 |

Table 5.42: difference in the tension values between simulation 14 and 13.

| | | Simulation 16 vs 15 |
|---|---|---|
| | | Difference in tension [kN] |
| **Line 1** | 3 h storm | 1.6555 |
| | 6 h storm | 1.6151 |
| **Line 3** | 3 h storm | 1.0505 |
| | 6 h storm | 0.9087 |

Table 5.43: difference in the tension values between simulation 16 and 15.

### 5.6.3 Forces at the anchors

The dynamic simulation for the forces at the anchors showed two different results for the two types of modelled solutions: for traditional anchors, the forces values barely differ from the static values (i.e. 10 N) and, for suction anchors, there are peaks of loading during the simulation.

In the first case, considering the little difference, the statistical analysis has not been implemented, while in the second solution, the procedure of extreme values statistics has been performed for the vertical loads at the suction anchors, the main parameter that will determine the characteristics of the anchor itself.

Suction anchors presents higher vertical loads during the dynamic simulation than the static one: for the chain cases, this discrepancy is higher than for the taut mooring system. The difference between simulations with the same mooring characteristics but different return period conditions is negligible (i.e. lower than 10 kN in every case), as well as for the different storm duration (i.e. less than 5 kN in every case). A comparison, between simulation with the

same modelled characteristics but different return period environmental conditions, has been made after the data exposition in the following paragraphs.
In Appendix G are reported:

- time history graphs of total loads for anchor 1 and anchor 3 (from simulation 1 to 8);
- time history graphs of vertical loads with thresholds for the statistical analysis performed for anchor 1 and anchor 3 (from simulation 9 to 16);
- fitted GPD parameters for anchor 1 and anchor 3 (from simulation 9 to 16).

## *Anchor*

For the traditional anchors, the dynamic simulations showed loads close to the static ones: the difference between the mean load values and the peaks is around 10 N. In addition, most of the load is distributed, like in the static conditions, in the horizontal directions with no sign of vertical forces that could lead to an uplift of the anchors. This happens in all the simulations from 1 to 8 and it is probably due to the important horizontal spread of the anchors that causes the mooring wire to be in contact with the sea bed for the most part.
For this fact, the statistical analysis of loads at the anchors has not been performed since it would have been superfluous: the difference of loads, during the time history of the simulations, is so little that the statistics would have presented results close to the static values. For the time history of the simulations, in which the small discrepancy is shown, refer to Appendix G.

## *Suction anchor*

Vertical loads at the suction anchors increases with the water depth and with the tension in the wire: the difference between location and mooring system is clear from the performed simulations. Considering different storm durations does not produce different result significantly.
Confidence intervals and the vertical load value for anchor 1 and 3 are reported in Table 5.45, Table 5.46, Table 5.47, Table 5.48, Table 5.49, Table 5.50 and Table 5.51. For list of simulation scenarios, see Table 5.8.

| | | **Simulation 9** | | |
|---|---|---|---|---|
| | | Lower CI [kN] | Vertical load [kN] | Upper CI [kN] |
| **Anchor 1** | 3 h storm | -61.0094 | -49.9729 | -48.5096 |
| | 6 h storm | -74.0212 | -50.9148 | -49.1416 |
| **Anchor 3** | 3 h storm | -71.1731 | -49.7770 | -46.2193 |
| | 6 h storm | -96.6320 | -52.6512 | -47.5213 |

Table 5.44: simulation 9 dynamic analysis results for vertical load.

| | | Simulation 10 | | |
|---|---|---|---|---|
| | | Lower CI [kN] | Vertical load [kN] | Upper CI [kN] |
| **Anchor 1** | 3 h storm | -78.9984 | -58.7646 | -55.2850 |
| | 6 h storm | -108.49 | -60.7833 | -56.8300 |
| **Anchor 3** | 3 h storm | -51.2062 | -48.7374 | -47.9425 |
| | 6 h storm | -52.5510 | -48.9781 | -48.4225 |

Table 5.45: simulation 10 dynamic analysis results for vertical load.

| | | Simulation 11 | | |
|---|---|---|---|---|
| | | Lower CI [kN] | Vertical load [kN] | Upper CI [kN] |
| **Anchor 1** | 3 h storm | -264.7087 | -214.1392 | -204.1001 |
| | 6 h storm | -313.0996 | -221.0871 | -208.1558 |
| **Anchor 3** | 3 h storm | -228.6065 | -198.2733 | -191.1933 |
| | 6 h storm | -253.0970 | -202.9855 | -194.1152 |

Table 5.46: simulation 11 dynamic analysis results for vertical load.

| | | Simulation 12 | | |
|---|---|---|---|---|
| | | Lower CI [kN] | Vertical load [kN] | Upper CI [kN] |
| **Anchor 1** | 3 h storm | -248.0107 | -217.3062 | -211.0725 |
| | 6 h storm | -273.9411 | -220.6232 | -214.1597 |
| **Anchor 3** | 3 h storm | -230.5207 | -196.4811 | -191.4907 |
| | 6 h storm | -271.8495 | -199.4784 | -193.8057 |

Table 5.47: simulation 12 dynamic analysis results for vertical load.

| | | Simulation 13 | | |
|---|---|---|---|---|
| | | Lower CI [kN] | Vertical load [kN] | Upper CI [kN] |
| **Anchor 1** | 3 h storm | -484.0728 | -483.0549 | -482.5474 |
| | 6 h storm | -484.6485 | -483.2331 | -482.8238 |
| **Anchor 3** | 3 h storm | -493.9372 | -484.6744 | -483.1882 |
| | 6 h storm | -505.7509 | -485.4398 | -483.9058 |

Table 5.48: simulation 13 dynamic analysis results for vertical load.

| | | Simulation 14 | | |
|---|---|---|---|---|
| | | Lower CI [kN] | Vertical load [kN] | Upper CI [kN] |
| **Anchor 1** | 3 h storm | -491.8359 | -487.5577 | -486.1590 |
| | 6 h storm | -494.5540 | -488.3851 | -486.8621 |
| **Anchor 3** | 3 h storm | -491.6917 | -485.9900 | -484.5580 |
| | 6 h storm | -496.1636 | -486.8979 | -485.2275 |

Table 5.49: simulation 14 dynamic analysis results for vertical load.

| | | Simulation 15 | | |
|---|---|---|---|---|
| | | Lower CI [kN] | Vertical load [kN] | Upper CI [kN] |
| **Anchor 1** | 3 h storm | -548.2415 | -547.1662 | -546.8064 |
| | 6 h storm | -548.8790 | -547.3789 | -546.9800 |
| **Anchor 3** | 3 h storm | -549.1728 | -548.1111 | -547.7205 |
| | 6 h storm | -549.7222 | -548.3359 | -547.9154 |

Table 5.50: simulation 15 dynamic analysis results for vertical load.

| | | Simulation 16 | | |
|---|---|---|---|---|
| | | Lower CI [kN] | Vertical load [kN] | Upper CI [kN] |
| **Anchor 1** | 3 h storm | -549.7819 | -548.1707 | -547.6436 |
| | 6 h storm | -550.9676 | -548.4821 | -547.9018 |
| **Anchor 3** | 3 h storm | -549.9160 | -548.4921 | -548.1236 |
| | 6 h storm | -550.7445 | -548.6922 | -548.3096 |

Table 5.51: simulation 16 dynamic analysis results for vertical load.

Difference in the vertical load between simulation performed with different return period, concerning environmental conditions, is low and it is always inferior than 10 kN. This outcome is shown in Table 5.52, Table 5.53, Table 5.54 and Table 5.55.

| | | Simulation 10 vs 9 |
|---|---|---|
| | | Difference in vertical load [kN] |
| **Line 1** | 3 h storm | -8.7917 |
| | 6 h storm | -9.8685 |
| **Line 3** | 3 h storm | 1.0396 |
| | 6 h storm | 3.6731 |

Table 5.52: difference in the vertical loads values between simulation 10 and 9.

| | | Simulation 12 vs 11 |
|---|---|---|
| | | Difference in vertical load [kN] |
| **Line 1** | 3 h storm | -3.1670 |
| | 6 h storm | 0.4639 |
| **Line 3** | 3 h storm | 1.7922 |
| | 6 h storm | 3.5071 |

Table 5.53: difference in the vertical loads values between simulation 12 and 11.

| | | Simulation 14 vs 13 |
|---|---|---|
| | | Difference in vertical load [kN] |
| **Line 1** | 3 h storm | -4.5028 |
| | 6 h storm | -5.1520 |
| **Line 3** | 3 h storm | -1.3156 |
| | 6 h storm | -1.4581 |

Table 5.54: difference in the vertical loads values between simulation 14 and 13.

| | | Simulation 16 vs 15 |
|---|---|---|
| | | Difference in vertical load [kN] |
| **Line 1** | 3 h storm | -1.0045 |
| | 6 h storm | -1.1032 |
| **Line 3** | 3 h storm | -0.3810 |
| | 6 h storm | -0.3563 |

Table 5.55: difference in the vertical loads values between simulation 16 and 15.

## 5.7 Discussion of the simulations

From all the simulations, a clear pattern emerged regarding the return period of the environmental conditions in which the floater and the moorings: running simulations, with 50 years return period waves and wind data, does not differ significantly from simulation with 100 years return period data implemented. This is due to the similarity of the results obtained from the statistical analysis of waves and wind data: the results, at the two different locations respectively, are very close both in term of wind speed (i.e. difference is around 2 m/s) and wave height (i.e. difference is around 40 cm).

Close values are also obtained from the statistical analysis of the simulations in terms of return period chosen or, in other terms, storm duration: results from a 3 hours storm are closely aligned to the 6 hours events.

The values referred to as our design values are the return parameters (tension or vertical load) found by using the maximum likelihood fitting procedure. The values, along with confidence intervals (CI) with a confidence level set to 95%, mean that the reported return parameter is defined to be the parameter whose expected number of exceedances in the specified storm duration is one (Orcina n.d.). In the present study, the values of CI come from a peak over threshold method analysis in which the threshold used is the one suggested by the software with no further considerations, see 5.6.1. An exceedance probability of one per storm should be acceptable as the actual design of the mooring lines take into account load factors to be multiplied with the load and material factors reducing the allowable capacity of the mooring line tension.

In the found design values some considerations are to be made considering the loads at the anchor: a traditional anchor must, in every case, avoid vertical loads and a suction anchor must be designed to withstand a certain dynamic vertical load. This capacity will depend on soil conditions and anchor design, aspects not considered in this study. These considerations, along with the uncertainty of the statistical analysis, must be considered during the detailed design of the mooring system.

The different solutions implemented and their related simulations results present advantages and disadvantages in terms of:

- mooring wire length: a longer line requires more material and this causes higher cost;
- mooring footprint: a larger footprint causes a larger area occupied by a hypothetical plant composed of several floating turbines, this aspect could arise environmental problems connected to possible damage to the sea bed and fishing areas;
- tension: higher tension in the wires requires materials that could withstand it and stronger materials rise construction cost;
- vertical forces at the anchors: especially suction anchors require structures, that connect the mooring wire to the sea bed, capable of withstanding significant vertical forces; as these forces increase, a more performant (and more expensive) anchor is required.

A comparison of these issues is given in Figure 5.19, Figure 5.20, Figure 5.21 and Figure 5.22, considering line 1, anchor 1 and 100 years return period environmental conditions and a 6 hours storm, pointing out the difference between the Adriatic Sea (sea depth 100 m) and the South Sicily (sea depth 400 m).

Comparing the mooring wire length, it is evident that, when the sea depth increases, the line length is higher. There is also a difference between anchors and suction anchors: the length required in the second case is less than a half of the one required in the first case (Figure 5.19).

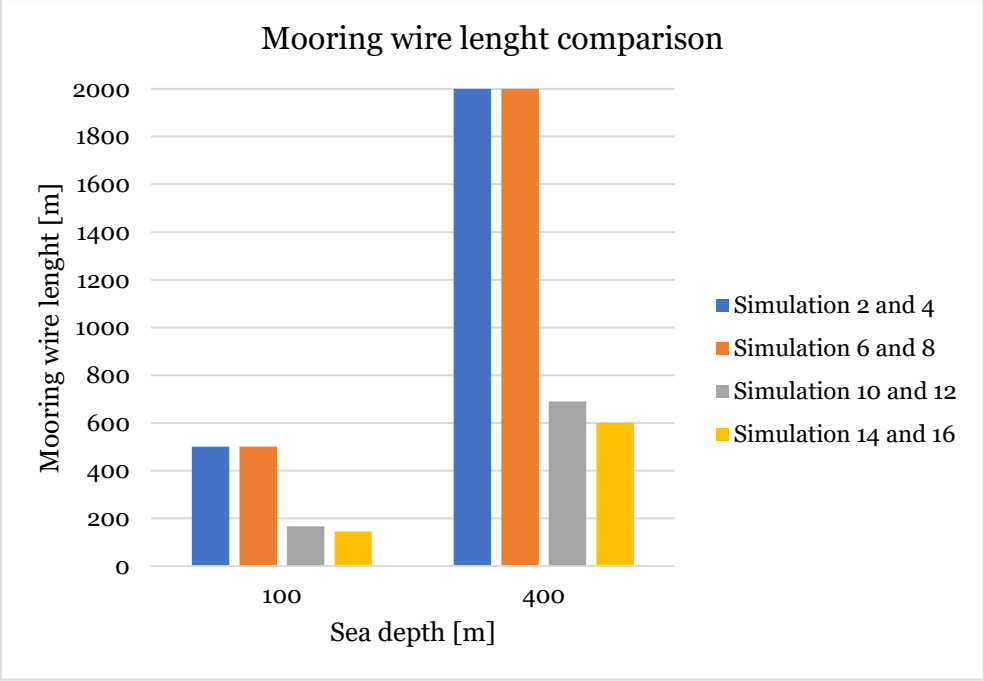


Figure 5.19: mooring wire length comparison (simulations 2/4/6/8/10/12/14/16).

As the sea depth increases, the mooring footprint is heavier (Figure 5.20): the area used for suction anchors in the South Sicily location is 15 times larger than the one used in the Adriatic Sea. A remarkable difference is present between traditional anchors and suction anchors: the first requires a much larger area than the second, in every case. See Figure 5.11 and Figure 5.14

for details about the horizontal spread chosen and its connected footprint shown in Figure 5.20.

As seen in 5.5.2, the small suction anchor footprint is increased when it is required a reduction in the vertical forces at the anchor: keeping the touchdown point of the mooring wire at the anchor, a rise of the mooring spread and a contemporary decrease of the angle between the line and the seabed cause vertical force to drop. So, at the cost of a larger footprint (Figure 5.15 and Figure 5.16) and a longer wire line, which uses more material, the decrease of vertical forces allows the use of a less performant and cheaper anchor.

The decision of whether or not applying this solution of vertical forces reduction must be analysed in terms of costs and environmental impact: the enlarged footprint of the suction anchor is near to a traditional anchor one and the increase of wire length could not be compensated by a cheaper anchor. At the end, the advantages of a suction anchor could disappear and this could make the use of a traditional anchor more convenient in terms of cost-efficiency.

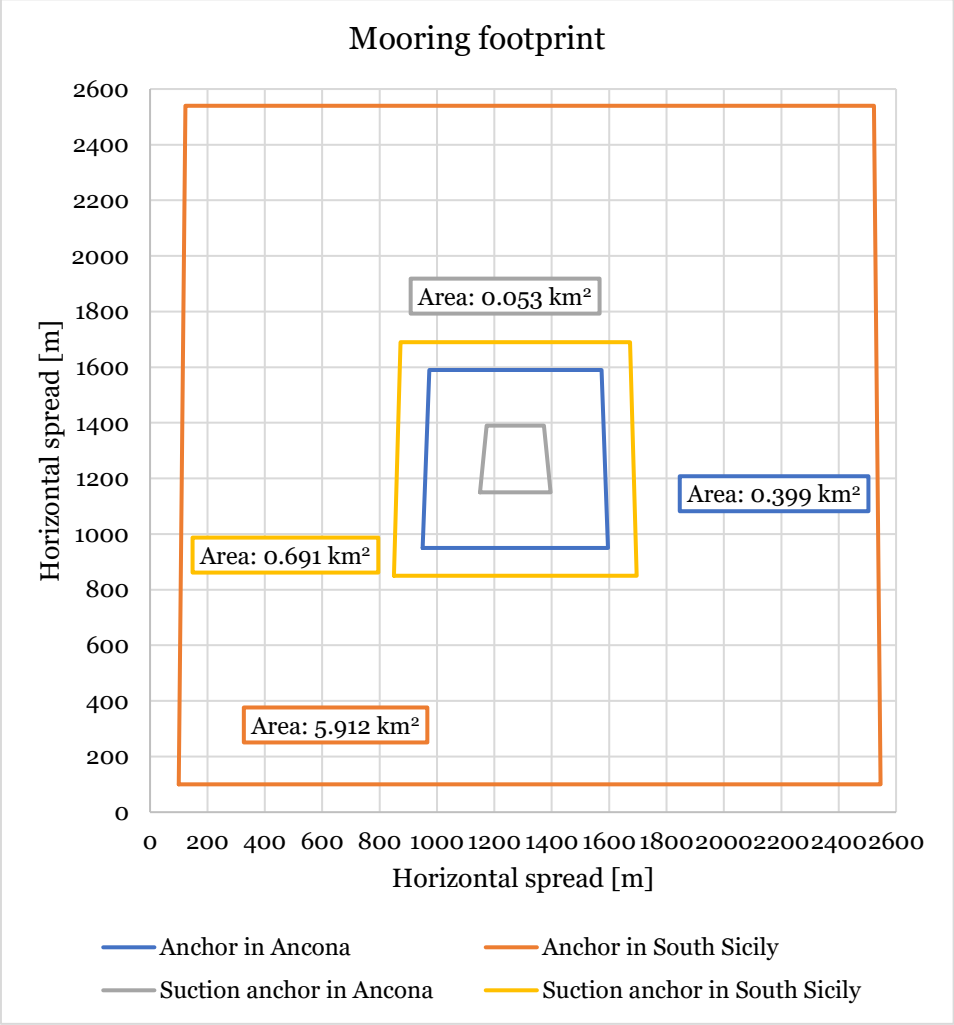


Figure 5.20: mooring footprint in the Adriatic Sea and South Sicily.

Tension increases with depth with different schemes (Figure 5.21): the presence of a mooring line entirely composed by chains causes a more significant increase. In general, suction anchor solutions cause more stress in the wires with respect to traditional anchors and, in particular, the solution that brings more tension in the lines is the taut mooring one. This fact, regarding suction anchors, leads to the need of choosing a stronger material regarding the lines: this, coupled with a high sea depth that requires long cables, could be make less desirable a similar solution. A limiting answer, concerning tension, could be the use of hybrid (chain and synthetic fibres) mooring line.

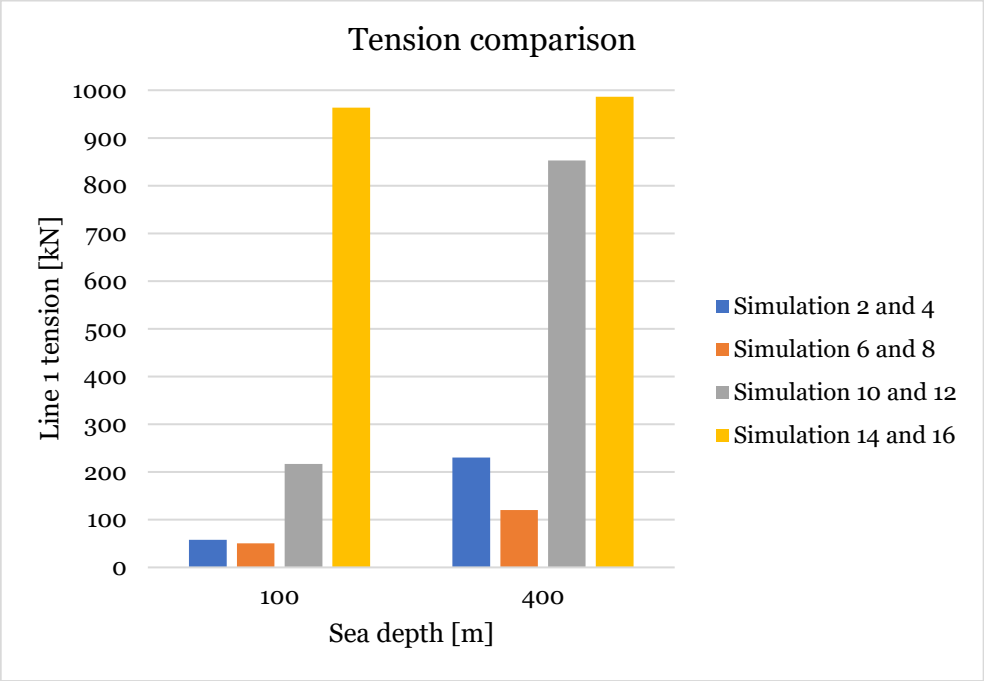


Figure 5.21: tension in the most stressed point of the mooring line comparison (simulations 2/4/6/8/10/12/14/16).

The analysis of vertical forces (Figure 5.22) could confirm the considerations made previously for the tension in the wire: as the sea depth increases, suction anchors could become a less desirable solution. The vertical forces, that the anchor must withstand, increase with the depth of the sea bed, requiring higher allowable vertical forces and more difficult to install, regarding the water depth, hardware. Traditional anchors, on the other hand, present only horizontal forces in the simulation performed, with no risk of uplifting.

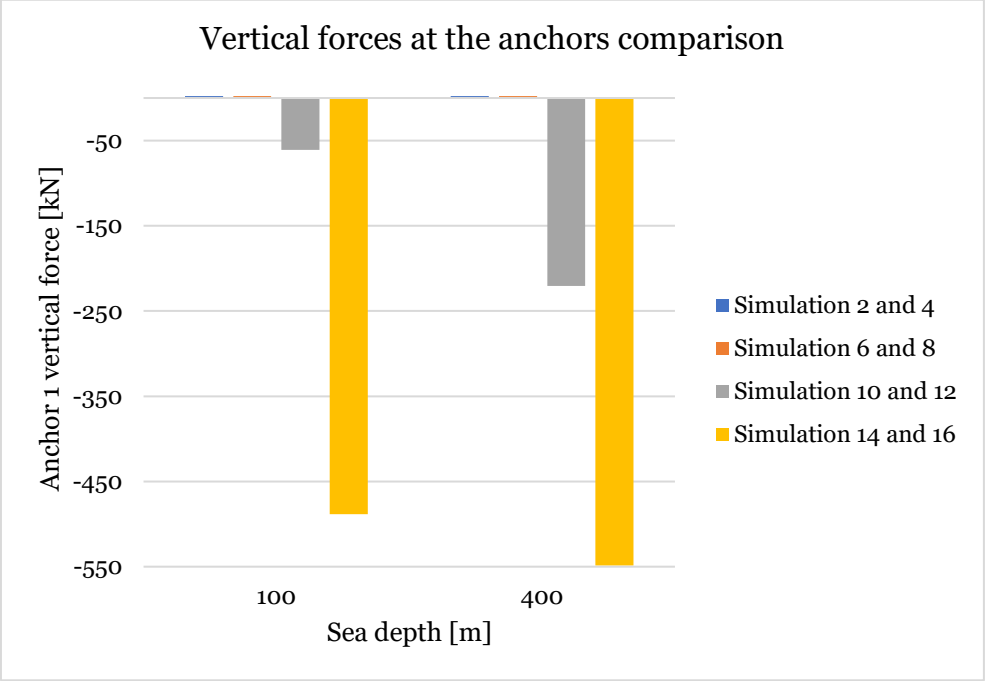


Figure 5.22: vertical forces at the anchors comparison (simulations 2*/4*/6*/8*/10/12/14/16, with * are reported static values refer to 5.6.3).

The process of choosing the best solution concerning mooring for a floating wind turbine must consider wire length, mooring footprint, tension and forces at the anchors and their interactions. For the cases in the study two different solution can be found: taut mooring system has been excluded for its high levels of tension in the wire and its performing anchors. Possible solutions, looking at the simulations results, could be:

- for the Adriatic Sea: suction anchors with chains;
- for South Sicily: traditional anchors with chains or chains with synthetic fibres.

For the Adriatic Sea, considering the low depth, a suction anchor with chain lines could be the best solution: reduced footprint and wire length and relative easiness of installation of this device with respect to water depth, could justify investing resources in the wire strength and anchor performance.

For South Sicily, on the other hand, it could be preferable focusing on traditional anchors: long wires and large footprint are compensated with less demanding material characteristics, with possibility of tension reduction using hybrid lines, and less expensive and easy to install anchors.

# Chapter 6
# Conclusions

## 6.1 Conclusions

This thesis deals essentially with finding the most suitable mooring solutions for the realization of a floating wind turbine farm in the Italian seas, focusing on two different locations. This has been obtained through the implementation of a 3D numerical model in the OrcaFlex software, which comprehends a common geometry of the floater, environmental loads and site characteristics in the two chosen study areas.

For the last two aspects, emerged that a different return period for wind speed and wave height made little difference in the results. The parameter that affected the most the outcomes, differentiating the two areas, is sea depth: when the depth increases, the lines' length, the mooring footprint, the wires' tension and the vertical forces at the anchors, for the suction ones, are higher.

A similar consideration can be drawn from the simulations for the mooring solutions: in the same depth conditions, when a traditional anchor is used, the lines' length and the mooring footprint are higher, while wires' tension is lower than a suction anchor. A suction anchor must cope with vertical forces too, not present in the traditional ones.

A general indication from the simulations has been obtained also for suction anchors: vertical forces at the anchors can be reduced with the increase of the horizontal spread of the moorings and the consequent reduction of the angle between sea bed and lines.

Considering the advantages and disadvantages of the previous aspects and the technical challenges of the installation and the design, in the end, the proposed numerical model was successful in providing a simple indication for the mooring of floating wind turbines in two different areas of the seas surrounding the Italian peninsula: for the Adriatic Sea (shallow waters), suction anchors with chains and for the Strait of Sicily (deeper waters), traditional anchors with chains or chains with synthetic fibres.

Generally, it can be derived that, for shallow waters, the suction anchors should be the preferred solution: the smaller occupied area and the shorter line compensate the design

difficulties of a similar device and the higher tensions of the wires. On the other hand, for deeper waters, the enlarged footprint and longer wires are the price to pay for the simplicity and the lower tension of traditional anchors.
In the finding of the environmental design parameters concerning wind speed and wave height, the best results are obtained with a Gumbel distribution, having parameters estimated with maximum goodness of fit procedure. An important issue emerged in the available data from the waves monitoring networks: the recordings are often discontinuous due to operational problems for the "Rete Ondametrica Nazionale", which has later been dismantled.
The modelled structure is the one that appears to be the most suitable in the Italian environment, with the current grade of development: a semi-submersible structure with the WindFloat design, developed in Portugal by Principle Power. It is particularly suitable for the Italian seas: its low draft allows transport and installation in shallow waters, like the Adriatic ones, without the need of specific vessels, apart simple tug boats, or good weather conditions. Italy can build this type of floating wind turbine, in ports with suitable drydocks for the construction of a similar structure, like Palermo, Livorno and Trieste. The possibility of commissioning in other EU countries in the Mediterranean area has been explored too: ports are available in Marseille (France), Skaramagas (Greece) and Valletta (Malta).
Potentially, the OrcaFlex numerical models, with the refinements explained in the next paragraph, can be applied in various environments all around the world, given the input parameter elaborated from on-site analysis, to provide an indication of a potential mooring solution for a semi-submersible floating structure.
The compiled R scripts can perform a statistical analysis for wind speed and wave height for any given location, with the input parameters made of a simple text file with the local recordings inside.

## 6.2 Recommendations for further works

Numerical models like the one used in this work can be a powerful tool in the assessment of a specific aspect of possible project, like moorings. Their accuracy is mainly based on the hypothesis made at the beginning of the elaboration process and the data gathered about the environment or, in other words, creating a numerical model means to recreate a simplified version of the reality but for the moment some aspects are still missing. These features can be a starting point for future works with the goal to improve the results and they are listed below:

- two main environmental variables have not been analysed, currents and sea floor composition: once located a more definite area, these aspects should be implemented in future works. Currents will be part of the external loading on the structure and sea

floor composition will influence the anchors' performance, especially influencing the design of the suction ones;

- other approaches could be followed in the statistical analysis of the environmental factors: the use of all records instead of the monthly maxima. If the data coverage is good enough, considering all the recordings could improve the data at disposal. This may require additional monitoring networks;
- structural resonance must be computed in a real project: if the natural frequency of the floater is close to the peak wave frequency, the resulting resonance could endanger the structural integrity. Further analysis on blades and tower are needed too, to assess that the average wind speed does not cause excitation that would lead to resonance;
- the RAO used in this thesis has not been computed specifically for a semi-submersible floating wind turbine: future works should face this issue with a specific elaboration process, which comprehends numerical analysis and test in tanks with scaled models of the floater-turbine system;
- this work does not address system economics: manufacturing, installation or decommissioning considerations or optimization of the floating wind turbine mooring system. These aspects could be a crucial factor in the realization of a floating wind farm project.

# References


American Bureau of Shipping. *Use of Synthetic Ropes in Deepwater Moorings: ABS guidance notes*. American Bureau of Shipping, 1999.

American Petroleum Institute. *Recommended Practice for the Analysis of Spread Mooring*. RP 2P, 1987.

Associazione Nazionale Energia dal Vento. "ANEV brochure." June 2017. http://www.anev.org/wp-content/uploads/2017/06/Anev_brochure_2017_10.pdf (accessed October 23, 2017).

Bureau of Ocean Energy Management. "WindFloat Pacific." 29 July 2014. https://www.boem.gov/NREL-WindFloat-Pacific-OSW-Project/ (accessed October 24, 2017).

Cantieri del Mediterraneo. *Dry docks info*. n.d. https://cantieridelmediterraneo.com/drydock-info/ (accessed October 25, 2017).

Chakrabarti, Subrata . *Handbook of Offshore Engineering (2-volume set)*. Elsevier Science, 2015.

Corriere di Taranto. *Parco eolico offshore: il progetto va avanti. Via ai lavori nel 2017, operativo nel 2018*. 15 March 2017. http://www.corriereditaranto.it/2017/03/15/parco-eolico-offshore-progetto-va-avanti-via-ai-lavori-nel-2017-operativo-nel-2018/ (accessed October 23, 2017).

Delignette-Muller, Marie-Laure, Christophe Dutang, Regis Pouillot, Jean-Baptiste Denis , and Aurélie Siberchicot. "Package 'fitdistrplus'." *CRAN*. 24 March 2017. https://cran.r-project.org/web/packages/fitdistrplus/fitdistrplus.pdf (accessed October 12, 2017).

DNV GL. "Offshore mooring chain." n.d. https://rules.dnvgl.com/docs/pdf/dnvgl/OS/2015-07/DNVGL-OS-E302.pdf (accessed November 29, 2017).

—. "Synthetic fibre ropes for towing, mooring and anchoring." March 2016. https://rules.dnvgl.com/docs/pdf/DNVGL/CP/2016-03/DNVGL-CP-0100.pdf (accessed November 29, 2017).

Ente bacini di Genova. *Facilities*. n.d. http://www.entebacinigenova.it/index.php/servizi/facilities (accessed October 25, 2017).

European Commission. *CO2 time series 1990-2013 per region/country*. 2014. http://edgar.jrc.ec.europa.eu/overview.php?v=CO2ts1990-2013&sort=des9 (accessed October 23, 2017).

European Union. *Renewable Energy Directive*. 2014. https://ec.europa.eu/energy/en/topics/renewable-energy/renewable-energy-directive (accessed October 23, 2017).

European Wind Energy Association. "Deep Water - The next step for offshore wind energy." 2013.

Fincantieri. "Ship repair services and conversions." 2010. https://www.fincantieri.com/globalassets/prodotti-servizi/riparazioni-e-trasformazione-navali/brochure-ship-repair-services.pdf (accessed October 25, 2017).

*Geoportale Nazionale, Bathymetry*. 3 February 2009. http://www.pcn.minambiente.it/geoportal/catalog/search/resource/livedata-preview.page?uuid=%7BA4B0E0DA-BC2F-4D36-B666-6102B1C423C7%7D&url=http%3A%2F%2Fwww.pcn.minambiente.it%2Fviewer%2Findex.php%3Fservices%3Dbatimetrica&info=%2Fgeoportal%2Frest%2Fdocument (accessed October 11, 2017).

*Geoportale Nazionale, INSPIRE*. n.d. http://www.pcn.minambiente.it/mattm/inspire/ (accessed October 10, 2017).

Glosten. *PelaStar*. 2012. http://pelastar.com/ (accessed October 24, 2017).

Gudmestad, Ove Tobias. *Marine Technology and Operations: Theory & Practice*. WIT Press, 2015.

Hellenic Shipyards. *Home*. n.d. http://www.hellenic-shipyards.gr/ (accessed October 30, 2017).

Holthuijsen, Leo H. *Waves in Oceanic and Coastal Waters*. Cambridge University Press, 2010.

*Istituto Superiore per la Protezione e la Ricerca Ambientale*. n.d. http://www.isprambiente.gov.it/it/ispra (accessed October 10, 2017).

Johnson, Norman L., Samuel Kotz, and N. Balakrishnan. *Continuous Univariate Distributions, Volume 1 and 2*. John Wiley and Sons, 1994.

La Stampa. *Pale eoliche, il no degli ambientalisti "Deturpano il nostro territorio"*. 4 February 2014. http://www.lastampa.it/2014/02/04/edizioni/savona/pale-eoliche-il-no-degli-ambientalisti-deturpano-il-nostro-territorio-3h70GyK63atEaPa6NjHPRM/pagina.html (accessed October 13, 2017).

Legambiente. *L'assurdo stop all'eolico off-shore in Italia*. 15 June 2015. https://www.legambiente.it/sites/default/files/docs/eolico_off-shore_dossier2015.pdf (accessed October 23, 2017).

Lindeboom, H J, et al. "Short-term ecological effects of an offshore wind farm in the Dutch coastal zone; a compilation." *Environmental Research Letters*, 2011 August 2011.

Marseille port. *Installations*. n.d. http://www.marseille-port.fr/fr/Page/Installations/14569 (accessed October 30, 2017).

Ministero dello Sviluppo Economico. “Strategia energetica nazionale.” 12 June 2017. http://dgsaie.mise.gov.it/sen/Strategia_Energetica_Nazionale_2017_-_documento_di_consultazione.pdf (accessed October 2017, 2017).

Naviravenna. *Facilities*. n.d. http://www.naviravenna.it/index.php/it/facilities (accessed October 25, 2017).

Orcina. *OrcaFlex*. n.d. https://www.orcina.com/SoftwareProducts/OrcaFlex/ (accessed November 28, 2017).

—. *OrcaFlex documentation*. n.d. https://www.orcina.com/SoftwareProducts/OrcaFlex/Documentation/Help/ (accessed November 28, 2017).

—. *OrcaFlex examples - A production risers*. n.d. https://www.orcina.com/SoftwareProducts/OrcaFlex/Examples/A%20Production%20Risers/index.php (accessed November 29, 2017).

Palumbo. *Malta*. n.d. http://www.palumbo.it/palumbo_eng/facili4_eng.html (accessed October 30, 2017).

Port de Barcelona. *Informacion genaral*. n.d. http://www.portdebarcelona.cat/en/web/el-port/informacion-general (accessed October 30, 2017).

Porto di livorno. *Bacini di carenaggio*. n.d. http://www.portolivorno.it/bacini_carenaggio/ (accessed October 25, 2017).

Priciple Power. *WindFloat*. n.d. http://www.principlepowerinc.com/en/windfloat (accessed 10 2017, 24).

*Rete Mareografica Nazionale (1998-2014)*. n.d. http://www.mareografico.it/ (accessed October 10, 2017).

*Rete Mareografica Nazionale (2014-2017)*. n.d. http://dati.isprambiente.it/dataset/rmn-la-rete-mareografica-nazionale/ (accessed October 10, 2017).

*Rete Ondametrica Nazionale*. n.d. http://dati.isprambiente.it/dataset/ron-rete-ondametrica-nazionale/ (accessed October 10, 2017).

*RMN Ancona*. n.d. http://www.mareografico.it/?session=0S178119609274M8878858884Y&syslng=ita&sysmen=-1&sysind=-1&syssub=-1&sysfnt=0&code=STAZ&idst=11&mode=INFO (accessed October 10, 2017).

*RMN Porto Empedocle*. n.d. http://www.mareografico.it/?session=0S658683622AQB89T658771&syslng=ita&sysmen=-1&sysind=-1&syssub=-1&sysfnt=0&code=STAZ&idst=1S&mode=INFO (accessed October 10, 2017).

Roddier, Dominique, Alexia Aubault, Antoine Peiffer, and Joshua Weinstein. “A generic 5 MW windfloat for numerical tool validation & comparison against a generic spar.” *ASME 2011 30th International Conference on Ocean, Offshore and Arctic Engineering*. Rotterdam, 2011.

*RON Ancona*. n.d. http://dati.isprambiente.it/id/buoy/ron/ancona-09/html (accessed October 10, 2017).

*RON Mazara del Vallo*. n.d. http://dati.isprambiente.it/id/buoy/ron/mazara-del-vallo-09/html (accessed October 10, 2017).

Statoil. *Hywind*. n.d. https://www.statoil.com/en/what-we-do/hywind-where-the-wind-takes-us.html (accessed October 24, 2017).

Structurae. *Grand Bassins Vauban*. n.d. https://structurae.net/structures/grands-bassins-vauban (accessed October 30, 2017).

Terna. *Dati statistici*. n.d. https://www.terna.it/it-it/sistemaelettrico/statisticheeprevisioni/datistatistici.aspx (accessed October 21, 2017).

UNFCCC. *The Paris agreement*. 4 November 2016. http://unfccc.int/paris_agreement/items/9485.php (accessed October 23, 2017).

Viktor Lenac Shipyards. *Facilities*. n.d. http://www.lenac.hr/Home.aspx?PageID=58 (accessed October 30, 2017).

# Appendix A
# SPARQL queries for wind and wave data

The queries have been submitted to the following website: http://dati.isprambiente.it/sparql.

## A.1 Ancona RMN

```
PREFIX : <http://dati.isprambiente.it/ontology/core#>
PREFIX gn: <http://www.geonames.org/ontology#>
PREFIX rdfs: <http://www.w3.org/2000/01/rdf-schema#>
PREFIX dcat: <http://www.w3.org/ns/dcat#>
select distinct ?station ?period ?csvUrl where {

#### Definire Parametro, Luogo e Periodo
?parameter a :Wind.
?place rdfs:label "Ancona".
FILTER ( str(?period) >= '1900-01' AND str(?period) <= '2017-12').

?parameter gn:nearbyFeature ?place.
?collection a :MeasurementCollection;
:measurementPeriod ?period;
:isDataOf ?parameter;
:generatedBy ?instrument;
dcat:downloadURL ?csvUrl.
?instrument :placedOn ?stat.
?stat rdfs:label ?station.
} ORDER BY ?period
```

## A.2 Porto Empedocle RMN

```
PREFIX : <http://dati.isprambiente.it/ontology/core#>
PREFIX gn: <http://www.geonames.org/ontology#>
PREFIX rdfs: <http://www.w3.org/2000/01/rdf-schema#>
PREFIX dcat: <http://www.w3.org/ns/dcat#>
select distinct ?station ?period ?csvUrl where {

#### Definire Parametro, Luogo e Periodo
?parameter a :Wind.
?place rdfs:label "Porto Empedocle".
FILTER ( str(?period) >= '1900-01' AND str(?period) <= '2017-12').

?parameter gn:nearbyFeature ?place.
```

```
?collection a :MeasurementCollection;
:measurementPeriod ?period;
:isDataOf ?parameter;
:generatedBy ?instrument;
dcat:downloadURL ?csvUrl.
?instrument :placedOn ?stat.
?stat rdfs:label ?station.
} ORDER BY ?period
```

# A.3 Ancona RON

```
PREFIX : <http://dati.isprambiente.it/ontology/core#>
PREFIX gn: <http://www.geonames.org/ontology#>
PREFIX rdfs: <http://www.w3.org/2000/01/rdf-schema#>
PREFIX dcat: <http://www.w3.org/ns/dcat#>
select distinct ?station ?period ?csvUrl where {

#### Definire Parametro, Luogo e Periodo
?parameter a :Wave.
?place rdfs:label "Ancona".
FILTER ( str(?period) >= '1900-01' AND str(?period) <= '2017-12').

?parameter gn:nearbyFeature ?place.
?collection a :MeasurementCollection;
:measurementPeriod ?period;
:isDataOf ?parameter;
:generatedBy ?instrument;
dcat:downloadURL ?csvUrl.
?instrument :placedOn ?stat.
?stat rdfs:label ?station.
} ORDER BY ?period
```

# A.4 Mazara del Vallo RON

```
PREFIX : <http://dati.isprambiente.it/ontology/core#>
PREFIX gn: <http://www.geonames.org/ontology#>
PREFIX rdfs: <http://www.w3.org/2000/01/rdf-schema#>
PREFIX dcat: <http://www.w3.org/ns/dcat#>
select distinct ?station ?period ?csvUrl where {

#### Definire Parametro, Luogo e Periodo
?parameter a :Wave.
?place rdfs:label "Mazara del Vallo".
FILTER ( str(?period) >= '1900-01' AND str(?period) <= '2017-12').

?parameter gn:nearbyFeature ?place.
?collection a :MeasurementCollection;
:measurementPeriod ?period;
:isDataOf ?parameter;
:generatedBy ?instrument;
dcat:downloadURL ?csvUrl.
?instrument :placedOn ?stat.
?stat rdfs:label ?station.
} ORDER BY ?period
```

# Appendix B
# Monthly data coverage

In these tables the ratio between data measured and expected measures is given for each of the months of a year, following the pattern explained in 2.1.1 and 2.1.2. The boxes with green background and green text represent a month with a coverage above or equal to 75% and the measurements in these months have been considered for the statistical analysis. The boxes with green text only (box without colour) in the RON tables represent a significant data, considered for the computations in a month with coverage less than 75% (refer to 2.1.2).

## B.1 Ancona RMN

| | Jan | Feb | Mar | Apr | May | Jun | Jul | Aug | Sep | Oct | Nov | Dec |
|---|---|---|---|---|---|---|---|---|---|---|---|---|
| **1999** | 0.0% | 87.2% | 100.0% | 100.0% | 79.4% | 94.6% | 100.0% | 100.0% | 100.0% | 99.9% | 100.0% | 100.0% |
| **2000** | 100.0% | 100.0% | 100.0% | 100.0% | 100.0% | 100.0% | 100.0% | 97.0% | 100.0% | 100.0% | 100.0% | 100.0% |
| **2001** | 100.0% | 100.0% | 100.0% | 100.0% | 100.0% | 100.0% | 100.0% | 100.0% | 100.0% | 100.0% | 100.0% | 100.0% |
| **2002** | 100.0% | 100.0% | 100.0% | 100.0% | 100.0% | 100.0% | 100.0% | 98.5% | 90.1% | 33.7% | 100.0% | 100.0% |
| **2003** | 100.0% | 100.0% | 100.0% | 100.0% | 100.0% | 100.0% | 100.0% | 100.0% | 100.0% | 100.0% | 100.0% | 100.0% |
| **2004** | 100.0% | 100.0% | 100.0% | 100.0% | 100.0% | 100.0% | 100.0% | 100.0% | 100.0% | 100.0% | 100.0% | 100.0% |

| 2017 | 2016 | 2015 | 2014 | 2013 | 2012 | 2011 | 2010 | 2009 | 2008 | 2007 | 2006 | 2005 |
|---|---|---|---|---|---|---|---|---|---|---|---|---|
| 99.1% | 96.1% | 98.7% | 99.6% | 99.6% | 92.9% | 98.8% | 98.0% | 100.0% | 100.0% | 100.0% | 96.9% | 100.0% |
| 97.8% | 98.4% | 99.3% | 99.9% | 99.7% | 91.0% | 96.3% | 100.0% | 100.0% | 100.0% | 100.0% | 100.0% | 100.0% |
| 97.4% | 98.2% | 98.8% | 99.7% | 99.7% | 86.5% | 98.0% | 100.0% | 100.0% | 100.0% | 100.0% | 100.0% | 100.0% |
| 98.0% | 97.3% | 98.3% | 99.9% | 99.5% | 98.4% | 93.8% | 99.9% | 100.0% | 100.0% | 100.0% | 100.0% | 100.0% |
| 98.7% | 97.5% | 98.7% | 99.9% | 99.9% | 99.9% | 95.7% | 100.0% | 100.0% | 100.0% | 100.0% | 100.0% | 100.0% |
| 98.0% | 98.1% | 97.2% | 100.0% | 99.4% | 99.8% | 97.7% | 100.0% | 100.0% | 100.0% | 100.0% | 100.0% | 100.0% |
| 98.5% | 94.7% | 97.1% | 99.9% | 99.8% | 99.8% | 98.1% | 100.0% | 99.6% | 100.0% | 100.0% | 100.0% | 100.0% |
| 98.3% | 98.1% | 98.8% | 100.0% | 99.6% | 99.7% | 96.1% | 100.0% | 100.0% | 100.0% | 100.0% | 100.0% | 100.0% |
| 0.0% | 98.7% | 99.2% | 99.7% | 99.8% | 100.0% | 99.6% | 100.0% | 94.7% | 100.0% | 100.0% | 100.0% | 100.0% |
| 0.0% | 99.4% | 97.5% | 99.6% | 99.9% | 100.0% | 97.5% | 99.9% | 100.0% | 100.0% | 100.0% | 100.0% | 100.0% |
| 0.0% | 99.0% | 97.2% | 99.2% | 95.9% | 99.8% | 98.5% | 99.5% | 100.0% | 100.0% | 100.0% | 100.0% | 100.0% |
| 0.0% | 97.6% | 96.1% | 98.8% | 99.6% | 99.8% | 98.1% | 99.9% | 100.0% | 100.0% | 100.0% | 100.0% | 100.0% |

# B.2 Porto Empedocle RMN

| | 1998 | 1999 | 2000 | 2001 | 2002 | 2003 | 2004 | 2005 | 2006 | 2007 | 2008 | 2009 | 2010 |
|---|---|---|---|---|---|---|---|---|---|---|---|---|---|
| Jan | 0.0% | 96.8% | 100.0% | 89.2% | 99.7% | 0.0% | 98.9% | 99.1% | 23.1% | 100.0% | 100.0% | 94.0% | 99.9% |
| Feb | 0.0% | 100.0% | 100.0% | 0.0% | 99.4% | 0.0% | 99.6% | 99.4% | 38.2% | 100.0% | 100.0% | 100.0% | 99.9% |
| Mar | 0.0% | 99.9% | 99.9% | 95.2% | 99.6% | 0.0% | 99.3% | 98.3% | 44.8% | 92.3% | 99.7% | 99.6% | 100.0% |
| Apr | 0.0% | 100.0% | 99.7% | 100.0% | 99.7% | 0.0% | 99.3% | 66.3% | 100.0% | 65.6% | 99.7% | 99.7% | 100.0% |
| May | 0.0% | 99.7% | 99.7% | 99.6% | 99.1% | 0.0% | 98.8% | 98.4% | 99.9% | 99.1% | 99.5% | 99.9% | 99.9% |
| Jun | 0.0% | 100.0% | 73.9% | 99.0% | 97.9% | 0.0% | 98.2% | 97.6% | 99.7% | 99.3% | 99.3% | 99.0% | 99.9% |
| Jul | 0.0% | 99.9% | 99.7% | 98.9% | 98.8% | 98.8% | 97.8% | 97.4% | 100.0% | 98.0% | 99.1% | 98.7% | 99.6% |
| Aug | 97.4% | 99.7% | 99.1% | 98.9% | 98.4% | 98.5% | 98.3% | 98.3% | 100.0% | 99.1% | 99.3% | 99.5% | 99.6% |
| Sep | 100.0% | 99.9% | 99.7% | 99.4% | 99.0% | 99.6% | 98.9% | 99.4% | 99.7% | 98.9% | 99.0% | 94.4% | 100.0% |
| Oct | 100.0% | 99.9% | 100.0% | 99.9% | 98.9% | 99.5% | 97.8% | 61.3% | 100.0% | 99.7% | 99.7% | 99.7% | 100.0% |
| Nov | 99.9% | 100.0% | 99.9% | 99.9% | 98.9% | 99.7% | 99.3% | 53.5% | 100.0% | 99.9% | 99.6% | 97.8% | 100.0% |
| Dec | 99.9% | 100.0% | 99.9% | 99.1% | 0.0% | 99.9% | 99.7% | 30.9% | 100.0% | 99.9% | 99.7% | 0.0% | 100.0% |

| 2017 | 2016 | 2015 | 2014 | 2013 | 2012 | 2011 |
|---|---|---|---|---|---|---|
| 98.4% | 99.9% | 100.0% | 93.7% | 99.9% | 99.8% | 99.7% |
| 93.3% | 99.3% | 100.0% | 88.6% | 100.0% | 100.0% | 100.0% |
| 85.3% | 98.7% | 100.0% | 82.3% | 99.8% | 99.6% | 100.0% |
| 60.9% | 98.9% | 100.0% | 98.6% | 98.9% | 98.9% | 100.0% |
| 25.0% | 98.3% | 99.8% | 100.0% | 99.8% | 99.3% | 99.9% |
| 0.0% | 98.4% | 99.8% | 100.0% | 98.0% | 90.6% | 99.5% |
| 0.0% | 78.0% | 94.2% | 99.9% | 97.3% | 99.7% | 97.9% |
| 0.0% | 92.0% | 97.9% | 99.9% | 96.1% | 99.8% | 99.9% |
| 0.0% | 96.9% | 96.9% | 99.9% | 93.0% | 99.8% | 100.0% |
| 0.0% | 97.7% | 99.2% | 100.0% | 89.0% | 100.0% | 100.0% |
| 0.0% | 99.6% | 99.5% | 100.0% | 96.3% | 99.9% | 100.0% |
| 0.0% | 98.9% | 99.2% | 99.9% | 99.8% | 99.7% | 99.8% |

# B.3 Ancona RON

| | 1999 | 2000 | 2001 | 2002 | 2003 |
|---|---|---|---|---|---|
| Jan | 0.0% | 99.2% | 0.0% | 0.0% | 95.1% |
| Feb | 0.0% | 62.5% | 0.0% | 0.0% | 66.7% |
| Mar | 71.4% | 99.2% | 0.0% | 0.0% | 82.5% |
| Apr | 100.0% | 31.7% | 0.0% | 0.0% | 94.7% |
| May | 99.6% | 66.1% | 0.0% | 100.0% | 91.3% |
| Jun | 99.2% | 39.2% | 0.0% | 81.7% | 90.3% |
| Jul | 100.0% | 100.0% | 0.0% | 100.0% | 82.0% |
| Aug | 99.6% | 100.0% | 0.0% | 30.2% | 92.5% |
| Sep | 97.5% | 92.1% | 0.0% | 70.9% | 98.9% |
| Oct | 96.8% | 98.0% | 0.0% | 57.1% | 98.8% |
| Nov | 100.0% | 99.2% | 0.0% | 96.1% | 99.5% |
| Dec | 100.0% | 75.0% | 0.0% | 98.5% | 57.7% |

| 2014 | 2013 | 2012 | 2011 | 2010 | 2009 | 2008 | 2007 | 2006 | 2005 | 2004 |
|---|---|---|---|---|---|---|---|---|---|---|
| 37.8% | 99.8% | 96.7% | 100.0% | 80.8% | 0.0% | 0.0% | 0.0% | 17.7% | 84.9% | 82.9% |
| 58.7% | 99.2% | 110.1% | 99.3% | 100.0% | 0.0% | 0.0% | 0.0% | 81.3% | 50.8% | 39.9% |
| 21.9% | 100.0% | 92.0% | 99.3% | 89.9% | 0.0% | 0.0% | 0.0% | 40.6% | 0.0% | 83.4% |
| 0.0% | 93.8% | 100.0% | 96.4% | 100.0% | 0.0% | 0.0% | 0.0% | 0.0% | 47.2% | 96.5% |
| 0.0% | 85.3% | 96.2% | 79.7% | 96.4% | 0.0% | 0.0% | 0.0% | 0.0% | 78.1% | 95.5% |
| 0.0% | 33.1% | 100.0% | 99.8% | 100.0% | 0.0% | 0.0% | 0.0% | 0.0% | 82.4% | 95.9% |
| 0.0% | 0.0% | 93.5% | 99.6% | 96.4% | 0.0% | 0.0% | 0.0% | 0.0% | 88.0% | 96.3% |
| 28.6% | 0.0% | 93.8% | 99.9% | 99.9% | 0.0% | 0.0% | 0.0% | 0.0% | 80.6% | 95.0% |
| 45.2% | 12.3% | 95.6% | 99.8% | 100.0% | 0.0% | 0.0% | 0.0% | 0.0% | 90.4% | 94.5% |
| 22.1% | 25.8% | 91.2% | 99.4% | 94.4% | 11.3% | 0.0% | 0.0% | 0.0% | 89.5% | 12.6% |
| 3.3% | 58.7% | 36.9% | 99.3% | 100.0% | 96.8% | 0.0% | 0.0% | 0.0% | 82.8% | 74.2% |
| 0.0% | 79.3% | 92.0% | 99.3% | 95.1% | 98.2% | 0.0% | 0.0% | 0.0% | 42.4% | 20.8% |

# B.4 Mazara del Vallo RON

| 1989 | Jan | Feb | Mar | Apr | May | Jun | Jul | Aug | Sep | Oct | Nov | Dec |
|---|---|---|---|---|---|---|---|---|---|---|---|---|
| 0.0% | 0.0% | 0.0% | 0.0% | 0.0% | 0.0% | 0.0% | 88.7% | 95.2% | 96.3% | 99.6% | 100.0% | 98.8% |

| 2003 | 2002 | 2001 | 2000 | 1999 | 1998 | 1997 | 1996 | 1995 | 1994 | 1993 | 1992 | 1991 | 1990 |
|---|---|---|---|---|---|---|---|---|---|---|---|---|---|
| 93.8% | 0.0% | 0.0% | 71.0% | 89.5% | 100.0% | 89.9% | 19.0% | 101.6% | 89.5% | 98.4% | 97.6% | 83.9% | 100.0% |
| 85.4% | 0.0% | 0.0% | 85.3% | 59.8% | 75.4% | 95.5% | 64.7% | 95.1% | 94.6% | 100.0% | 97.8% | 89.7% | 77.7% |
| 99.3% | 78.2% | 0.0% | 100.0% | 50.4% | 65.7% | 84.7% | 72.2% | 98.0% | 87.9% | 96.0% | 94.4% | 92.7% | 82.3% |
| 99.5% | 55.4% | 0.0% | 86.7% | 60.4% | 59.6% | 98.8% | 88.8% | 98.3% | 72.9% | 97.9% | 100.0% | 101.3% | 95.0% |
| 99.1% | 49.0% | 0.0% | 99.2% | 73.8% | 50.8% | 87.1% | 82.7% | 89.5% | 94.0% | 98.0% | 98.8% | 96.4% | 94.8% |
| 57.8% | 59.6% | 0.0% | 99.6% | 76.3% | 45.8% | 84.2% | 91.7% | 97.9% | 89.6% | 97.5% | 97.9% | 69.2% | 94.2% |
| 0.0% | 94.0% | 0.0% | 98.0% | 14.9% | 49.6% | 85.5% | 96.4% | 96.8% | 84.3% | 0.0% | 99.6% | 95.6% | 89.1% |
| 81.6% | 90.3% | 0.0% | 71.8% | 0.0% | 38.7% | 87.5% | 98.8% | 96.0% | 90.7% | 95.2% | 100.0% | 87.9% | 98.0% |
| 98.4% | 89.1% | 0.0% | 90.4% | 25.8% | 71.3% | 92.1% | 90.4% | 89.2% | 80.0% | 70.4% | 98.8% | 97.1% | 97.9% |
| 94.4% | 98.7% | 0.0% | 93.5% | 75.8% | 78.6% | 66.9% | 83.5% | 81.5% | 83.9% | 84.3% | 95.6% | 99.2% | 60.5% |
| 100.0% | 89.2% | 0.0% | 99.6% | 81.3% | 87.5% | 82.9% | 70.0% | 0.0% | 84.2% | 94.6% | 90.8% | 100.0% | 100.0% |
| 95.5% | 60.8% | 0.0% | 64.1% | 60.1% | 80.6% | 97.2% | 96.8% | 28.6% | 88.3% | 94.0% | 88.3% | 100.0% | 100.0% |

| 2014 | 2013 | 2012 | 2011 | 2010 | 2009 | 2008 | 2007 | 2006 | 2005 | 2004 |
|---|---|---|---|---|---|---|---|---|---|---|
| 40.9% | 0.0% | 93.2% | 98.8% | 98.2% | 0.0% | 97.0% | 0.0% | 61.6% | 95.4% | 77.3% |
| 41.6% | 0.0% | 95.0% | 97.9% | 64.7% | 0.0% | 100.4% | 0.0% | 59.1% | 66.5% | 53.1% |
| 74.5% | 0.0% | 99.6% | 98.8% | 0.0% | 0.0% | 74.5% | 0.0% | 56.4% | 80.3% | 83.7% |
| 58.3% | 0.0% | 98.0% | 97.3% | 68.5% | 0.0% | 6.1% | 0.0% | 40.7% | 89.4% | 53.8% |
| 80.2% | 0.0% | 99.5% | 97.2% | 97.9% | 0.0% | 0.0% | 23.5% | 36.4% | 72.8% | 64.7% |
| 95.6% | 0.0% | 99.9% | 99.7% | 92.7% | 0.0% | 0.0% | 68.4% | 40.4% | 92.3% | 99.0% |
| 99.6% | 0.0% | 98.2% | 99.8% | 99.5% | 0.0% | 0.0% | 72.1% | 39.9% | 87.5% | 99.7% |
| 99.2% | 0.0% | 92.9% | 95.9% | 99.5% | 0.0% | 0.0% | 96.1% | 39.0% | 90.6% | 100.0% |
| 61.1% | 0.0% | 98.7% | 75.3% | 98.9% | 0.0% | 0.0% | 93.6% | 39.8% | 97.0% | 99.0% |
| 45.6% | 0.0% | 98.7% | 46.6% | 96.5% | 0.0% | 0.0% | 44.3% | 37.8% | 92.8% | 97.5% |
| 0.0% | 76.5% | 98.9% | 66.2% | 94.5% | 11.7% | 0.0% | 0.0% | 4.2% | 90.0% | 94.0% |
| 0.0% | 80.2% | 23.7% | 95.4% | 98.9% | 96.0% | 0.0% | 90.1% | 0.0% | 49.3% | 54.2% |

# Appendix C
# R codes

For the Gumbel and Weibull distributions, PDFs and CDFs refer to 2.2.2 and 2.2.3 with the following notation used in the scripts to represent the different parameters:

- beta = β: shape parameter;
- mu = μ: location parameter;
- s = σ: scale parameter.

## C.1 Ancona (design wind speed)

```
ancona = read.table("wind_ancona.txt", header = TRUE)
ancona

#histogram
windows()
hist(ancona$WS, probability = TRUE, main = "Histogram of the wind speed",
xlab = "Wind speed [m/s]")

library(fitdistrplus)

T50 = 50
T100 = 100

F50 = (T50-1)/T50
F50
F100 = (T100-1)/T100
F100

#maximum likelihood estimation
dgumbel = function(x,mu,s){ # PDF
  exp((mu - x)/s - exp((mu - x)/s))/s}

pgumbel = function(q,mu,s){ # CDF
  exp(-exp(-((q - mu)/s)))}

qgumbel = function(p, mu, s){ # quantile function
  mu-s*log(-log(p))}

gumbel_mle    =    fitdist(ancona$WS,    "gumbel",    start=list(mu=5,    s=5),
method="mle")
```

```
summary(gumbel_mle)

gof_gmle = gofstat(gumbel_mle, discrete=FALSE)
gof_gmle

windows()
par(cex=1.2, bg="white")
plot(gumbel_mle, lwd=2, col="cornflowerblue")

#wind speed estimations (mle)
mu_gmle = getElement(gumbel_mle$estimate, "mu")
s_gmle = getElement(gumbel_mle$estimate, "s")

W50_gmle = mu_gmle-s_gmle*log(log(F50^(-1)))
W50_gmle

W100_gmle = mu_gmle-s_gmle*log(log(F100^(-1)))
W100_gmle

#maximum goodness of fit
gumbel_mge   =   fitdist(ancona$WS,   "gumbel",   start=list(mu=5,   s=5),
method="mge", gof="KS")

summary(gumbel_mge)

gof_gmge = gofstat(gumbel_mge, discrete=FALSE)
gof_gmge

windows()
par(cex=1.2, bg="white")
plot(gumbel_mge, lwd=2, col="cornflowerblue")

#Wind speed estimations (mge)
mu_gmge = getElement(gumbel_mge$estimate, "mu")
s_gmge = getElement(gumbel_mge$estimate, "s")

W50_gmge = mu_gmge-s_gmge*log(log(F50^(-1)))
W50_gmge

W100_gmge = mu_gmge-s_gmge*log(log(F100^(-1)))
W100_gmge
```

## C.2 Porto Empedocle (design wind speed)

```
porto_empedocle = read.table("wind_portoempedocle.txt", header = TRUE)
porto_empedocle

#histogram
windows()
hist(porto_empedocle$WS, probability = TRUE, main = "Histogram of the wind
speed", xlab = "Wind speed [m/s]")

library(fitdistrplus)

T50 = 50
T100 = 100

F50 = (T50-1)/T50
F50
F100 = (T100-1)/T100
```

```
F100

#maximum likelihood estimation
dgumbel = function(x,mu,s){ # PDF
  exp((mu - x)/s - exp((mu - x)/s))/s}

pgumbel = function(q,mu,s){ # CDF
  exp(-exp(-((q - mu)/s)))}

qgumbel = function(p, mu, s){ # quantile function
  mu-s*log(-log(p))}

gumbel_mle = fitdist(porto_empedocle$WS, "gumbel", start=list(mu=5, s=5),
method="mle")

summary(gumbel_mle)

gof_gmle = gofstat(gumbel_mle, discrete=FALSE)
gof_gmle

windows()
par(cex=1.2, bg="white")
plot(gumbel_mle, lwd=2, col="cornflowerblue")

#wind speed estimations (mle)
mu_gmle = getElement(gumbel_mle$estimate, "mu")
s_gmle = getElement(gumbel_mle$estimate, "s")

W50_gmle = mu_gmle-s_gmle*log(log(F50^(-1)))
W50_gmle

W100_gmle = mu_gmle-s_gmle*log(log(F100^(-1)))
W100_gmle

#maximum goodness of fit
gumbel_mge = fitdist(porto_empedocle$WS, "gumbel", start=list(mu=5, s=5),
method="mge", gof="KS")

summary(gumbel_mge)

gof_gmge = gofstat(gumbel_mge, discrete=FALSE)
gof_gmge

windows()
par(cex=1.2, bg="white")
plot(gumbel_mge, lwd=2, col="cornflowerblue")

#Wind speed estimations (mge)
mu_gmge = getElement(gumbel_mge$estimate, "mu")
s_gmge = getElement(gumbel_mge$estimate, "s")

W50_gmge = mu_gmge-s_gmge*log(log(F50^(-1)))
W50_gmge

W100_gmge = mu_gmge-s_gmge*log(log(F100^(-1)))
W100_gmge
```

## C.3 Ancona (design wave height, complete dataset)

```
ancona = read.table("wave_ancona.txt", header = TRUE)
```

```
ancona

#histogram
windows()
hist(ancona$Hm, probability = TRUE, main = "Histogram of the wave height",
xlab = "Wave height [m]")

library(fitdistrplus)

T50 = 50
T100 = 100

F50 = (T50-1)/T50
F50
F100 = (T100-1)/T100
F100

{#gumbel
  #maximum likelihood estimation
  dgumbel = function(x,mu,s){ # PDF
  exp((mu - x)/s - exp((mu - x)/s))/s}

  pgumbel = function(q,mu,s){ # CDF
  exp(-exp(-((q - mu)/s)))}

  qgumbel = function(p, mu, s){ # quantile function
  mu-s*log(-log(p))}

  gumbel_mle   =   fitdist(ancona$Hm,   "gumbel",   start=list(mu=5,   s=5),
method="mle")

  summary(gumbel_mle)

  gof_gmle = gofstat(gumbel_mle, discrete=FALSE)
  gof_gmle

  windows()
  par(cex=1.2, bg="white")
  plot(gumbel_mle, lwd=2, col="cornflowerblue")

  #wave height estimations (mle)
  mu_gmle = getElement(gumbel_mle$estimate, "mu")
  s_gmle = getElement(gumbel_mle$estimate, "s")

  W50_gmle = mu_gmle-s_gmle*log(log(F50^(-1)))
  W50_gmle

  W100_gmle = mu_gmle-s_gmle*log(log(F100^(-1)))
  W100_gmle

  #maximum goodness of fit
  gumbel_mge   =   fitdist(ancona$Hm,   "gumbel",   start=list(mu=5,   s=5),
method="mge", gof="KS")

  summary(gumbel_mge)

  gof_gmge = gofstat(gumbel_mge, discrete=FALSE)
  gof_gmge

  windows()
  par(cex=1.2, bg="white")
  plot(gumbel_mge, lwd=2, col="cornflowerblue")
```

```
  #wave height estimations (mge)
  mu_gmge = getElement(gumbel_mge$estimate, "mu")
  s_gmge = getElement(gumbel_mge$estimate, "s")

  W50_gmge = mu_gmge-s_gmge*log(log(F50^(-1)))
  W50_gmge

  W100_gmge = mu_gmge-s_gmge*log(log(F100^(-1)))
  W100_gmge
}

{#weibull
  #maximum likelihood estimation

  dwei = function(x, s, beta){ # PDF
    beta/s*(x/s)^(beta-1)*exp(-(x/s)^beta)}

  pwei = function(q, s, beta){ # CDF
    1-exp(-(q/s)^beta)}

  qwei = function(p, s, beta){ # quantile function
    s*(-log(1-p))^(1/s)}

  weibull_mle = fitdist(ancona$Hm, distr = "wei", start=list(s=5, beta=5),
method="mle")

  summary(weibull_mle)

  gof_wmle = gofstat(weibull_mle, discrete=FALSE)
  gof_wmle

  windows()
  par(cex=1.2, bg="white")
  plot(weibull_mle, lwd=2, col="cornflowerblue")

  #wave height estimations (mle)
  s_wmle = getElement(weibull_mle$estimate, "s")
  beta_wmle = getElement(weibull_mle$estimate, "beta")

  H50_wmle = s_wmle*(-log(1-F50))^(1/beta_wmle)
  H50_wmle

  H100_wmle = s_wmle*(-log(1-F100))^(1/beta_wmle)
  H100_wmle

  #maximum goodness of fit
  weibull_mge   =   fitdist(ancona$Hm,   "wei",   start=list(s=5,   beta=5),
method="mge", gof="KS")

  summary(weibull_mge)

  gof_wmge = gofstat(weibull_mge, discrete=FALSE)
  gof_wmge

  windows()
  par(cex=1.2, bg="white")
  plot(weibull_mge, lwd=2, col="cornflowerblue")

  #wave height estimations (mge)
  s_wmge = getElement(weibull_mge$estimate, "s")
  beta_wmge = getElement(weibull_mge$estimate, "beta")

  H50_wmge = s_wmge*(-log(1-F50))^(1/beta_wmge)
```

```
  H50_wmge

  H100_wmge = s_wmge*(-log(1-F100))^(1/beta_wmge)
  H100_wmge
}
```

# C.4 Ancona (design wave height, >3 m dataset)

```
ancona = read.table("wave_ancona.txt", header = TRUE)
ancona

Hm3 = ancona$Hm [ancona$Hm > 3]

#histogram
windows()
hist(Hm3, probability = TRUE, main = "Histogram of the wave height", xlab =
"Wave height [m]")

library(fitdistrplus)

T50 = 50
T100 = 100

F50 = (T50-1)/T50
F50
F100 = (T100-1)/T100
F100

{#gumbel
  #maximum likelihood estimation
  dgumbel = function(x,mu,s){ # PDF
    exp((mu - x)/s - exp((mu - x)/s))/s}

  pgumbel = function(q,mu,s){ # CDF
    exp(-exp(-((q - mu)/s)))}

  qgumbel = function(p, mu, s){ # quantile function
    mu-s*log(-log(p))}

  gumbel_mle = fitdist(Hm3, "gumbel", start=list(mu=5, s=5), method="mle")

  summary(gumbel_mle)

  gof_gmle = gofstat(gumbel_mle, discrete=FALSE)
  gof_gmle

  windows()
  par(cex=1.2, bg="white")
  plot(gumbel_mle, lwd=2, col="cornflowerblue")

  #wave height estimations (mle)
  mu_gmle = getElement(gumbel_mle$estimate, "mu")
  s_gmle = getElement(gumbel_mle$estimate, "s")

  W50_gmle = mu_gmle-s_gmle*log(log(F50^(-1)))
  W50_gmle

  W100_gmle = mu_gmle-s_gmle*log(log(F100^(-1)))
  W100_gmle
```

```
  #maximum goodness of fit
  gumbel_mge = fitdist(Hm3, "gumbel", start=list(mu=5, s=5), method="mge",
gof="KS")

  summary(gumbel_mge)

  gof_gmge = gofstat(gumbel_mge, discrete=FALSE)
  gof_gmge

  windows()
  par(cex=1.2, bg="white")
  plot(gumbel_mge, lwd=2, col="cornflowerblue")

  #wave height estimations (mge)
  mu_gmge = getElement(gumbel_mge$estimate, "mu")
  s_gmge = getElement(gumbel_mge$estimate, "s")

  W50_gmge = mu_gmge-s_gmge*log(log(F50^(-1)))
  W50_gmge

  W100_gmge = mu_gmge-s_gmge*log(log(F100^(-1)))
  W100_gmge
}

{#weibull
  #maximum likelihood estimation

  dwei = function(x, s, beta){ # PDF
    beta/s*(x/s)^(beta-1)*exp(-(x/s)^beta)}

  pwei = function(q, s, beta){ # CDF
    1-exp(-(q/s)^beta)}

  qwei = function(p, s, beta){ # quantile function
    s*(-log(1-p))^(1/s)}

  weibull_mle = fitdist(Hm3, distr = "wei", start=list(s=5, beta=5),
method="mle")

  summary(weibull_mle)

  gof_wmle = gofstat(weibull_mle, discrete=FALSE)
  gof_wmle

  windows()
  par(cex=1.2, bg="white")
  plot(weibull_mle, lwd=2, col="cornflowerblue")

  #wave height estimations (mle)
  s_wmle = getElement(weibull_mle$estimate, "s")
  beta_wmle = getElement(weibull_mle$estimate, "beta")

  H50_wmle = s_wmle*(-log(1-F50))^(1/beta_wmle)
  H50_wmle

  H100_wmle = s_wmle*(-log(1-F100))^(1/beta_wmle)
  H100_wmle

  #maximum goodness of fit
  weibull_mge = fitdist(Hm3, "wei", start=list(s=5, beta=5), method="mge",
gof="KS")

  summary(weibull_mge)
```

```
  gof_wmge = gofstat(weibull_mge, discrete=FALSE)
  gof_wmge

  windows()
  par(cex=1.2, bg="white")
  plot(weibull_mge, lwd=2, col="cornflowerblue")

  #wave height estimations (mge)
  s_wmge = getElement(weibull_mge$estimate, "s")
  beta_wmge = getElement(weibull_mge$estimate, "beta")

  H50_wmge = s_wmge*(-log(1-F50))^(1/beta_wmge)
  H50_wmge

  H100_wmge = s_wmge*(-log(1-F100))^(1/beta_wmge)
  H100_wmge
}
```

# C.5 Ancona (design wave height, >3.5 m dataset)

```
ancona = read.table("wave_ancona.txt", header = TRUE)
ancona

Hm35 = ancona$Hm [ancona$Hm > 3.5]

#histogram
windows()
hist(Hm35, probability = TRUE, main = "Histogram of the wave height", xlab =
"Wave height [m]")

library(fitdistrplus)

T50 = 50
T100 = 100

F50 = (T50-1)/T50
F50
F100 = (T100-1)/T100
F100

{#gumbel
  #maximum likelihood estimation
  dgumbel = function(x,mu,s){ # PDF
    exp((mu - x)/s - exp((mu - x)/s))/s}

  pgumbel = function(q,mu,s){ # CDF
    exp(-exp(-((q - mu)/s)))}

  qgumbel = function(p, mu, s){ # quantile function
    mu-s*log(-log(p))}

  gumbel_mle = fitdist(Hm35, "gumbel", start=list(mu=5, s=5), method="mle")

  summary(gumbel_mle)

  gof_gmle = gofstat(gumbel_mle, discrete=FALSE)
  gof_gmle

  windows()
```

```
  par(cex=1.2, bg="white")
  plot(gumbel_mle, lwd=2, col="cornflowerblue")

  #wave height estimations (mle)
  mu_gmle = getElement(gumbel_mle$estimate, "mu")
  s_gmle = getElement(gumbel_mle$estimate, "s")

  W50_gmle = mu_gmle-s_gmle*log(log(F50^(-1)))
  W50_gmle

  W100_gmle = mu_gmle-s_gmle*log(log(F100^(-1)))
  W100_gmle

  #maximum goodness of fit
  gumbel_mge = fitdist(Hm35, "gumbel", start=list(mu=5, s=5), method="mge",
gof="KS")

  summary(gumbel_mge)

  gof_gmge = gofstat(gumbel_mge, discrete=FALSE)
  gof_gmge

  windows()
  par(cex=1.2, bg="white")
  plot(gumbel_mge, lwd=2, col="cornflowerblue")

  #wave height estimations (mge)
  mu_gmge = getElement(gumbel_mge$estimate, "mu")
  s_gmge = getElement(gumbel_mge$estimate, "s")

  W50_gmge = mu_gmge-s_gmge*log(log(F50^(-1)))
  W50_gmge

  W100_gmge = mu_gmge-s_gmge*log(log(F100^(-1)))
  W100_gmge
}

{#weibull
  #maximum likelihood estimation

  dwei = function(x, s, beta){ # PDF
    beta/s*(x/s)^(beta-1)*exp(-(x/s)^beta)}

  pwei = function(q, s, beta){ # CDF
    1-exp(-(q/s)^beta)}

  qwei = function(p, s, beta){ # quantile function
    s*(-log(1-p))^(1/s)}

  weibull_mle = fitdist(Hm35, distr = "wei", start=list(s=5, beta=5),
method="mle")

  summary(weibull_mle)

  gof_wmle = gofstat(weibull_mle, discrete=FALSE)
  gof_wmle

  windows()
  par(cex=1.2, bg="white")
  plot(weibull_mle, lwd=2, col="cornflowerblue")

  #wave height estimations (mle)
  s_wmle = getElement(weibull_mle$estimate, "s")
```

```
  beta_wmle = getElement(weibull_mle$estimate, "beta")

  H50_wmle = s_wmle*(-log(1-F50))^(1/beta_wmle)
  H50_wmle

  H100_wmle = s_wmle*(-log(1-F100))^(1/beta_wmle)
  H100_wmle

  #maximum goodness of fit
  weibull_mge = fitdist(Hm35, "wei", start=list(s=5, beta=5), method="mge",
gof="KS")

  summary(weibull_mge)

  gof_wmge = gofstat(weibull_mge, discrete=FALSE)
  gof_wmge

  windows()
  par(cex=1.2, bg="white")
  plot(weibull_mge, lwd=2, col="cornflowerblue")

  #wave height estimations (mge)
  s_wmge = getElement(weibull_mge$estimate, "s")
  beta_wmge = getElement(weibull_mge$estimate, "beta")

  H50_wmge = s_wmge*(-log(1-F50))^(1/beta_wmge)
  H50_wmge

  H100_wmge = s_wmge*(-log(1-F100))^(1/beta_wmge)
  H100_wmge
}
```

## C.6 Mazara del vallo (design wave height, complete dataset)

```
mazara = read.table("wave_mazara.txt", header = TRUE)
mazara

#histogram
windows()
hist(mazara$Hm, probability = TRUE, main = "Histogram of the wave height",
xlab = "Wave height [m]")

library(fitdistrplus)

T50 = 50
T100 = 100

F50 = (T50-1)/T50
F50
F100 = (T100-1)/T100
F100

{#gumbel
  #maximum likelihood estimation
  dgumbel = function(x,mu,s){ # PDF
    exp((mu - x)/s - exp((mu - x)/s))/s}
```

```
  pgumbel = function(q,mu,s){ # CDF
    exp(-exp(-((q - mu)/s)))}

  qgumbel = function(p, mu, s){ # quantile function
    mu-s*log(-log(p))}

  gumbel_mle   =   fitdist(mazara$Hm,   "gumbel",   start=list(mu=5,   s=5),
method="mle")

  summary(gumbel_mle)

  gof_gmle = gofstat(gumbel_mle, discrete=FALSE)
  gof_gmle

  windows()
  par(cex=1.2, bg="white")
  plot(gumbel_mle, lwd=2, col="cornflowerblue")

  #wave height estimations (mle)
  mu_gmle = getElement(gumbel_mle$estimate, "mu")
  s_gmle = getElement(gumbel_mle$estimate, "s")

  W50_gmle = mu_gmle-s_gmle*log(log(F50^(-1)))
  W50_gmle

  W100_gmle = mu_gmle-s_gmle*log(log(F100^(-1)))
  W100_gmle

  #maximum goodness of fit
  gumbel_mge   =   fitdist(mazara$Hm,   "gumbel",   start=list(mu=5,   s=5),
method="mge", gof="KS")

  summary(gumbel_mge)

  gof_gmge = gofstat(gumbel_mge, discrete=FALSE)
  gof_gmge

  windows()
  par(cex=1.2, bg="white")
  plot(gumbel_mge, lwd=2, col="cornflowerblue")

  #wave height estimations (mge)
  mu_gmge = getElement(gumbel_mge$estimate, "mu")
  s_gmge = getElement(gumbel_mge$estimate, "s")

  W50_gmge = mu_gmge-s_gmge*log(log(F50^(-1)))
  W50_gmge

  W100_gmge = mu_gmge-s_gmge*log(log(F100^(-1)))
  W100_gmge
}

{#weibull
  #maximum likelihood estimation

  dwei = function(x, s, beta){ # PDF
    beta/s*(x/s)^(beta-1)*exp(-(x/s)^beta)}

  pwei = function(q, s, beta){ # CDF
    1-exp(-(q/s)^beta)}

  qwei = function(p, s, beta){ # quantile function
    s*(-log(1-p))^(1/s)}
```

```
  weibull_mle = fitdist(mazara$Hm, distr = "wei", start=list(s=5, beta=5),
method="mle")

  summary(weibull_mle)

  gof_wmle = gofstat(weibull_mle, discrete=FALSE)
  gof_wmle

  windows()
  par(cex=1.2, bg="white")
  plot(weibull_mle, lwd=2, col="cornflowerblue")

  #wave height estimations (mle)
  s_wmle = getElement(weibull_mle$estimate, "s")
  beta_wmle = getElement(weibull_mle$estimate, "beta")

  H50_wmle = s_wmle*(-log(1-F50))^(1/beta_wmle)
  H50_wmle

  H100_wmle = s_wmle*(-log(1-F100))^(1/beta_wmle)
  H100_wmle

  #maximum goodness of fit
  weibull_mge = fitdist(mazara$Hm, "wei", start=list(s=5, beta=5),
method="mge", gof="KS")

  summary(weibull_mge)

  gof_wmge = gofstat(weibull_mge, discrete=FALSE)
  gof_wmge

  windows()
  par(cex=1.2, bg="white")
  plot(weibull_mge, lwd=2, col="cornflowerblue")

  #wave height estimations (mge)
  s_wmge = getElement(weibull_mge$estimate, "s")
  beta_wmge = getElement(weibull_mge$estimate, "beta")

  H50_wmge = s_wmge*(-log(1-F50))^(1/beta_wmge)
  H50_wmge

  H100_wmge = s_wmge*(-log(1-F100))^(1/beta_wmge)
  H100_wmge
}
```

## C.7 Mazara del vallo (design wave height, >3 m dataset)

```
mazara = read.table("wave_mazara.txt", header = TRUE)
mazara

Hm3 = mazara$Hm [mazara$Hm > 3]

#histogram
windows()
```

```
hist(Hm3, probability = TRUE, main = "Histogram of the wave height", xlab =
"Wave height [m]")

library(fitdistrplus)

T50 = 50
T100 = 100

F50 = (T50-1)/T50
F50
F100 = (T100-1)/T100
F100

{#gumbel
  #maximum likelihood estimation
  dgumbel = function(x,mu,s){ # PDF
    exp((mu - x)/s - exp((mu - x)/s))/s}

  pgumbel = function(q,mu,s){ # CDF
    exp(-exp(-((q - mu)/s)))}

  qgumbel = function(p, mu, s){ # quantile function
    mu-s*log(-log(p))}

  gumbel_mle = fitdist(Hm3, "gumbel", start=list(mu=5, s=5), method="mle")

  summary(gumbel_mle)

  gof_gmle = gofstat(gumbel_mle, discrete=FALSE)
  gof_gmle

  windows()
  par(cex=1.2, bg="white")
  plot(gumbel_mle, lwd=2, col="cornflowerblue")

  #wave height estimations (mle)
  mu_gmle = getElement(gumbel_mle$estimate, "mu")
  s_gmle = getElement(gumbel_mle$estimate, "s")

  W50_gmle = mu_gmle-s_gmle*log(log(F50^(-1)))
  W50_gmle

  W100_gmle = mu_gmle-s_gmle*log(log(F100^(-1)))
  W100_gmle

  #maximum goodness of fit
  gumbel_mge = fitdist(Hm3, "gumbel", start=list(mu=5, s=5), method="mge",
gof="KS")

  summary(gumbel_mge)

  gof_gmge = gofstat(gumbel_mge, discrete=FALSE)
  gof_gmge

  windows()
  par(cex=1.2, bg="white")
  plot(gumbel_mge, lwd=2, col="cornflowerblue")

  #wave height estimations (mge)
  mu_gmge = getElement(gumbel_mge$estimate, "mu")
  s_gmge = getElement(gumbel_mge$estimate, "s")

  W50_gmge = mu_gmge-s_gmge*log(log(F50^(-1)))
```

```
  W50_gmge

  W100_gmge = mu_gmge-s_gmge*log(log(F100^(-1)))
  W100_gmge
}

{#weibull
  #maximum likelihood estimation

  dwei = function(x, s, beta){ # PDF
    beta/s*(x/s)^(beta-1)*exp(-(x/s)^beta)}

  pwei = function(q, s, beta){ # CDF
    1-exp(-(q/s)^beta)}

  qwei = function(p, s, beta){ # quantile function
    s*(-log(1-p))^(1/s)}

  weibull_mle  =  fitdist(Hm3,  distr  =  "wei",  start=list(s=5,  beta=5),
method="mle")

  summary(weibull_mle)

  gof_wmle = gofstat(weibull_mle, discrete=FALSE)
  gof_wmle

  windows()
  par(cex=1.2, bg="white")
  plot(weibull_mle, lwd=2, col="cornflowerblue")

  #wave height estimations (mle)
  s_wmle = getElement(weibull_mle$estimate, "s")
  beta_wmle = getElement(weibull_mle$estimate, "beta")

  H50_wmle = s_wmle*(-log(1-F50))^(1/beta_wmle)
  H50_wmle

  H100_wmle = s_wmle*(-log(1-F100))^(1/beta_wmle)
  H100_wmle

  #maximum goodness of fit
  weibull_mge = fitdist(Hm3, "wei", start=list(s=5, beta=5), method="mge",
gof="KS")

  summary(weibull_mge)

  gof_wmge = gofstat(weibull_mge, discrete=FALSE)
  gof_wmge

  windows()
  par(cex=1.2, bg="white")
  plot(weibull_mge, lwd=2, col="cornflowerblue")

  #wave height estimations (mge)
  s_wmge = getElement(weibull_mge$estimate, "s")
  beta_wmge = getElement(weibull_mge$estimate, "beta")

  H50_wmge = s_wmge*(-log(1-F50))^(1/beta_wmge)
  H50_wmge

  H100_wmge = s_wmge*(-log(1-F100))^(1/beta_wmge)
  H100_wmge
}
```

## C.8 Mazara del vallo (design wave height, >3.5 m dataset)

```
mazara = read.table("wave_mazara.txt", header = TRUE)
mazara

Hm35 = mazara$Hm [mazara$Hm > 3.5]

#histogram
windows()
hist(Hm35, probability = TRUE, main = "Histogram of the wave height", xlab =
"Wave height [m]")

library(fitdistrplus)

T50 = 50
T100 = 100

F50 = (T50-1)/T50
F50
F100 = (T100-1)/T100
F100

{#gumbel
  #maximum likelihood estimation
  dgumbel = function(x,mu,s){ # PDF
    exp((mu - x)/s - exp((mu - x)/s))/s}

  pgumbel = function(q,mu,s){ # CDF
    exp(-exp(-((q - mu)/s)))}

  qgumbel = function(p, mu, s){ # quantile function
    mu-s*log(-log(p))}

  gumbel_mle = fitdist(Hm35, "gumbel", start=list(mu=5, s=5), method="mle")

  summary(gumbel_mle)

  gof_gmle = gofstat(gumbel_mle, discrete=FALSE)
  gof_gmle

  windows()
  par(cex=1.2, bg="white")
  plot(gumbel_mle, lwd=2, col="cornflowerblue")

  #wave height estimations (mle)
  mu_gmle = getElement(gumbel_mle$estimate, "mu")
  s_gmle = getElement(gumbel_mle$estimate, "s")

  W50_gmle = mu_gmle-s_gmle*log(log(F50^(-1)))
  W50_gmle

  W100_gmle = mu_gmle-s_gmle*log(log(F100^(-1)))
  W100_gmle

  #maximum goodness of fit
  gumbel_mge = fitdist(Hm35, "gumbel", start=list(mu=5, s=5), method="mge",
gof="KS")
```

```
  summary(gumbel_mge)

  gof_gmge = gofstat(gumbel_mge, discrete=FALSE)
  gof_gmge

  windows()
  par(cex=1.2, bg="white")
  plot(gumbel_mge, lwd=2, col="cornflowerblue")

  #wave height estimations (mge)
  mu_gmge = getElement(gumbel_mge$estimate, "mu")
  s_gmge = getElement(gumbel_mge$estimate, "s")

  W50_gmge = mu_gmge-s_gmge*log(log(F50^(-1)))
  W50_gmge

  W100_gmge = mu_gmge-s_gmge*log(log(F100^(-1)))
  W100_gmge
}

{#weibull
  #maximum likelihood estimation

  dwei = function(x, s, beta){ # PDF
    beta/s*(x/s)^(beta-1)*exp(-(x/s)^beta)}

  pwei = function(q, s, beta){ # CDF
    1-exp(-(q/s)^beta)}

  qwei = function(p, s, beta){ # quantile function
    s*(-log(1-p))^(1/s)}

  weibull_mle = fitdist(Hm35, distr = "wei", start=list(s=5, beta=5),
method="mle")

  summary(weibull_mle)

  gof_wmle = gofstat(weibull_mle, discrete=FALSE)
  gof_wmle

  windows()
  par(cex=1.2, bg="white")
  plot(weibull_mle, lwd=2, col="cornflowerblue")

  #wave height estimations (mle)
  s_wmle = getElement(weibull_mle$estimate, "s")
  beta_wmle = getElement(weibull_mle$estimate, "beta")

  H50_wmle = s_wmle*(-log(1-F50))^(1/beta_wmle)
  H50_wmle

  H100_wmle = s_wmle*(-log(1-F100))^(1/beta_wmle)
  H100_wmle

  #maximum goodness of fit
  weibull_mge = fitdist(Hm35, "wei", start=list(s=5, beta=5), method="mge",
gof="KS")

  summary(weibull_mge)

  gof_wmge = gofstat(weibull_mge, discrete=FALSE)
  gof_wmge
```

```
windows()
par(cex=1.2, bg="white")
plot(weibull_mge, lwd=2, col="cornflowerblue")

#wave height estimations (mge)
s_wmge = getElement(weibull_mge$estimate, "s")
beta_wmge = getElement(weibull_mge$estimate, "beta")

H50_wmge = s_wmge*(-log(1-F50))^(1/beta_wmge)
H50_wmge

H100_wmge = s_wmge*(-log(1-F100))^(1/beta_wmge)
H100_wmge
```

# Appendix D
# JONSWAP spectra

In all the following paragraphs:

- $\alpha$ is the modified Philips constant;
- $\gamma$ is the peak enhancement factor;
- $f_P$ is the frequency at the spectral peak;
- $T_P$ is the spectral peak period;
- $H_S$ is the significant wave height;
- $T_z$ is the zero-crossing period;
- $U_{10}$ is the wind speed 10 meters above the sea surface.

## D.1 Adriatic Sea, 50 years return period

| Parameter | Value |
|---|---|
| $H_S$ | 5.62 m |
| $T_z$ | 7.18 s |
| $U_{10}$ | 20.90 m/s |
| $\gamma$ | 2.329 |
| $\alpha$ | 0.0149 |
| $f_P$ | 0.1053 Hz |
| $T_P$ | 9.5 s |

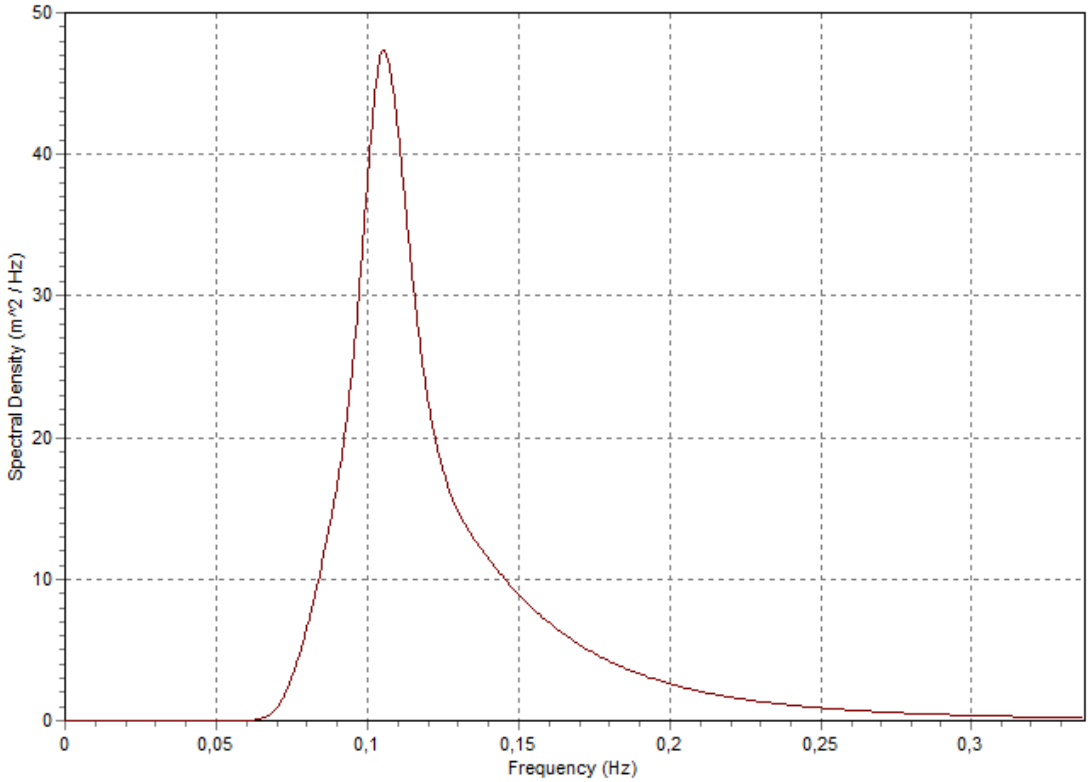


## D.2 Adriatic Sea, 100 years return period

| Parameter | Value |
|---|---|
| $H_S$ | 6.01 m |
| $T_z$ | 7.20 s |
| $U_{10}$ | 22.64 m/s |
| $\gamma$ | 2.4102 |
| $\alpha$ | 0.0168 |
| $f_P$ | 0.1053 Hz |
| $T_P$ | 9.5 s |

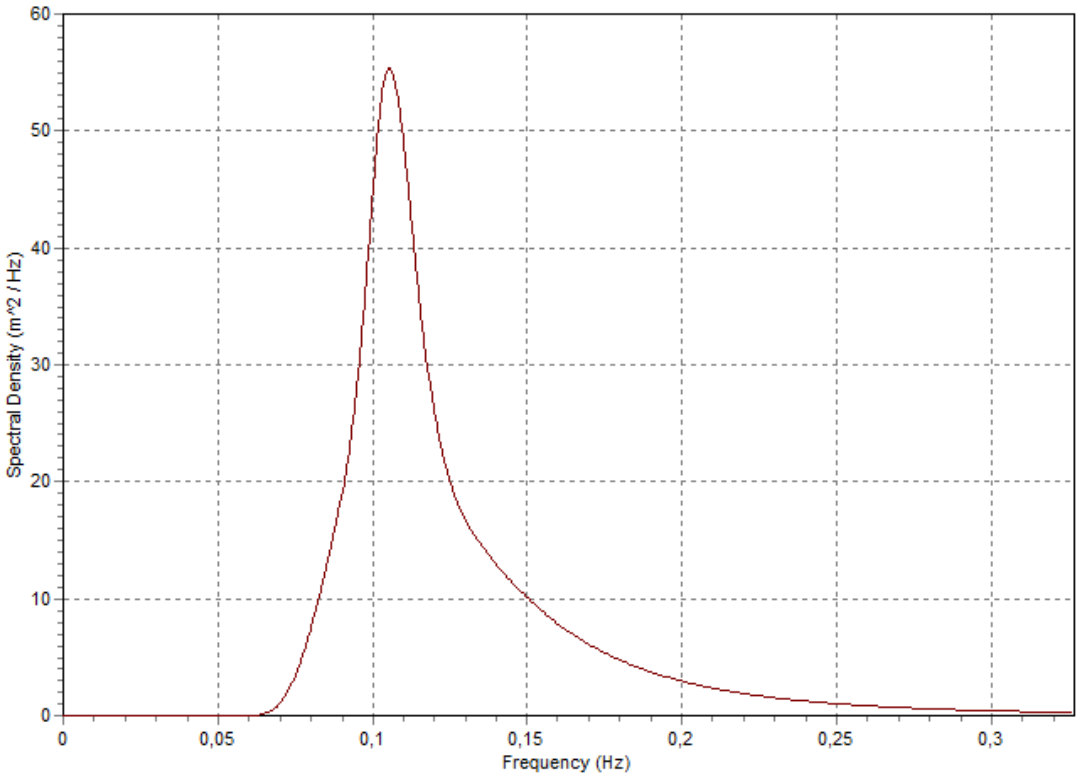


# D.3 South Sicily, 50 years return period

| Parameter | Value |
|---|---|
| $H_S$ | 6.21 m |
| $T_z$ | 8.29 s |
| $U_{10}$ | 22.41 m/s |
| $\gamma$ | 2.329 |
| $\alpha$ | 0.0149 |
| $f_P$ | 0.0909 Hz |
| $T_P$ | 9.5 s |

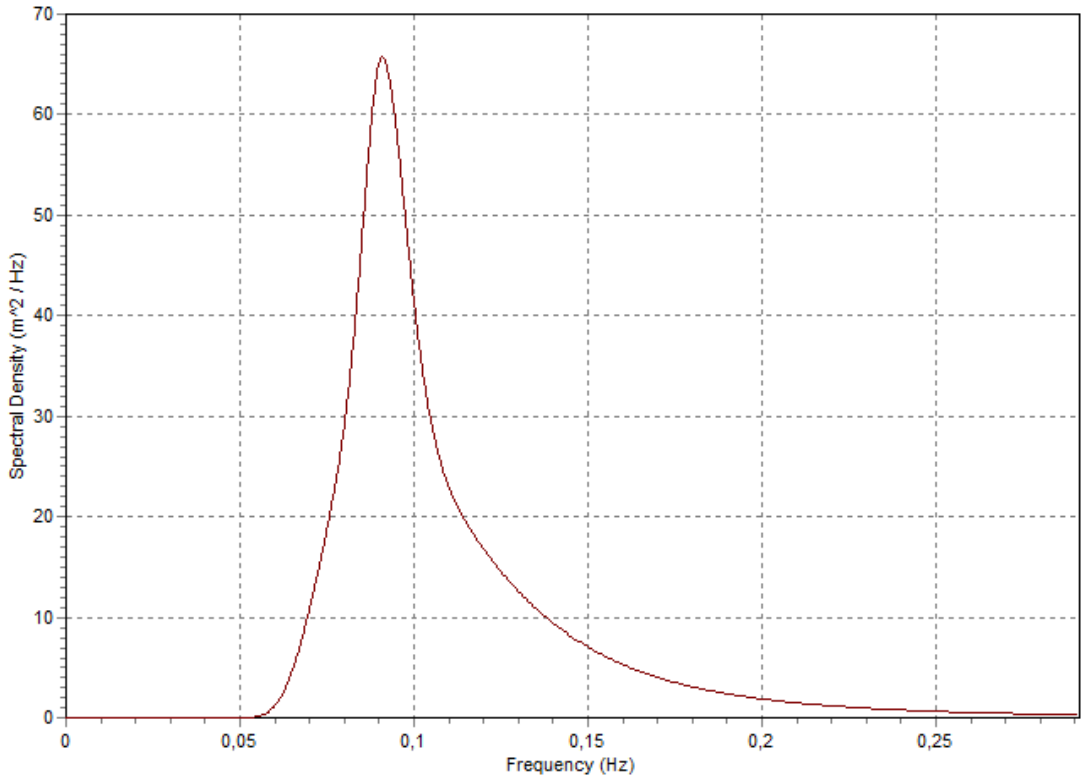


# D.4 South Sicily, 100 years return period

| Parameter | Value |
|---|---|
| $H_S$ | 6.66 m |
| $T_z$ | 8.31 s |
| $U_{10}$ | 23.83 m/s |
| $\gamma$ | 2.3137 |
| $\alpha$ | 0.0117 |
| $f_P$ | 0.0909 Hz |
| $T_P$ | 9.5 s |

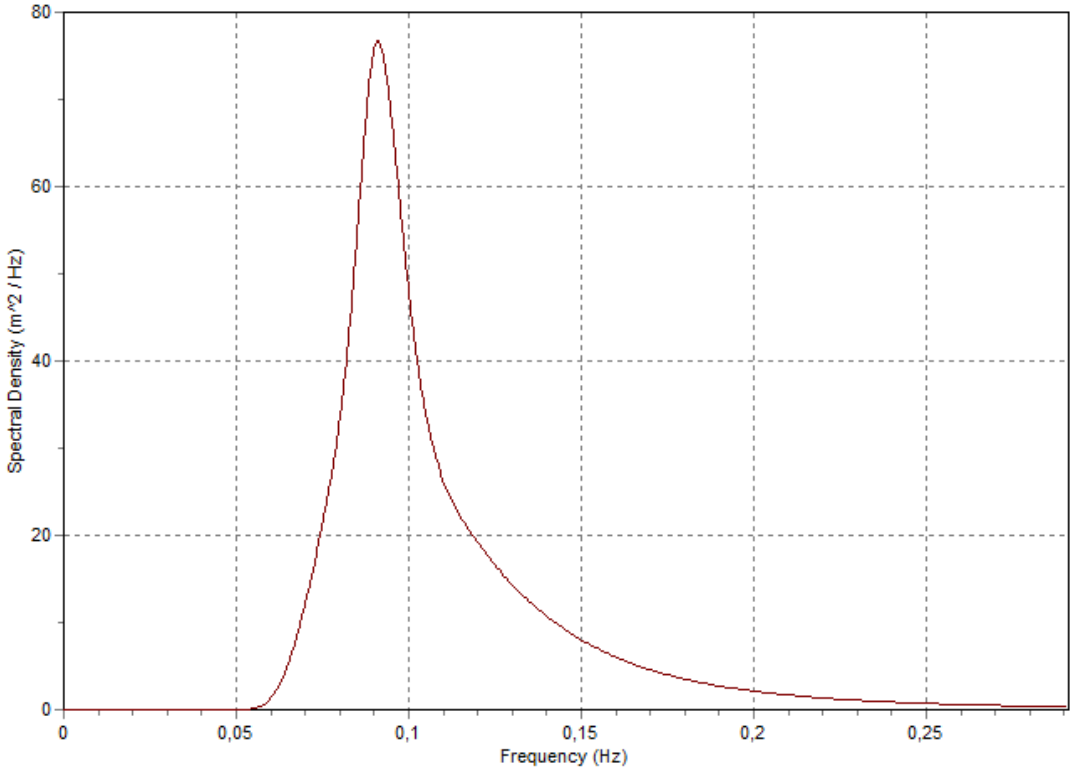
80
60
40
20
0
Spectral Density (m^2 / Hz)
0
0,05
0,1
0,15
0,2
0,25
Frequency (Hz)

# Appendix E
# RAOs

The RAO tables and images are directly taken and converted from the example's page in the Orcina website, regarding a semi-submersible oil platform (Orcina n.d.).

## E.1 0°

| Period [s] | Surge | | Sway | | Heave | |
|---|---|---|---|---|---|---|
| | Amplitude [m/m] | Phase [deg] | Amplitude [m/m] | Phase [deg] | Amplitude [m/m] | Phase [deg] |
| 0.00 | 0.00 | 0.00 | 0.00 | 0.00 | 0.00 | 0.00 |
| 4.00 | 0.06 | 267.75 | 0.00 | 0.00 | 0.01 | 12.79 |
| 4.50 | 0.07 | 246.33 | 0.00 | 0.00 | 0.00 | -8.12 |
| 5.00 | 0.08 | 66.48 | 0.00 | 0.00 | 0.01 | 164.45 |
| 5.50 | 0.09 | 71.12 | 0.00 | 0.00 | 0.02 | -170.40 |
| 6.00 | 0.10 | 75.86 | 0.00 | 0.00 | 0.01 | -148.64 |
| 6.50 | 0.11 | 83.88 | 0.00 | 0.00 | 0.01 | -155.97 |
| 7.00 | 0.13 | 90.64 | 0.00 | 0.00 | 0.01 | 0.81 |
| 7.50 | 0.15 | 94.06 | 0.00 | 0.00 | 0.03 | -18.48 |
| 8.00 | 0.16 | 92.30 | 0.00 | 0.00 | 0.04 | -25.41 |
| 9.00 | 0.21 | 279.85 | 0.00 | 0.00 | 0.12 | -22.24 |
| 10.00 | 0.26 | 276.13 | 0.00 | 0.00 | 0.21 | -12.52 |
| 11.00 | 0.31 | 274.46 | 0.00 | 0.00 | 0.28 | -5.69 |
| 12.00 | 0.38 | 273.67 | 0.00 | 0.00 | 0.32 | -2.17 |
| 13.00 | 0.44 | 273.29 | 0.00 | 0.00 | 0.34 | -0.87 |
| 14.00 | 0.51 | 273.08 | 0.00 | 0.00 | 0.35 | -0.65 |
| 15.00 | 0.58 | 272.98 | 0.00 | 0.00 | 0.34 | -1.20 |
| 16.00 | 0.64 | 272.93 | 0.00 | 0.00 | 0.30 | -2.85 |
| 17.00 | 0.70 | 272.91 | 0.00 | 0.00 | 0.25 | -7.85 |
| 18.00 | 0.76 | 272.93 | 0.00 | 0.00 | 0.13 | -34.33 |

| | | | | | | |
|---|---|---|---|---|---|---|
| 19.00 | 0.81 | 272.97 | 0.00 | 0.00 | 0.25 | -133.61 |
| 20.00 | 0.85 | 273.09 | 0.00 | 0.00 | 1.12 | -139.27 |
| 21.00 | 0.88 | 273.48 | 0.00 | 0.00 | 3.61 | -74.17 |
| 22.00 | 0.91 | 273.34 | 0.00 | 0.00 | 2.26 | -20.20 |
| 23.00 | 0.92 | 273.57 | 0.00 | 0.00 | 1.65 | -9.50 |
| 24.00 | 0.92 | 274.23 | 0.00 | 0.00 | 1.41 | -5.67 |
| 25.00 | 0.92 | 276.31 | 0.00 | 0.00 | 1.28 | -3.92 |
| 26.00 | 0.90 | 286.63 | 0.00 | 0.00 | 1.20 | -3.04 |
| 27.00 | 0.91 | 285.20 | 0.00 | 0.00 | 1.15 | -2.32 |
| 28.00 | 0.93 | 275.97 | 0.00 | 0.00 | 1.12 | -1.90 |
| 29.00 | 0.95 | 274.15 | 0.00 | 0.00 | 1.09 | -1.59 |
| 30.00 | 1.00 | 270.00 | 0.00 | 0.00 | 1.08 | -1.35 |
| Infinity | 1.00 | 270.00 | 0.00 | 0.00 | 1.00 | -1.36 |

| Period [s] | Roll | | Pitch | | Yaw | |
|---|---|---|---|---|---|---|
| | Amplitude [deg/m] | Phase [deg] | Amplitude [deg/m] | Phase [deg] | Amplitude [deg/m] | Phase [deg] |
| 0.00 | 0.00 | 0.00 | 0.00 | 0.00 | 0.00 | 0.00 |
| 4.00 | 0.00 | 0.00 | 0.03 | -97.22 | 0.00 | 0.00 |
| 4.50 | 0.00 | 0.00 | 0.02 | -117.34 | 0.00 | 0.00 |
| 5.00 | 0.00 | 0.00 | 0.02 | 13.25 | 0.00 | 0.00 |
| 5.50 | 0.00 | 0.00 | 0.04 | 69.28 | 0.00 | 0.00 |
| 6.00 | 0.00 | 0.00 | 0.07 | 75.48 | 0.00 | 0.00 |
| 6.50 | 0.00 | 0.00 | 0.09 | 82.85 | 0.00 | 0.00 |
| 7.00 | 0.00 | 0.00 | 0.12 | 90.69 | 0.00 | 0.00 |
| 7.50 | 0.00 | 0.00 | 0.14 | 95.52 | 0.00 | 0.00 |
| 8.00 | 0.00 | 0.00 | 0.15 | 101.16 | 0.00 | 0.00 |
| 9.00 | 0.00 | 0.00 | 0.38 | 96.12 | 0.00 | 0.00 |
| 10.00 | 0.00 | 0.00 | 0.21 | 95.88 | 0.00 | 0.00 |
| 11.00 | 0.00 | 0.00 | 0.22 | 90.95 | 0.00 | 0.00 |
| 12.00 | 0.00 | 0.00 | 0.22 | 91.97 | 0.00 | 0.00 |
| 13.00 | 0.00 | 0.00 | 0.21 | 91.97 | 0.00 | 0.00 |
| 14.00 | 0.00 | 0.00 | 0.20 | 88.78 | 0.00 | 0.00 |
| 15.00 | 0.00 | 0.00 | 0.18 | 90.44 | 0.00 | 0.00 |
| 16.00 | 0.00 | 0.00 | 0.16 | 88.70 | 0.00 | 0.00 |
| 17.00 | 0.00 | 0.00 | 0.14 | 87.00 | 0.00 | 0.00 |
| 18.00 | 0.00 | 0.00 | 0.11 | 83.28 | 0.00 | 0.00 |
| 19.00 | 0.00 | 0.00 | 0.08 | 80.03 | 0.00 | 0.00 |
| 20.00 | 0.00 | 0.00 | 0.06 | 57.99 | 0.00 | 0.00 |
| 21.00 | 0.00 | 0.00 | 0.06 | 17.07 | 0.00 | 0.00 |

| | | | | | | |
|---|---|---|---|---|---|---|
| 22.00 | 0.00 | 0.00 | 0.05 | -31.54 | 0.00 | 0.00 |
| 23.00 | 0.00 | 0.00 | 0.12 | -59.35 | 0.00 | 0.00 |
| 24.00 | 0.00 | 0.00 | 0.25 | -63.50 | 0.00 | 0.00 |
| 25.00 | 0.00 | 0.00 | 0.51 | -57.15 | 0.00 | 0.00 |
| 26.00 | 0.00 | 0.00 | 1.22 | -21.68 | 0.00 | 0.00 |
| 27.00 | 0.00 | 0.00 | 1.14 | 52.10 | 0.00 | 0.00 |
| 28.00 | 0.00 | 0.00 | 0.66 | 74.95 | 0.00 | 0.00 |
| 29.00 | 0.00 | 0.00 | 0.47 | 81.45 | 0.00 | 0.00 |
| 30.00 | 0.00 | 0.00 | 0.38 | 84.73 | 0.00 | 0.00 |
| Infinity | 0.00 | 0.00 | 0.38 | 84.94 | 0.00 | 0.00 |

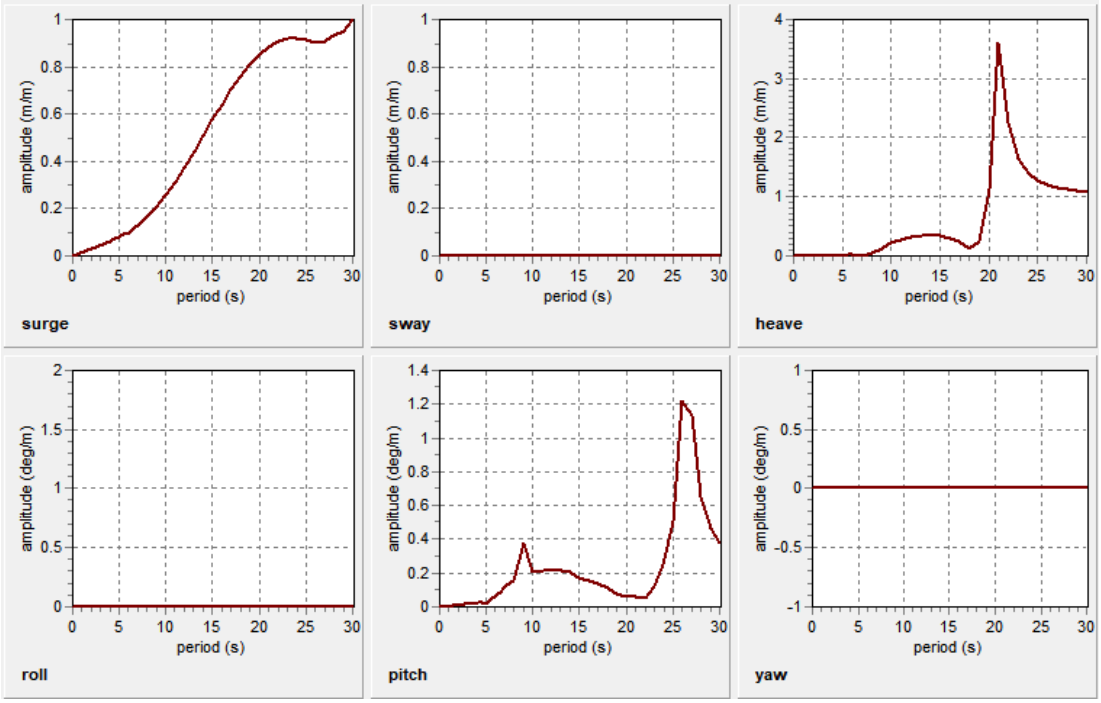


# E.2 45°

| Period [s] | Surge | | Sway | | Heave | |
|---|---|---|---|---|---|---|
| | Amplitude [m/m] | Phase [deg] | Amplitude [m/m] | Phase [deg] | Amplitude [m/m] | Phase [deg] |
| 0.00 | 0.00 | 0.00 | 0.00 | 0.00 | 0.00 | 0.00 |
| 4.00 | 0.06 | 34.24 | 0.06 | 34.22 | 0.01 | -44.08 |
| 4.50 | 0.07 | 266.31 | 0.07 | -97.29 | 0.01 | 170.55 |
| 5.00 | 0.08 | 255.48 | 0.08 | -108.13 | 0.00 | 107.27 |
| 5.50 | 0.09 | 250.62 | 0.09 | -112.99 | 0.02 | 136.53 |
| 6.00 | 0.10 | 258.10 | 0.10 | -105.50 | 0.02 | 164.64 |
| 6.50 | 0.11 | 317.27 | 0.11 | -46.59 | 0.02 | 178.62 |

| | | | | | | |
|---|---|---|---|---|---|---|
| 7.00 | 0.13 | 23.84 | 0.13 | 23.48 | 0.02 | 9.53 |
| 7.50 | 0.15 | 46.89 | 0.15 | 46.48 | 0.02 | -10.08 |
| 8.00 | 0.16 | 19.73 | 0.16 | 11.94 | 0.05 | -15.99 |
| 9.00 | 0.21 | 270.53 | 0.21 | -93.13 | 0.11 | -17.72 |
| 10.00 | 0.26 | 273.06 | 0.26 | -90.57 | 0.20 | -10.55 |
| 11.00 | 0.31 | 273.42 | 0.31 | -90.20 | 0.26 | -4.91 |
| 12.00 | 0.38 | 273.29 | 0.38 | -90.32 | 0.31 | -1.87 |
| 13.00 | 0.44 | 273.11 | 0.44 | -90.49 | 0.34 | -0.74 |
| 14.00 | 0.51 | 272.99 | 0.51 | -90.61 | 0.34 | -0.56 |
| 15.00 | 0.58 | 272.92 | 0.58 | -90.69 | 0.33 | -1.09 |
| 16.00 | 0.64 | 272.88 | 0.64 | -90.73 | 0.31 | -2.68 |
| 17.00 | 0.70 | 272.87 | 0.70 | -90.74 | 0.24 | -7.39 |
| 18.00 | 0.76 | 272.88 | 0.76 | -90.73 | 0.13 | -33.16 |
| 19.00 | 0.81 | 272.91 | 0.81 | -90.70 | 0.25 | -134.85 |
| 20.00 | 0.85 | 273.03 | 0.85 | -90.60 | 1.13 | -143.45 |
| 22.00 | 0.91 | 273.25 | 0.91 | -90.43 | 2.28 | -19.18 |
| 23.00 | 0.92 | 273.45 | 0.92 | -90.30 | 1.66 | -8.84 |
| 24.00 | 0.92 | 274.02 | 0.92 | -89.97 | 1.41 | -5.35 |
| 25.00 | 0.92 | 275.88 | 0.92 | -89.15 | 1.27 | -3.84 |
| 26.00 | 0.90 | 287.23 | 0.90 | -86.70 | 1.21 | -2.89 |
| 27.00 | 0.89 | 281.84 | 0.89 | -72.28 | 1.15 | -2.31 |
| 28.00 | 0.87 | 275.63 | 0.87 | -79.64 | 1.12 | -1.81 |
| 29.00 | 0.86 | 273.97 | 0.86 | -88.09 | 1.09 | -1.56 |
| 30.00 | 0.86 | 273.46 | 0.86 | -89.62 | 1.07 | -1.30 |
| Infinity | 0.86 | 270.75 | 0.61 | -88.73 | 1.00 | -1.30 |

| Period [s] | Roll | | Pitch | | Yaw | |
|---|---|---|---|---|---|---|
| | Amplitude [deg/m] | Phase [deg] | Amplitude [deg/m] | Phase [deg] | Amplitude [deg/m] | Phase [deg] |
| 0.00 | 0.00 | 0.00 | 0.00 | 0.00 | 0.00 | 0.00 |
| 4.00 | 0.01 | 36.47 | 0.01 | 36.47 | 0.00 | 0.00 |
| 4.50 | 0.02 | -100.81 | 0.02 | -100.81 | 0.00 | 0.00 |
| 5.00 | 0.04 | -109.38 | 0.04 | -109.38 | 0.00 | 0.00 |
| 5.50 | 0.03 | -115.67 | 0.03 | -115.67 | 0.00 | 0.00 |
| 6.00 | 0.01 | -112.22 | 0.01 | -112.22 | 0.00 | 0.00 |
| 6.50 | 0.03 | 48.25 | 0.03 | 48.25 | 0.00 | 0.00 |
| 7.00 | 0.07 | 56.12 | 0.07 | 56.12 | 0.00 | 0.00 |
| 7.50 | 0.12 | 63.62 | 0.12 | 63.62 | 0.00 | 0.00 |
| 8.00 | 0.16 | 75.07 | 0.16 | 75.07 | 0.00 | 0.00 |
| 9.00 | 0.20 | 86.35 | 0.20 | 86.35 | 0.00 | 0.00 |

| | | | | | | |
|---|---|---|---|---|---|---|
| 10.00 | 0.20 | 91.10 | 0.20 | 91.10 | 0.00 | 0.00 |
| 11.00 | 0.20 | 92.55 | 0.20 | 92.55 | 0.00 | 0.00 |
| 12.00 | 0.20 | 90.84 | 0.20 | 90.84 | 0.00 | 0.00 |
| 13.00 | 0.18 | 91.24 | 0.18 | 91.24 | 0.00 | 0.00 |
| 14.00 | 0.16 | 92.13 | 0.16 | 92.13 | 0.00 | 0.00 |
| 15.00 | 0.15 | 91.19 | 0.15 | 91.19 | 0.00 | 0.00 |
| 16.00 | 0.14 | 88.94 | 0.14 | 88.94 | 0.00 | 0.00 |
| 17.00 | 0.11 | 88.84 | 0.11 | 88.84 | 0.00 | 0.00 |
| 18.00 | 0.10 | 85.84 | 0.10 | 85.84 | 0.00 | 0.00 |
| 19.00 | 0.08 | 81.44 | 0.08 | 81.44 | 0.00 | 0.00 |
| 20.00 | 0.05 | 70.50 | 0.05 | 70.50 | 0.00 | 0.00 |
| 22.00 | 0.03 | -7.88 | 0.03 | -7.88 | 0.00 | 0.00 |
| 23.00 | 0.07 | -57.17 | 0.07 | -57.17 | 0.00 | 0.00 |
| 24.00 | 0.15 | -63.94 | 0.15 | -63.94 | 0.00 | 0.00 |
| 25.00 | 0.34 | -59.93 | 0.34 | -59.93 | 0.00 | 0.00 |
| 26.00 | 0.95 | -26.39 | 0.95 | -26.39 | 0.00 | 0.00 |
| 27.00 | 0.76 | 63.18 | 0.76 | 63.18 | 0.00 | 0.00 |
| 28.00 | 0.45 | 74.87 | 0.45 | 74.87 | 0.00 | 0.00 |
| 29.00 | 0.32 | 82.89 | 0.32 | 82.89 | 0.00 | 0.00 |
| 30.00 | 0.26 | 85.20 | 0.26 | 85.20 | 0.00 | 0.00 |
| Infinity | 0.26 | 86.48 | 0.26 | 86.48 | 0.00 | 0.00 |

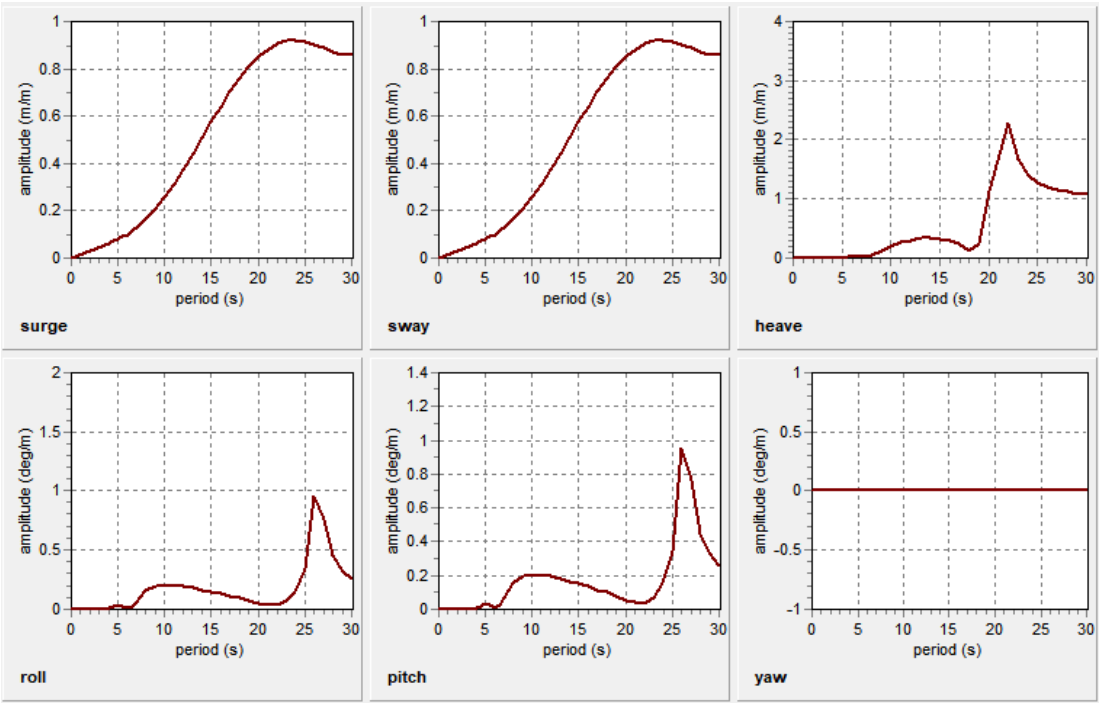

# E.3 90°

| Period [s] | Surge | | Sway | | Heave | |
|---|---|---|---|---|---|---|
| | Amplitude [m/m] | Phase [deg] | Amplitude [m/m] | Phase [deg] | Amplitude [m/m] | Phase [deg] |
| 0.00 | 0.00 | 0.00 | 0.00 | 0.00 | 0.00 | 0.00 |
| 4.00 | 0.00 | 0.00 | 0.06 | -95.87 | 0.01 | -8.27 |
| 4.50 | 0.00 | 0.00 | 0.07 | -117.28 | 0.01 | 165.19 |
| 5.00 | 0.00 | 0.00 | 0.08 | 66.55 | 0.02 | -172.90 |
| 5.50 | 0.00 | 0.00 | 0.09 | 71.12 | 0.01 | -148.18 |
| 6.00 | 0.00 | 0.00 | 0.10 | 75.85 | 0.01 | -154.82 |
| 6.50 | 0.00 | 0.00 | 0.11 | 83.87 | 0.01 | 0.84 |
| 7.00 | 0.00 | 0.00 | 0.13 | 90.62 | 0.02 | -17.98 |
| 7.50 | 0.00 | 0.00 | 0.15 | 94.02 | 0.04 | -25.26 |
| 8.00 | 0.00 | 0.00 | 0.16 | 92.13 | 0.12 | -22.18 |
| 9.00 | 0.00 | 0.00 | 0.21 | -83.79 | 0.22 | -12.65 |
| 10.00 | 0.00 | 0.00 | 0.26 | -87.50 | 0.27 | -5.61 |
| 11.00 | 0.00 | 0.00 | 0.31 | -89.15 | 0.32 | -2.20 |
| 12.00 | 0.00 | 0.00 | 0.38 | -89.94 | 0.34 | -0.86 |
| 13.00 | 0.00 | 0.00 | 0.44 | -90.32 | 0.34 | -0.67 |
| 14.00 | 0.00 | 0.00 | 0.51 | -90.53 | 0.33 | -1.23 |
| 15.00 | 0.00 | 0.00 | 0.58 | -90.63 | 0.30 | -2.88 |
| 16.00 | 0.00 | 0.00 | 0.64 | -90.68 | 0.24 | -7.99 |
| 17.00 | 0.00 | 0.00 | 0.70 | -90.69 | 0.14 | -34.61 |
| 18.00 | 0.00 | 0.00 | 0.76 | -90.69 | 0.26 | -133.55 |
| 19.00 | 0.00 | 0.00 | 0.81 | -90.65 | 1.12 | -139.42 |
| 20.00 | 0.00 | 0.00 | 0.85 | -90.55 | 3.60 | -72.31 |
| 21.00 | 0.00 | 0.00 | 0.88 | -90.21 | 2.26 | -20.18 |
| 22.00 | 0.00 | 0.00 | 0.91 | -90.35 | 1.65 | -9.27 |
| 23.00 | 0.00 | 0.00 | 0.92 | -90.21 | 1.41 | -5.69 |
| 24.00 | 0.00 | 0.00 | 0.92 | -89.85 | 1.28 | -3.98 |
| 25.00 | 0.00 | 0.00 | 0.92 | -88.98 | 1.20 | -2.98 |
| 26.00 | 0.00 | 0.00 | 0.90 | -86.11 | 1.15 | -2.35 |
| 27.00 | 0.00 | 0.00 | 0.89 | -72.69 | 1.12 | -1.88 |
| 28.00 | 0.00 | 0.00 | 0.87 | -79.05 | 1.10 | -1.60 |
| 29.00 | 0.00 | 0.00 | 0.86 | -87.48 | 1.07 | -1.35 |
| 30.00 | 0.00 | 0.00 | 0.86 | -89.28 | 1.00 | -1.36 |
| Infinity | 0.00 | 0.00 | 0.86 | -88.40 | 1.07 | -1.33 |

| Period [s] | Roll | | Pitch | | Yaw | |
|---|---|---|---|---|---|---|
| | Amplitude [deg/m] | Phase [deg] | Amplitude [deg/m] | Phase [deg] | Amplitude [deg/m] | Phase [deg] |
| 0.00 | 0.00 | 0.00 | 0.00 | 0.00 | 0.00 | 0.00 |
| 4.00 | 0.02 | 84.83 | 0.00 | 0.00 | 0.00 | 0.00 |
| 4.50 | 0.02 | 65.69 | 0.00 | 0.00 | 0.00 | 0.00 |
| 5.00 | 0.02 | 195.06 | 0.00 | 0.00 | 0.00 | 0.00 |
| 5.50 | 0.04 | 250.22 | 0.00 | 0.00 | 0.00 | 0.00 |
| 6.00 | 0.06 | 260.89 | 0.00 | 0.00 | 0.00 | 0.00 |
| 6.50 | 0.09 | 260.61 | 0.00 | 0.00 | 0.00 | 0.00 |
| 7.00 | 0.11 | 270.94 | 0.00 | 0.00 | 0.00 | 0.00 |
| 7.50 | 0.14 | 282.85 | 0.00 | 0.00 | 0.00 | 0.00 |
| 8.00 | 0.15 | 278.23 | 0.00 | 0.00 | 0.00 | 0.00 |
| 9.00 | 0.17 | 286.34 | 0.00 | 0.00 | 0.00 | 0.00 |
| 10.00 | 0.20 | 282.57 | 0.00 | 0.00 | 0.00 | 0.00 |
| 11.00 | 0.21 | 278.10 | 0.00 | 0.00 | 0.00 | 0.00 |
| 12.00 | 0.21 | 270.22 | 0.00 | 0.00 | 0.00 | 0.00 |
| 13.00 | 0.21 | 279.17 | 0.00 | 0.00 | 0.00 | 0.00 |
| 14.00 | 0.19 | 274.77 | 0.00 | 0.00 | 0.00 | 0.00 |
| 15.00 | 0.17 | 275.14 | 0.00 | 0.00 | 0.00 | 0.00 |
| 16.00 | 0.15 | 272.08 | 0.00 | 0.00 | 0.00 | 0.00 |
| 17.00 | 0.13 | 265.32 | 0.00 | 0.00 | 0.00 | 0.00 |
| 18.00 | 0.11 | 266.87 | 0.00 | 0.00 | 0.00 | 0.00 |
| 19.00 | 0.08 | 261.82 | 0.00 | 0.00 | 0.00 | 0.00 |
| 20.00 | 0.04 | 236.14 | 0.00 | 0.00 | 0.00 | 0.00 |
| 21.00 | 0.05 | 202.04 | 0.00 | 0.00 | 0.00 | 0.00 |
| 22.00 | 0.05 | 152.20 | 0.00 | 0.00 | 0.00 | 0.00 |
| 23.00 | 0.10 | 122.40 | 0.00 | 0.00 | 0.00 | 0.00 |
| 24.00 | 0.18 | 116.60 | 0.00 | 0.00 | 0.00 | 0.00 |
| 25.00 | 0.33 | 118.11 | 0.00 | 0.00 | 0.00 | 0.00 |
| 26.00 | 0.67 | 127.13 | 0.00 | 0.00 | 0.00 | 0.00 |
| 27.00 | 1.51 | 174.48 | 0.00 | 0.00 | 0.00 | 0.00 |
| 28.00 | 1.15 | 235.35 | 0.00 | 0.00 | 0.00 | 0.00 |
| 29.00 | 0.69 | 253.77 | 0.00 | 0.00 | 0.00 | 0.00 |
| 30.00 | 0.50 | 263.73 | 0.00 | 0.00 | 0.00 | 0.00 |
| Infinity | 0.49 | 268.78 | 0.00 | 0.00 | 0.00 | 0.00 |

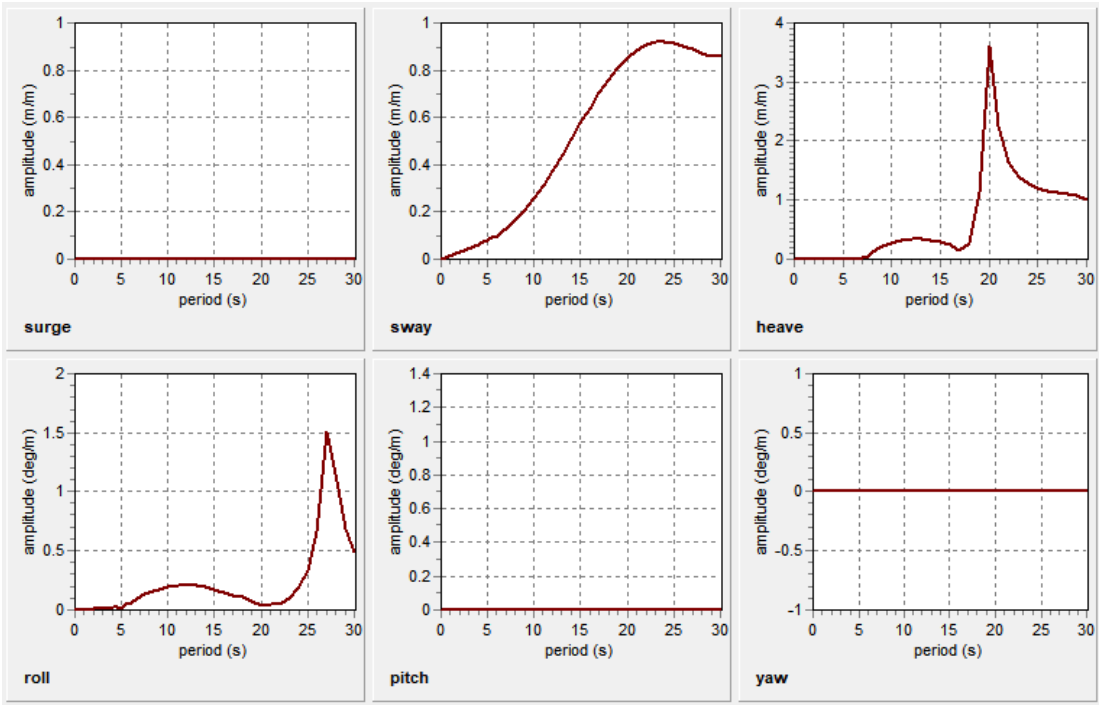
amplitude (m/m)
period (s)
surge
sway
heave
amplitude (deg/m)
roll
pitch
yaw

# Appendix F
# Wire tensions

Generalize Pareto distribution (GPD) parameters:

- β: shape parameter;
- μ: location parameter;
- σ: scale parameter.

## F.1 Simulation 1

**Range graph**

Line 1

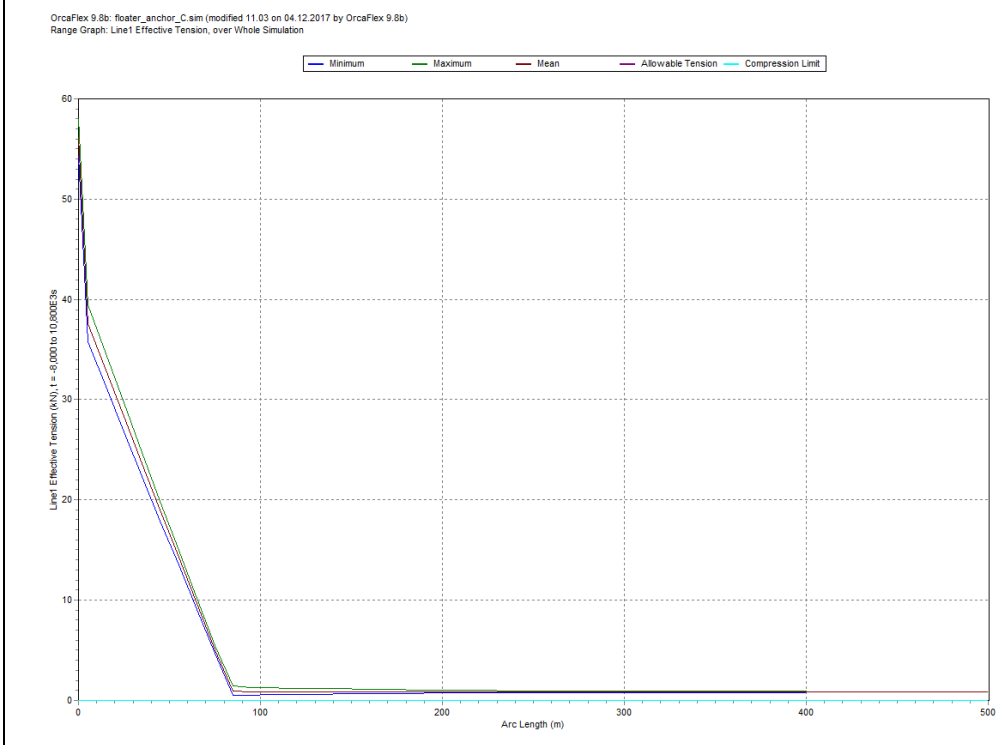

Line 3

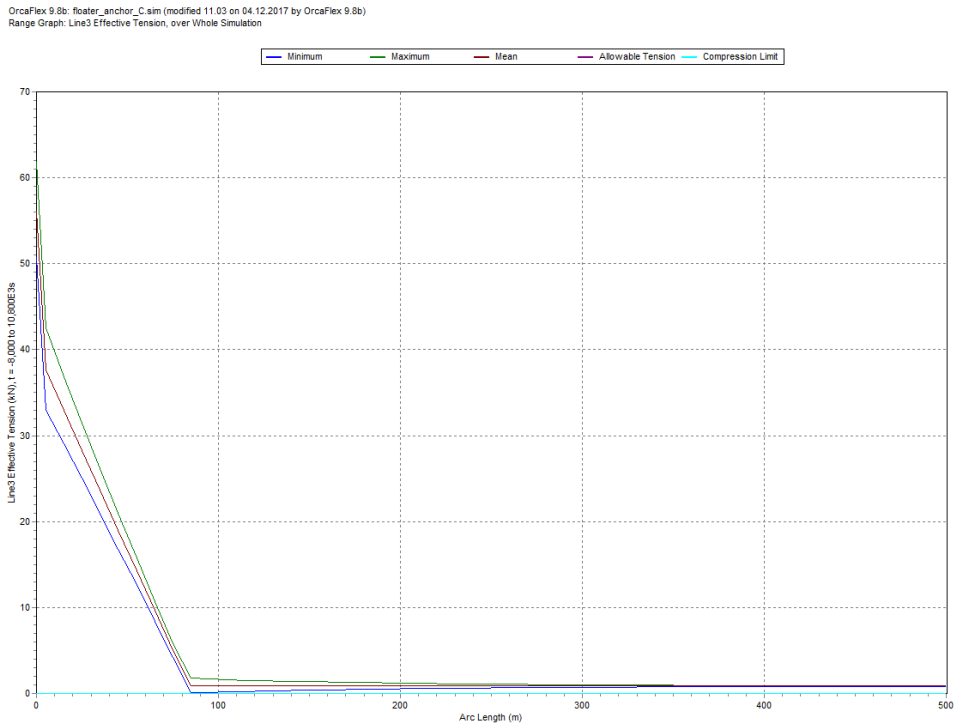


**Time history**

Line 1

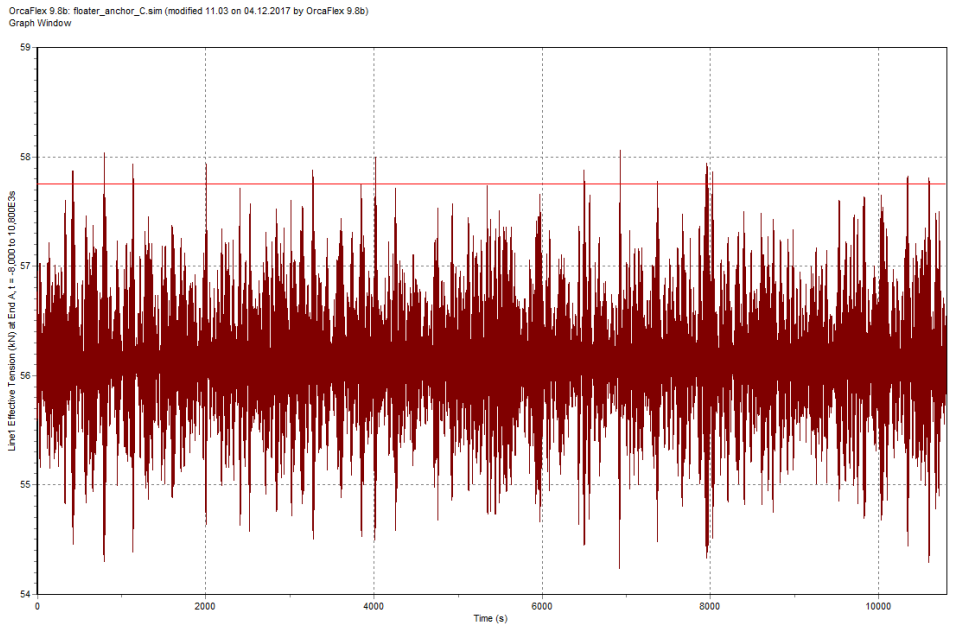

| | |
|---|---|
| Line 3 | 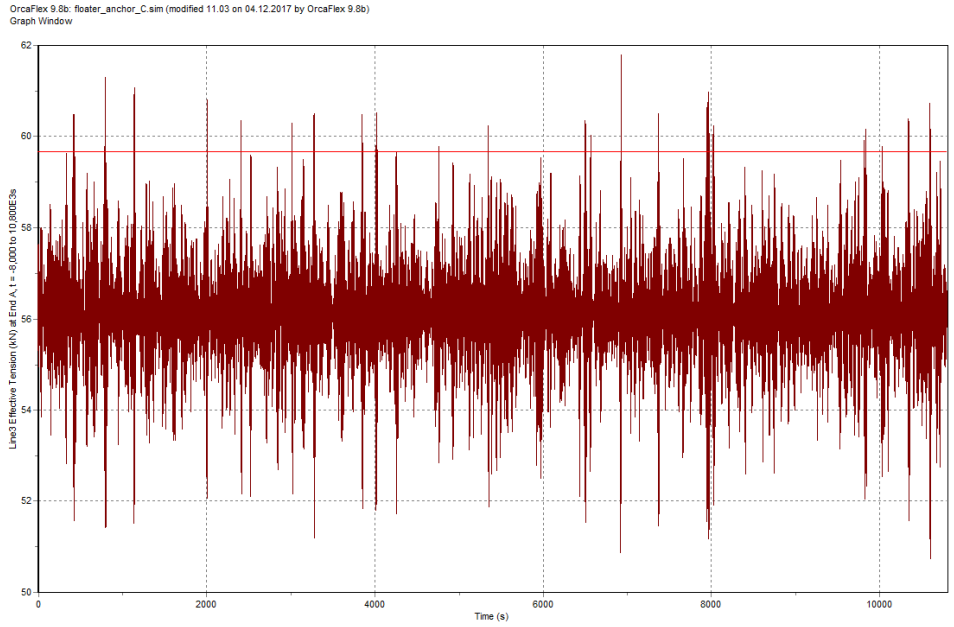 |

| **GPD parameters (line 1)** | |
|---|---|
| β | -0.331 |
| μ | 0 |
| σ | 0.227 |
| Points fitted | 8 |
| Threshold [kN] | 57.63 |
| **GPD parameters (line 3)** | |
| β | 0.018 |
| μ | 0 |
| σ | 0.632 |
| Points fitted | 22 |
| Threshold [kN] | 59.30 |

# F.2 Simulation 2

| **Range graph** |
|---|

| | |
|---|---|
| Line 1 | 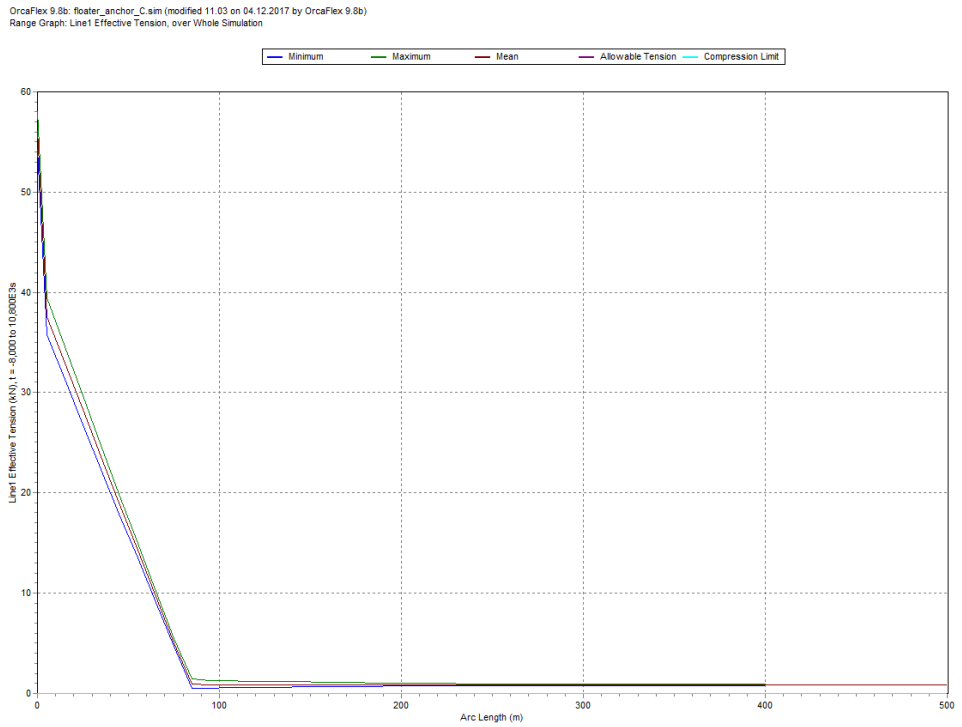 |
| Line 3 | 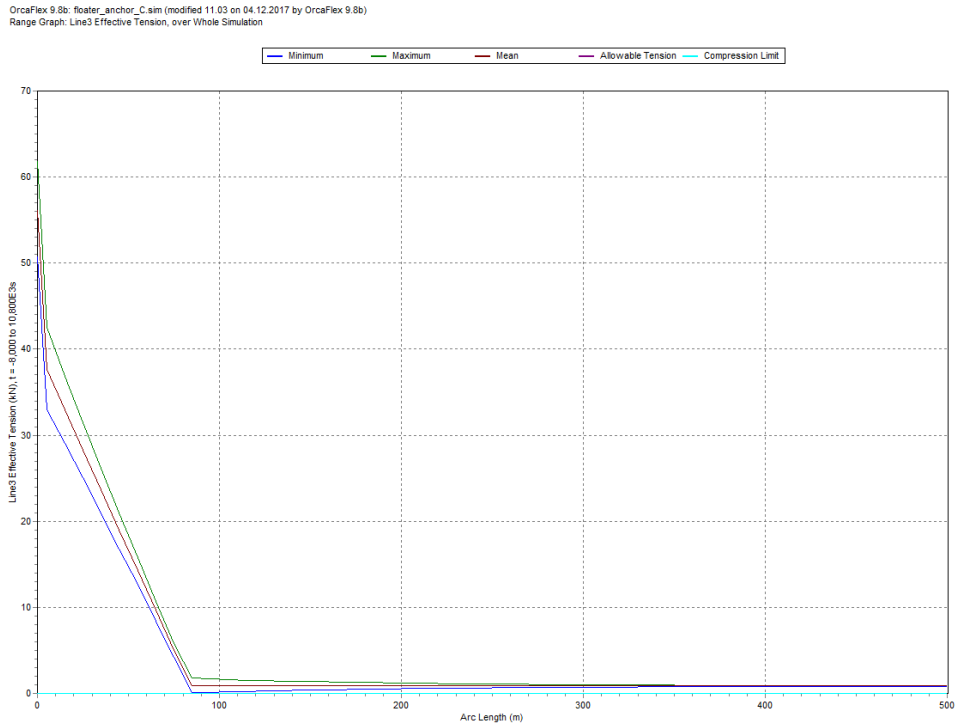 |
| **Time history** | |

| | |
|---|---|
| Line 1 | 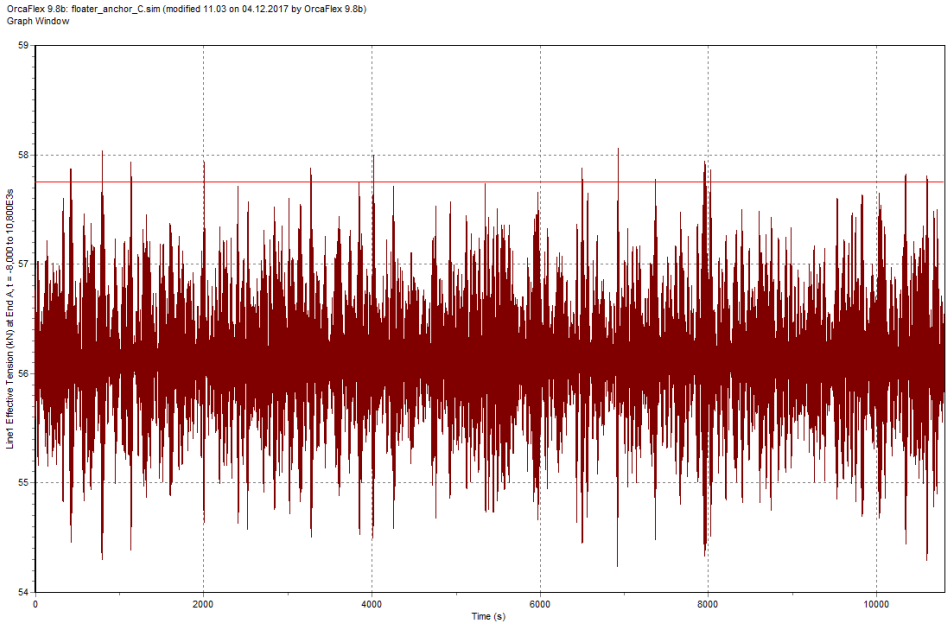 |
| Line 3 | 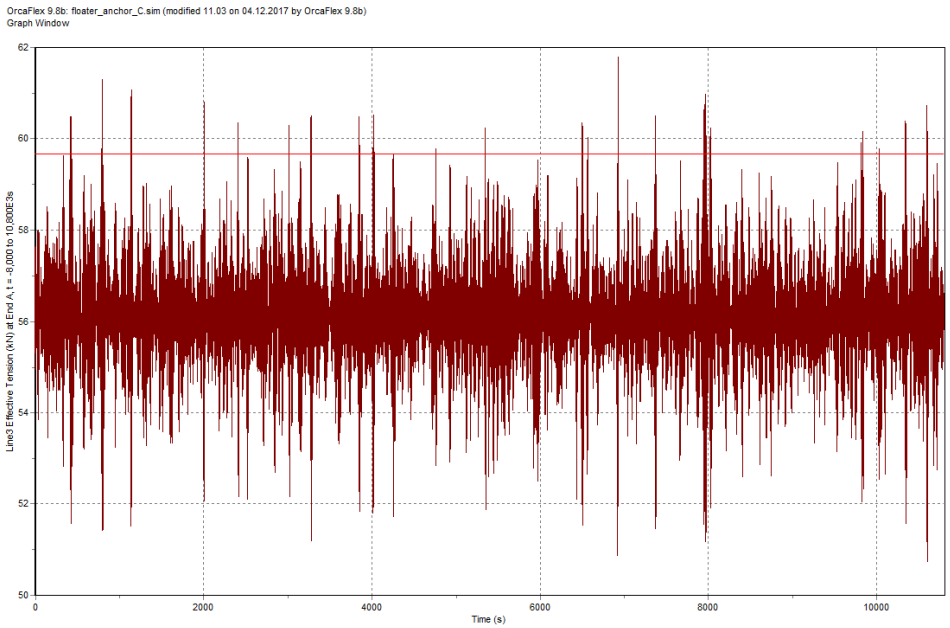 |

| **GPD parameters (line 1)** | |
|---|---|
| β | -0.646 |
| μ | 0 |
| σ | 0.210 |
| Points fitted | 21 |
| Threshold [kN] | 57.75 |
| **GPD parameters (line 3)** | |
| β | -0.389 |

| | |
|---|---|
| μ | 0 |
| σ | 0.945 |
| Points fitted | 36 |
| Threshold [kN] | 59.66 |

# F.3 Simulation 3

**Range graph**

Line 1

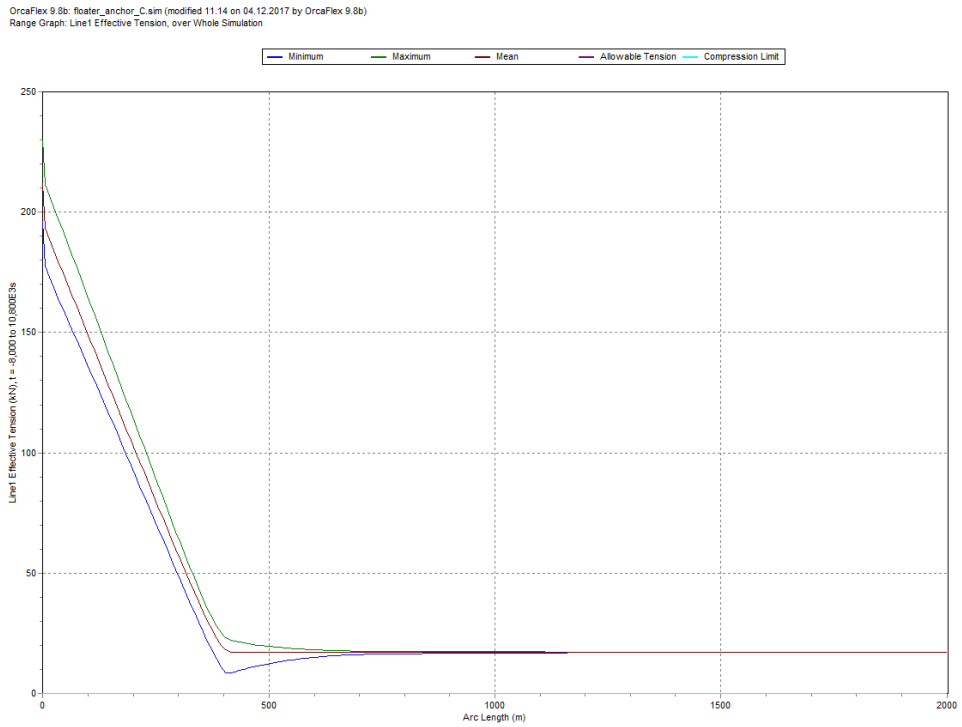

Line 3

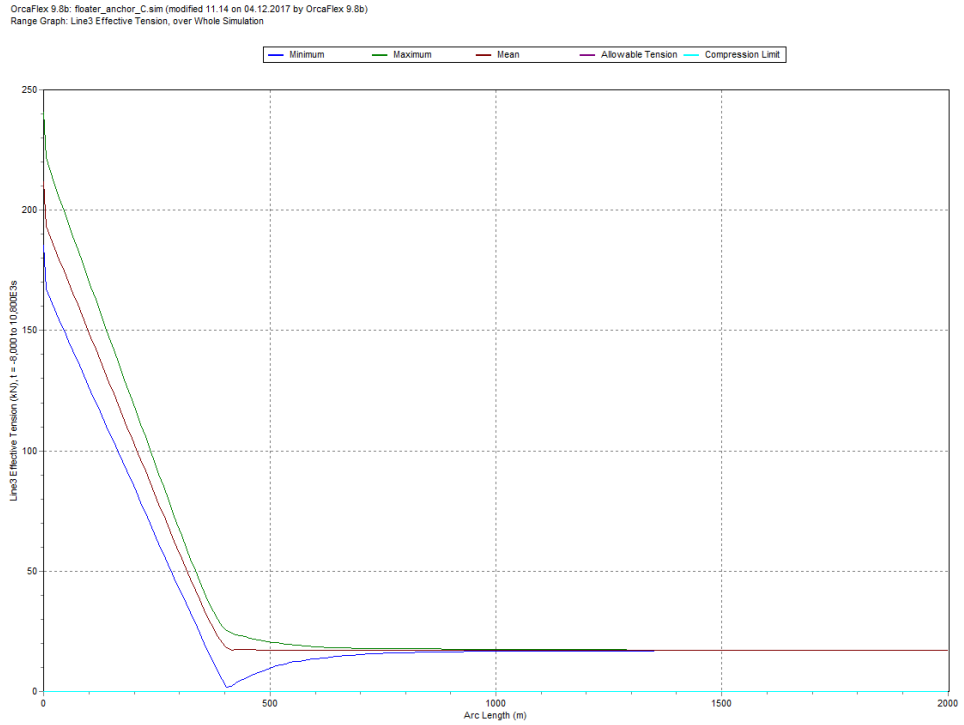


**Time history**

Line 1

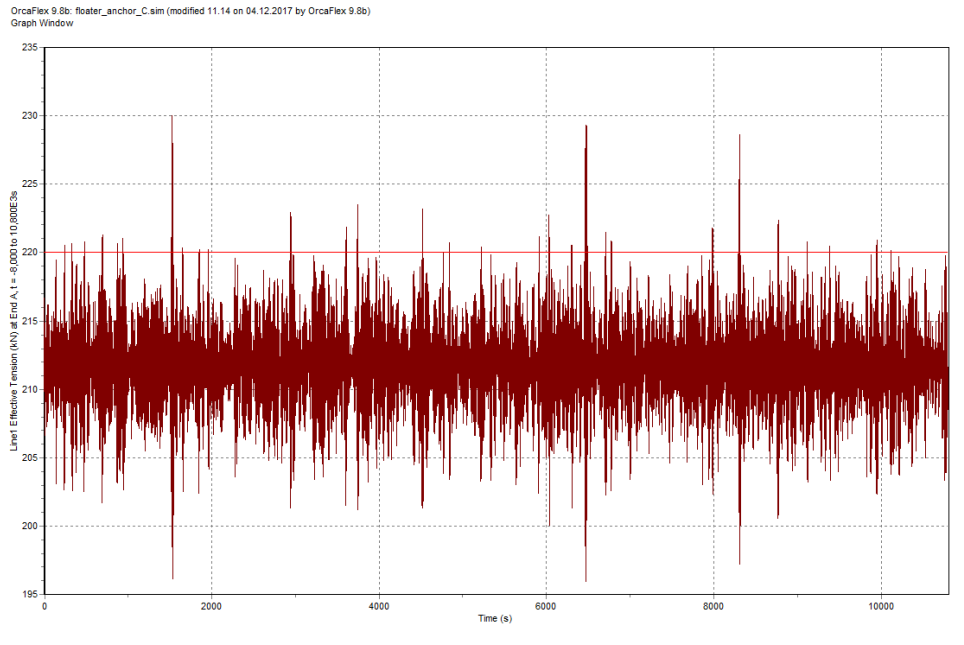

| | |
|---|---|
| Line 3 | 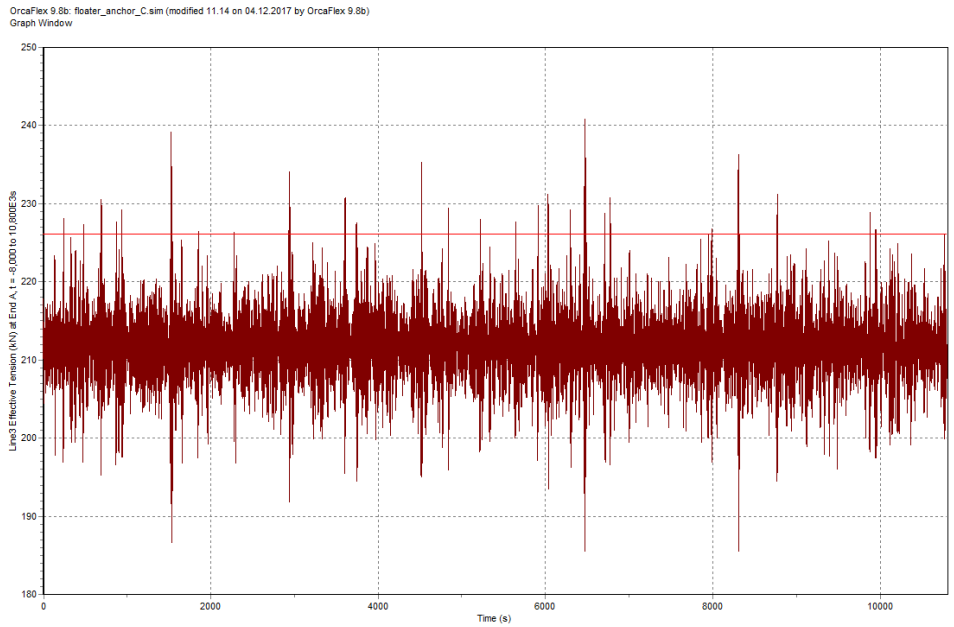 |

| **GPD parameters (line 1)** | |
|---|---|
| β | 0.327 |
| μ | 0 |
| σ | 1.511 |
| Points fitted | 41 |
| Threshold [kN] | 220.00 |
| **GPD parameters (line 3)** | |
| β | -0.169 |
| μ | 0 |
| σ | 4.852 |
| Points fitted | 35 |
| Threshold [kN] | 226.10 |

# F.4 Simulation 4

| **Range graph** |
|---|

| | |
|---|---|
| Line 1 | 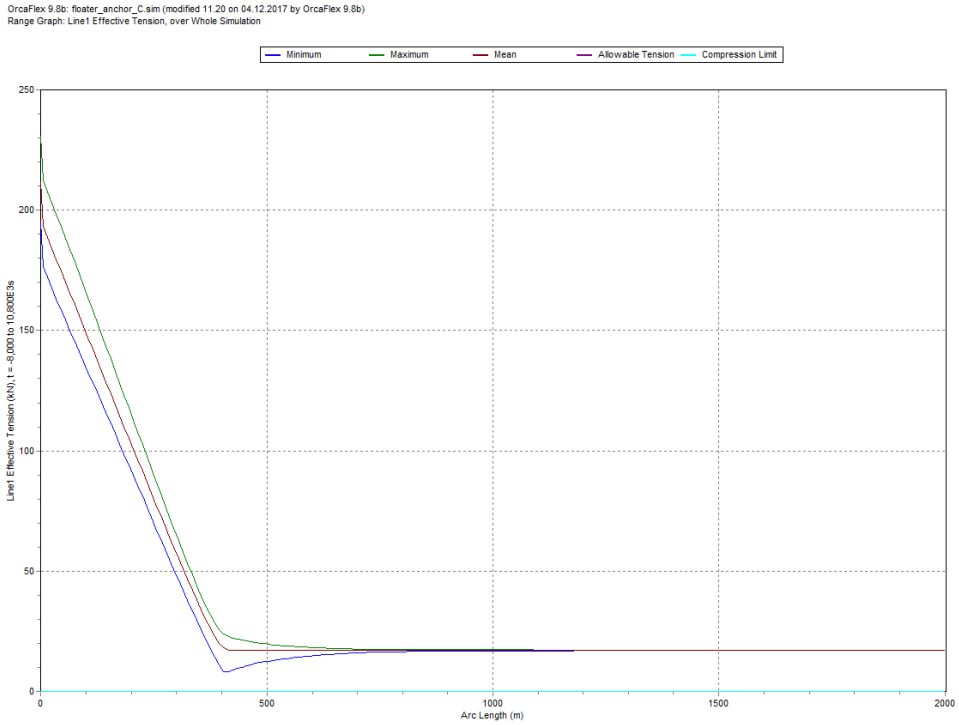 |
| Line 3 | 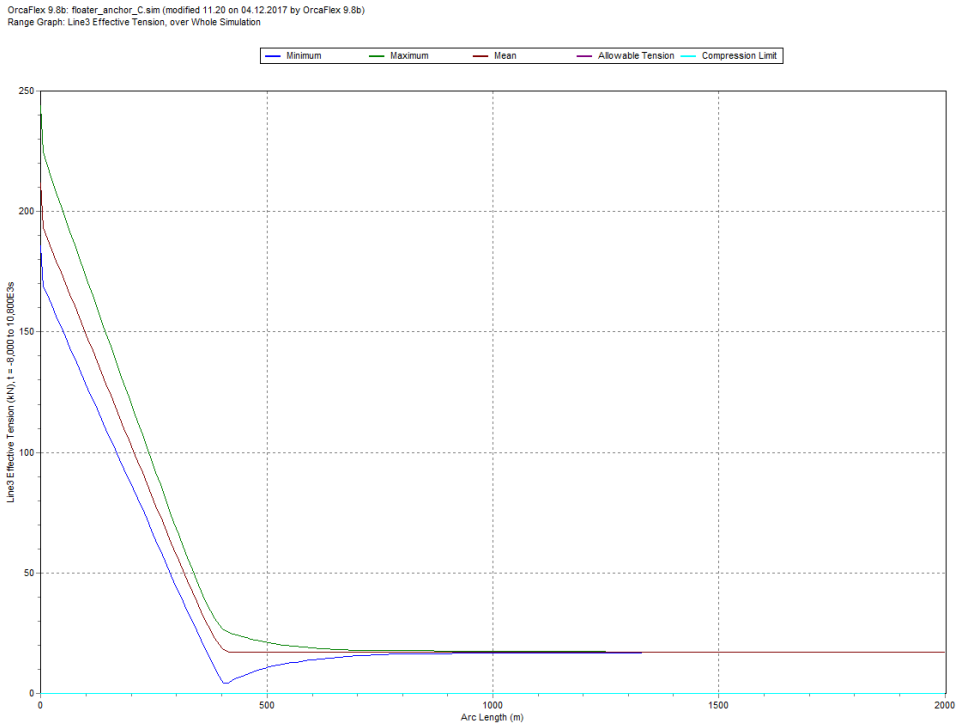 |
| **Time history** | |

| | |
|---|---|
| Line 1 | 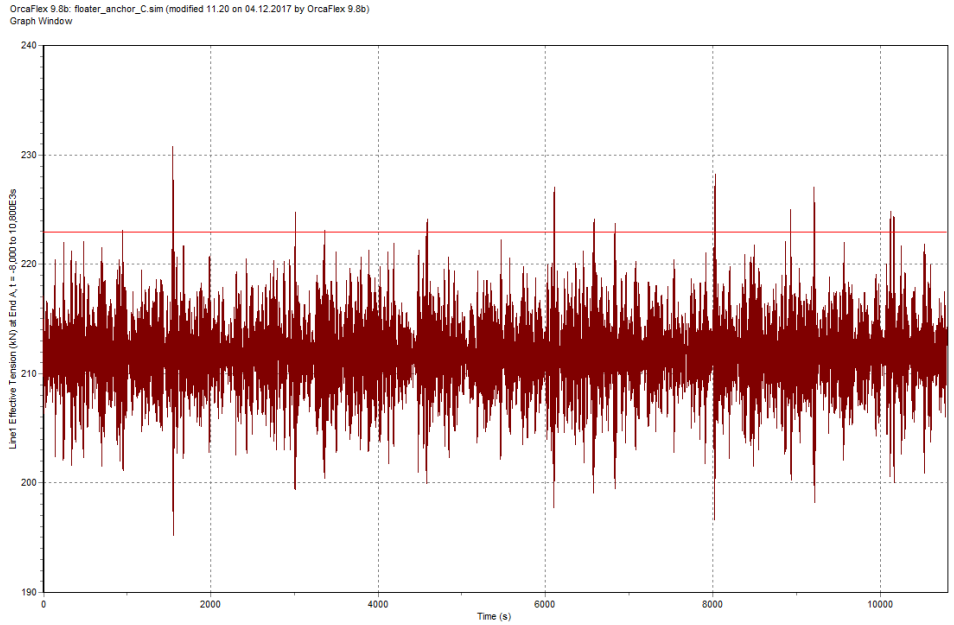 |
| Line 3 | 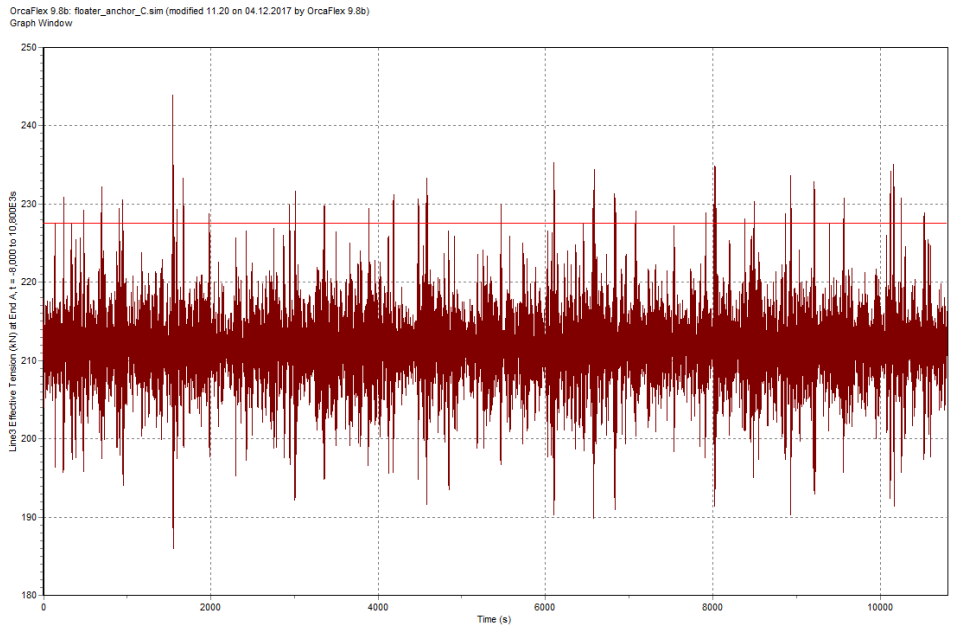 |

| **GPD parameters (line 1)** | |
|---|---|
| β | -0.291 |
| μ | 0 |
| σ | 3.192 |
| Points fitted | 19 |
| Threshold [kN] | 222.90 |
| **GPD parameters (line 3)** | |
| β | -0.183 |

| | |
|---|---|
| μ | 0 |
| σ | 4.426 |
| Points fitted | 45 |
| Threshold [kN] | 227.60 |

# F.5 Simulation 5

**Range graph**

Line 1

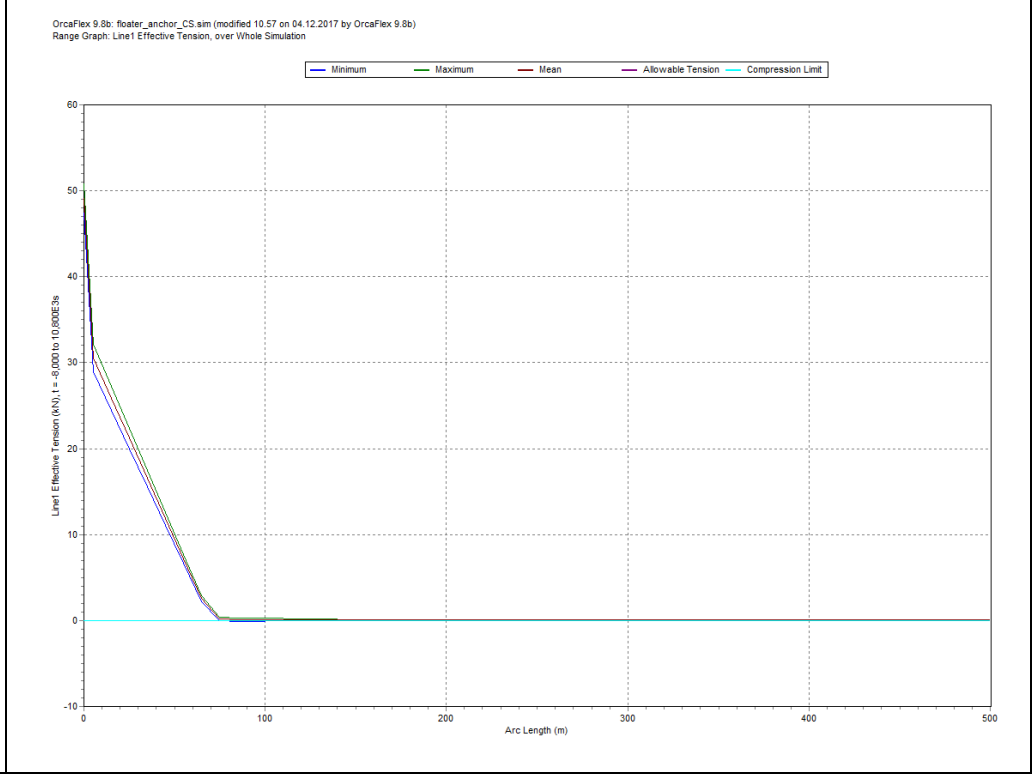

Line 3

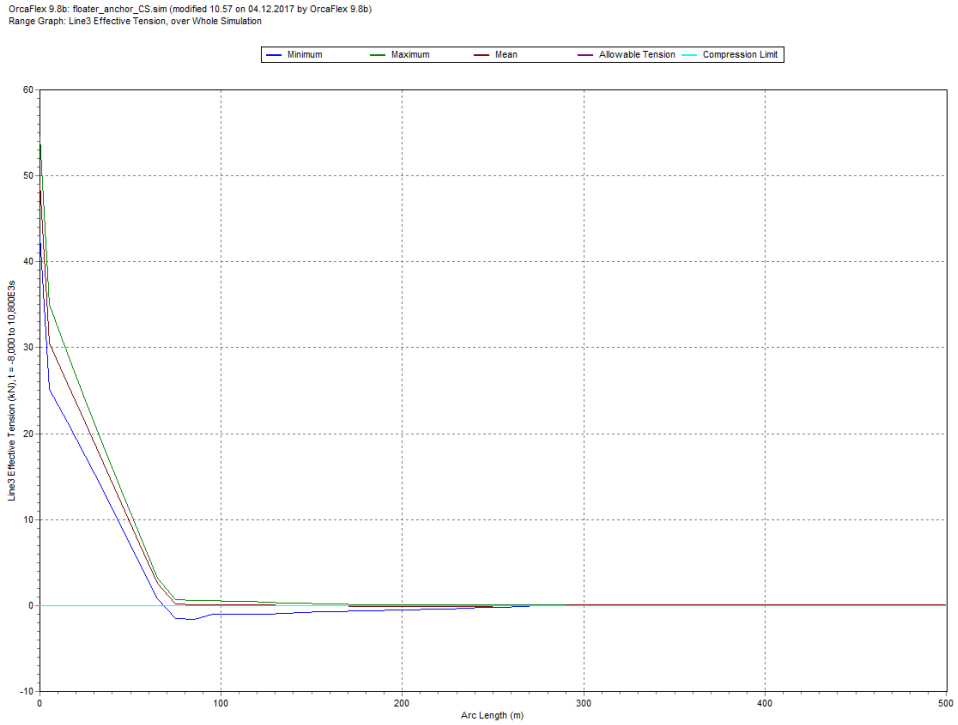


**Time history**

Line 1

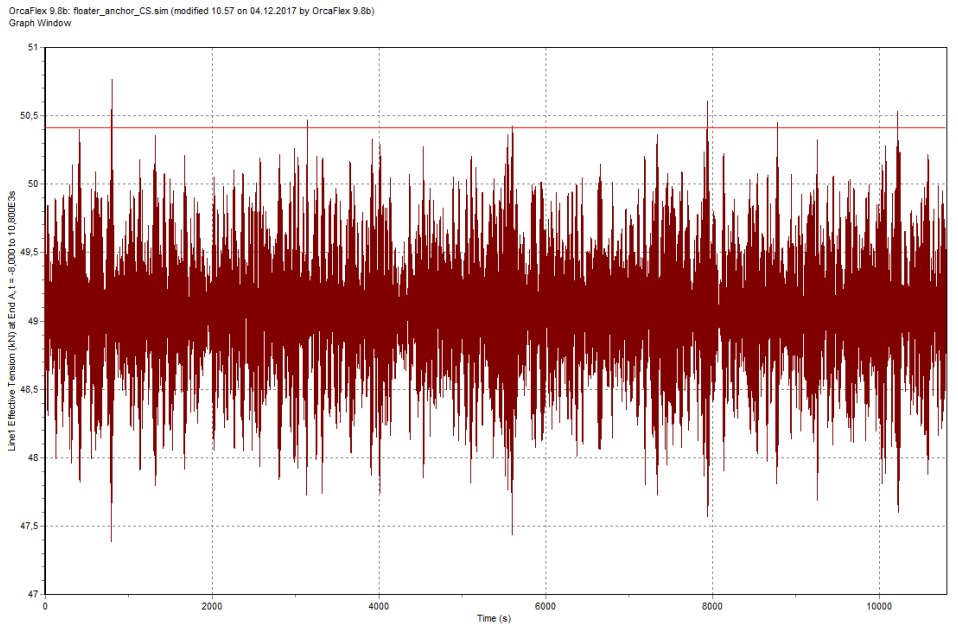

| | |
|---|---|
| Line 3 | 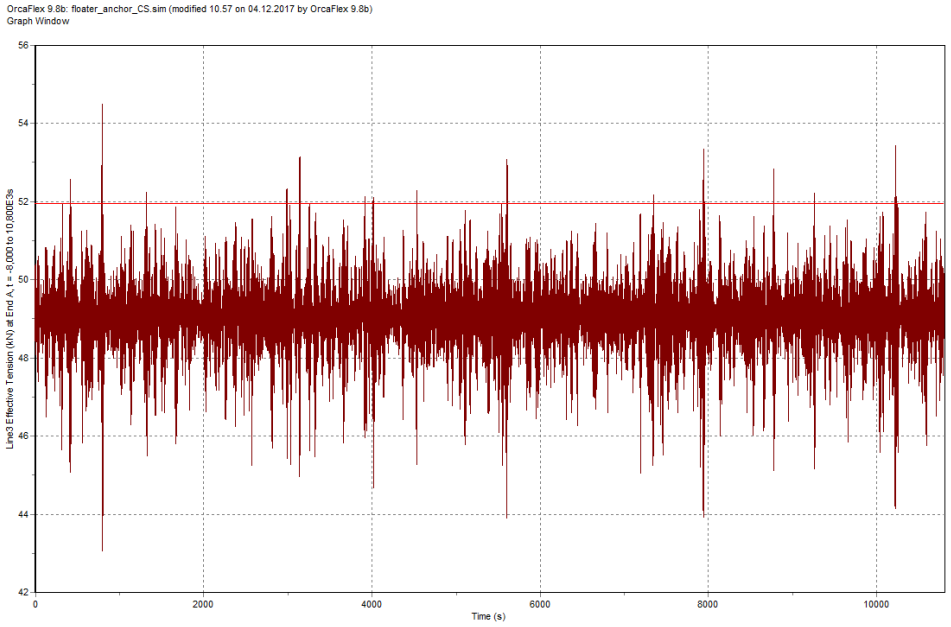 |

| **GPD parameters (line 1)** | |
|---|---|
| β | -0.397 |
| μ | 0 |
| σ | 0.192 |
| Points fitted | 7 |
| Threshold [kN] | 50.41 |
| **GPD parameters (line 3)** | |
| β | 0.084 |
| μ | 0 |
| σ | 0.540 |
| Points fitted | 24 |
| Threshold [kN] | 51.95 |

# F.6 Simulation 6

| **Range graph** |
|---|

| | |
|---|---|
| Line 1 | 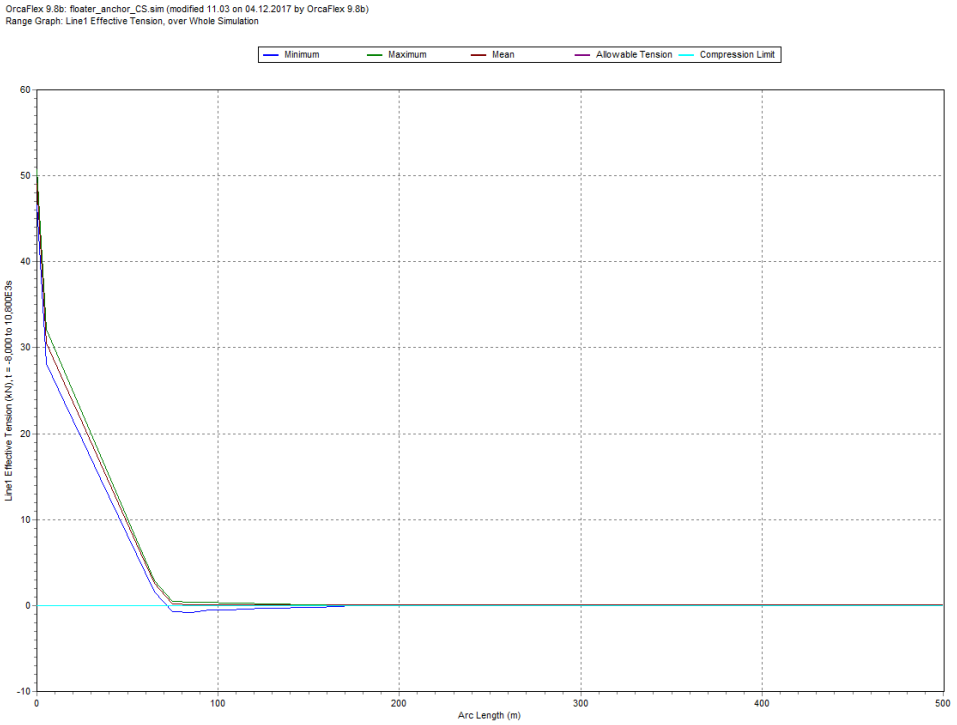 |
| Line 3 | 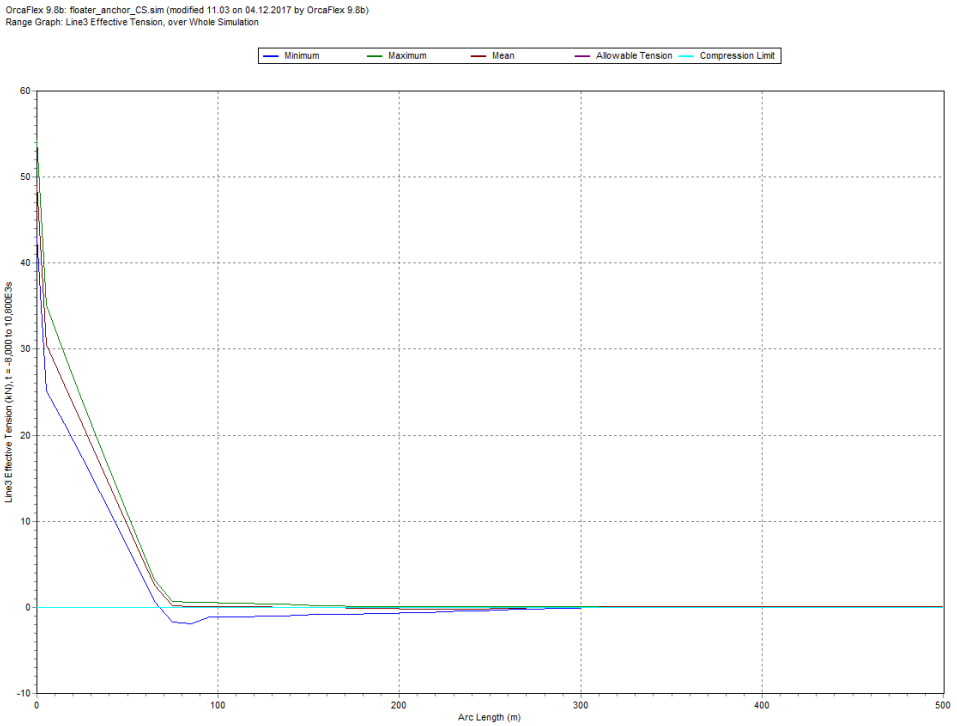 |
| **Time history** | |

Line 1

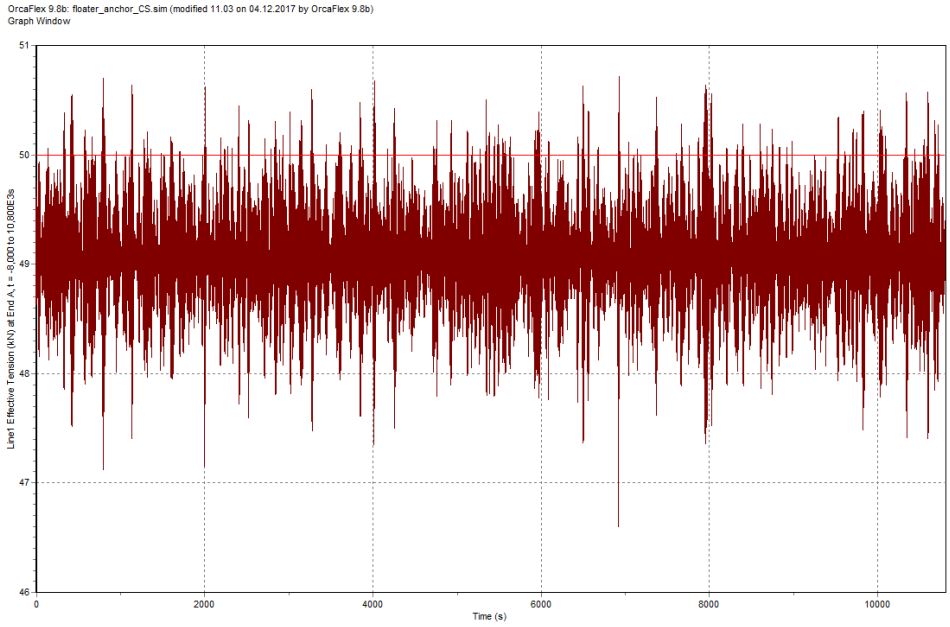


Line 3

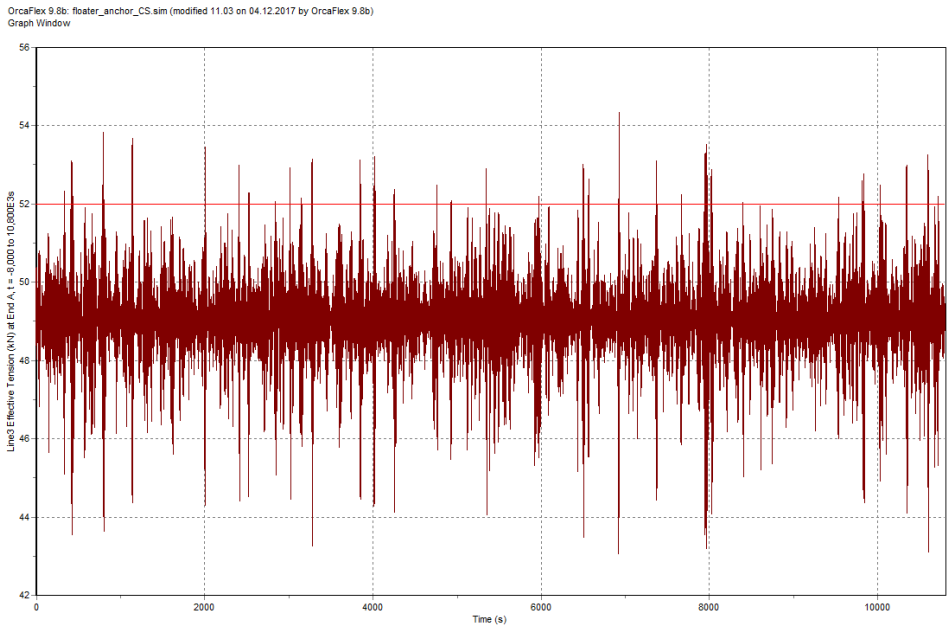


| GPD parameters (line 1) | |
|---|---|
| β | -0.277 |
| μ | 0 |
| σ | 0.267 |
| Points fitted | 189 |
| Threshold [kN] | 50.00 |
| **GPD parameters (line 3)** | |
| β | -0.344 |

| | |
|---|---|
| μ | 0 |
| σ | 0.938 |
| Points fitted | 55 |
| Threshold [kN] | 52.00 |

# F.7 Simulation 7

| Range graph | |
|---|---|
| Line 1 | 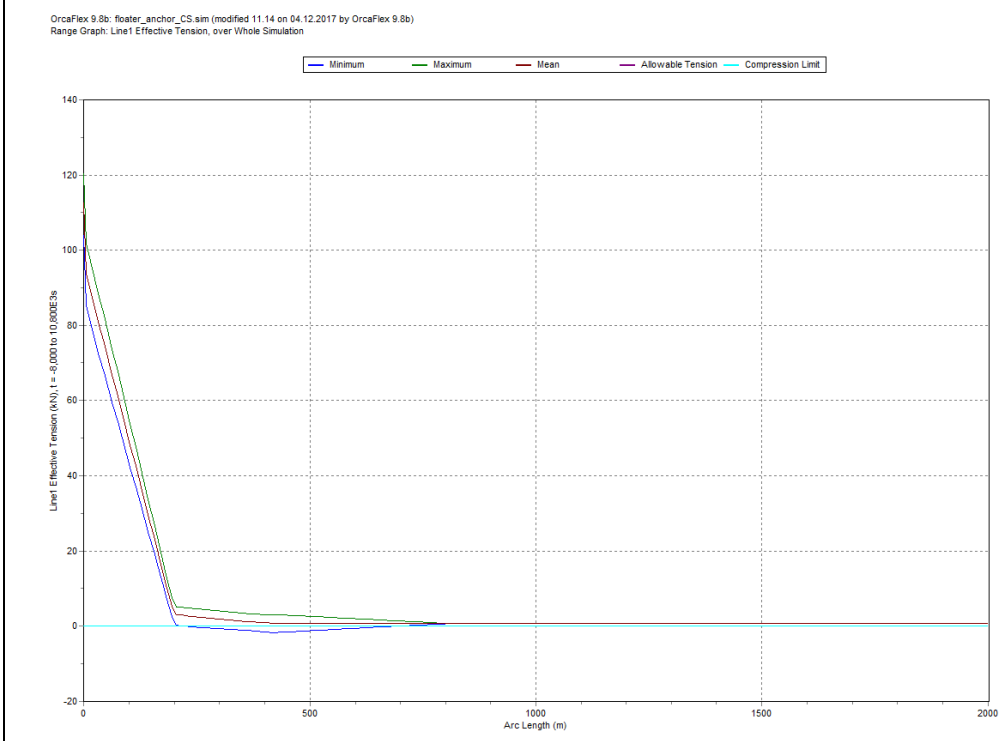 |

Line 3

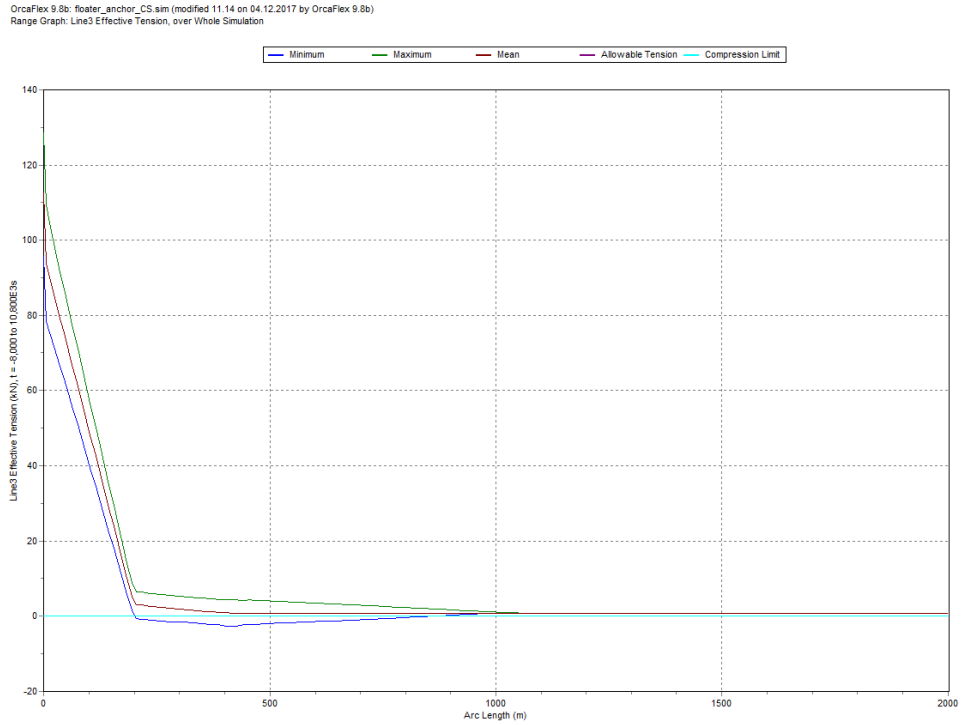


**Time history**

Line 1

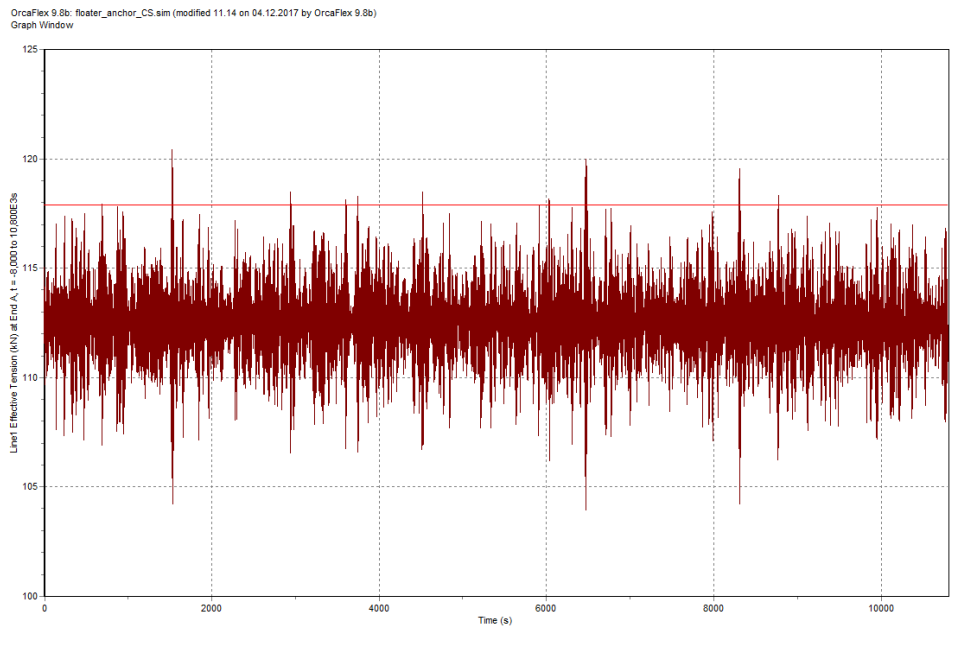

| | |
|---|---|
| Line 3 | 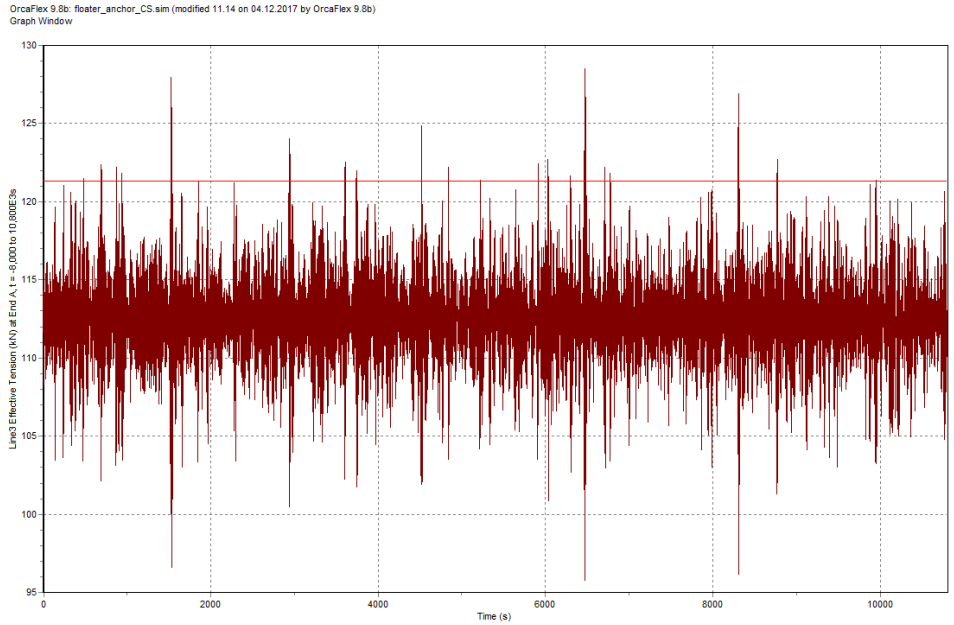 |

| **GPD parameters (line 1)** | |
|---|---|
| β | -0.673 |
| μ | 0 |
| σ | 1.783 |
| Points fitted | 14 |
| Threshold [kN] | 117.90 |
| **GPD parameters (line 3)** | |
| β | 0.290 |
| μ | 0 |
| σ | 1.413 |
| Points fitted | 27 |
| Threshold [kN] | 121.30 |

# F.8 Simulation 8

| **Range graph** |
|---|

| | |
|---|---|
| Line 1 | 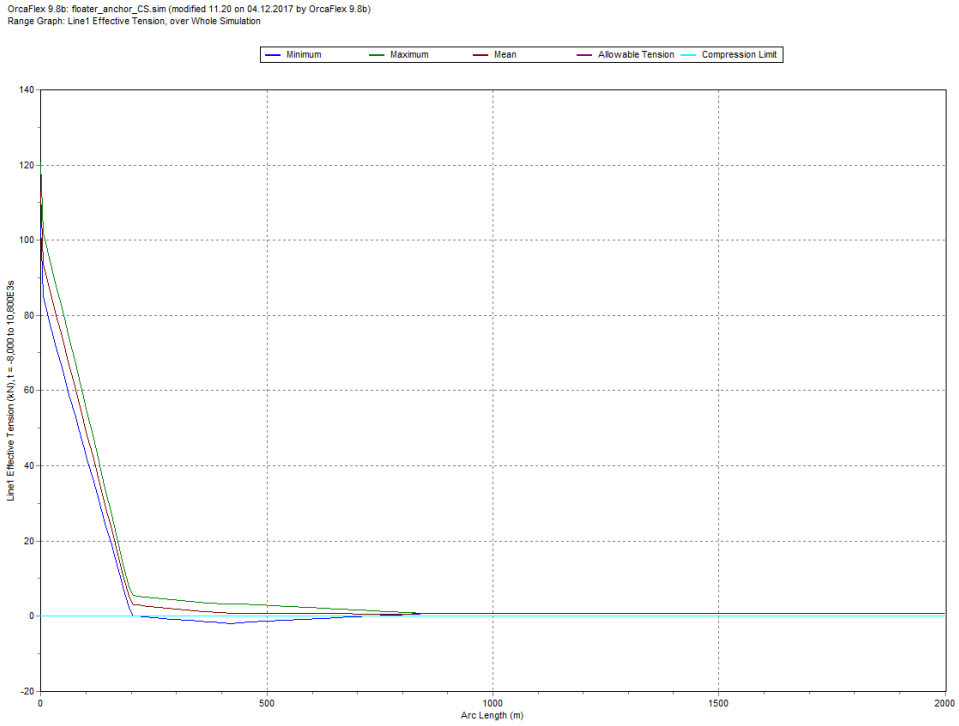 |
| Line 3 | 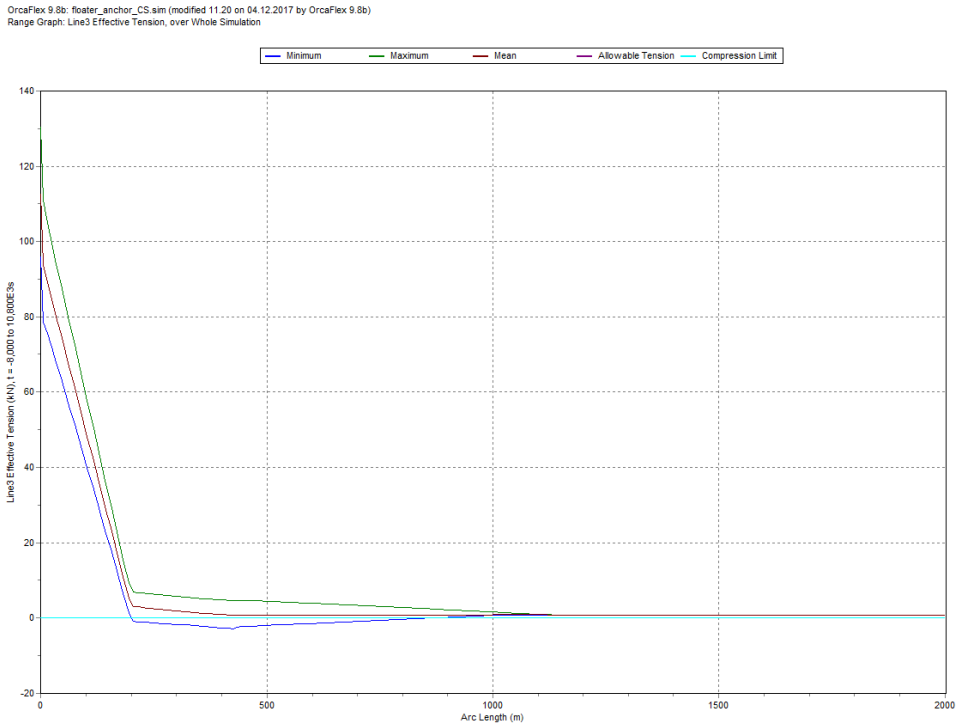 |
| **Time history** | |

Line 1

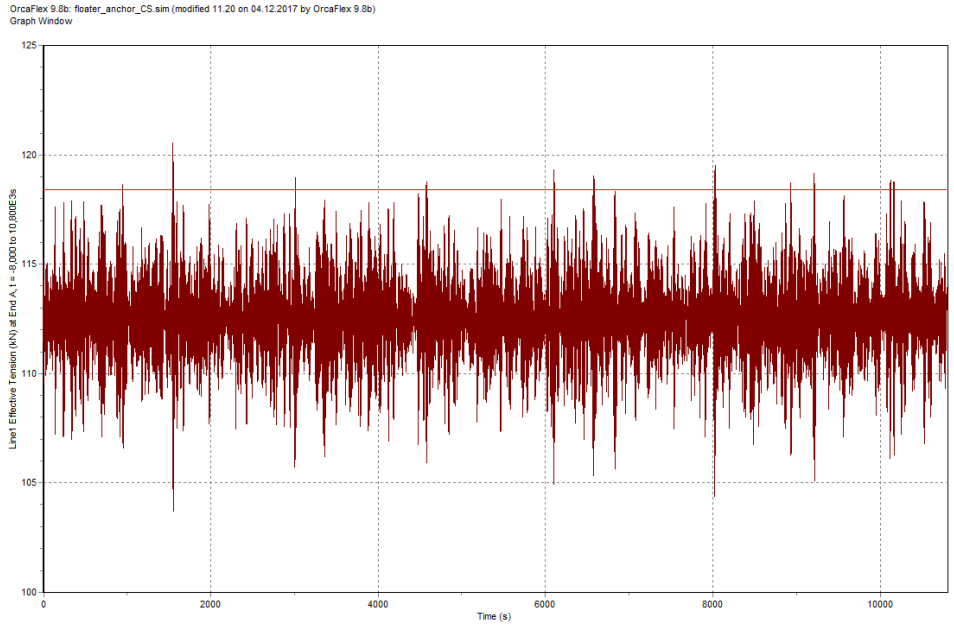


Line 3

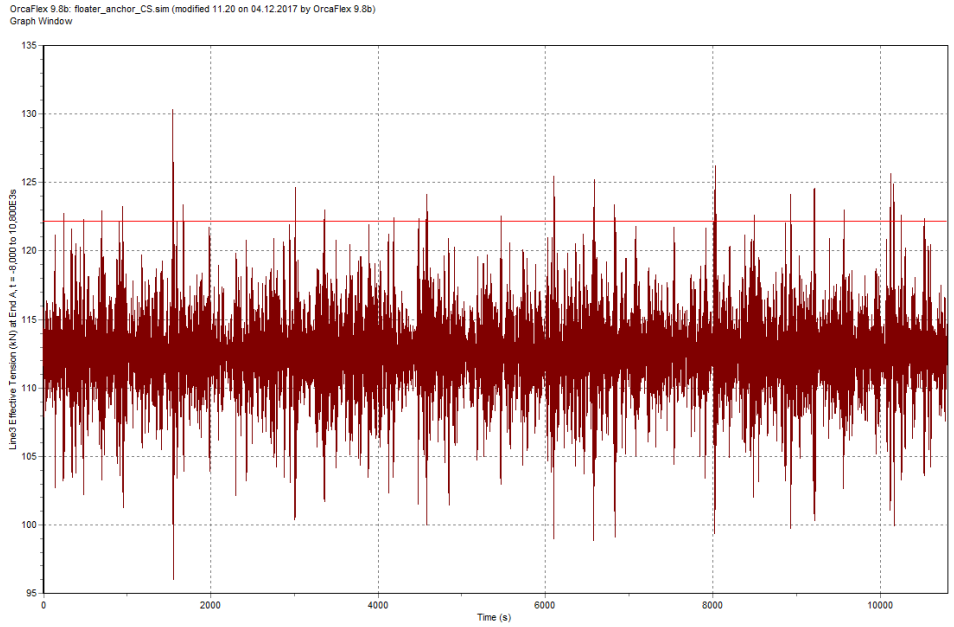


| **GPD parameters (line 1)** | |
|---|---|
| β | -0.229 |
| μ | 0 |
| σ | 0.779 |
| Points fitted | 16 |
| Threshold [kN] | 118.40 |
| **GPD parameters (line 3)** | |
| β | 0.018 |

| | |
|---|---|
| μ | 0 |
| σ | 1.605 |
| Points fitted | 33 |
| Threshold [kN] | 122.20 |

# F.9 Simulation 9

**Range graph**

Line 1

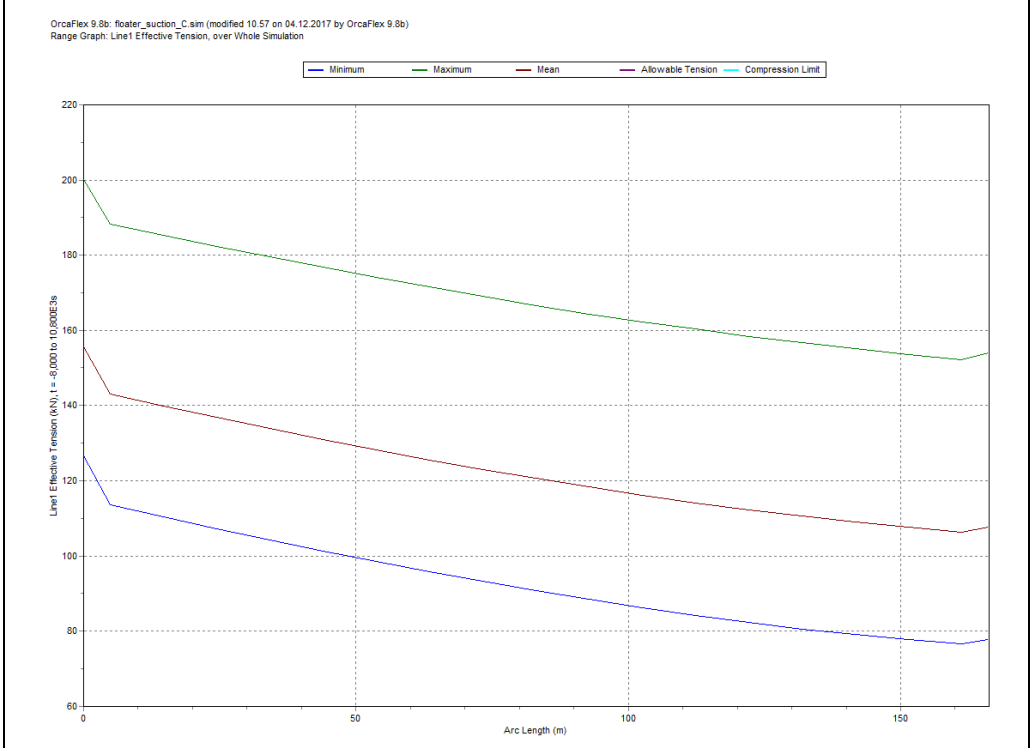

Line 3

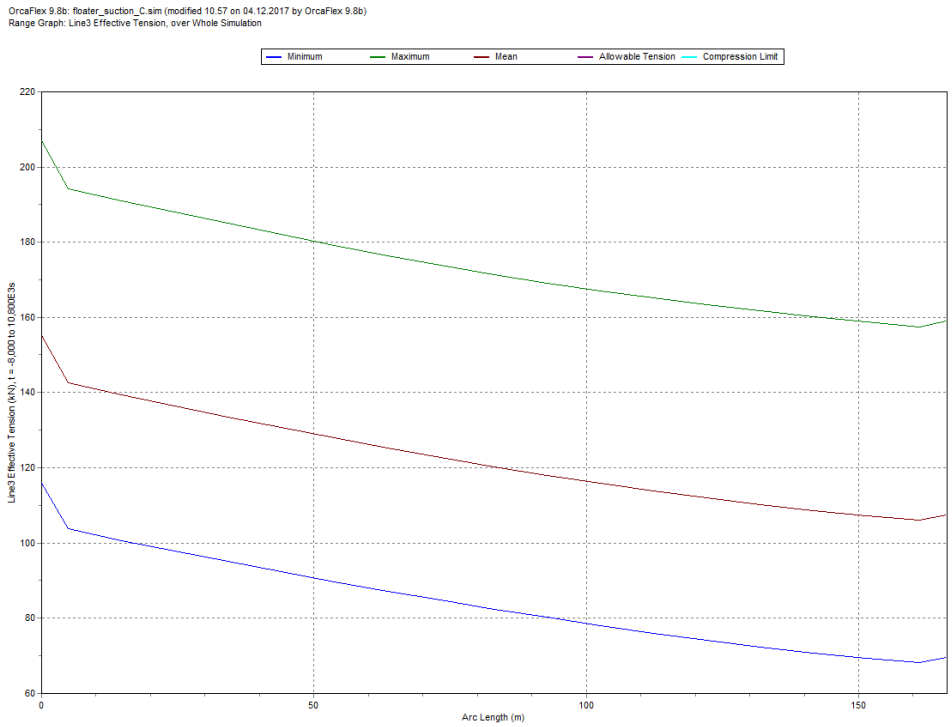


**Time history**

Line 1

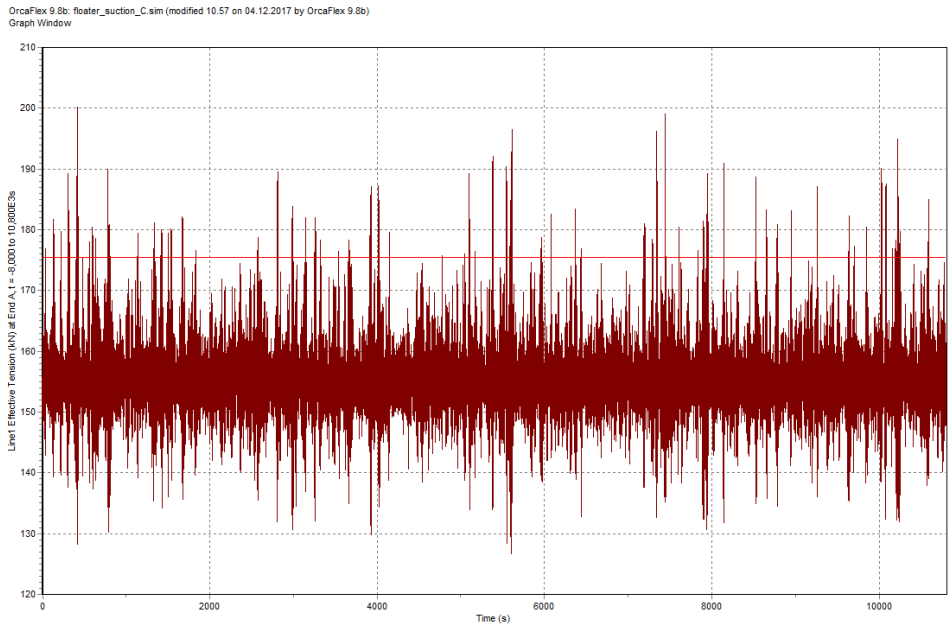

| | |
|---|---|
| Line 3 | 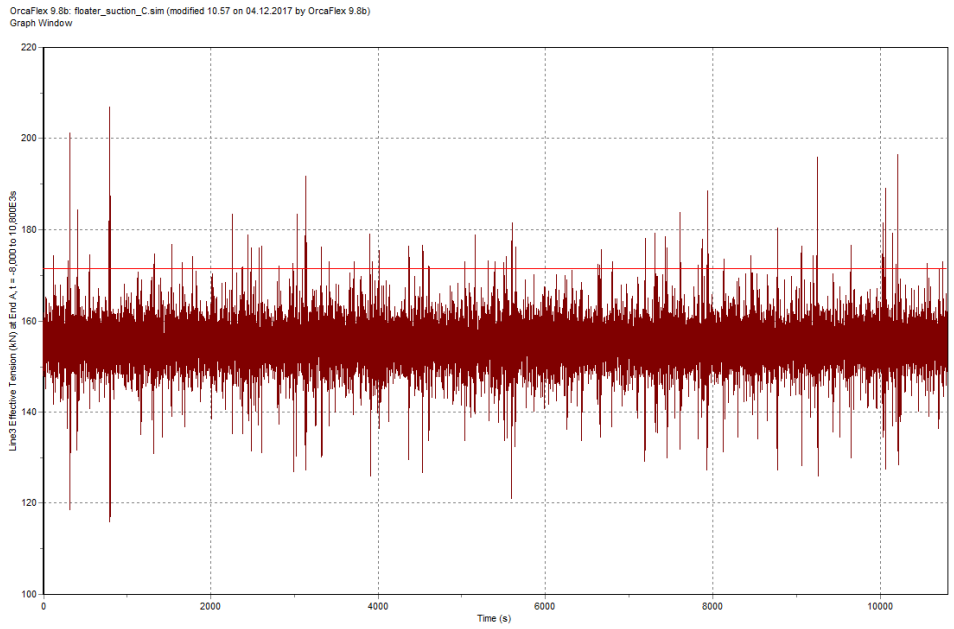 |

| **GPD parameters (line 1)** | |
|---|---|
| β | -0.260 |
| μ | 0 |
| σ | 8.574 |
| Points fitted | 104 |
| Threshold [kN] | 175.50 |
| **GPD parameters (line 3)** | |
| β | 0.112 |
| μ | 0 |
| σ | 5.432 |
| Points fitted | 79 |
| Threshold [kN] | 171.50 |

# F.10 Simulation 10

| **Range graph** |
|---|

| | |
|---|---|
| Line 1 | 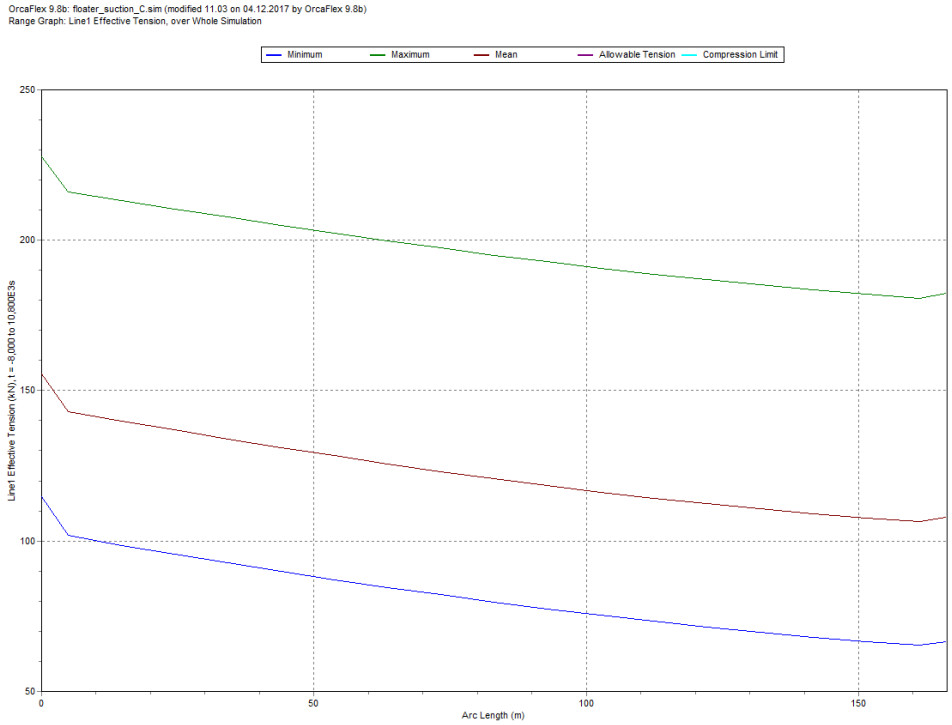 |
| Line 3 | 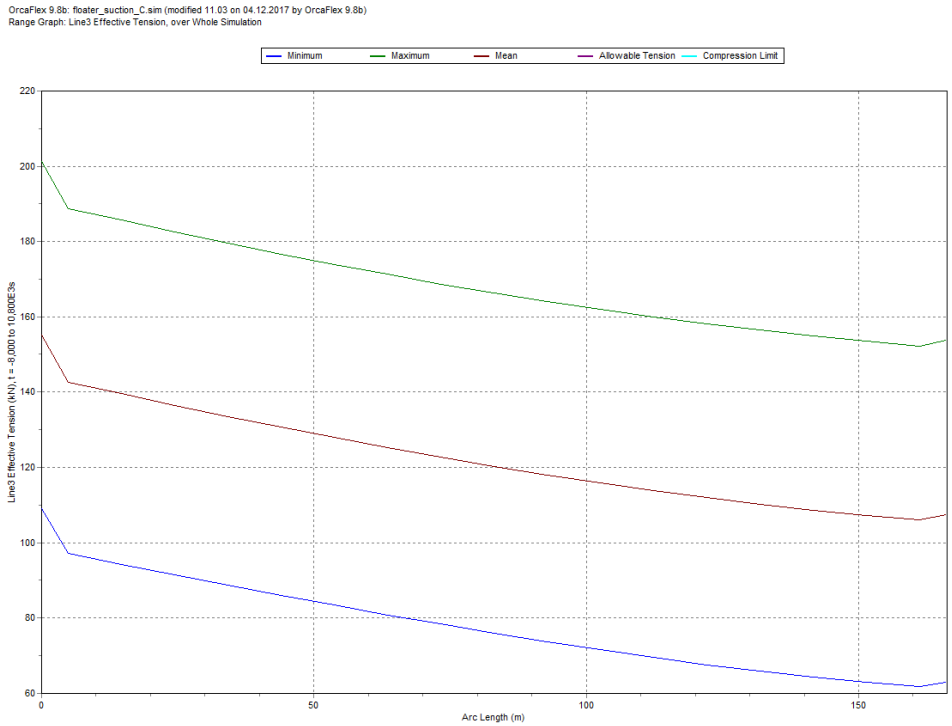 |
| **Time history** | |

| | |
|---|---|
| Line 1 | 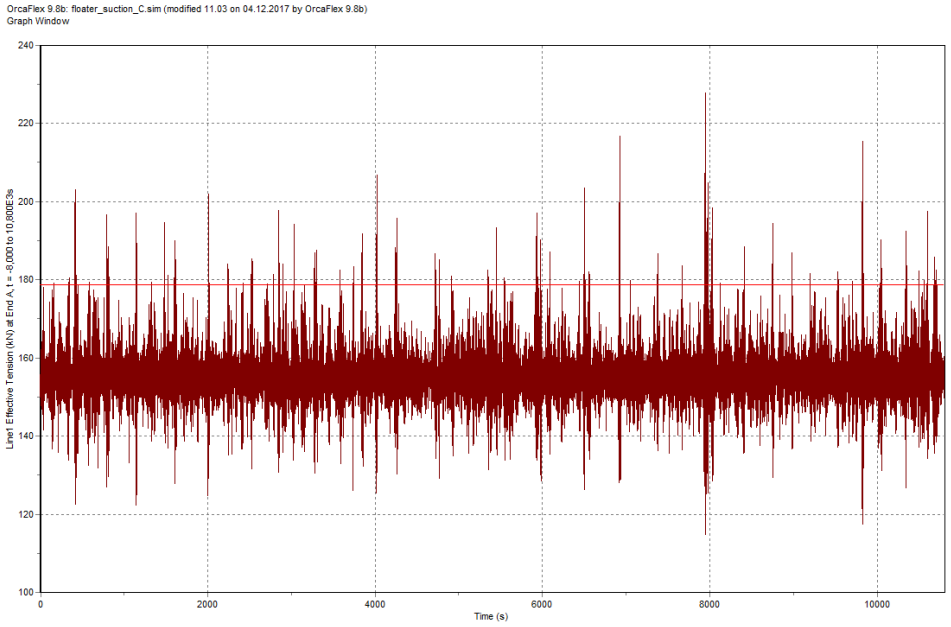 |
| Line 3 | 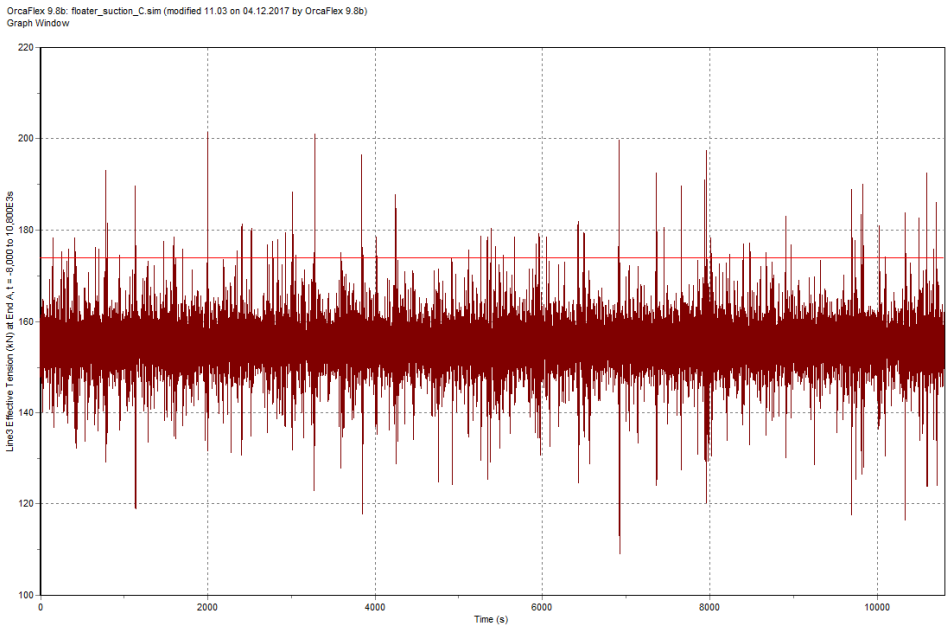 |

| **GPD parameters (line 1)** | |
|---|---|
| β | 0.063 |
| μ | 0 |
| σ | 8.444 |
| Points fitted | 101 |
| Threshold [kN] | 178.70 |
| **GPD parameters (line 3)** | |
| β | -0.034 |

| | |
|---|---|
| μ | 0 |
| σ | 7.018 |
| Points fitted | 87 |
| Threshold [kN] | 179.90 |

# F.11 Simulation 11

| Range graph | |
|---|---|
| Line 1 | 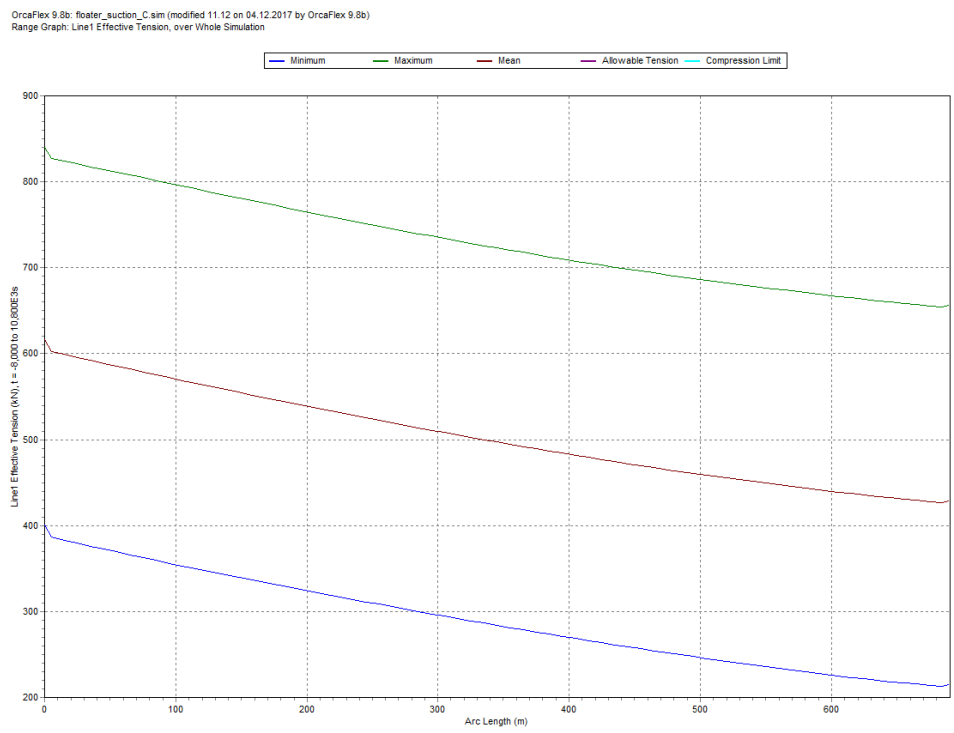 |

Line 3

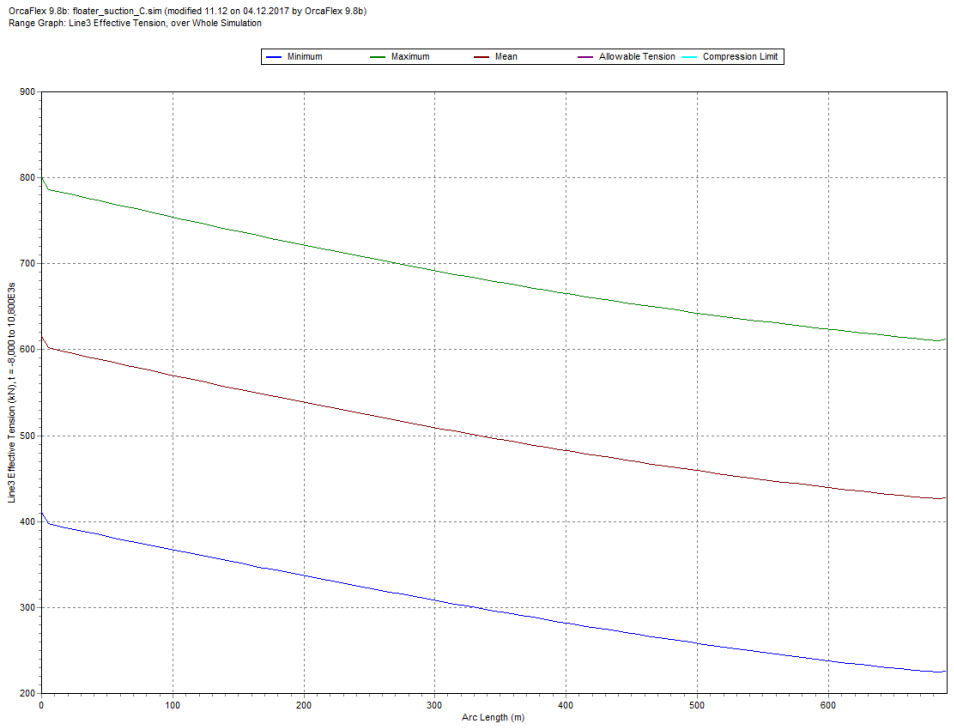


**Time history**

Line 1

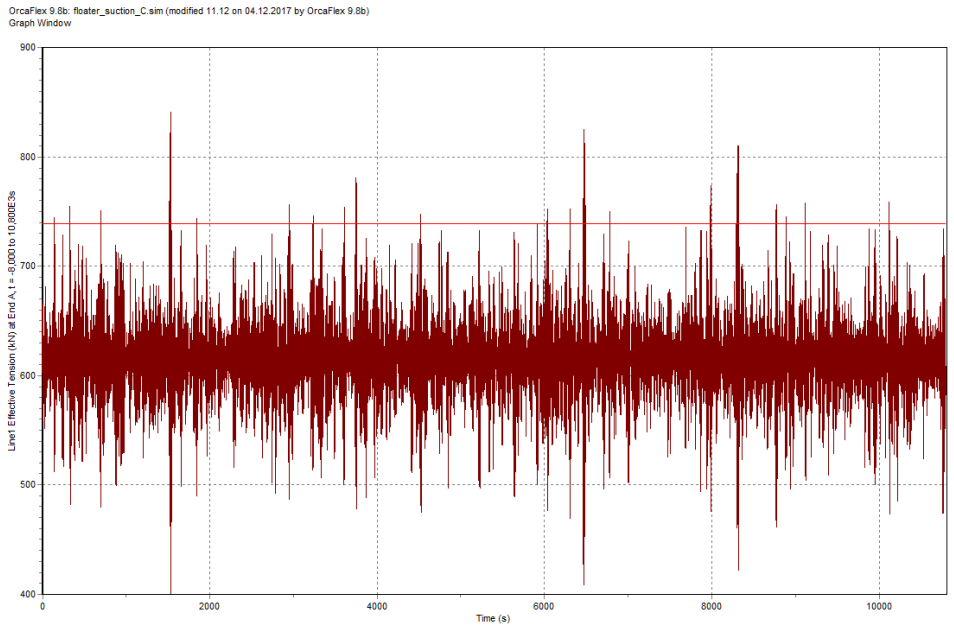

| | |
|---|---|
| Line 3 | 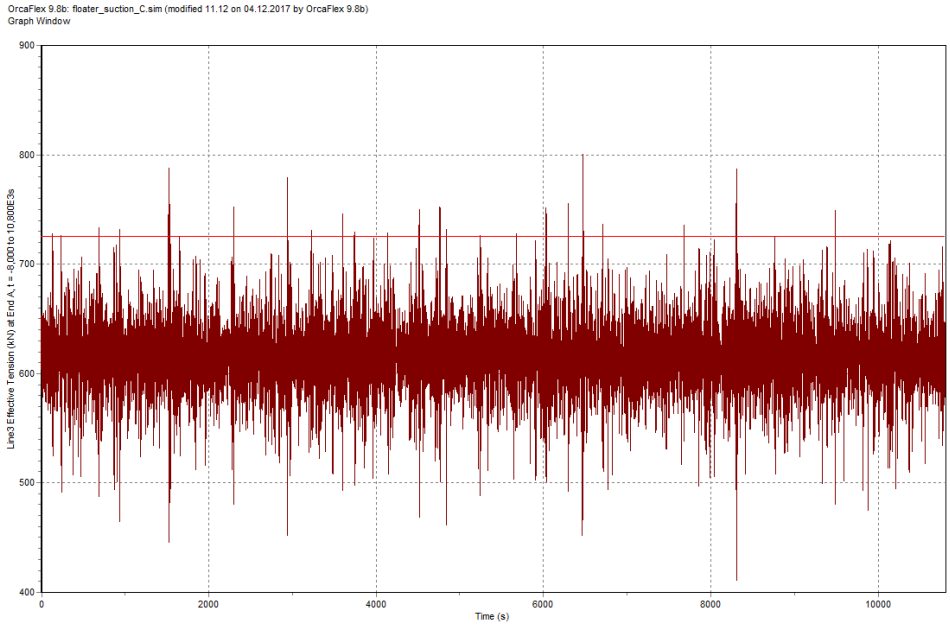 |

| **GPD parameters (line 1)** | |
|---|---|
| β | -0.051 |
| μ | 0 |
| σ | 30.005 |
| Points fitted | 28 |
| Threshold [kN] | 738.80 |
| **GPD parameters (line 3)** | |
| β | 0.033 |
| μ | 0 |
| σ | 19.272 |
| Points fitted | 28 |
| Threshold [kN] | 725.30 |

# F.12 Simulation 12

| **Range graph** |
|---|

| | |
|---|---|
| Line 1 | 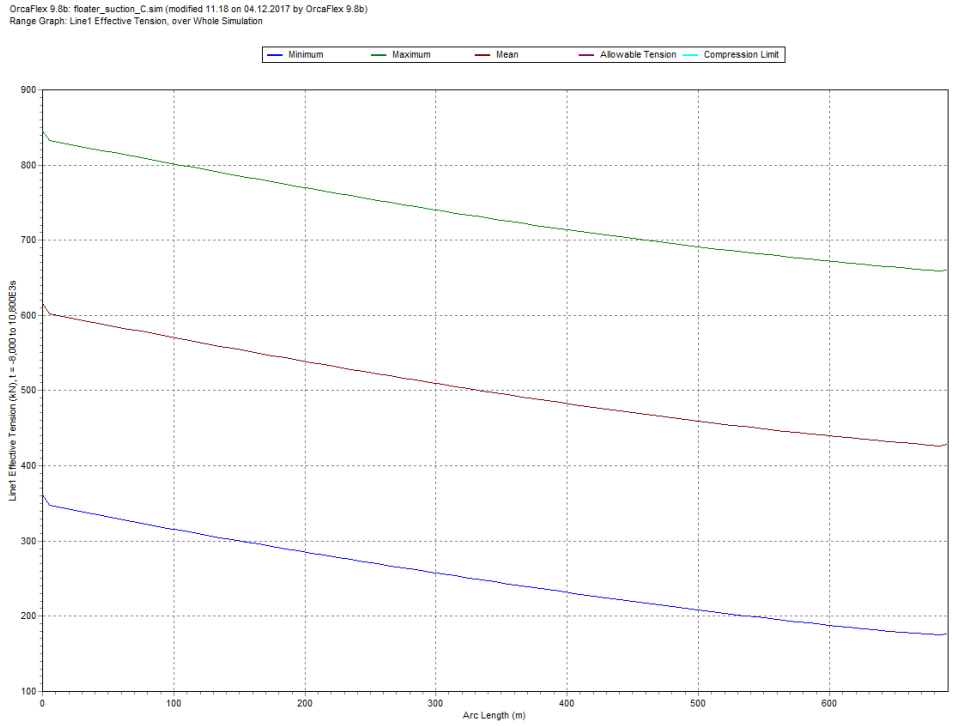 |
| Line 3 | 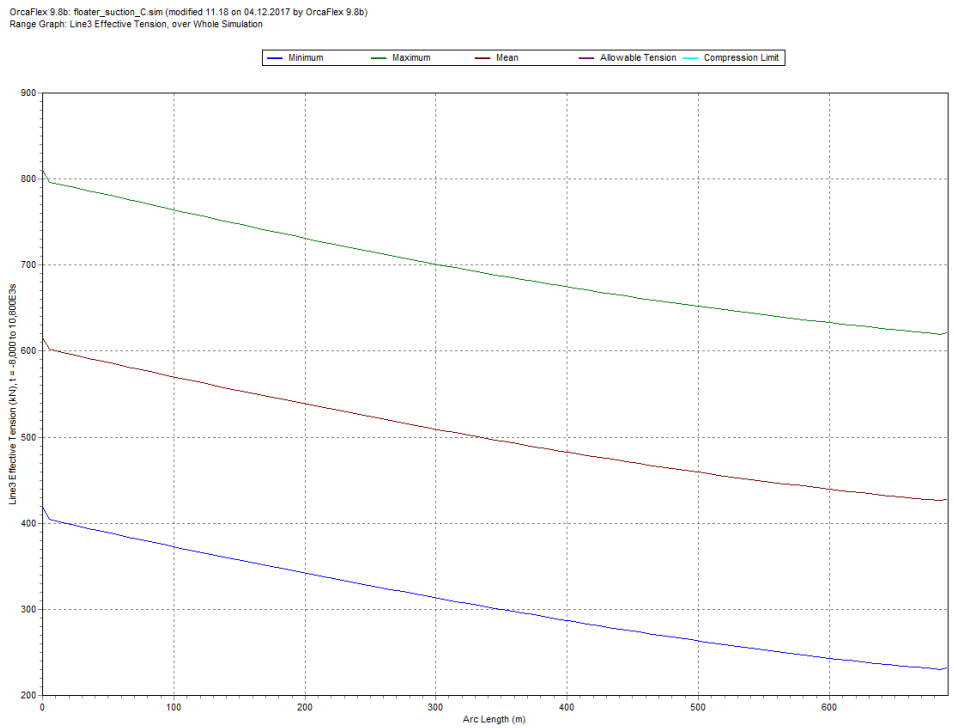 |
| **Time history** | |

Line 1

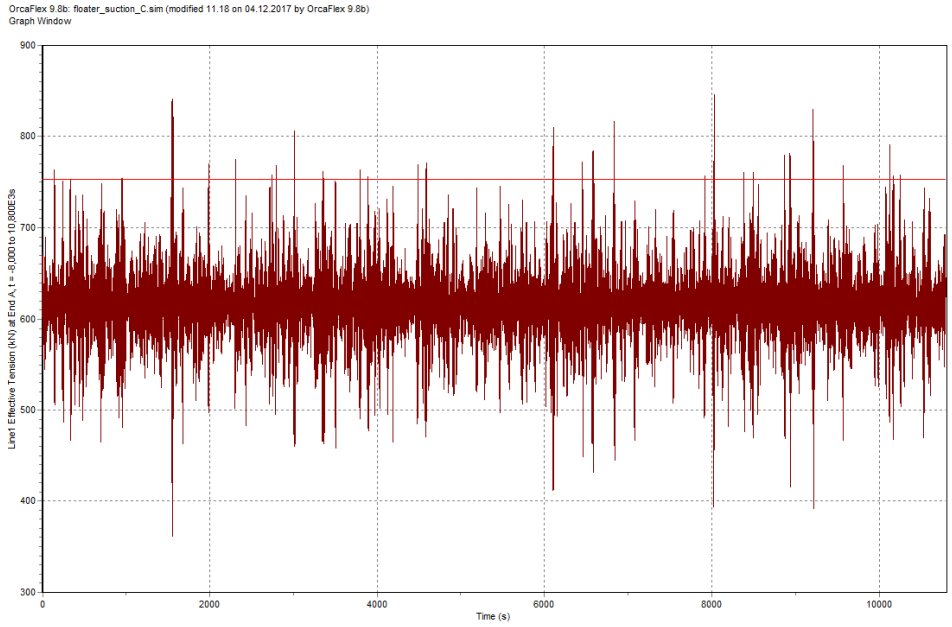


Line 3

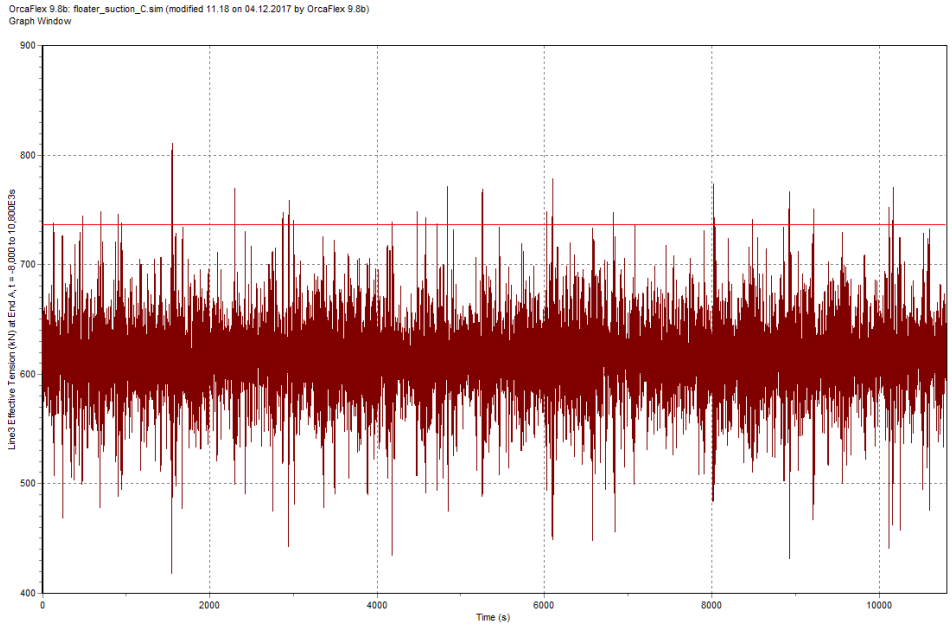


| **GPD parameters (line 1)** | |
|---|---|
| β | -0.137 |
| μ | 0 |
| σ | 30.952 |
| Points fitted | 35 |
| Threshold [kN] | 753.10 |
| **GPD parameters (line 3)** | |
| β | -0.029 |

| | |
|---|---|
| μ | 0 |
| σ | 17.444 |
| Points fitted | 28 |
| Threshold [kN] | 736.70 |

# F.13 Simulation 13

**Range graph**

Line 1

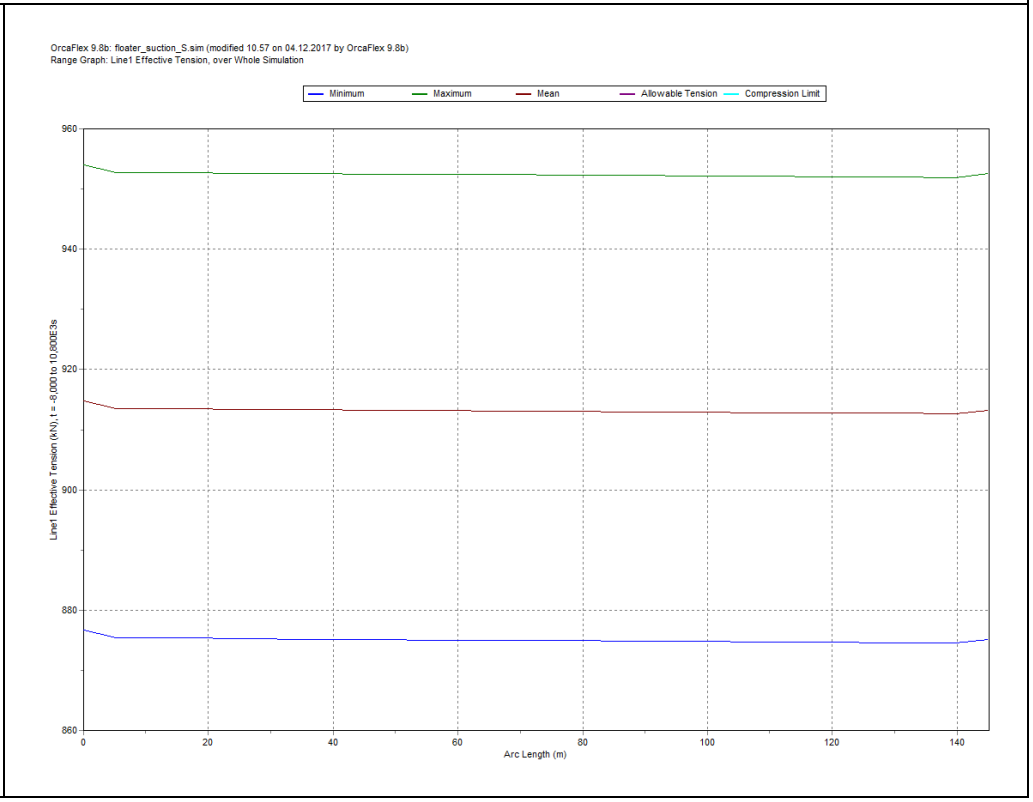

Line 3

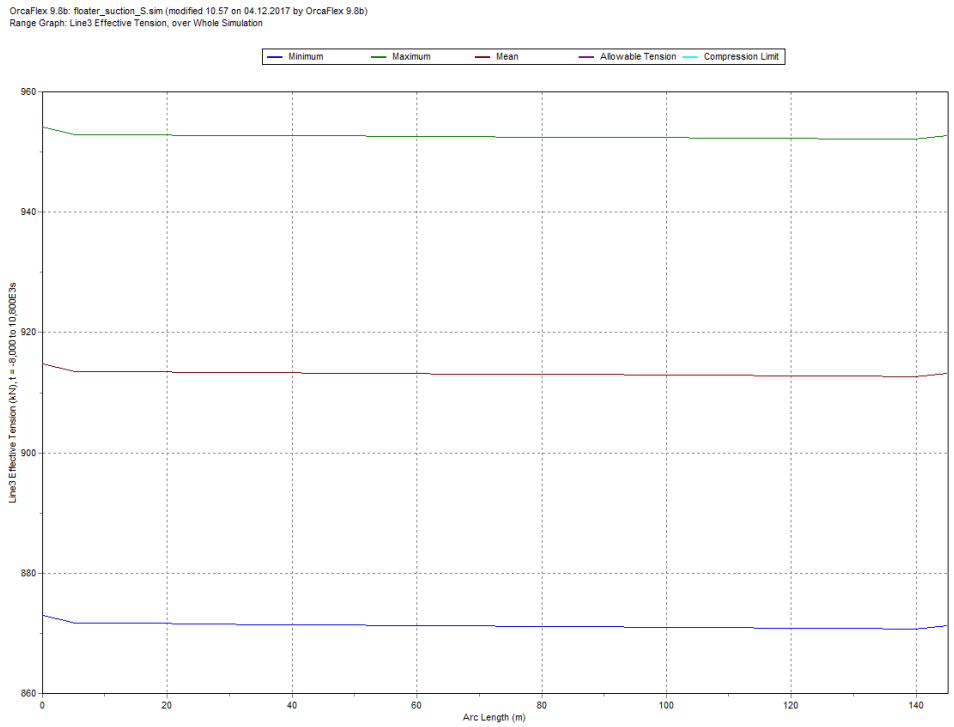


**Time history**

Line 1

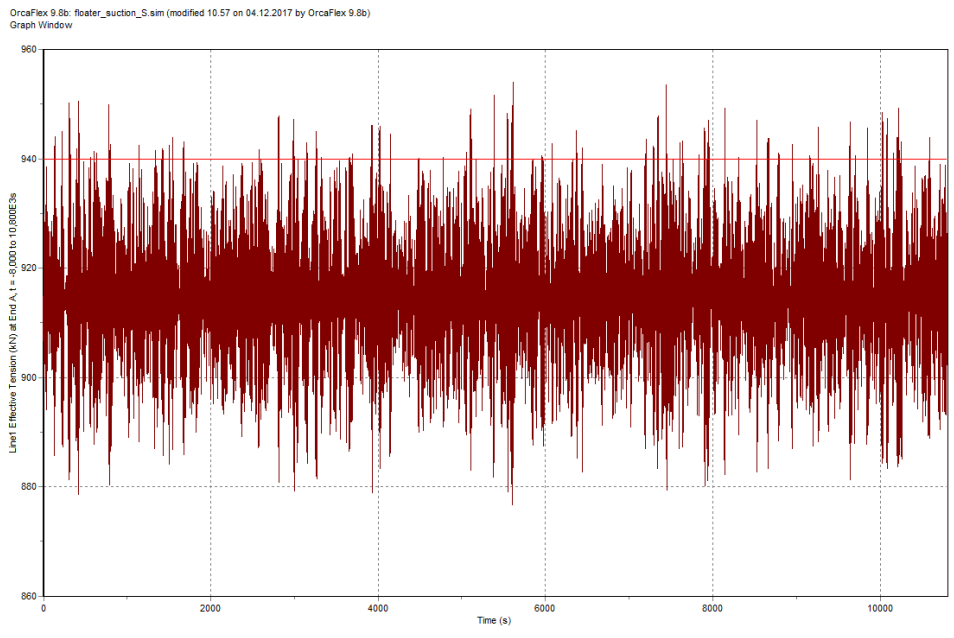

| | |
|---|---|
| Line 3 | 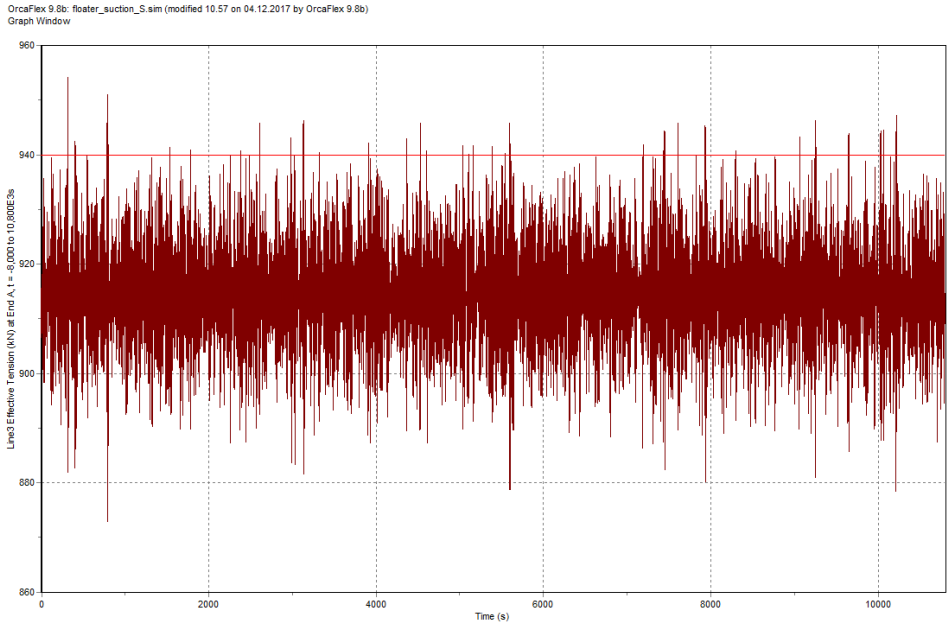 |

| **GPD parameters (line 1)** | |
|---|---|
| β | -0.304 |
| μ | 0 |
| σ | 5.272 |
| Points fitted | 100 |
| Threshold [kN] | 940.00 |
| **GPD parameters (line 3)** | |
| β | -0.195 |
| μ | 0 |
| σ | 4.400 |
| Points fitted | 41 |
| Threshold [kN] | 940.00 |

# F.14 Simulation 14

| **Range graph** |
|---|

| | |
|---|---|
| Line 1 | 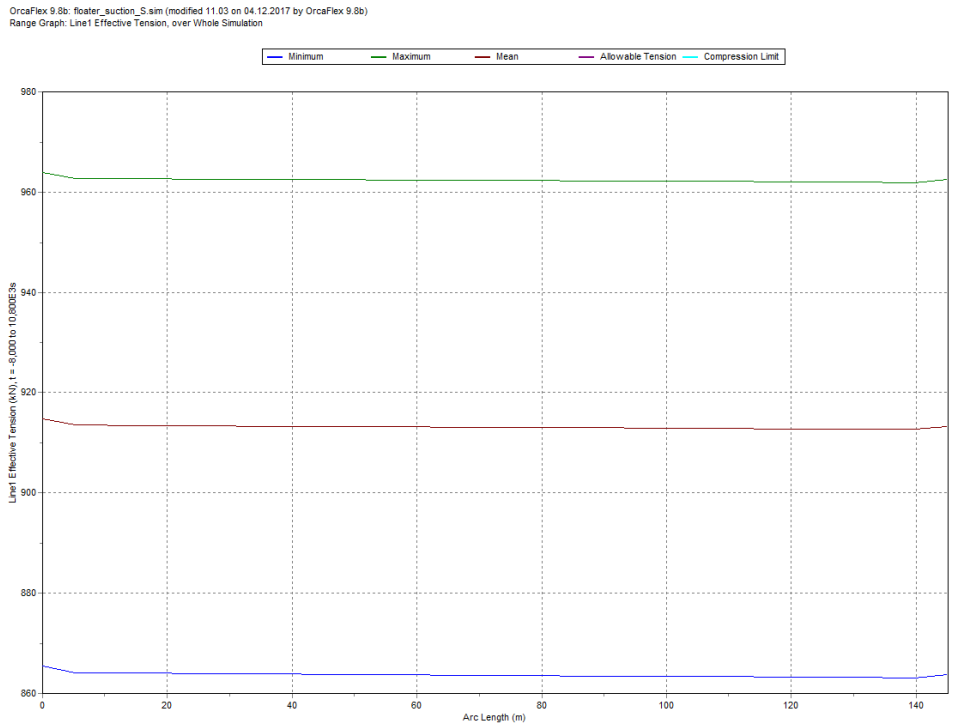 |
| Line 3 | 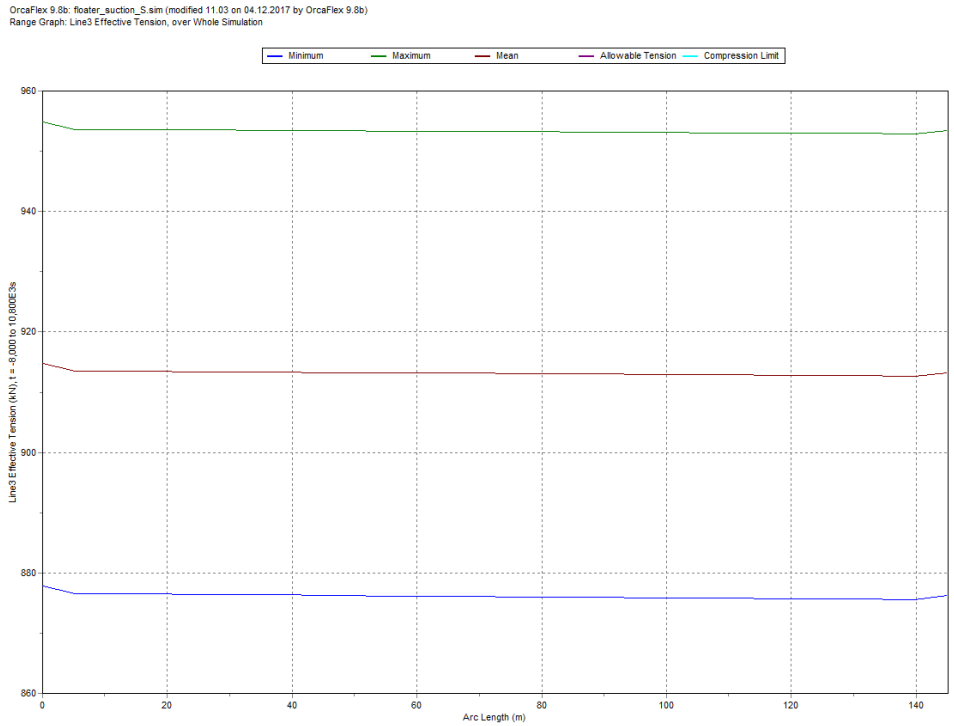 |
| **Time history** | |

| | |
|---|---|
| Line 1 | 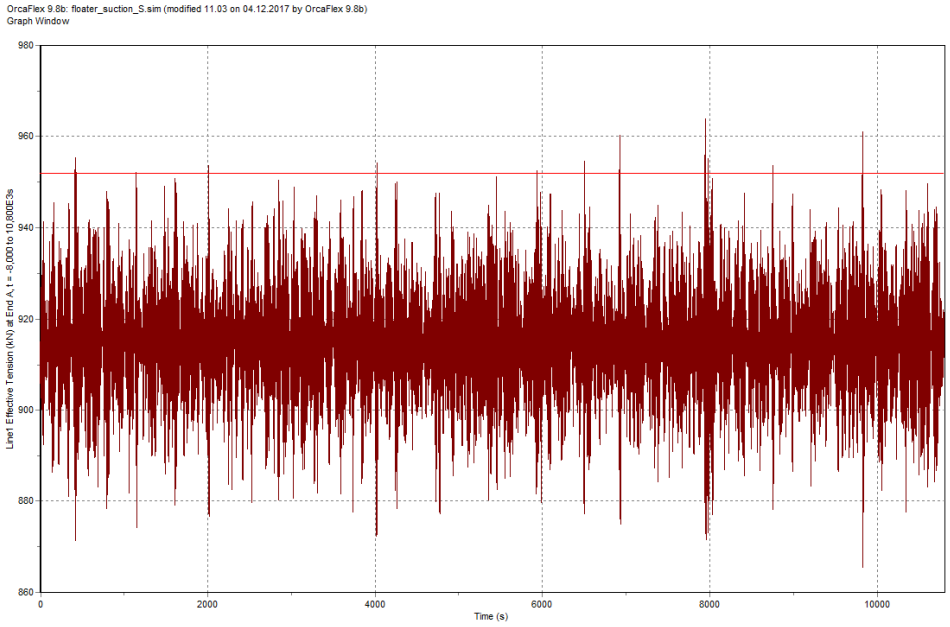 |
| Line 3 | 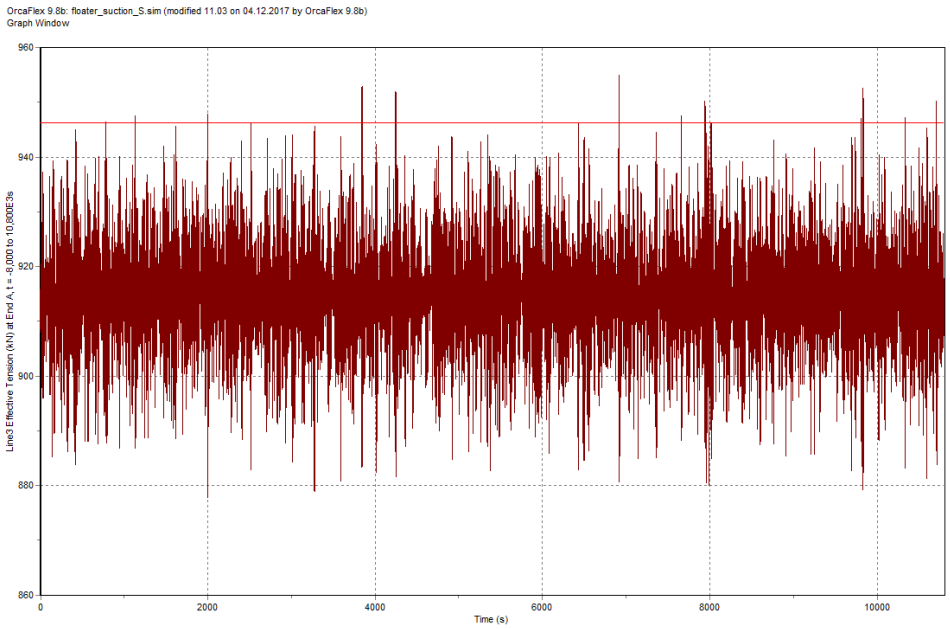 |

| **GPD parameters (line 1)** | |
|---|---|
| β | -0.041 |
| μ | 0 |
| σ | 3.706 |
| Points fitted | 14 |
| Threshold [kN] | 952.00 |
| **GPD parameters (line 3)** | |
| β | -0.644 |

| | |
|---|---|
| μ | 0 |
| σ | 6.015 |
| Points fitted | 13 |
| Threshold [kN] | 946.20 |

# F.15 Simulation 15

| Range graph | |
|---|---|
| Line 1 | 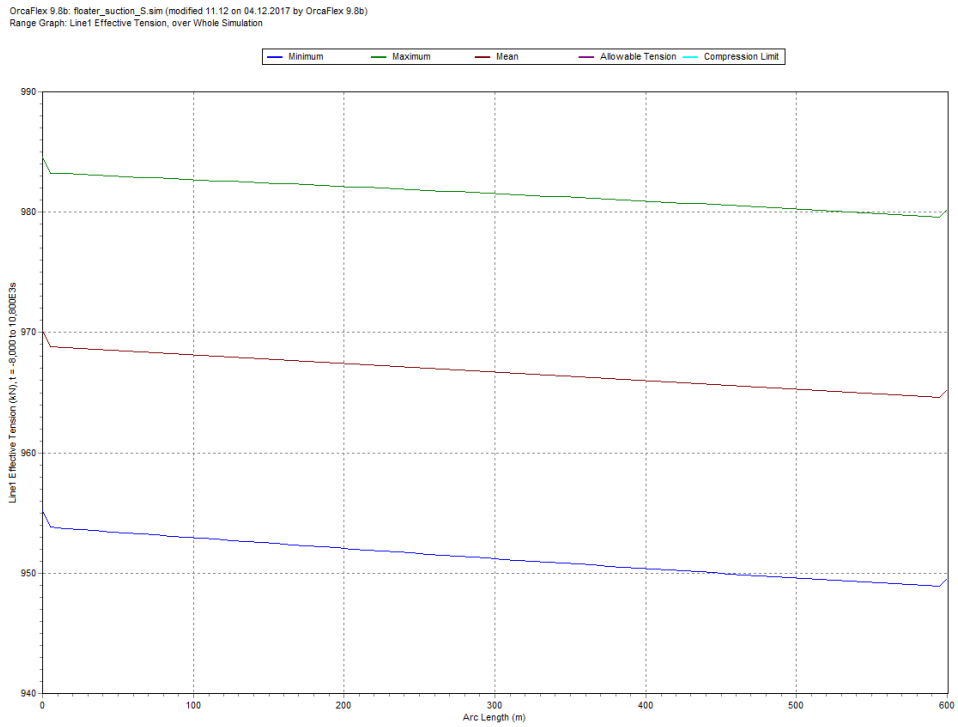 |

Line 3

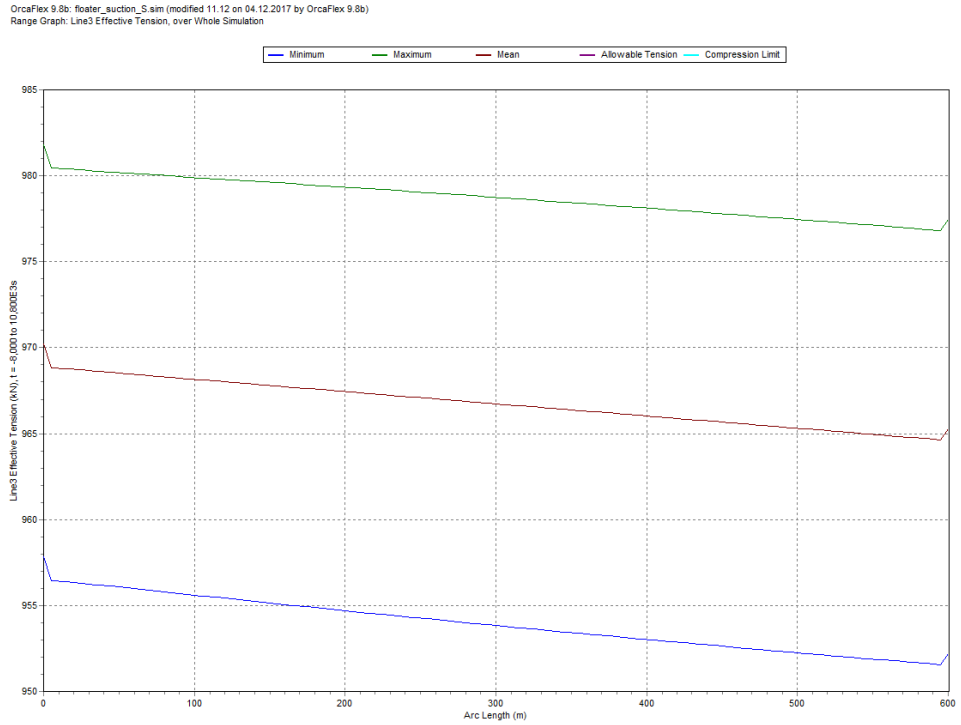


**Time history**

Line 1

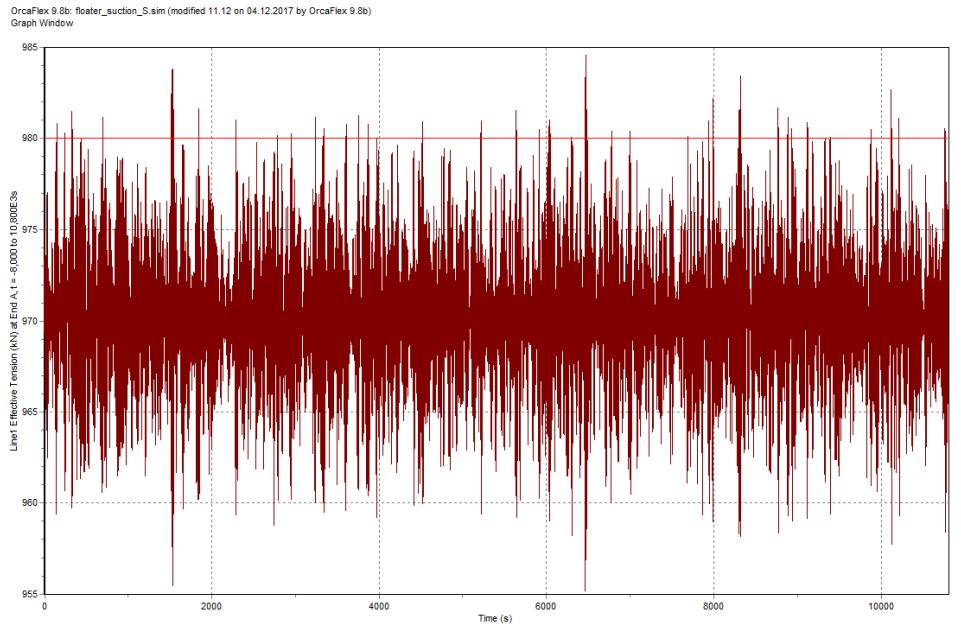

| | |
|---|---|
| Line 3 | 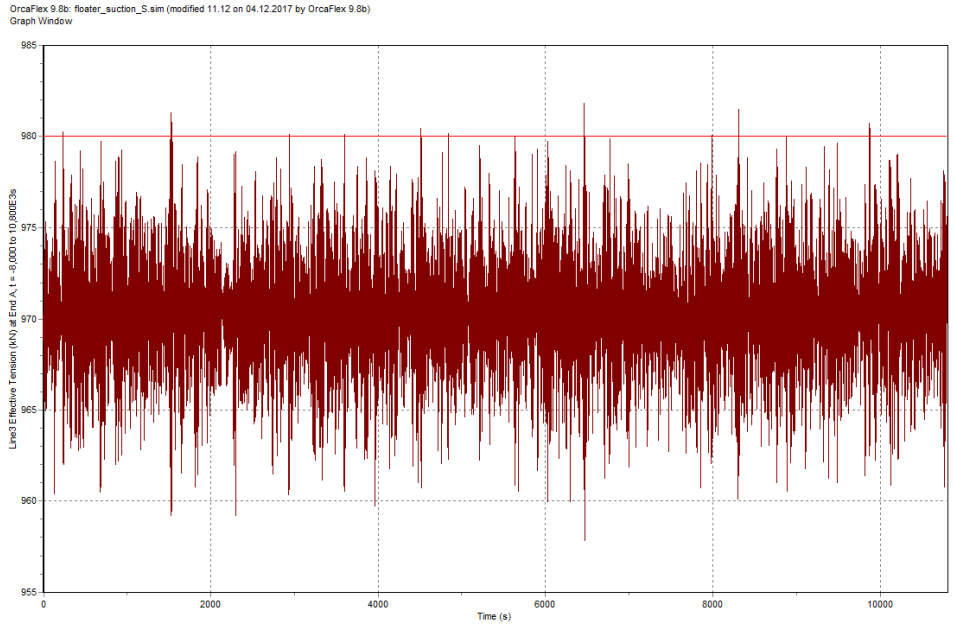 |

| **GPD parameters (line 1)** | |
|---|---|
| β | -0.053 |
| μ | 0 |
| σ | 1.182 |
| Points fitted | 52 |
| Threshold [kN] | 980.00 |
| **GPD parameters (line 3)** | |
| β | -0.125 |
| μ | 0 |
| σ | 0.687 |
| Points fitted | 12 |
| Threshold [kN] | 980.00 |

# F.16 Simulation 16

| **Range graph** |
|---|

| | |
|---|---|
| Line 1 | 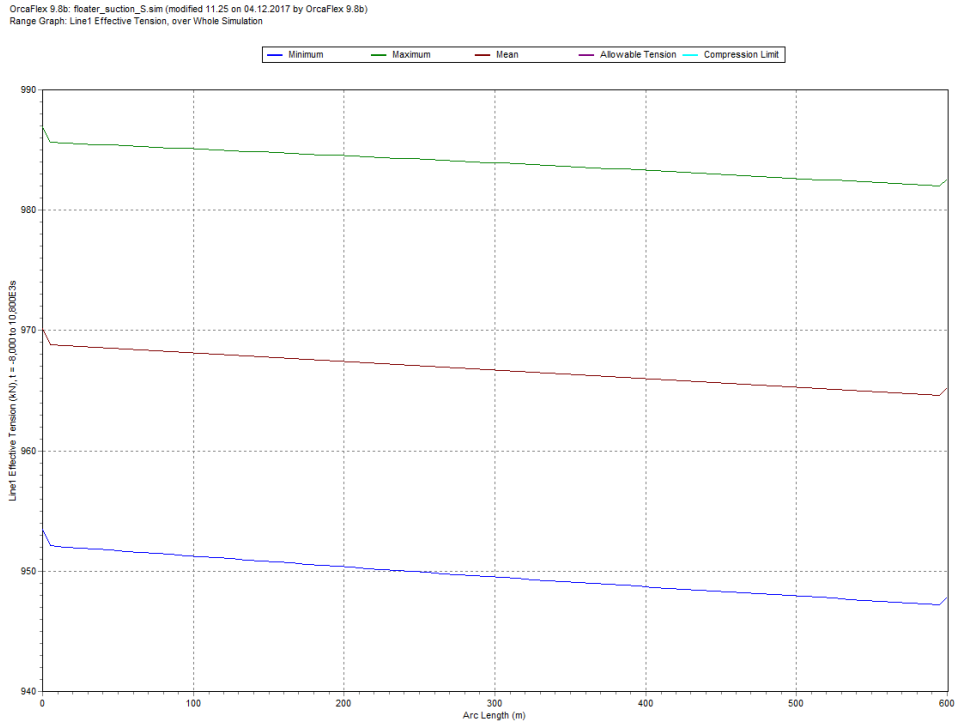 |
| Line 3 | 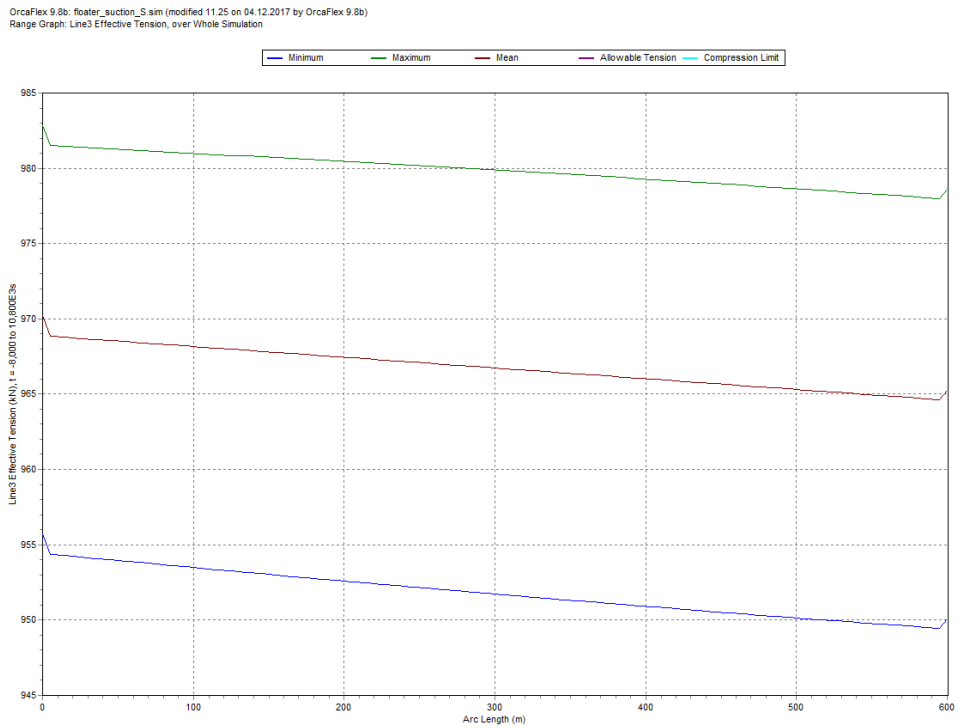 |
| **Time history** | |

Line 1

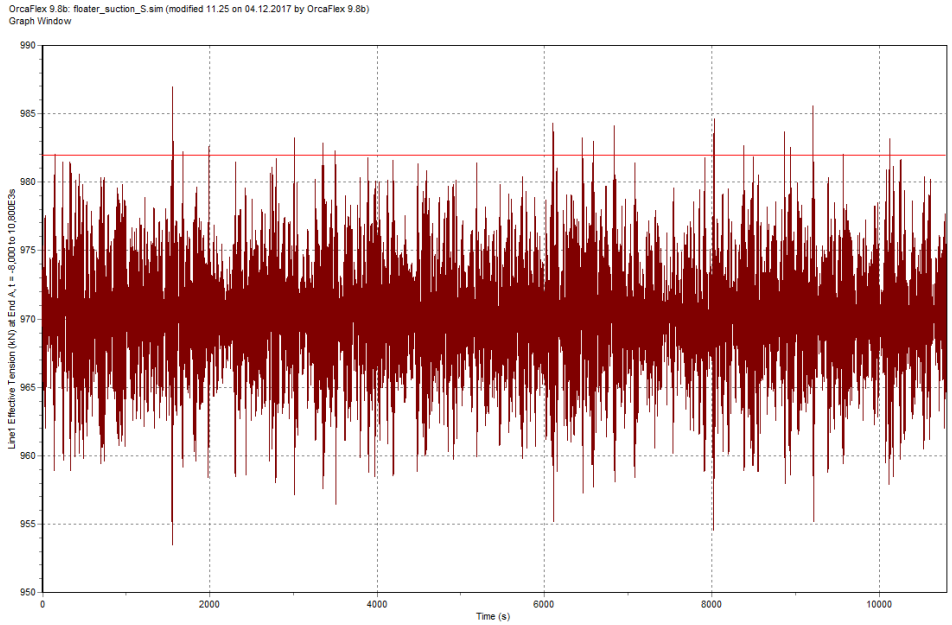


Line 3

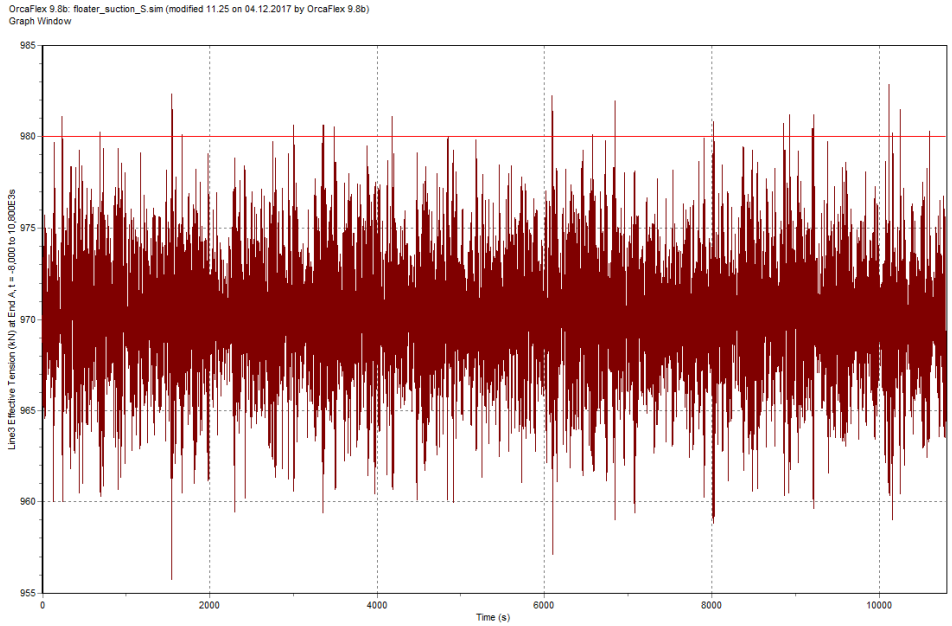


| **GPD parameters (line 1)** | |
|---|---|
| β | -0.192 |
| μ | 0 |
| σ | 1.667 |
| Points fitted | 21 |
| Threshold [kN] | 982.00 |
| **GPD parameters (line 3)** | |
| β | -0.517 |

| | |
|---|---|
| μ | 0 |
| σ | 1.632 |
| Points fitted | 22 |
| Threshold [kN] | 980.00 |

# Appendix G
# Anchor forces

Generalize Pareto distribution (GPD) parameters:

- β: shape parameter;
- μ: location parameter;
- σ: scale parameter.

## G.1 Simulation 1

| Time history | |
|---|---|
| Anchor 1 | 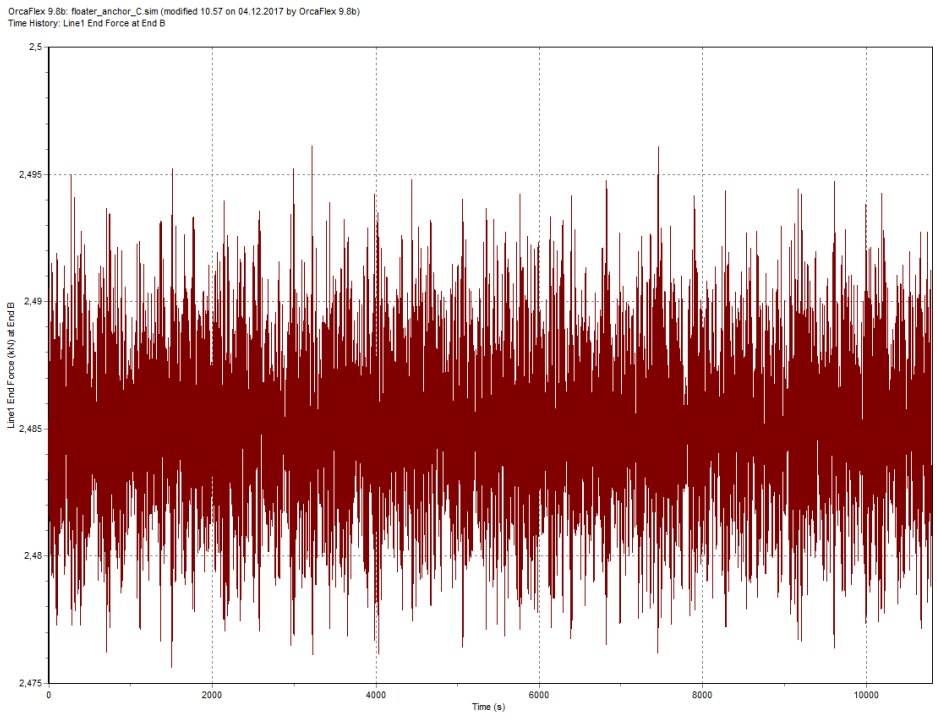 |

| | |
|---|---|
| Anchor 3 | 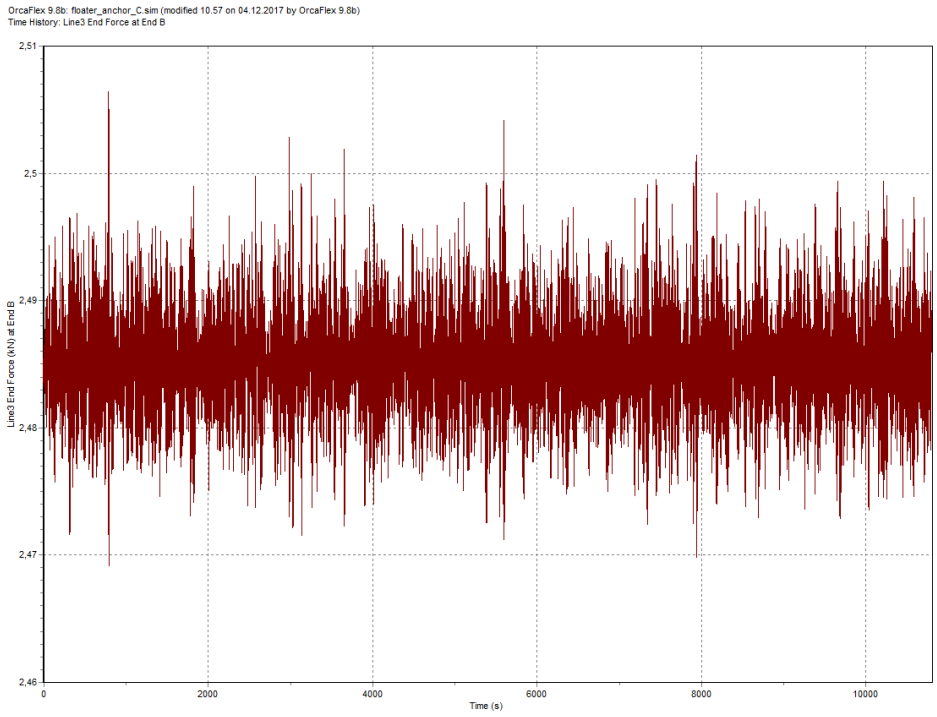 |

## G.2 Simulation 2

| Time history |
|---|

| | |
|---|---|
| Anchor 1 | 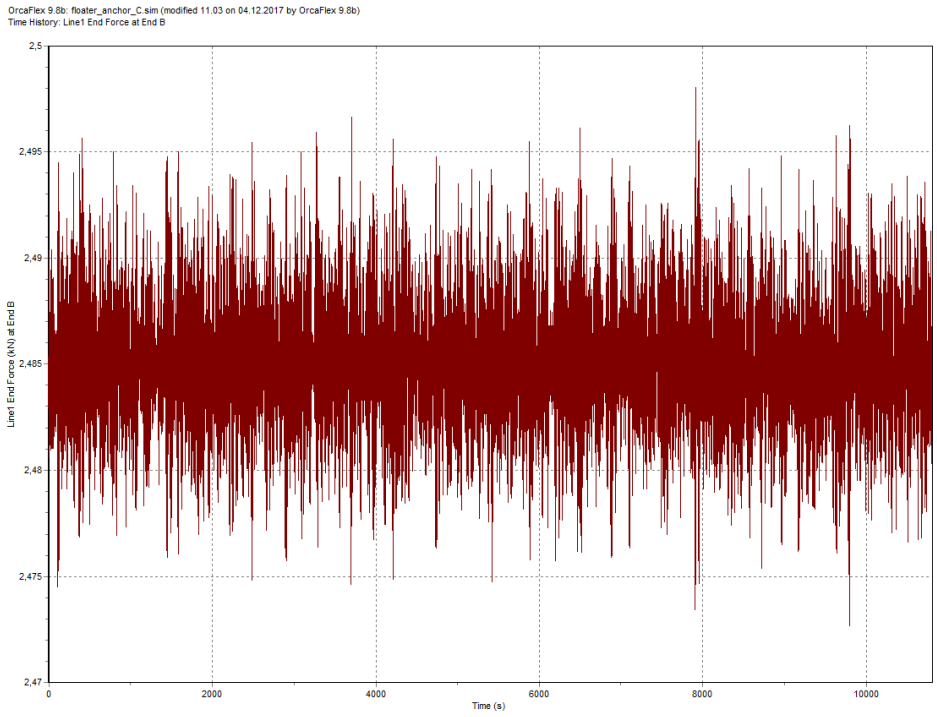 |
| Anchor 3 | 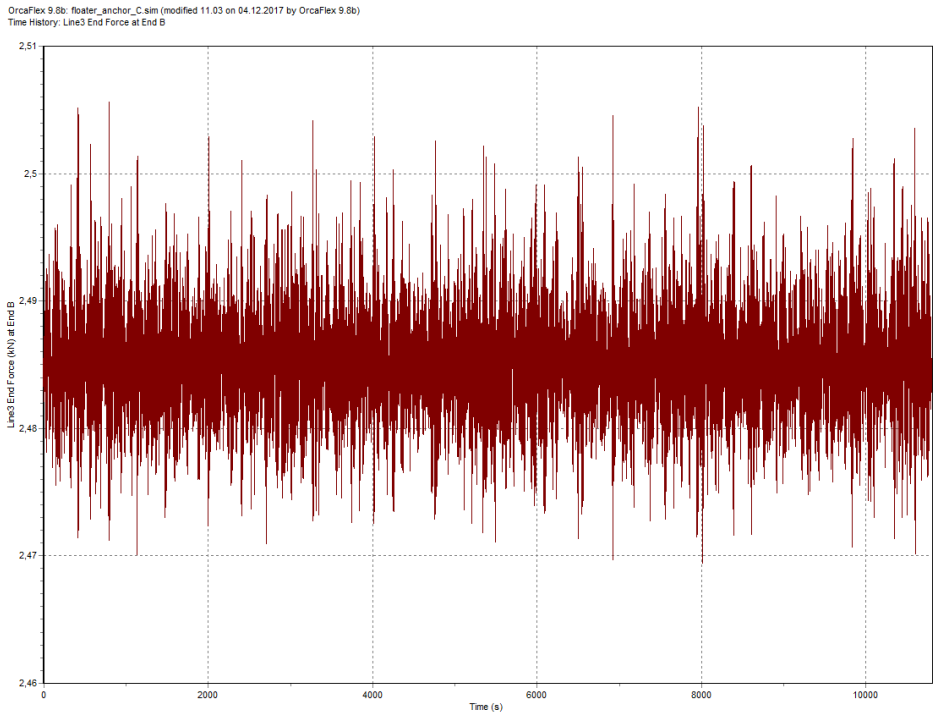 |

# G.3 Simulation 3

| | Time history |
|---|---|
| Anchor 1 | 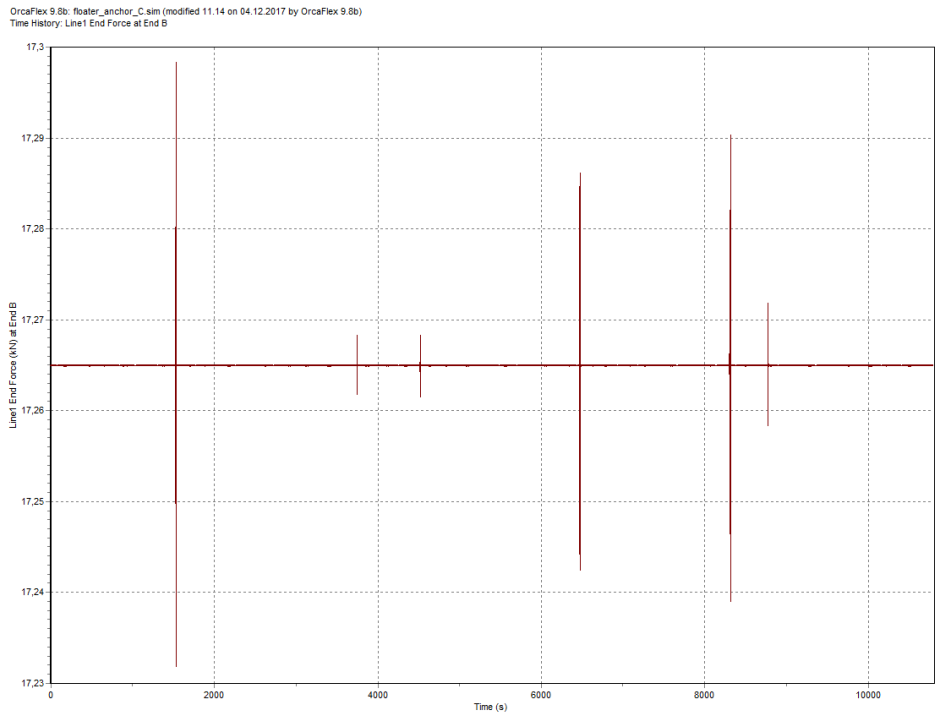 |
| Anchor 3 | 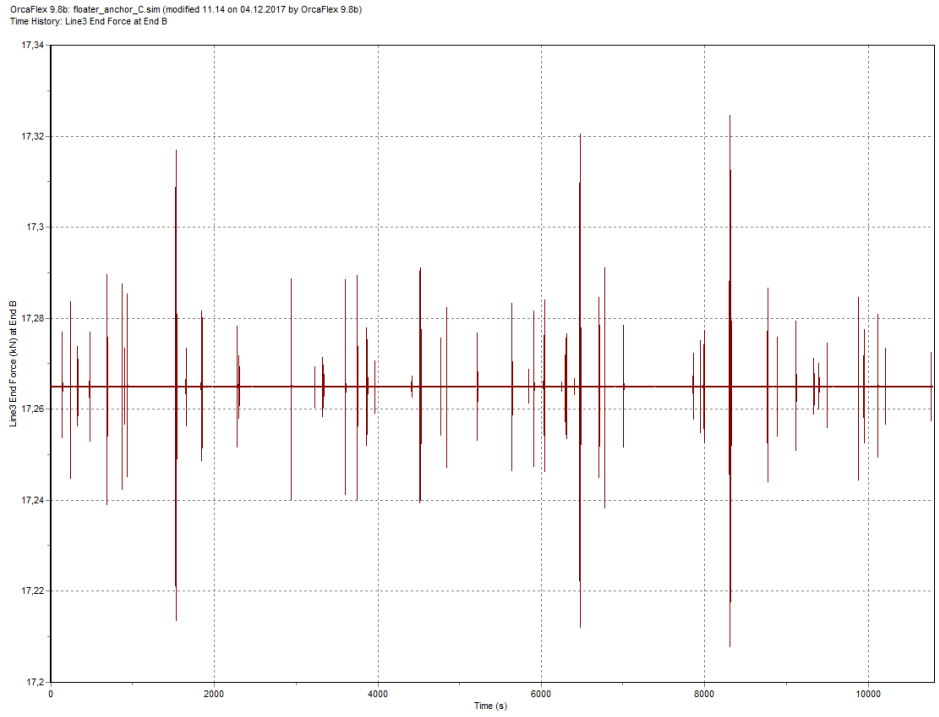 |

# G.4 Simulation 4

| | Time history |
|---|---|
| Anchor 1 | 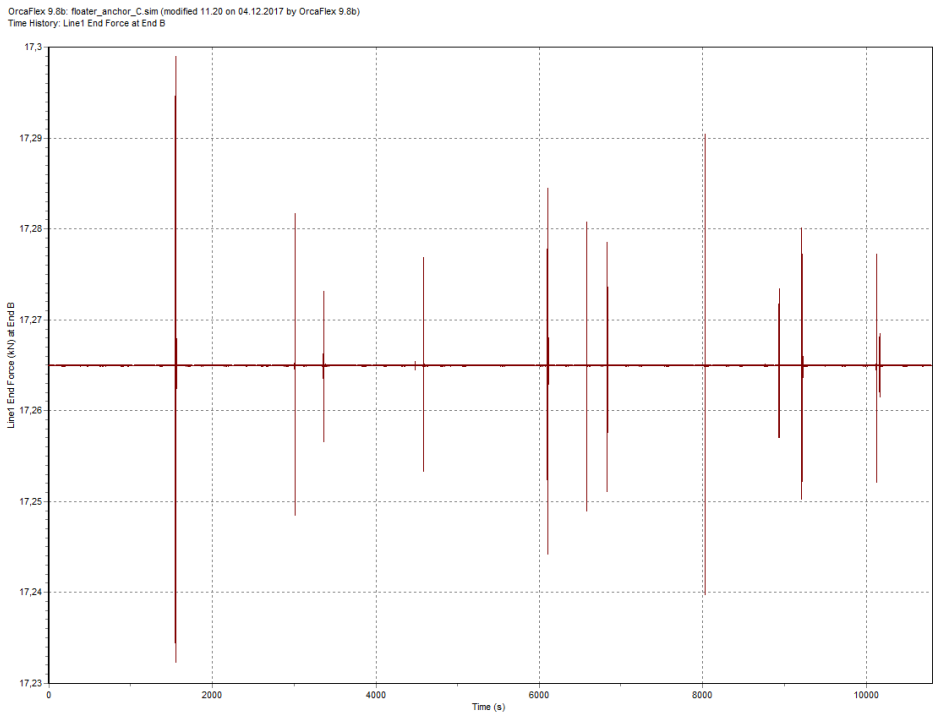 |
| Anchor 3 | 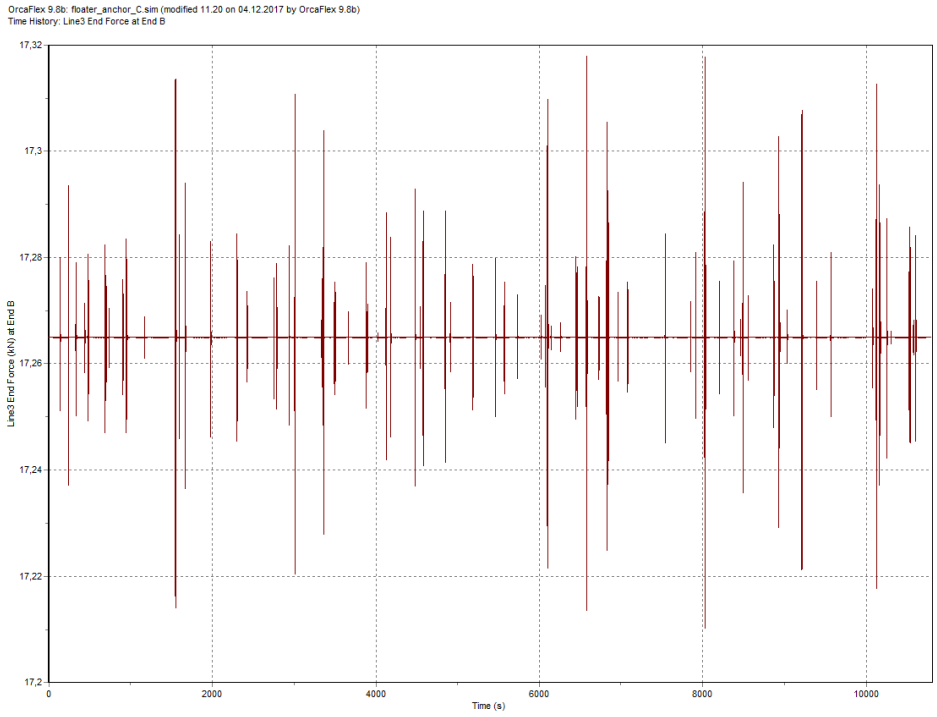 |

# G.5 Simulation 5

| | Time history |
|---|---|
| Anchor 1 | 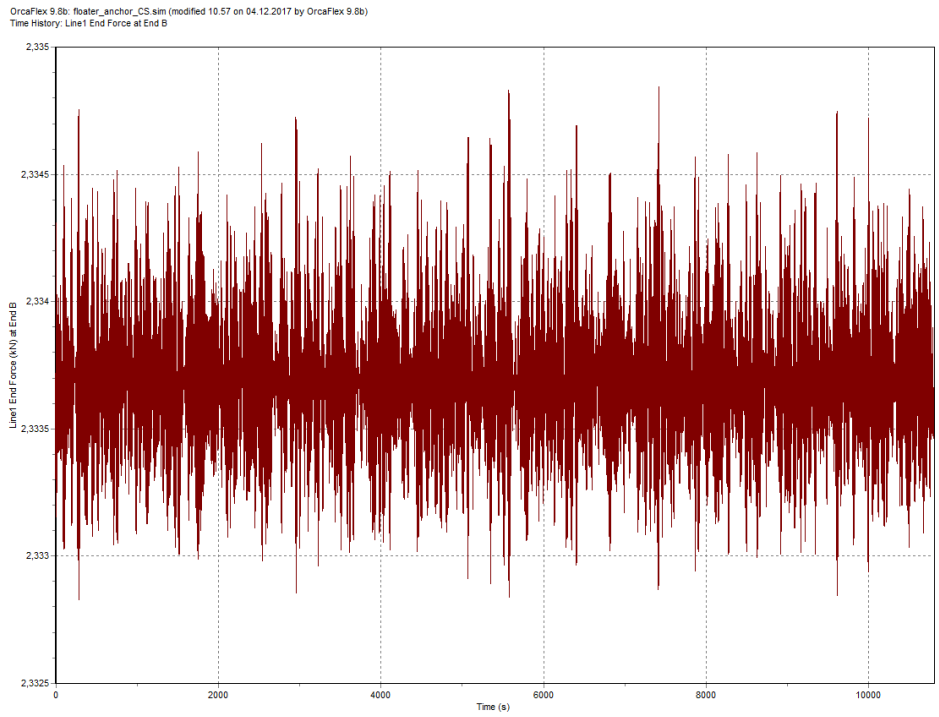 |
| Anchor 3 | 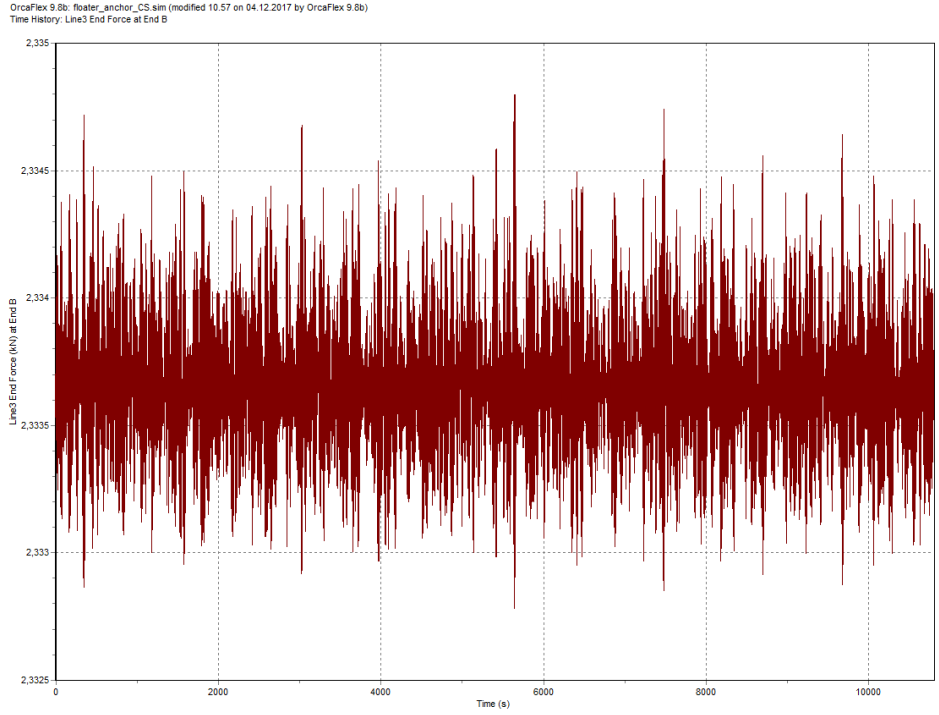 |

# G.6 Simulation 6

| | Time history |
|---|---|
| Anchor 1 | 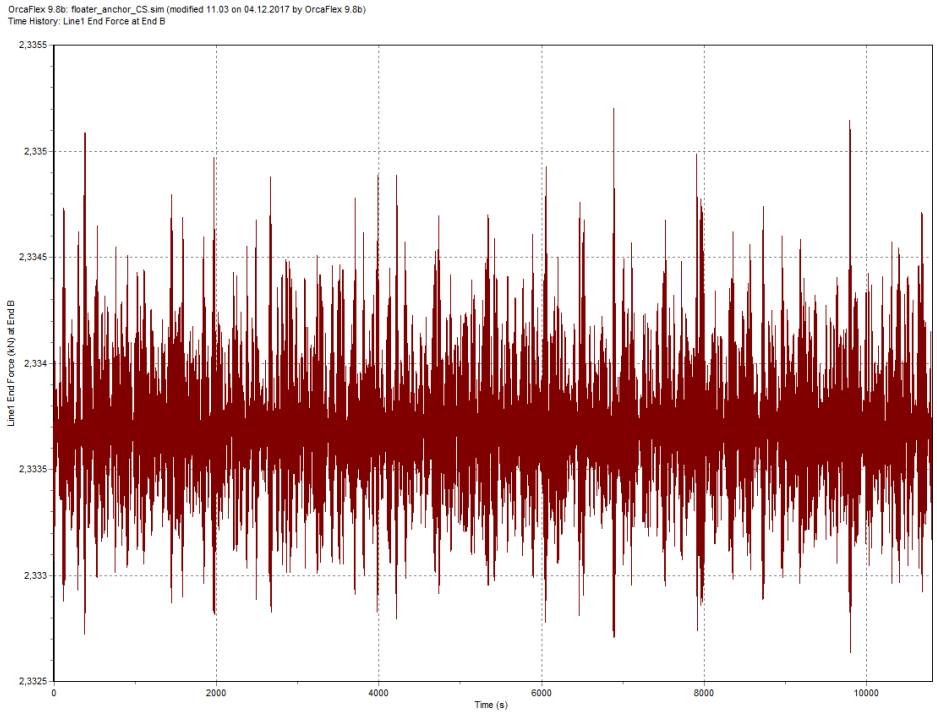 |
| Anchor 3 | 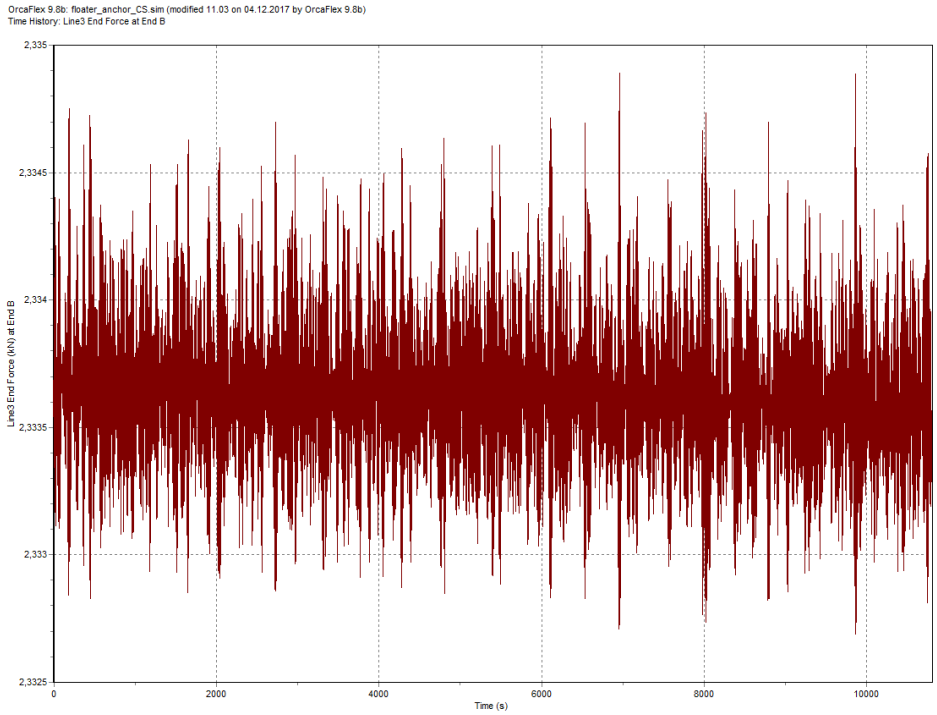 |

# G.7 Simulation 7

| | Time history |
|---|---|
| Anchor 1 | 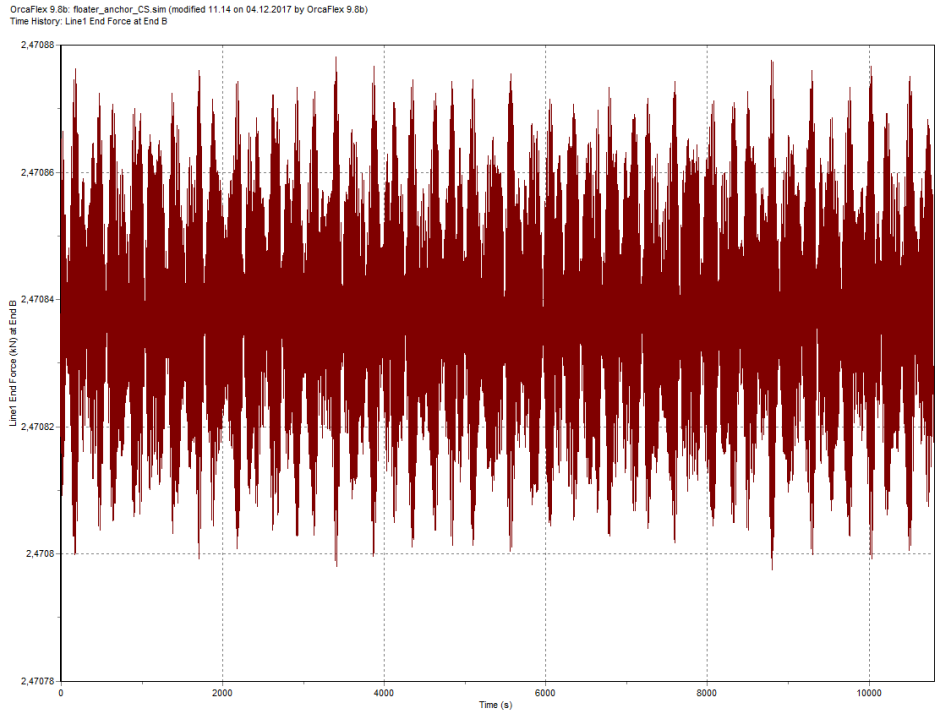 |
| Anchor 3 | 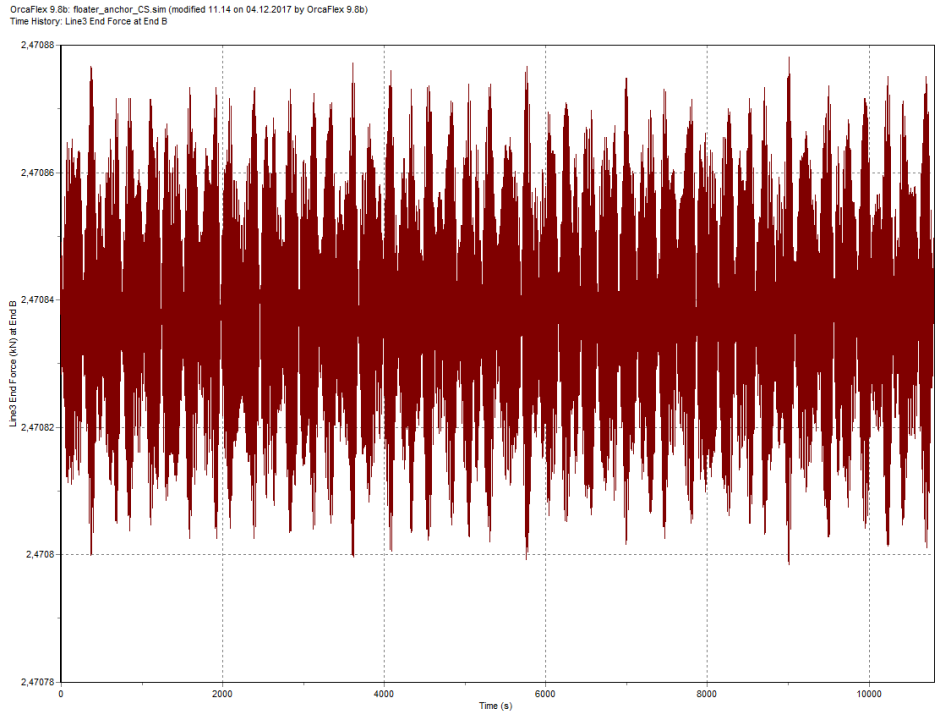 |

# G.8 Simulation 8

| Time history | |
|---|---|
| Anchor 1 | 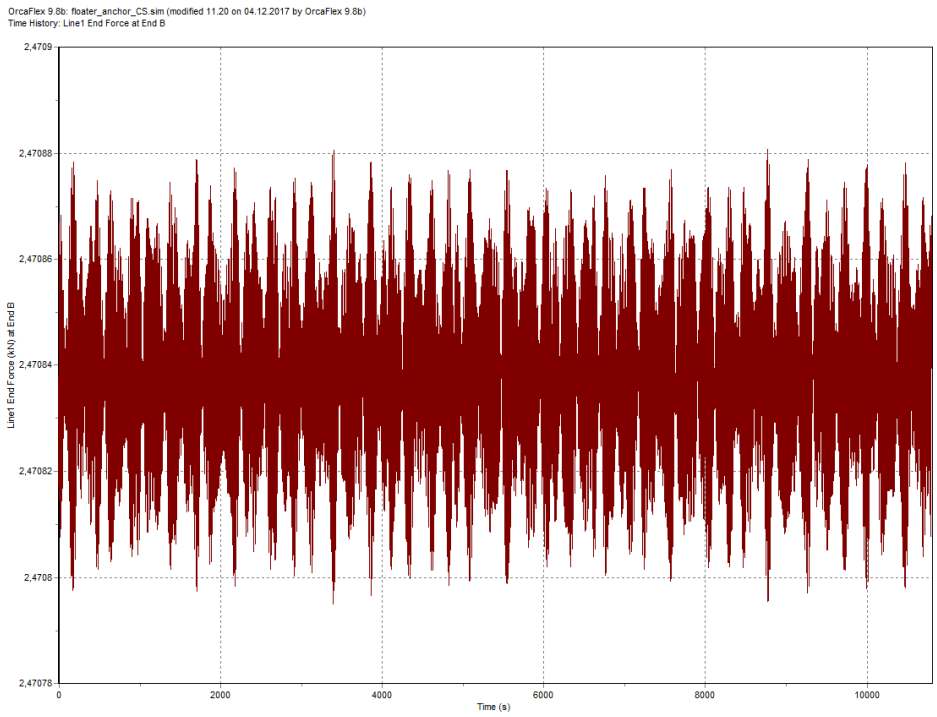 |
| Anchor 3 | 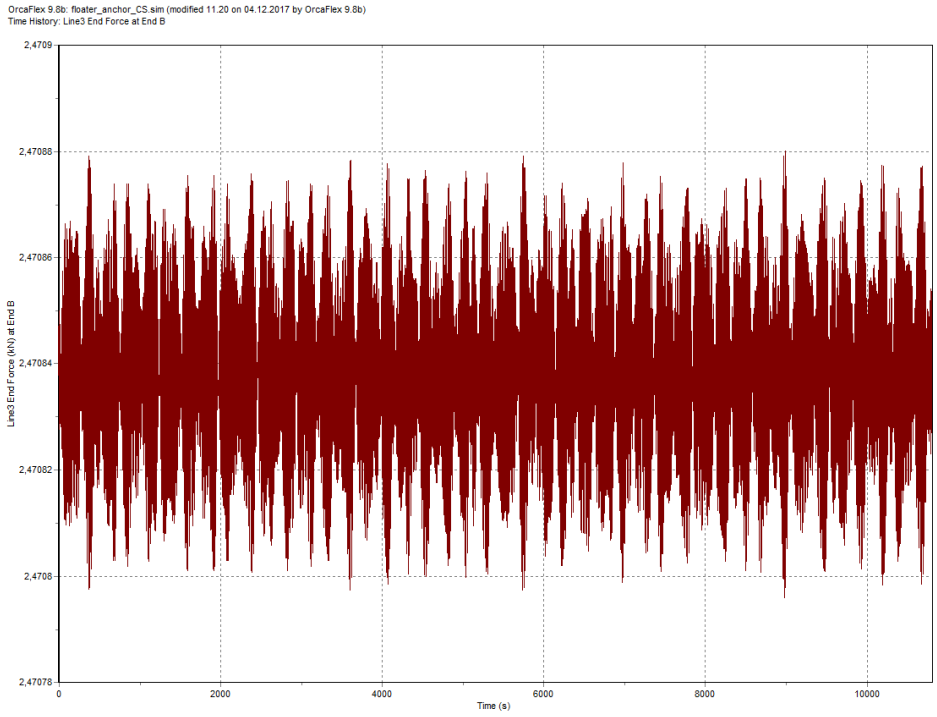 |

# G.9 Simulation 9

| Vertical forces time history | |
|---|---|
| Anchor 1 | 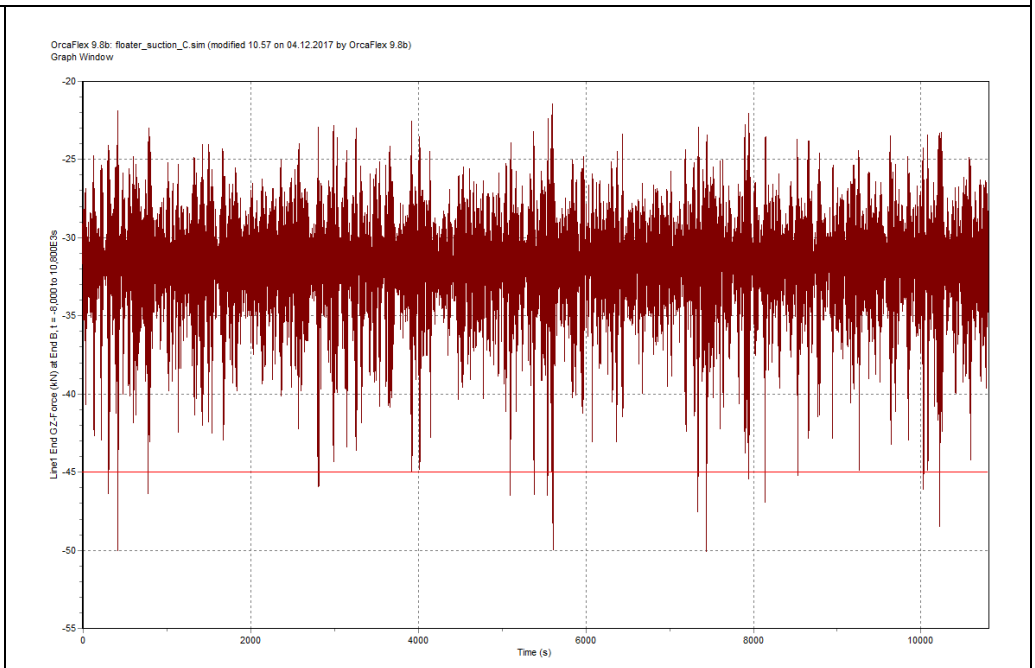 |
| Anchor 3 | 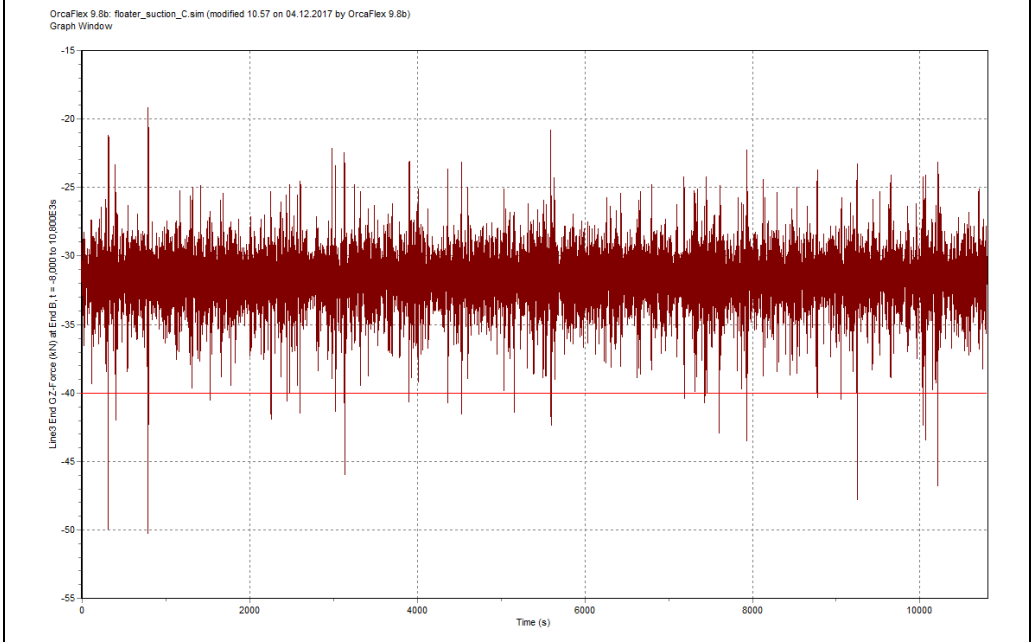 |

| GPD parameters (anchor 1) | |
|---|---|
| β | -0.088 |
| μ | 0 |
| σ | 1.838 |

| | |
|---|---|
| Points fitted | 22 |
| Threshold [kN] | -45.00 |
| **GPD parameters (anchor 3)** | |
| β | 0.194 |
| μ | 0 |
| σ | 1.980 |
| Points fitted | 32 |
| Threshold [kN] | -40.00 |

# G.10 Simulation 10

| **Vertical forces time history** | |
|---|---|
| Anchor 1 | 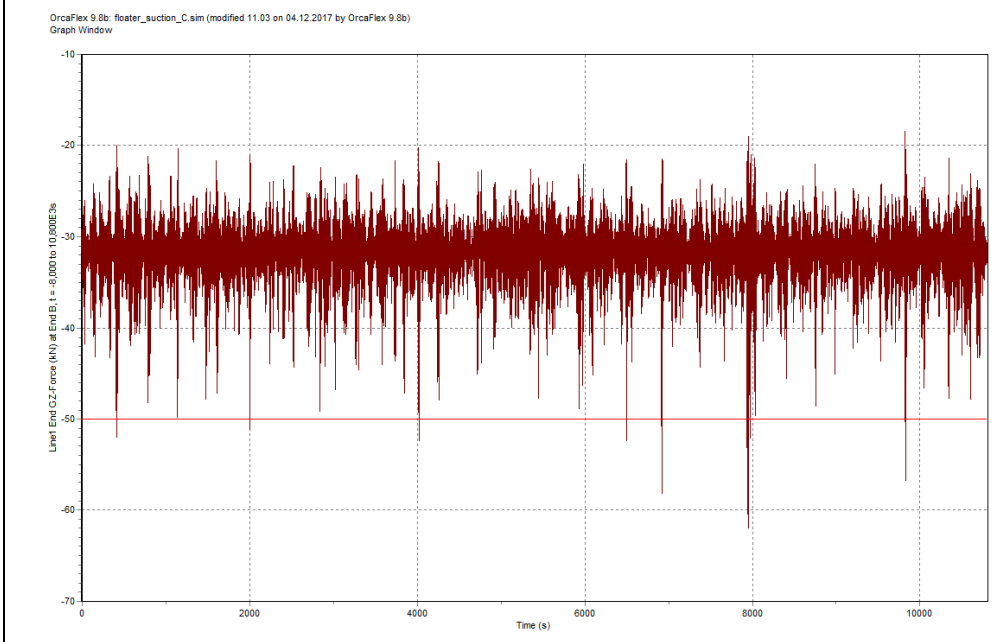 |

| | |
|---|---|
| Anchor 3 | 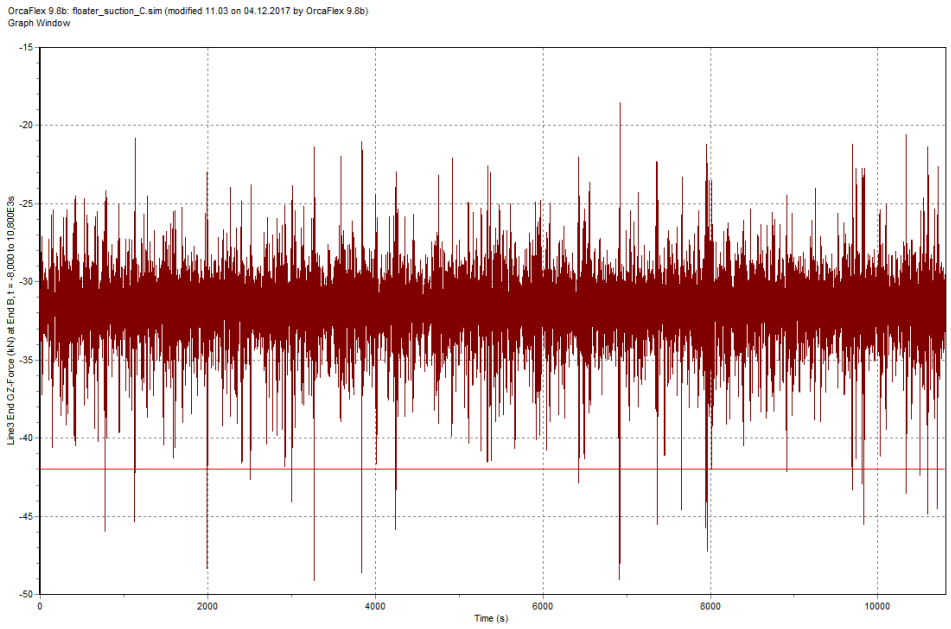 |

| **GPD parameters (anchor 1)** | |
|---|---|
| β | -0.144 |
| μ | 0 |
| σ | 4.325 |
| Points fitted | 11 |
| Threshold [kN] | -50.00 |
| **GPD parameters (anchor 3)** | |
| β | -0.793 |
| μ | 0 |
| σ | 5.795 |
| Points fitted | 25 |
| Threshold [kN] | -40.00 |

# G.11 Simulation 11

| **Vertical forces time history** |
|---|

Anchor 1

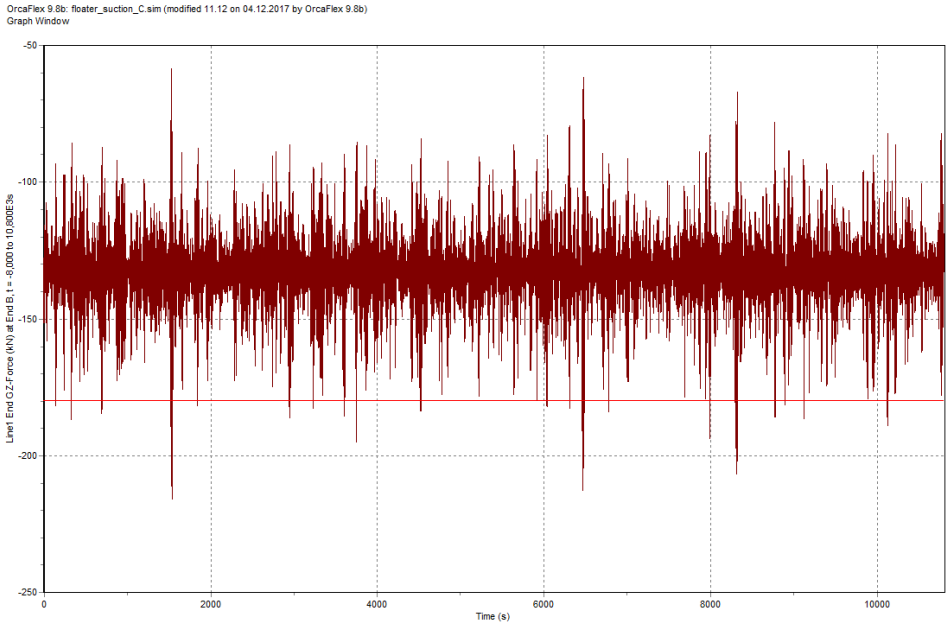


Anchor 3

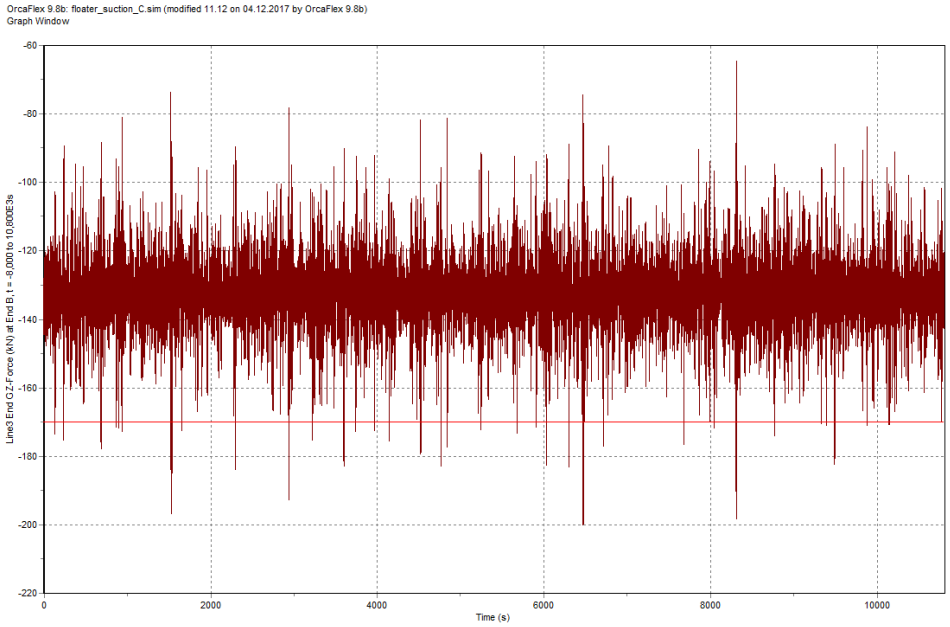


| GPD parameters (anchor 1) | |
|---|---|
| β | -0.0057 |
| μ | 0 |
| σ | 10.238 |
| Points fitted | 29 |
| Threshold [kN] | -180.00 |
| **GPD parameters (anchor 3)** | |
| β | -0.057 |

| | |
|---|---|
| μ | 0 |
| σ | 8.560 |
| Points fitted | 39 |
| Threshold [kN] | -170.00 |

# G.12 Simulation 12

**Vertical forces time history**

Anchor 1

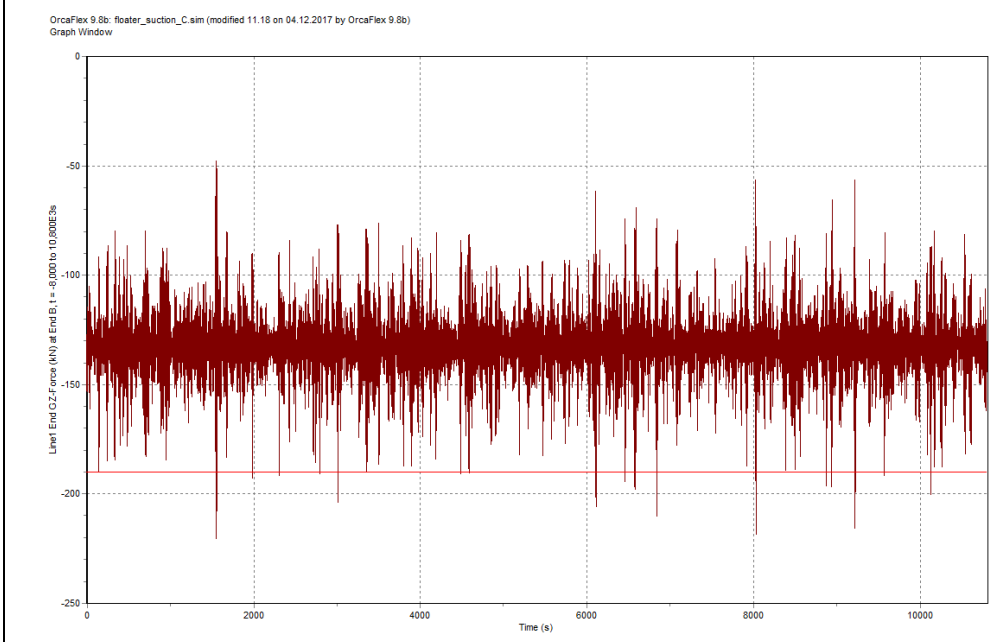

| Anchor 3 | 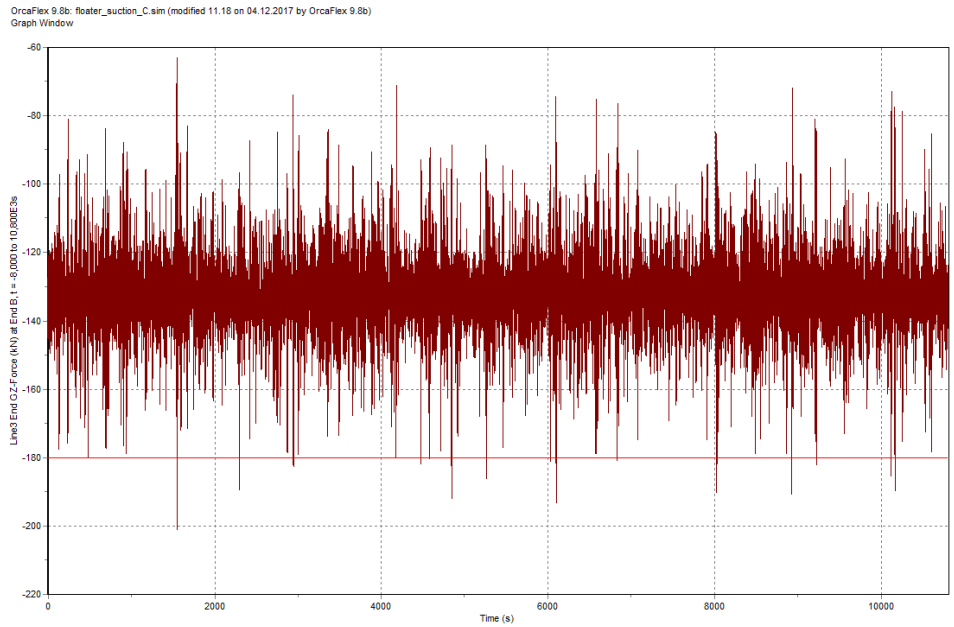 |
|---|---|

| GPD parameters (anchor 1) | |
|---|---|
| β | -0.306 |
| μ | 0 |
| σ | 13.657 |
| Points fitted | 22 |
| Threshold [kN] | -190.00 |
| **GPD parameters (anchor 3)** | |
| β | -0.150 |
| μ | 0 |
| σ | 7.032 |
| Points fitted | 18 |
| Threshold [kN] | -180.00 |

# G.13 Simulation 13

| Vertical forces time history |
|---|

| | |
|---|---|
| Anchor 1 | 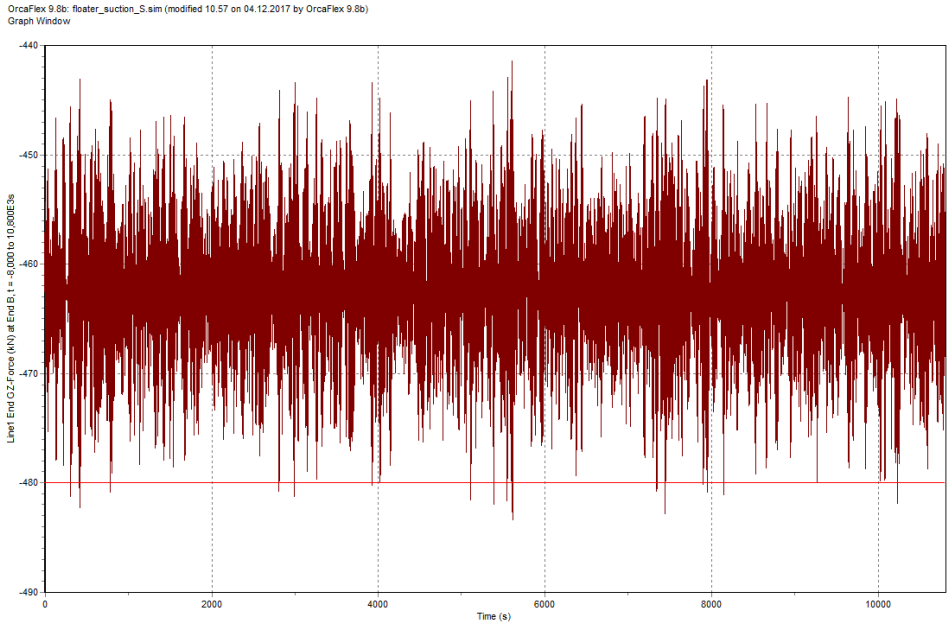 |
| Anchor 3 | 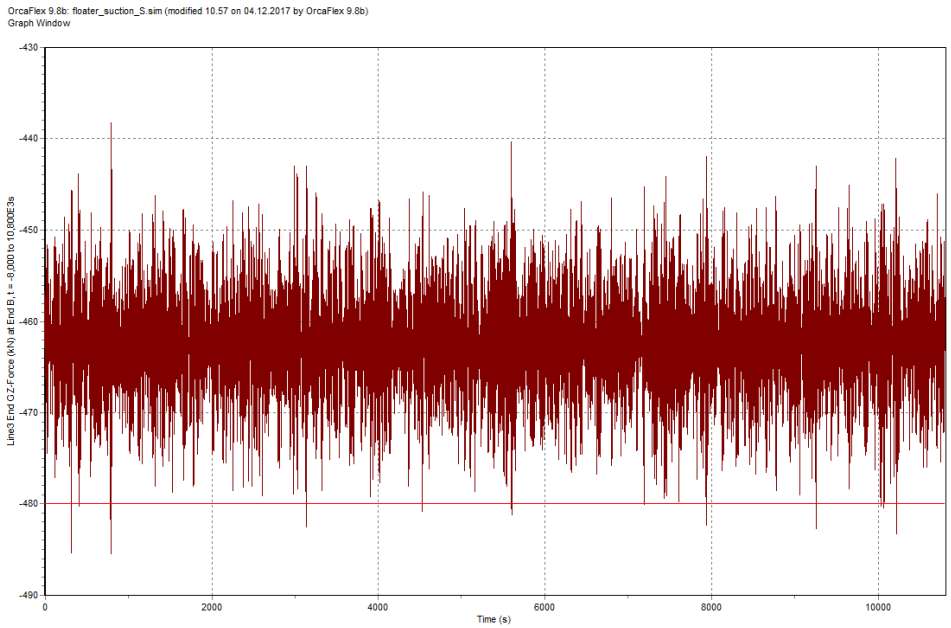 |

| **GPD parameters (anchor 1)** | |
|---|---|
| β | -0.702 |
| μ | 0 |
| σ | 2.470 |
| Points fitted | 18 |
| Threshold [kN] | -480.00 |
| **GPD parameters (anchor 3)** | |
| β | -0.272 |

| | |
|---|---|
| μ | 0 |
| σ | 2.483 |
| Points fitted | 14 |
| Threshold [kN] | -480.00 |

# G.14 Simulation 14

| Vertical forces time history | |
|---|---|
| Anchor 1 | 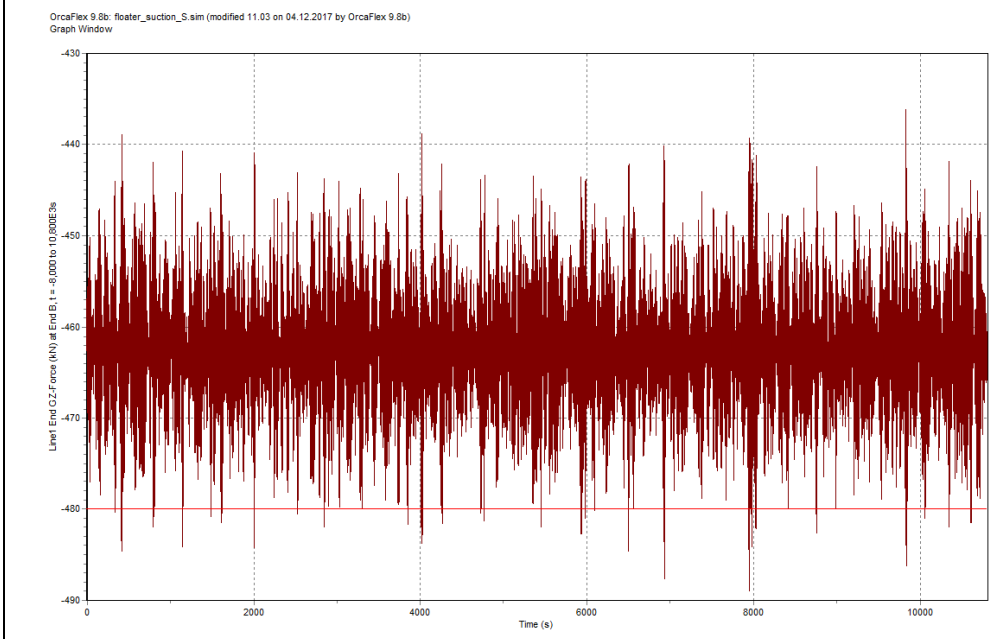 |

| | |
|---|---|
| Anchor 3 | 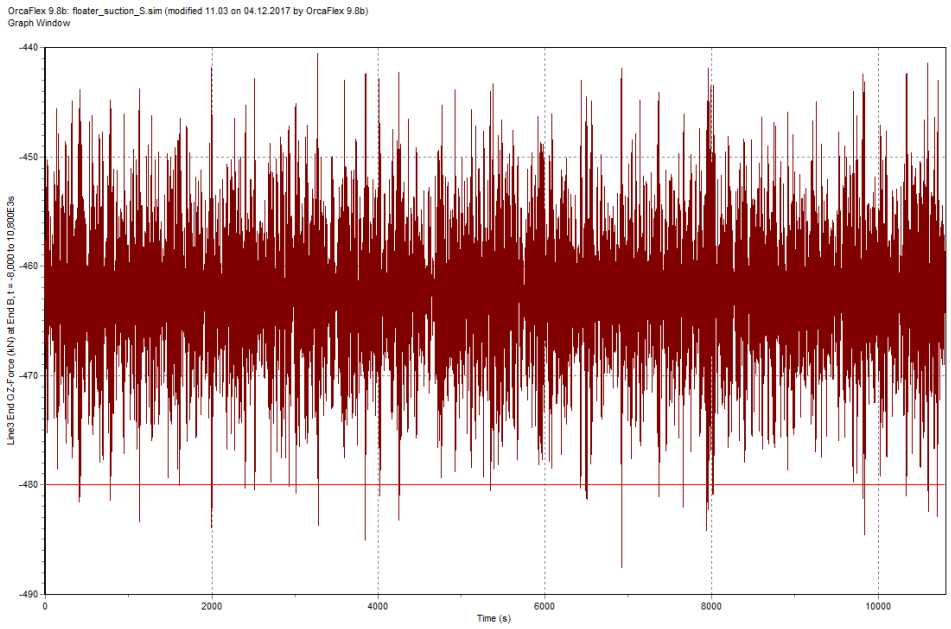 |

| **GPD parameters (anchor 1)** | |
|---|---|
| β | -0.237 |
| μ | 0 |
| σ | 3.089 |
| Points fitted | 39 |
| Threshold [kN] | -480.00 |
| **GPD parameters (anchor 3)** | |
| β | -0.130 |
| μ | 0 |
| σ | 2.146 |
| Points fitted | 32 |
| Threshold [kN] | -480.00 |

# G.15 Simulation 15

| **Vertical forces time history** |
|---|

Anchor 1

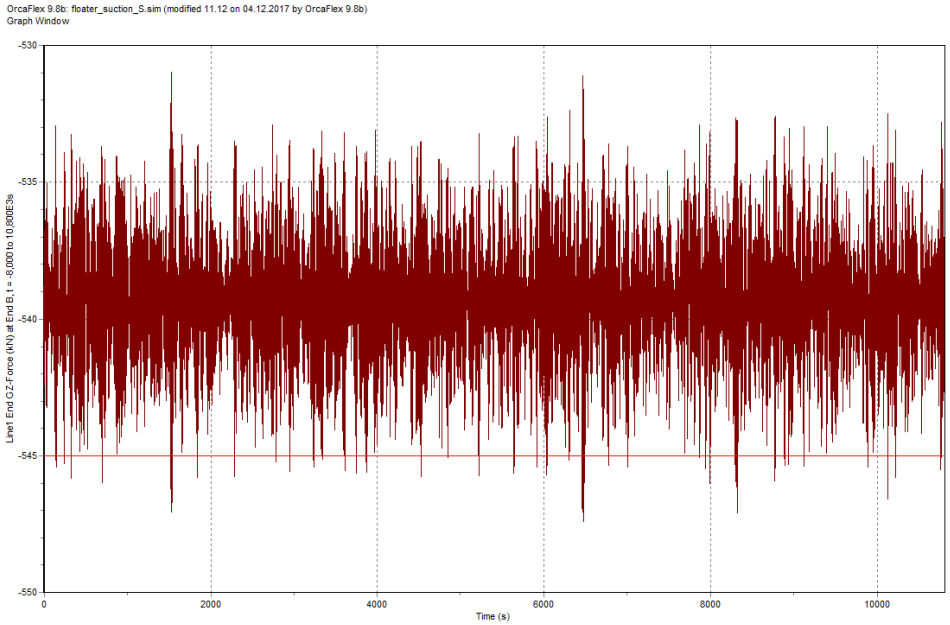


Anchor 3

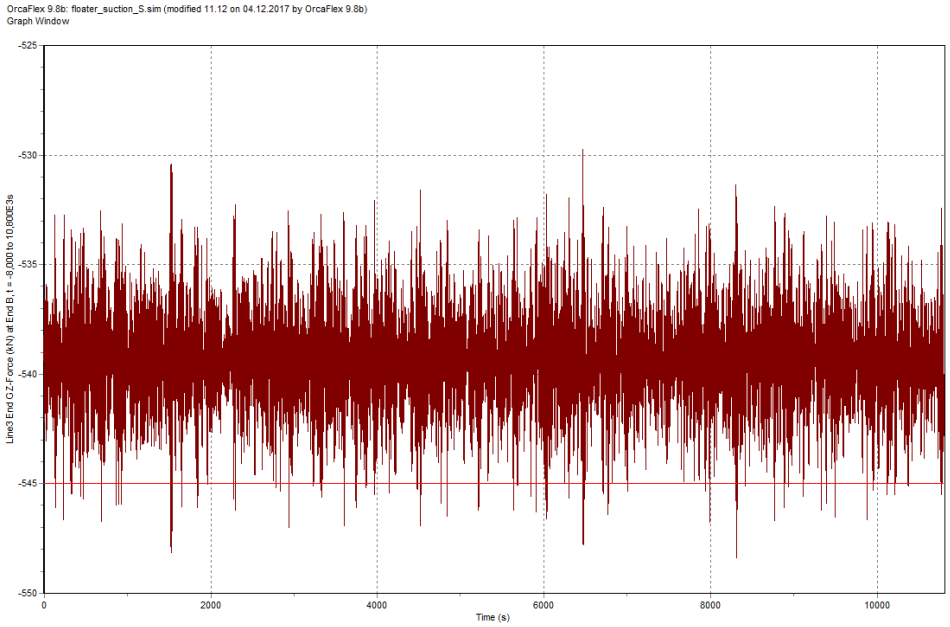


| **GPD parameters (anchor 1)** | |
|---|---|
| β | -0.244 |
| μ | 0 |
| σ | 0.863 |
| Points fitted | 49 |
| Threshold [kN] | -545.00 |
| **GPD parameters (anchor 3)** | |
| β | -0.305 |

| | |
|---|---|
| μ | 0 |
| σ | 1.309 |
| Points fitted | 69 |
| Threshold [kN] | -545.00 |

# G.16 Simulation 16

**Vertical forces time history**

Anchor 1

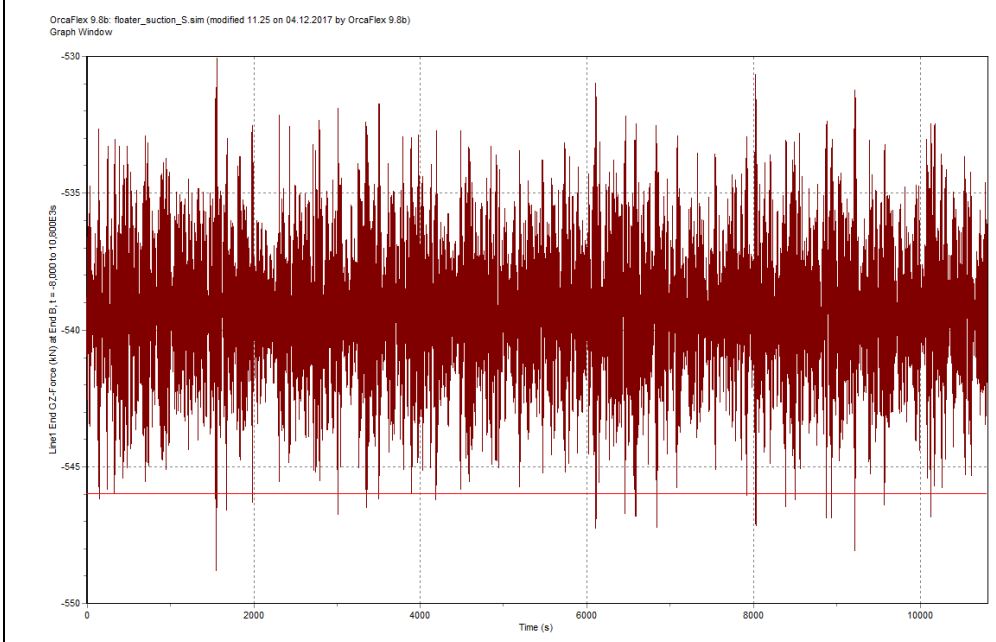

Anchor 3

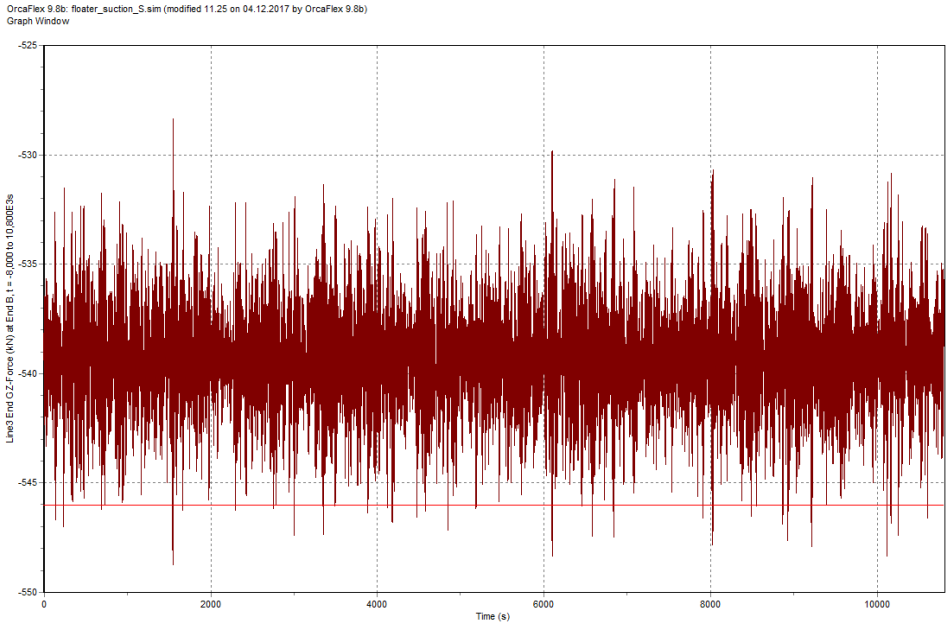


| GPD parameters (anchor 1) | |
|---|---|
| β | -0.199 |
| μ | 0 |
| σ | 0.914 |
| Points fitted | 25 |
| Threshold [kN] | -546.00 |
| **GPD parameters (anchor 3)** | |
| β | -0.348 |
| μ | 0 |
| σ | 1.192 |
| Points fitted | 42 |
| Threshold [kN] | -546.00 |